Andreas WEBER

Dissertation

Andreas WEBER

Dissertation

Polymeric Thermotropic Glazings for Overheating Protection:
Systematic Polymer Science Based Optimisation
of Performance Characteristics

November 2013

Polymer Competence Center Leoben GmbH
Department Polymer Engineering and Science, University of Leoben

About the Dissertation

This cumulative Dissertation was authored by

DI Andreas Weber
born 07. September 1984
in Bludenz (Vorarlberg, Republik Österreich)

Submitted to

Materials Science and Testing of Polymers
Department Polymer Engineering and Science
University of Leoben

Conducted at

Polymer Competence Center Leoben GmbH

Supervisor

Dr. Katharina Resch
Materials Science and Testing of Polymers
Department Polymer Engineering and Science
University of Leoben

Academic Supervisor

Univ.-Prof. Dr. Gerald Pinter
Materials Science and Testing of Polymers
Department Polymer Engineering and Science
University of Leoben

Referees

Univ.-Prof. Dr. Gerald Pinter
Materials Science and Testing of Polymers
Department Polymer Engineering and Science
University of Leoben

Univ.-Prof. Dr. Wolfgang Kern
Chemistry of Polymers
Department Polymer Engineering and Science
University of Leoben

Part I.

Preamble

Affidavit

I declare in lieu of oath, that I wrote this thesis and performed the associated research myself, using only literature cited in this volume.

Andreas Weber
Thüringen (Vorarlberg, Republik Österreich) | November 2013

Funding

The majority of the research work of this Dissertation was performed within the Non-COMET-project “Smart Windows – Smart Collectors: Entwicklung, Modellierung und Vermessung von Überhitzungsschutzverglasungen für Fassaden- und Kollektoranwendungen” (project-no.: 5019) at the Polymer Competence Center Leoben GmbH (PCCL, Austria) with contributions by Department Polymer Engineering, University of Leoben (Austria) and Advanced Polymer Compounds (A.P.C., Austria). The project was funded by the State Government of Styria, Department Zukunftsfonds.

Minor parts of the research work of this Dissertation were performed within the COMET-project “Special topics of polymer science and advanced characterization methods” (project-no.: 4393) at the Polymer Competence Center Leoben GmbH (PCCL, Austria) within the framework of the COMET-program of the Federal Ministry for Transport, Innovation and Technology and Federal Ministry of Economy, Family and Youth. The PCCL is funded by the Austrian Government and the State Governments of Styria and Upper Austria.

Acknowledgement

On this occasion, I want to express my gratitude to all persons who supported my work while performing this thesis.

First of all, I want to thank my supervisor Dr. Katharina Resch (Materials Science and Testing of Polymers, Department Polymer Engineering and Science, University of Leoben) for her support throughout the recent years. Furthermore, I much appreciated working together with Katharina. She trusted in my scientific skills, never shied away from discussion and supported me in order to realize my ideas whenever necessary and gave me the possibility to significantly improve my academic writing skills. It was a privilege to me getting supervised by Katharina during writing this thesis.

Furthermore I want to express my gratitude to Univ.-Prof. Dr. Gerald Pinter (Materials Science and Testing of Polymers, Department Polymer Engineering and Science, University of Leoben), Univ.-Prof. Dr. Wolfgang Kern (Chemistry of Polymeric Materials, Department Polymer Engineering and Science, University of Leoben) and Mag. Martin Payer (CEO of PCCL) for offering me the possibility to perform this thesis.

I want to thank DI Karl Schnetzinger (A.P.C. Advanced Polymer Compounds) for compounding thermoplast based materials. Furthermore he provided valuable insight into critical aspects of compounding technology.

Special thanks go to Dr. Sandra Schlögl (PCCL) who was always helpful when it came to the setup of equipment in the chemistry laboratories I have never used before.

I am thankful for the pleasure to work with Jörg Schauberger, Archim Wolfberger, Rebecca Kramer, Evelyn Sattler, Dietmar Lenko and Jakob Manhart at the chemistry laboratories, who were always willing to provide a helping hand when more than two

hands were required. But I especially want to thank them for providing such a nice atmosphere in the lab.

Furthermore, I had the pleasure to supervise Alexander Klutz, Andrea Schmid, Daniel Holzer and Georg M. Smole with regard to scientific work during the time they were working in the relevant fields of our projects. On this occassion I want to express my gratitude to them for their contributions.

My gratitude is also dedicated to my colleague Astrid Rauschenbach (PCCL). Thanks to her excellent work in the measurement tasks she conducted, progress of my work was significantly improved. Special thanks go also to my colleagues Marlene, Bettina, Daniel, Andreas, Ines, Bernd, Nici, Barbara, Gilbert and others I might forgot for their fidelity, friendship and the lively debates also apart from scientific work.

I also want to express my gratitude to my former teacher Dr. Josef Mäser, providing knowledge and academic skills to me that were relevant for me also upon performing this thesis.

My friends Steffi, Christiane, Philipp, Christof, Markus, Christian, Max and Aaron I want to thank for the hours we had a good time together. Especially I want to express my gratitude to my life-long friends Alexander, Lukas, Mathias and Matthias. Our friendship and our common past in the Ortsfeuerwehr Thüringen are the reasons why I appreciate them so much.

On this occasion I do not want to miss the opportunity to express my gratitude to the most important beings in my life: My parents Marion and Edgar, my sister Carmen, my brother Johannes and his friend Yvonne and my grandparents Albert and Heidi who always stood behind me.

Special thanks go also to my Aikido colleagues Günther, Wolfgang, Valentin, Ezra, Valentina and Gerald. Aikido always helped me to keep balance, shaped my character and was a great accomplishment for my life.

Kurzfassung

Diese Dissertation befasst sich mit der – auf einem systematischen polymerwissenschaftlichen Ansatz beruhenden – Überhitzungsschutzleistungsoptimierung von Polymer-basierten thermotropen Überhitzungsschutzverglasungen. Die untersuchten thermotropen Verglasungen, die bevorzugt eine Transmissionsreduktion bei Überschreiten einer vordefinierten Schalttemperatur zeigen, sind für die Verwendung als Überhitzungsschutzverglasung für Gebäude und speziell für solar-thermische Kollektoren gedacht. Der Fokus lag dabei auf der Formulierung von thermotropen Systemen mit fixen Domänen (TSFD), welche aus einer Polymermatrix und einem darin fein dispergierten thermotropen Additiv (der aktiven Komponente, die die Streudomänen ausbildet) bestehen. Aus der Streutheorie war bekannt, dass die Brechungsindexdifferenz zwischen Matrix und Additiv sowie die Streudomänengröße die wichtigsten die Überhitzungsschutzleistung von TSFD beeinflussenden Parameter sind. Deswegen wurde die Erhebung von Struktur-Eigenschafts-Beziehungen zwischen den thermo-refraktiven Eigenschaften der TSFD-Komponenten (Matrix, thermotropes Additiv), der Überhitzungsschutzleistung und der Morphologie der TSFD prioritär behandelt. Dies wurde auf Basis einer – in diesem Umfang bis dato nicht bewerkstelligten – systematischen Materialformulierungsstrategie mittles umfassender polymerphysikalischen Charakterisierung der TSFD-Komponenten (3 Thermoplaste und 4 UV-härtbare Harze als Matrix; 21 thermotrope Additive) als auch der 41 hergestellten TSFD bewerkstelligt. Die thermo-refraktiven Eigenschaften der TSFD-Komponenten waren (überwiegend) dermaßen ausgeprägt, dass theoretisch TSFD mit effizienter Überhitzungsschutzleistung erhalten werden konnten. Jedoch waren die tatsächlich erzielten Überhitzungsleistungen limitiert. Dies wurde einerseits den in unzureichender Form und/oder Größe entwickelten Streudomänen zugeschrieben.

So zeigten TSFD mit in unzureichender Form (z.B. plättchenartig) und Größe ausgebildeten Streudomänen eine moderate Reduktion der solar hemisphärischen Transmission. Andere TSFD, die zwar in zweckmäßiger Form (kugelförmig) ausgeprägte aber zu große Streudomänen aufwiesen, waren durch geringfügige Änderungen der solar hemisphärischen Transmission gekennzeichnet. Andererseits war die unzureichende Überhitzungsschutzleistung – in Teilen der TSFD – auch aufgetretenen Defekten geschuldet. Defektbehaftete TSFD mit in unzureichender Größe ausgeprägten sphärischen Streudomänen zeigten i.A. eine Zunahme der solar hemisphärischen Transmission. Die Ausbildung der unterschiedlichen Domänenformen wurde den Unterschieden bezüglich der Wechselwirkungen der verschiedenen Matrices und der thermotropen Additiven zugeschrieben. Jene Additive, die in flüssiger Form in der Matrix löslich waren, bildeten während der Kristallisation aus der homogenen Mischung energetisch günstige Domänenformen (v.a. nicht sphärische) mit entsprechender Größe aus. Bei den in den Matrices nicht löslichen thermotropen Additiven verhinderten die Viskositätsunterschiede von Matrixmaterial und flüssigem thermotropen Additiv vermutlich die Ausbildung der sphärischen Streudomänen in einer zweckmäßigen Größe. Die Defektbildung in einigen TSFD wurde unzureichender Adhäsion an den Grenzflächen von Matrix und Additiv sowie thermisch induzierten Effekten zugeordnet. Diese thermisch induzierten Effekte waren entweder größere Expansion/Kontraktion des thermotropen Additivs im Vergleich zur Matrix zufolge der auftretenden Temperaturen während der TSFD Herstellung oder thermisch induzierte Diffusion des geschmolzenen Additivs. Die Vermeidung der Defektbildung durch systematische Optimierung der Herstellbedingungen und der Materialformulierung verbesserte die Überhitzungsschutzleistung einer prototypischen TSFD markant: Während das defektbehaftete Ausgangsmaterial eine signifikante Transmissionszunahme zeigte, wies die defektbefreite Schicht eine moderate Transmissionsreduktion bei Überschreiten der Schalttemperatur auf. Allerdings waren die Durchmesser der sphärischen Streudomänen nach wie vor unzureichend. Die Einstellung der Streudomänengröße über ein speziell entwickeltes photoinitiiertes Miniemulsionspolymerisationsverfahren zur Einkapselung des thermotropen Additivs führte zu einer signifikant verbesserten Transmissionsreduktion der mit diesen Domänen formulierten Schicht bei Überschreiten der Schalttemperatur.

Abstract

This dissertation deals with the optimisation of the performance characteristics of polymeric thermotropic glazings for overheating protection purposes employing a systematic polymer scientific approach. The thermotropic glazings investigated – preferably exhibiting a transmittance reduction upon exceeding a pre-defined temperature threshold – are intended for use as overheating protection glazings for buildings and especially for solar thermal collectors. More specifically, focus was on formulation of thermotropic systems with fixed domains (TSFD), consisting of a thermotropic additive as the active component finely dispersed (forming scattering domains) in a polymeric matrix material. From scattering theory the refractive index difference between matrix and additive as well as the scattering domain size were recognised to be the most important parameters affecting the light-shielding efficiency of TSFD. Thus, structure-property-relationships between thermo-refractive properties of TSFD constituents (matrix, thermotropic additive), the light-shielding efficiency and the internal material structure (morphology) of the established TSFD was of major interest and were studied employing an – in its extent unique – systematic material formulations strategy based on sound polymer physical characterisation of numerous TSFD constituents (3 thermoplastic and 4 UV-curable resin matrices; 21 thermotropic additives) and of the 41 established TSFD. The thermo-refractive properties of TSFD constituents were (majorly) sufficient in order to achieve TSFD with efficient overheating protection performance. However, the actually obtained overheating protection performance was limited. This was ascribed to inappropriate shape and/or size of scattering domains on the one hand side and to defects formed in parts of the TSFD on the other hand side. TSFD with inappropriately shaped (e.g. plate-like) and sized scattering domains exhibited a moderate reduction in solar hemispheric transmittance.

TSFD with appropriately shaped (spherical) but inappropriately sized scattering domains showed only minor changes in solar hemispheric transmittance in general. TSFD with inappropriately sized spherical scattering domains and with defects displayed an increase in solar hemispheric transmittance. The formation of different scattering domain shapes was ascribed to differences in the interactions between the individual matrix materials and the thermotropic additives. Additives which were soluble in the matrix resin when they were liquid, were subject to crystallisation from a homogeneous mixture upon TSFD formulation yielding formation of an energetically favourable shape (i.e. non-spherical) and size. For insoluble thermotropic additives – forming spherical scattering domains –, the different viscosities of matrix material and thermotropic additive in the liquid state were suspected to prevent formation of appropriately sized scattering domains. The defect formation in several TSFD was attributed to limited adhesion at the interface of matrix material and thermotropic additive and to thermally induced effects. These thermally induced effects were either stronger expansion/contraction of the thermotropic additive compared to the matrix due to apparent temperature conditions during processing or thermally induced diffusion of the thermotropic additive in the molten state. The prevention of defect formation by systematic optimisation of processing conditions and material formulation improved the solar hemispheric transmittance change of a specific TSFD: Whereas the initial layer with defects showed a significant transmittance increase, the layer lacking defects showed a moderate transmittance reduction upon exceeding the threshold temperature. Nevertheless, the diameters of the spherical scattering domains were inappropriate. Adjustment of the scattering domain size via a specifically developed photo-initiated miniemulsion polymerisation mediated encapsulation process for the thermotropic additive resulted in a significantly enhanced transmittance reduction of the layer formulated with these domains upon exceeding the threshold temperature.

Contents

Part II.

Introduction to the Thesis

1 Motivation

1.1 Energy, Human Development and Climate Change

Ensuring access to modern energy is identified as challenging issue for the future [1]. A paper by United Nations [2] outlines the significant importance of energy in order to achieve every single of the Millenium Development Goals (MDG) [2]. The MDG are (reproduced from [2]):

1. Eradicate extreme poverty and hunger
2. Achieve universal primary education
3. Promote gender equality and empower women
4. Reduce child mortality
5. Improve maternal health
6. Combat HIV/AIDS, malaria and other disease
7. Ensure environmental sustainability
8. Develop a global partnership for development

This is illustrated by the close correlation of Human Development Index (HDI) and the per capital energy consumption [2]: The higher the per capital energy consumption, the higher the HDI. Thus, energy supply is important for social development in general, also apart from the MDG. However, when improving availability of energy, sustainability of both, energy supply and consumption, has to be improved as well [2]. This includes improving energy efficiency, introduction of modern energy production and utilisation technologies, substitution of polluting fuels by less polluting fuels and introduction of renewable energy [2]. All these aspects are of vital importance because the mitigation of climate change is directly interrelated with the challenge

of ensuring access to modern energy [1]. The following considerations may illustrate these close interrelationships.

Climate change will tend to increase the risk of hunger and malnutrition due to reduced global agricultural production and subsequent increases in food prices [3], [4]. Hence, climate change will constrain at least achieving the MDG number 1 and likely have impact on the other MDG. Reasons for the climate change are changes in the energy balance of the Earth which is affected by absorption, scattering and emission of radiation at the Earth's surface and within the atmosphere [4]. Parameters that affect absorption, scattering and emission are the atmospheric concentration of greenhouse gases and aerosols, land cover and solar radiation [4]. Although aerosols have a net cooling effect (Radiative Forcing compared to year 1750 (RF): $-1.2\,W\,m^{-2}$), emission of greenhouse gases (RF: $2.64\,W\,m^{-2}$) together with other factors yield a net positive energy balance of anthropogenic activities (RF: $1.6\,W\,m^{-2}$) [4]. Thereby, the greenhouse gases carbon dioxide (CO_2; RF: $1.66\,W\,m^{-2}$) – which is the most important greenhouse gas –, methane (CH_4; RF: $0.48\,W\,m^{-2}$), halocarbons (RF: $0.34\,W\,m^{-2}$) and nitrous oxides (RF: $0.16\,W\,m^{-2}$) have the highest effects on the energy balance of the Earth [4]. The highest share (56.6 %) with regard to global anthropogenic greenhouse gas emissions between 1970 and 2004 in terms of CO_2-equivalents is related to emission of CO_2 due to fossil fuel use [4].

As pointed out previously, CO_2 contributes to a high fraction to global warming. Its emission is attributed to a high extent to fossil fuel usage. However, the intention when using fossil fuels is to release and subsequently utilise their chemically stored energy (e.g. combustion). For example in terms of CO_2-equivalents, the sectors energy supply, transportation and industry together have a share of approximately 58 % with regard to the global annual emission of anthropogenic greenhouse gases [4]. In view of these aspects, the forecasted grow in global energy demand by more than one-third till 2035 [5], [6] might be alarming. Accordingly, the emission of greenhouse gases will increase [4], [6]. Furthermore the costs of fossil fuels will increase as well due to the mechanisms of demand and supply. With growing energy demand, the oil price will gain from USD 125 per barrel in 2011 to more than USD 215 per barrel in 2035 [5]. Another question is, if economies are willing to face the enormous costs of increased consumption of subsidised fossil fuels: Subsidies for fossil fuels globally totalled USD

523 billions in 2011, which was almost 30 % higher than in 2010 [6]. Thus, a major challenge is to cover the energy demand of mankind and simultaneously mitigate greenhouse gas emission.

Accordingly, a global initiative launched by the Secretary-General of United Nations Ban – which is called Sustainable Energy for All (SE4ALL) – outlines three objectives to be achieved by 2030 [1], [7]. Several development goals are closely related with these three objectives. The three objectives and associated development goals are (reproduced from [7]):

1. Ensuring universal energy access
    - Improved health
    - Improved agricultural productivity
    - Empowerment of women
    - Business and employment creation
    - Economic development
    - Achievment of the MDG

2. Doubling the share of renewable energy
    - Affordable energy even where grid does not reach
    - New opportunities for small entrepreneurs
    - Decreased variability in energy costs
    - Energy security and reduced import bills
    - Reduced environmental impacts

3. Doubling the rate of improvement in energy efficiency
    - Lighting/appliances that require less power
    - Fossil fuel resources used more effectively
    - Reduced energy costs for consumers
    - Redistribution of electricity that now is wasted or lost
    - More reliable electricity systems

The related action agenda is presented in reference [8]. As outlined above, making more efficient use of energy is playing a key role as a greenhouse gas emission mitiga-

tion strategy and is thus important for a more sustainable energy future as well as for improving energy security [4], [6], [9]. Nevertheless, as acknowledged in the SE4ALL initiative [7], [8], substitution of fossil fuels with energy from renewable sources is a prerequisite in order to mitigate greenhouse gas emission and also to contribute to energy security by diversification of energy sources [4], [10]. Therefore, the role of renewables is discussed more in detail in the next section.

1.2 The Current and Future Role of Renewables for Sustainable Energy Supply

Today, energy from renewable sources has a share of estimated 16.7 % with regard to global final energy consumption (year 2010) [9] (remark: The calculations in the Renewables 2012 Report [9] are based on an estimation for final energy consumption, which is slightly higher (3.69×10^{20} J) than the actual consumption (3.63×10^{20} J [11]). Whereas a fraction of 8.5 % of the so called "total final energy" was attributed to traditional biomass (mainly for cooking and heating purposes), modern renewables (modern biomass, biofuels, geothermal, hydropower, wind and solar) accounted for round about 8.2 % [9]. Wind, solar, modern biomass and geothermal energy generation together had a share of 0.9 % only [9]. Solar thermal and photovoltaics (PV) contributed 0.16 and 0.06 %, respectively [9].

However, renewables will approach coal as primary source of global electricity by 2035 and thus will provide almost one-third of total electricity output [5], [6]. Simultaneously, contribution of solar energy will grow faster than other renewables [5]. That is no wonder because solar energy has the largest theoretical potential of the renewable energy sources and is available abundantly. The sun provides more energy to the earth within an hour (4.3×10^{20} J) than is consumed within a year (final energy consumption in 2010: 3.63×10^{20} J) [11], [12]. The International Energy Agency's (IEA) World Energy Outlook 2012 [13] sees a tremendous potential for solar energy, especially for solar energy from solar thermal technologies: Solar heat generated may gain from 7.95×10^{17} J (221 TW h) in 2010 to 2.93×10^{18} J (814 TW h) in 2035. FANINGER [14] outlines that currently solar thermal provides only around

0.5 % of the estimated heating and cooling energy demand in the world, although the potential for the EU-27 is around 47 % in 2050. In 2050, specific scenarios in the technology roadmap for solar heating and cooling of IEA [10] forecast a total yield of approximately 1.8×10^{19} J (5000 TW h) from solar thermal technologies in heating and cooling applications and thus a saving of 800×10^6 t CO_2-emission. The major contribution of solar thermal technologies in the field of heating and cooling is ascribed to domestic hot water and space heating appliances and process heat for industry. The detailed figures are presented in Table 1.1 . Just for comparison, electricity output from concentrating solar power facilities (CSP) and PV can increase from 5.76×10^{15} J (1.6 TW h) and 1.15×10^{17} J (32 TW h) in 2010 to 1.01×10^{18} J (280 TW h) and 3.05×10^{18} J (846 TW h), respectively [13]. However, the numbers for CSP and PV are significantly lower than the estimated contribution of solar thermal systems for heating and cooling. Hence, the figures presented outline the huge potential of solar thermal technologies in general and of solar thermal technologies for heating[1] and cooling specifically. Therefore, the next section is devoted to harvesting solar energy via solar thermal systems with a focus on the solar thermal collector.

Table 1.1

Table 1.1.: Forecast of installed capacity and annual yield of solar thermal technologies for heating and cooling for different applications for year 2050 (data from [10])

Application	Installed Capacity	Annual yield		Market share
	[GW_{th}]	[J]	[TW h]	[%]
Domestic hot water and space heating	3500	8.9×10^{18}	2472	14
Process heat in industry (<120 °C)	3200	7.2×10^{18}	2000	20
Solar cooling	>1000	1.5×10^{18}	417	17
Swimming pool heating	200	0.4×10^{18}	111	

[1] Energy demand for space heating may be partially covered directly from solar gains via solar passive systems (i.e. windows, transparent insulation)

1.3 Harvesting Solar Energy via Solar Thermal Systems

The basic physical principle of solar thermal systems is the conversion of solar radiation with short wavelength into heat (photo-thermal conversion) [15], [16]. For the photo-thermal conversion in solar thermal systems, absorbers are necessary [15]. Usually, this absorber is part of a collector [15]. Collectors can be divided in two major classes [15], [16]:

1. Non-concentrating collectors
2. Concentrating collectors

Furthermore, heat carrier medium (either gaseous or liquid) is indispensable in order to transport the gained heat, yielding the sub-division into air- and liquid-collectors [15]. Depending on the solar thermal system concept (natural or forced circulation), further components are necessary (e.g. storage tank, piping, circulation pump (facultative), heat exchanger (facultative), etc.) [10], [15]. The most common collector is the non-concentrating fluid collector [15]. The simplest form is the absorber itself. However, usually the absorber is part of a collector either consisting of frame, insulation, glazing and absorber (flat-plate collector (FPC)) or the absorber is placed inside an evacuated tube (evacuated tube collector (ETC)) in order to mitigate losses and thus provide heat carrier fluid with higher temperature compared to the sole absorber [10], [15], [16]. Non-concentrating collectors like FPC and ETC can supply heat carrier fluid with temperatures up to 120 °C or even higher, and thus are sufficient collector types for domestic hot water generation, space heating, solar cooling and parts of process heat in industry (<120 °C) [10], [16], [17]. Thus, there is no wonder that these two collector types are currently the most important ones: FPC, ETC, unglazed water collectors and glazed/unglazed air collectors account for 62.1 GW_{th} (88.8×10^6 m^2), 111 GW_{th} (158.5×10^6 m^2), 21.5 GW_{th} (30.7×10^6 m^2) and 1.3 GW_{th} (1.8×10^6 m^2) with regard to installed capacity, respectively [18]. However, the market share of ETC and FPC is not evenly distributed over the globe. In terms of installed capacity, China (PRC) is world market leader for both collector concepts FPC (9.4 GW_{th}) and ETC (108.2 GW_{th}) [18]. On the contrary, the FPC system is more

popular in the other top ten solar countries compared to the ETC (e.g. Austria: FPC 2724.6 MW_{th} vs. ETC 46.5 MW_{th}) with regard to market share [18]. For comparison, the total installed solar thermal collector area by the end of 2010 was 279.7×10^6 m^2 corresponding to an installed capacity of 195.8 GW_{th}, whereby the majority is installed in PRC (117.6 GW_{th}) and Europe (36.0 GW_{th}) [18]. Furthermore, IEA sees ETC and FPC to be key collector types for heat applications also in future because domestic hot water generation, space heating and process heat in industry (<120 °C) will account for the highest market share with regard to installed solar thermal capacity in 2050 [10].

Nevertheless, further actions are necessary in order to promote a deeper market penetration of solar thermal systems. Therefor IEA defined actions and milestones with regard to technology development in the solar heating and cooling sector [10]. The use of alternative materials – polymeric materials are explicitly mentioned in the technology roadmap [10] – shall contribute to a reduction in life-cycle cost and thus improve economics of solar thermal systems. The gaining importance of polymeric materials is reflected by the establishment of Task 39 within IEA's Solar Heating and Cooling Programme (IEA SHC) which is devoted exclusively to polymeric materials for solar thermal applications [19]. An important outcome of this task is a handbook dealing with polymeric materials for solar thermal applications [20].

However, with the introduction of polymeric materials in solar thermal systems, the stagnation of solar thermal systems has to be addressed even more carefully than in traditional solar thermal systems. Harrison [21] describes stagnation in the following manner:

> *"Stagnation occurs when the solar energy absorbed by a solar collector exceeds the capability of its heat transfer fluid circuit to adequately cool it, resulting in excessive absorber temperatures."*

This is due to a change in the energy balance of the collector: Incoming (solar gains, etc.) and outgoing (losses, etc.) energy flows establish a new equilibrium due to a smaller flow of outgoing energy yielding a higher equilibrium temperature of the collector. The equilibrium temperature or stagnation temperature of a conventional solar thermal collector can reach approximately 180 °C or even higher temperatures,

which exceeds the long-term service temperature of cost-efficient polymeric materials [16], [21], [22]. For a polymeric FPC with parts made from cost-efficient polymeric materials, limiting the stagnation temperature to temperatures below 130 °C would be sufficient [23]. However, stagnation is also a problem in conventional solar thermal collectors, yielding high potential for deterioration and failure of heat carrier fluid and collector components [21]. Therefore, stagnation control has to be carefully addressed.

Several approaches for stagnation control on the collector, system and array level exist [21]. On the collector level potential solutions for stagnation control are derived from the energy balance of the collector and thus are related to its equilibrium temperature upon stagnation, which has to be reduced to the desired temperature level:

- Less efficient photo-thermal conversion process
- Improving collector losses
- Supply excess heat to heat sinks (e.g. via heat carrier medium)
- Adjustment of solar gains to energy demand

A rather conservative approach on the collector level would be the deterioration of the collector efficiency by eliminating selective absorber coating (deterioration of photo-thermal conversion process; high effectiveness but low efficiency approach) and/or less sophisticated insulation (improved collector losses; low effectiveness (heating the surroundings is *not* effective) but high efficiency approach) of the collector in order to limit stagnation temperature. However, that concept takes a reduced energy yield into account but it is sometimes defined as prerequisite for polymeric materials utilisation in solar thermal collectors in order to maintain long lifetime [24]. However, from a stance requiring effectiveness (heating the heat carrier fluid, not the surrounding) and efficiency also in utilisation of resources one might come to another conlusion: Not trying to achieve the potential maximum yield of a solar thermal system by intentionally designing a “poor” performing system is a poor compromise in order to meet the construction materials’ requirements. Supplying energy to heat sinks (heat dumps, venting) is another option for limiting stagnation temperature [21] but poses a waste of already obtained energy if it is not getting stored for later utilisation. The

stagnation control solutions already discussed would infringe the requirements for an energy efficient solar thermal collector outlined by Kalogirou [16]:

> *"An energy efficient solar collector should absorb incident solar radiation, convert it to thermal energy and deliver the thermal energy to a heat transfer medium with minimum losses at each step."*

In view of this opinion, the most straight-forward method would be the adjustment of solar gains of the collector to the actual energy demand and thereby maintaining high collector efficiency in the desired temperature range. Harrison [21] outlines two potential approaches in order to adjust solar gains: shading or intentional degradation of the collector's optical properties (e.g. via thermo variable glazings) during stagnation. However, shades require an actively operated control system with sensors, control unit and actuators, which are all prone to possible malfunction or defect. These pitfalls may also arise for actively operated thermo variable glazings (e.g. temperature-controlled electro-chromic glazings), but do not apply for passively operated thermo variable glazings. Prominent examples of the latter type of smart glazings are thermotropic glazings [25]. Their temperature-triggered reduction in solar transmittance can provide efficient overheating protection for solar thermal collectors [23], [26]. In order to limit stagnation temperatures of an all-polymeric FPC to temperatures not exceeding 130 °C – without affecting collector efficiency significantly –, solar transmittances >85 and <60 % are required below and above the threshold temperature, respectively [23]. Depending on the installation situation of the thermotropic glazing – either mounted in the collector glazing or directly on the absorber – required switching threshold of thermotropic glazings vary (55 to 60 °C for thermotropic glazings and 75 to 80 °C for thermotropic absorbers) [23].

1.4 Thermotropic Glazings

Thermotropic glazings change their optical appearance from highly light-transmitting to intensively light-scattering upon exceeding a pre-defined threshold temperature, reversibly [27], [28]. The way this performance is achieved, is slightly different for the

different types of thermotropic glazings. Basically, phase-separating and non-phase-separating systems can be distinguished [25], [27]. In phase-separating systems at least two components are homogeneously mixed below the threshold temperature [25], [27]. When exceeding the threshold temperature, these components establish separated phases [25], [27]. If these phases exhibit different refractive indices, intense light-scattering occurs [25], [27], [28]. Prominent examples of this kind of material class are thermotropic hydrogels and thermotropic polymer blends [25], [27], [29].

Non-phase-separating systems consist of a thermotropic additive (minor phase) finely dispersed in a matrix material (major phase), also recognised under the term thermotropic systems with fixed domains (TSFD) [25], [27], [30]. Below the threshold temperature, the refractive indices of matrix and additive are almost equal, yielding the incident radiation to pass through the thermotropic layer almost un-scattered [27]. Upon exceeding the threshold temperature, the thermotropic additive undergoes a steep change in refractive index with the onset of intense light-scattering, yielding a reduction in solar transmittance [27].

Whereas the switching process in phase-separating systems is diffusion-controlled, it is not for TSFD. Thus, yielding fast switching response of TSFD, consequently resulting in low hysteresis [30]. Further advantages of TSFD are ease of adjustment of switching threshold, presumptive long-term stability, high reversibility and steep switching process [30].

From a historical point of view, investigations on thermotropic glazings were primarily conducted with a focus on the buildings sector and with phase-separating systems being of primary interest [25], [27]–[39]. The following considerations might illustrate the motivation for that kind of research: Efficient utilisation of solar gains can reduce energy demand for artificial daylighting in a building significantly [25]. Furthermore, these solar gains can reduce the energy demand for space heating during winter [25]. However, during summer these solar gains together with internal thermal loads (persons, equipment) increase cooling energy demand [25]. Thermotropic glazings installed in a building's facade would be feasible in order to prevent buildings from overheating and thus enhance the thermal and – as welcome side effect – the visual comfort of building occupants [25]. Furthermore, energy demand for space heating,

artificial daylighting and cooling energy demand can be reduced, thus resulting in a reduction of primary energy consumption of a building [34], [35]. Nevertheless, depending on the individual architectural situation, overheating protection of a building might be rather complex and global statements on performance requirements for thermotropic overheating protection glazing cannot be made [32], [34]. However, in the more "standardised" field of solar thermal collectors, this may be easier, as already outlined in section 1.3.

Notwithstanding, the application of thermotropic glazings for overheating protection of polymeric solar thermal collectors is a relatively new field of research [23], [30]. As outlined in section 1.3, this was motivated by the intention to limit the stagnation temperature of solar thermal collectors. In this specific field of research, the advantages of TSFD (outlined above) made them the most attractive type of thermotropic glazing and they thus gained interest in recent research. A good overview on the current status of research in the field of TSFD is still presented by the review by Resch and Wallner [30], also because limited external research activities were recognised in the field of TSFD since the review was published (e.g. references [40]–[42]). On the contrary, a joint group at University of Leoben and Polymer Competence Center Leoben GmbH contributed significantly in the field of TSFD during the last years [22], [43]–[54].

Nevertheless, knowledge on the theoretically achievable overheating protection potential of TSFD was missing until 2012. Although such information was available for phase-separating thermotropic glazings from the dissertation of Nitz [31], the results had limited significance for TSFD due to their different mode of operation. Nevertheless, an important outcome of his thesis is that the maximum overheating protection potential of a thermotropic glazing [2] is achievable with spherical scattering domains exhibiting diameters in the range between 200 and 400 nm [31]. Other parameters affecting the scattering performance and thus overheating protection performance of a thermotropic glazing are the refractive index difference between matrix and thermo-

[2] This generalisation is valid because it makes no difference wether a scattering domain is formed before the scattering event taking place (like in phase-separating systems) or if the scattering domain is existing permanently (like in non-phase-separating systems, including TSFD) if all other relevant parameters of the thermotropic systems are equal

tropic additive, the concentration of scattering domains and the layer thickness [31]. As a consequence, theoretical modelling of the overheating protection potential of TSFD was conducted. Within these investigations, the scattering domain size was kept constant: Diameters of spherical scattering domains were implemented to resemble a distribution between 200 and 400 nm [55]. On the contrary, the refractive indices of matrix and thermotropic additive, the concentration of scattering domains and the thickness of the TSFD were varied upon simulation. For example, a hypothetical TSFD with refractive indices of 1.50 (matrix) and 1.50 (additive) below the threshold temperature and 1.50 (matrix) and 1.45 (additive) above the threshold temperature, a scattering domain concentration of 5 % and a thickness of 1 mm would achieve a theoretical transmittance reduction from 92.3 to 64.4 % at a wavelength of 589 nm upon exceeding the threshold temperature [55]. If the refractive index of the additive above the threshold temperature is 1.40 (instead of 1.45) and all other parameters remain as previously stated, a theoretical transmittance reduction from 92.3 to 45.0 % upon exceeding the threshold temperature is obtainable. The values chosen for these examples resemble a realistic assumption for actually obtained TSFD [47], [48], [50]. Furthermore, the examples illustrate a general trend: the higher the refractive index difference between matrix and additive, the lower the transmittance. Consequently, the refractive index difference has to be as low as possible at temperatures below the threshold temperature. On the contrary, the refractive index difference has to be as high as possible upon exceeding the threshold temperature. In general, the simulation results were promising with regard to overheating protection potential of TSFD [55].

However, the overheating protection performance of TSFD established so far – especially for overheating protection of solar thermal collectors – is limited [22], [30], [47], [48], [50] (For example, one of the best performing TSFD obtained so far exhibited a reduction in solar hemispheric transmittance from 83 to 69 % [47]; The solar transmittance is defined in equation 1.1). This was primarily ascribed to inappropriate scattering domain shape and/or size [46], [48], [54]: Spherical as well as non-spherical scattering domains were detected, which exhibited dimensions not being in the optimal range. Furthermore, so far no structure-property-relationship was established

that would reasonably distinguish the reasons for formation of either spherical or non-spherical scattering domains upon TSFD formulation.

From all these considerations one can conclude that TSFD – despite their significant overheating protection potential for buildings and especially for solar thermal collectors – require serious efforts in establishment/improvement of structure-property-relationships between the TSFD constituents' properties, the overheating protection performance of the TSFD and their internal material structure (morphology). Thorough understanding of these structure-property-relationships are indispensable for optimisation of the overheating protection performance of TSFD.

$$\tau_{solar} = \frac{\int_{250\,nm}^{2500\,nm} \tau(\lambda) \times AM1.5(\lambda) \times d\lambda}{\int_{250\,nm}^{2500\,nm} AM1.5(\lambda) \times d\lambda} \tag{1.1}$$

τ_{solar} . . . solar transmittance (hemispheric or diffuse)
λ . . . wavelength
$\tau(\lambda)$ . . . transmittance as a function of the wavelength (hemispheric or diffuse)
$AM1.5(\lambda)$ . . . AM1.5 solar irradiance source function

1.5 References

[1] F. Birol, A. Brew-Hammond, D. Dorner, S. Gitonga, V. Iyer, C. Jones, V. Modi, P. Nore, V. R. Putti and L. Srivastava, *Sustainable Energy for All: Technical Report of Task Force 1: in Support of the Objective to Achieve Universal Access to Modern Energy Services by 2030*, United Nations, Ed., 2012. [Online]. Available: www.sustainableenergyforall.org/about-us/item/download/44_b4eed262c898809a2c307206ce227dfd (visited on 12/08/2013).

[2] United Nations, *The Energy Challenge for Achieving the Millenium Development Goals*, United Nations, Ed., 2005. [Online]. Available: http://www.un-energy.org/sites/default/files/share/une/un-enrg_paper.pdf (visited on 12/08/2013).

[3] M. Parry, A. Evans, M. W. Rosegrant and T. Wheeler, *Climate Change and Hunger: Responding to the Challenge*, World Food Programme, Ed., Rome, 2009. [Online]. Available: home.wfp.org/stellent/groups/public/documents/newsroom/wfp212536.pdf (visited on 12/08/2013).

[4] IPCC, *Climate Change 2007: Synthesis Report*, IPCC, Ed., 2007. [Online]. Available: www.ipcc.ch/pdf/assessment-report/ar4/syr/ar4_syr.pdf (visited on 12/08/2013).

[5] IEA, *World Energy Outlook 2012: Executive Summary*, IEA, Ed., Paris, 2012. [Online]. Available: www.iea.org/publications/freepublications/publication/English.pdf (visited on 12/08/2013).

[6] IEA, *World Energy Outlook 2012 Factsheet: How will global energy markets evolve to 2035?*, IEA, Ed., Paris, 2012. [Online]. Available: www.worldenergyoutlook.org/media/weowebsite/2012/factsheets.pdf (visited on 12/08/2013).

[7] United Nations, *Sustainable Energy for All: A global action agenda: Pathways for concerted action toward sustainable energy for all*, United Nations, Ed., 2012. [Online]. Available: http://www.sustainableenergyforall.org/images/content/SE4ALL-ActionAgenda.pdf (visited on 12/08/2013).

[8] N. Nakićenović, D. Kammen, J. Jewell, N. Al-Hosany, A. Cooper, R. Detchon, D. Elis, S. Foster, M. Fulton, D. Gielen, I. Giner-Reichl, M. Hopkins, R. Kempner, B. Lebot, G. Guimarães, M. Ploutakhina, M. Radka, A. Sakar and P. Schulz, *Sustainable Energy for all: Technical Report of Task Force 2: in Support of Doubling the Global Rate of Energy Efficiency; Improvment and Doubling the Share of Renewable Energy in the Global Energy Mix by 2030*, United Nations, Ed., 2012. [Online]. Available: http://www.sustainableenergyforall.org/about-us/item/download/46_60ad99d05ed07e6c49cff5eb02d2c967 (visited on 13/08/2013).

[9] REN 21, *Renewables 2012: Global Status Report*, REN 21, Ed., 2012. [Online]. Available: http://www.map.ren21.net/GSR/GSR2012_low.pdf (visited on 12/08/2013).

[10] IEA, *Technology Roadmap: Solar Heating and Cooling*, IEA, Ed., Paris, 2012. [Online]. Available: www.iea.org/publications/freepublications/publication/2012_SolarHeatingCooling_Roadmap_FINAL_WEB.pdf (visited on 12/08/2013).

[11] IEA, *Key World Energy Statistics 2012*, IEA, Ed., Paris, 2012. [Online]. Available: www.iea.org/publications/freepublications/publication/kwes.pdf (visited on 12/08/2013).

[12] U.S. Department of Energy, *Basic Research Needs for Solar Energy Utilization: Report of the Basic Energy Sciences Workshop on Solar Energy Utilization*, U.S. Department of Energy, Ed., 2005. [Online]. Available: science.energy.gov/~/media/bes/pdf/reports/files/seu_rpt.pdf (visited on 12/08/2013).

[13] IEA, *World Energy Outlook 2012: Renewable Energy Outlook: Chapter 7*, IEA, Ed., Paris, 2012. [Online]. Available: www.worldenergyoutlook.org/media/weowebsite/2012/WEO2012_Renewables.pdf (visited on 12/08/2013).

[14] G. Faninger, *The Potential of Solar Thermal Technologies in a Sustainable Energy Future: Results from 32 Years of International R&D Cooperation*, IEA SHC, Ed., 2010. [Online]. Available: http://www.iea-shc.org/data/sites/1/publications/Potential_of_Solar_Thermal_Technologies_2010.pdf (visited on 12/08/2013).

[15] M. Kaltschmitt, W. Streicher and A. Wiese, Eds., *Erneuerbare Energien: Systemtechnik, Wirtschaftlichkeit, Umweltaspekte*, 4th ed. Berlin and Heidelberg: Springer, 2006, ISBN: 978-3-540-28205-1.

[16] S. A. Kalogirou, 'Solar thermal collectors and applications', *Progress in Energy and Combustion Science*, vol. 30, no. 3, pp. 231–295, 2004, ISSN: 03601285. DOI: 10.1016/j.pecs.2004.02.001.

[17] G. Faninger, *The potential of solar heat in the future energy system*, 2010. [Online]. Available: http://www.aee-intec.at/0uploads/dateien868.pdf (visited on 05/05/2013).

[18] W. Weiss and F. Mauthner, *Solar Heat Worldwide: Markets and Contribution to the Energy Supply 2010: 2012 Edition*, AEE INTEC and IEA SHC, Eds., Gleisdorf, 2012. [Online]. Available: http://www.iea-shc.org/data/sites/1/publications/Solar_Heat_Worldwide-2012.pdf (visited on 12/08/2013).

[19] IEA SHC, *Homepage of IEA SHC Task 39*, IEA SHC, Ed., 2013. [Online]. Available: http://task39.iea-shc.org/ (visited on 10/05/2013).

[20] M. Köhl, M. G. Meir, P. Papillon, G. M. Wallner and S. Saile, Eds., *Polymeric materials for solar thermal applications*, 1st ed. Weinheim: Wiley-VCH, 2012, ISBN: 978-3-527-33246-5.

[21] S. Harrison and C. A. Cruickshank, 'A review of strategies for the control of high temperature stagnation in solar collectors and systems', *Energy Procedia*, vol. 30, pp. 793–804, 2012, ISSN: 18766102. DOI: 10.1016/j.egypro.2012.11.090.

[22] K. Resch and G. M. Wallner, 'Thermotropic Resin Systems: Relationships Between Formulation Parameters, Material Structure and Optical Properties', in *Proceedings of ISES Solar World Congress 2007*, D. Y. Goswami and Y. Zhao, Eds., Berlin: Springer, 2007, pp. 541–545, ISBN: 978-3-540-75996-6. DOI: 10.1007/978-3-540-75997-3_98.

[23] G. M. Wallner, K. Resch and R. Hausner, 'Property and performance requirements for thermotropic layers to prevent overheating in an all polymeric flat-plate collector', *Solar Energy Materials and Solar Cells*, vol. 92, no. 6, pp. 614–620, 2008, ISSN: 09270248. DOI: 10.1016/j.solmat.2007.12.005.

[24] S. Banse, 'Polymeric collector materials: Fantastic plastics - revolution or devolution?', *Sun & Wind Energy*, vol. 4, pp. 84–89, 2011.

[25] P. Nitz and A. Wagner, 'Schaltbare und regelbare Verglasungen', *BINE Themeninfo*, vol. I/02, no. I/02, pp. 1–12, 2002, ISSN: 1610-8302.

[26] K. Resch, R. Hausner and G. M. Wallner, 'All Polymeric Flat-Plate Collector — Potential of Thermotropic Layers to Prevent Overheating', in *Proceedings of ISES Solar World Congress 2007*, D. Y. Goswami and Y. Zhao, Eds., Berlin: Springer, 2007, pp. 561–565, ISBN: 978-3-540-75996-6. DOI: 10.1007/978-3-540-75997-3_102.

[27] P. Nitz and H. Hartwig, 'Solar control with thermotropic layers', *Solar Energy*, vol. 79, no. 6, pp. 573–582, 2005, ISSN: 0038092X. DOI: 10.1016/j.solener.2004.12.009.

[28] A. Seeboth, J. Schneider and A. Patzak, 'Materials for intelligent sun protecting glazing', *Solar Energy Materials and Solar Cells*, vol. 60, no. 3, pp. 263–277, 2000, ISSN: 09270248. DOI: 10.1016/S0927-0248(99)00087-2.

[29] K. Fuchs, 'Entwicklung und Charakterisierung thermotroper Polymerblends', Dissertation, Albert-Ludwigs-University, Freiburg i.B., 2001.

[30] K. Resch and G. M. Wallner, 'Thermotropic layers for flat-plate collectors—A review of various concepts for overheating protection with polymeric materials', *Solar Energy Materials and Solar Cells*, vol. 93, no. 1, pp. 119–128, 2009, ISSN: 09270248. DOI: 10.1016/j.solmat.2008.09.004.

[31] P. Nitz, 'Optical modelling and characterisation of thermotropic systems', Dissertation, Albert-Ludwigs-University, Freiburg i.B., 1999.

[32] H. Hartwig, 'Konzepte für die Integration selbstregelnder, thermotroper Schichten in moderne Gebäudehüllen zur passiven Nutzung der Sonnenenergie', Dissertation, Technische Universität München, München, 2003.

[33] A. Raicu, H. R. Wilson, P. Nitz, W. Platzer, V. Wittwer and E. Jahns, 'Facade systems with variable solar control using thermotropic polymer blends', *Solar Energy*, vol. 72, no. 1, pp. 31–42, 2002, ISSN: 0038092X. DOI: 10.1016/S0038-092X(01)00093-7.

[34] J. Yao and N. Zhu, 'Evaluation of indoor thermal environmental, energy and daylighting performance of thermotropic windows', *Building and Environment*, vol. 49, pp. 283–290, 2012, ISSN: 03601323. DOI: 10.1016/j.buildenv.2011.06.004.

[35] T. Inoue, 'Solar shading and daylighting by means of autonomous responsive dimming glass: practical application', *Energy and Buildings*, vol. 35, no. 5, pp. 463–471, 2003, ISSN: 03787788. DOI: 10.1016/S0378-7788(02)00143-3.

[36] A. Goetzberger, M. Müller and M. Goller, 'A self-regulating glare protection system using concentrated solar radiation and thermotropic coating', *Solar Energy*, vol. 69, pp. 45–57, 2001, ISSN: 0038092X. DOI: 10.1016/S0038-092X(01)00015-9.

[37] A. Georg, W. Graf, D. Schweiger, V. Wittwer, P. Nitz and H. R. Wilson, 'Switchable glazing with a large dynamic range in total solar energy transmittance (TSET)', *Solar Energy*, vol. 62, no. 3, pp. 215–228, 1998, ISSN: 0038092X. DOI: 10.1016/S0038-092X(98)00014-0.

[38] A. Beck, T. Hoffmann, W. Körner and J. Fricke, 'Thermochromic gels for control of insolation', *Solar Energy*, vol. 50, no. 5, pp. 407–414, 1993, ISSN: 0038092X. DOI: 10.1016/0038-092X(93)90061-R.

[39] A. Beck, W. Körner, H. Scheller, J. Fricke, W. Platzer and V. Wittwer, 'Control of solar insolation via thermochromic light-switching gels', *Solar Energy Materials and Solar Cells*, vol. 36, no. 4, pp. 339–347, 1995, ISSN: 09270248. DOI: 10.1016/0927-0248(94)00171-N.

[40] O. Muehling, A. Seeboth, T. Haeusler, R. Ruhmann, E. Potechius and R. Vetter, 'Variable solar control using thermotropic core/shell particles', *Solar Energy Materials and Solar Cells*, vol. 93, no. 9, pp. 1510–1517, 2009, ISSN: 09270248. DOI: 10.1016/j.solmat.2009.03.029.

[41] R. Ruhmann, A. Seeboth, O. Muehling and D. Loetzsch, 'Thermotropic Materials for Adaptive Solar Control', *Advances in Science and Technology*, vol. 77, pp. 124–131, 2012, ISSN: 1662-0356. DOI: 10.4028/www.scientific.net/AST.77.124.

[42] A. Gladen, J. H. Davidson, S. C. Mantell, J. Zhang and Y. Xu, 'A Model of the Optical Properties of a Non-absorbing Media with Application to Thermotropic Materials for Overheat Protection', *Energy Procedia*, vol. 30, pp. 116–124, 2012, ISSN: 18766102. DOI: 10.1016/j.egypro.2012.11.015.

[43] M. Knausz, 'Untersuchung des Schaltverhaltens von thermotropen Gießharzen', Bachelorarbeit, University of Leoben, Leoben, 2009.

[44] M. J. Mikl, 'Herstellung und Charakterisierung von thermotropen Systemen mit fixierten Domänen', Diplomarbeit, University of Leoben, Leoben, 2010.

[45] K. Resch, R. Hausner, G. M. Wallner and R. W. Lang, 'Thermotropic Layers for Overheating Protection of all-Polymeric Flat Plate Solar Collectors', in *Polymeric materials for solar thermal applications*, M. Köhl, M. G. Meir, P. Papillon, G. M. Wallner and S. Saile, Eds., Weinheim: Wiley-VCH, 2012, pp. 255–266, ISBN: 978-3-527-33246-5.

[46] K. Resch and G. M. Wallner, 'Morphology of phase-separated thermotropic layers based on UV cured acrylate resins', *Polymers for Advanced Technologies*, vol. 20, no. 12, pp. 1163–1167, 2009, ISSN: 10427147. DOI: 10.1002/pat.1393.

[47] K. Resch, G. M. Wallner and R. Hausner, 'Phase separated thermotropic layers based on UV cured acrylate resins – Effect of material formulation on overheating protection properties and application in a solar collector', *Solar Energy*, vol. 83, no. 9, pp. 1689–1697, 2009, ISSN: 0038092X. DOI: 10.1016/j.solener.2009.06.006.

[48] K. Resch, G. M. Wallner and R. W. Lang, 'Spectroscopic Investigations of Phase-Separated Thermotropic Layers Based on UV Cured Acrylate Resins', *Macromolecular Symposia*, vol. 265, no. 1, pp. 49–60, 2008, ISSN: 10221360. DOI: 10.1002/masy.200850506.

[49] K. Resch and A. Weber, 'Smart Windows - Smart Collectors: Entwicklung von funktionalen Überhitzungsschutzverglasungen für Gebäudeverglasungen und thermische Solarkollektoren', *Berg- und Hüttenmännische Monatshefte*, vol. 156, no. 11, pp. 429–433, 2011, ISSN: 0005-8912. DOI: 10.1007/s00501-011-0031-2.

[50] K. Resch, 'Polymeric Thermotropic Materials for Overheating Protection of Solar Collectors', Dissertation, University of Leoben, Leoben, 2008.

[51] A. Schmid, 'Untersuchung der Zusammenhänge zwischen Morphologie und den Überhitzungsschutzeigenschaften von thermotropen Systemen mit fixierten Domänen', Bachelorarbeit, Montanuniversität Leoben, Leoben, 2012. (visited on 14/03/2012).

[52] M. Seemann, 'Charakterisierung des Lichtstreuverhaltens und der Morphologie von thermotropen Verglasungen auf Thermoplastbasis', Masterarbeit, University of Leoben, Leoben, 2010.

[53] A. Weber, 'Analyse der Morphologie und des Schaltvorganges von thermotropen Polymeren mittels Rasterkraftmikroskopie', Master Thesis, University of Leoben, Leoben, 2010.

[54] A. Weber and K. Resch, 'Effect of Temperature-Cycling on the Morphology of Polymeric Thermotropic Glazings for Overheating Protection Applications', *Journal of Polymer Research*, vol. 19:9888, no. 6, pp. 1–8, 2012, ISSN: 1022-9760. DOI: 10.1007/s10965-012-9888-3.

[55] K. Resch, A. Weber, D. Gruber, K. Schnetzinger and W. Kern, *Smart Windows - Smart Collectors: Entwicklung, Modellierung und Vermessung von Überhitzungsschutzverglasungen für Fassaden- und Kollektoranwendungen: Zwischenbericht 2: WPR-NKP.09.014-02*, Leoben, 2012.

2 Objectives

The definition of the objectives of this thesis requires the definition of boundary conditions for this investigation in the first place:

- Boundary conditions from a theoretical point of view
  - A numerical feasibility study [1] confirmed the viability of overheating protection of solar thermal collectors (i.e. FPC) by thermotropic glazings (i.e. TSFD) and thus the potential of TSFD to significantly reduce the collector's stagnation temperature.
  - Furthermore, numerical simulation confirmed that TSFD are – theoretically – able to fulfill the performance requirements for overheating protection of a solar thermal FPC [1], [2].
- Boundary conditions from a practical point of view
  - The overheating protection performance of TSFD established so far is limited.
  - This is attributed to inappropriate shape and/or size of scattering domains.
  - Furthermore, knowledge on the structure-property-relationships of TSFD is limited, especially with regard to the effects governing the formation of either spherical or non-spherical scattering domains.

Furthermore – according to numerical simulation – the parameters governing the overheating protection performance of TSFD are *refractive index difference* between matrix and thermotropic additive, *scattering domain size*, *concentration* of scattering

domains [1] and the *layer thickness* [2]. From these parameters, the refractive index difference between matrix and additive and the scattering domain size are of primary importance because they govern the scattering process at a single scattering domain (single scattering) [3], [4]. A photon undergoing several subsequent single scattering processes upon its track through a TSFD is subject to multiple scattering [3], [4]. Thus, the concentration of the scattering domains and the layer thickness are additional important parameters for multiple scattering (like in a TSFD) [3], [4]. However, they are of secondary importance compared to the parameters affecting single scattering. Thus, an important objective of this study was to generate a highly inefficient single scattering process below the threshold temperature and a highly efficient single scattering process above the threshold temperature. Therefore potential TSFD constituents (matrix, thermotropic additive) exhibiting a refractive index difference as low as possible and as high as possible below and above the hypothetical threshold temperature, respectively, had to be identified. Furthermore optimally shaped and sized scattering domains had to be achieved in order to meet this objective. To meet this objective was a prerequisite in order to establish an efficient multiple scattering process and to obtain a TSFD with efficient overheating protection performance – especially for a solar thermal FPC –, which represented the primary objective of this thesis.

Thus, in order to sufficiently address all these aspects, a material formulation strategy was established. The material formulation strategy and the associated goals were defined in the following manner:

1. Pre-selection and characterisation of potential matrix materials and potential thermotropic additives with regard to application relevant properties applying sound polymer-physical principles

[1] The scattering domain size distribution together with the concentration of the thermotropic additive define the concentration of scattering domains. At a specific concentration of thermotropic additive, the smaller the domains are, the bigger is the domain concentration.

2. Assessment of refractive index match/mismatch between matrix and thermotropic additives
    - Refractive index difference below threshold temperature:
      as low as possible
    - Refractive index difference above threshold temperature:
      as high as possible
3. Formulation of promising TSFD, which were likely to exhibit proper overheating protection performance
4. Characterisation of the overheating protection performance of the established TSFD
5. Characterisation of the morphology of the established TSFD
6. Establishment of structure-property-relationships between properties of TSFD components, overheating protection performance and morphology
7. Deduction of strategies for optimisation of TSFD and experimental validation
    - Identification of issues, that prevent established TSFD
      from exhibiting efficient overheating protection performance
    - Identification of potential approaches and deduction of feasible measures in order to address the previously identified issues
    - Practical realisation of these measures and subsequent assessment of performance characteristics
    - Evaluation of the effectiveness of the applied measures

Thereby, points 3–7 are inside a feedback-loop in order to achieve continuous improvement of overheating protection performance and structure-property-relationships. Finally, an important remark for all these considerations is introduced: As outlined above, the primary objective of this study was to establish a TSFD providing efficient overheating especially for solar thermal FPC. That issue is indeed more straight forward than establishment of a TSFD providing efficient overheating protection for a building. The reason is that for overheating protection of buildings such general

performance requirements like for solar thermal collectors do not exist. That is due to the complex situation of overheating protection glazings in the architectural context, which require individual assessment of the requirements for overheating protection [5].

2.1 References

[1] G. M. Wallner, K. Resch and R. Hausner, 'Property and performance requirements for thermotropic layers to prevent overheating in an all polymeric flat-plate collector', *Solar Energy Materials and Solar Cells*, vol. 92, no. 6, pp. 614–620, 2008, ISSN: 09270248. DOI: 10.1016/j.solmat.2007.12.005.

[2] K. Resch, A. Weber, D. Gruber, K. Schnetzinger and W. Kern, *Smart Windows - Smart Collectors: Entwicklung, Modellierung und Vermessung von Überhitzungsschutzverglasungen für Fassaden- und Kollektoranwendungen: Zwischenbericht 2: WPR-NKP.09.014-02*, Leoben, 2012.

[3] P. Nitz, 'Optical modelling and characterisation of thermotropic systems', Dissertation, Albert-Ludwigs-University, Freiburg i.B., 1999.

[4] P. Nitz, J. Ferber, R. Stangl, H. R. Wilson and V. Wittwer, 'Simulation of multiply scattering media', *Solar Energy Materials and Solar Cells*, vol. 54, no. 1-4, pp. 297–307, 1998, ISSN: 09270248. DOI: 10.1016/S0927-0248(98)00081-6.

[5] H. Hartwig, 'Konzepte für die Integration selbstregelnder, thermotroper Schichten in moderne Gebäudehüllen zur passiven Nutzung der Sonnenenergie', Dissertation, Technische Universität München, München, 2003.

3 Structure of the Thesis

According to the objectives outlined above, the thesis presents a series of subsequent publications illustrating the steady progress in development of thermotropic glazings for overheating protection of buildings and solar thermal collectors. The thesis is divided in six parts. The parts are:

1. Preamble
2. Introduction to the thesis
3. Systematic material formulation strategy
4. In-situ optimisation strategies
5. Ex-situ optimisation strategy
6. Summary, conclusion and outlook

The first part presents mandatory (e.g. affidavit) and content related sections (e.g. table of content).

The second part presents an introduction to the motivation and the technological background of the thesis. Furthermore the objectives of the thesis are outlined. In the third part, a systematic material formulation strategy for TSFD based on thermo-plastics and UV-curable resin systems is developed. Based on an extensive literature review, potential matrix materials and thermotropic additives were surveyed with regard to thermo-mechanical, thermal and thermo-refractive properties. Based on the assessment of thermo-refractive properties promising material combinations

were selected, manufactured and comprehensively characterised with regard to solar-optical properties and morphology. Subsequently, structure-property-relationships were established, from which optimisation strategies for the TSFD were derived.

The fourth part deals with in-situ optimisation strategies derived from structure-property-relationships already established in the third part. The term “in-situ” means that all optimisation measures take effect *during* the assembly of the TSFD. Thus, the manufacturing process remains a two-step process (mixing matrix material and thermotropic additive; moulding). As the processing conditions were suspected to have detrimental effects on the performance of specific TSFD, the effect of curing and other parameters on the light-shielding efficiency and morphology of these TSFD was evaluated in one chapter. Another chapter deals with strategies in order to adjust scattering domain size: The effect of the addition of functional additives during manufacturing process and applied variations in the processing conditions upon manufacturing process on the morphology and thus light-shielding efficiency of TSFD is studied systematically applying tools of design of experiments (DoE). Obtained changes in overheating protection performance are correlated with the individual levels of the applied factors.

On the contrary, the fifth part deals with an ex-situ optimisation strategy. The term “ex-situ” means that the optimisation measures take effect *before* the assembly of the TSFD. Thus, the manufacturing process is extended to a three-step process (adjustment of scattering domain size; mixing matrix material and scattering domains; moulding): A mini-emulsion polymerisation is applied in order to adjust scattering domain size. Encapsulated thermotropic additive is subsequently mixed into matrix materials and evaluated with regard to solar-optical properties.

The individual parts three, four and five are opened by a brief introduction to the most relevant information for the specific topic. Thereby, the introduction shall outline central aspects addressed within the respective paper(s). Furthermore, the major concept of the paper is presented. Subsequently, the relevant papers published by the main-author of this thesis along with co-authors are presented in each individual section. The individual papers present detailed scientific background and considerations, materials, experimental details, data and conclusions of the scientific work.

In the sixth part the thesis is reviewed briefly and conclusions are drawn from the key findings of the thesis. Finally, the outlook points to challenges not addressed so far, and outlines recommendations for potential solutions and future work.

Part III.

Systematic Material Formulation Strategy

4 Introduction to Publications 1 and 2

Although preceding fundamental studies on TSFD [1]–[5] took all the considerations outlined in chapter 2 with regard to single and multiple scattering into account, the formulated TSFD nevertheless did not display the desired extent of overheating protection performance in order to efficiently prevent a solar thermal collector from overheating. Primarily, that was ascribed to inappropriately shaped and/or sized scattering domains, which prevented single and thus multiple scattering processes to be highly efficient at temperatures exceeding the switching threshold. Consequently, the authors recommended optimisation of scattering domain size and/or shape in order to achieve TSFD with improved overheating protection performance. However, open questions remaining were also the reasons for formation of inappropriately shaped and sized scattering domains. Thus, gaining a deeper insight into the structure-property-relationships of TSFD was identified as an imperative for this study in order to achieve TSFD with highly inefficient single scattering and thus highly inefficient multiple scattering below the threshold temperature and with highly efficient single scattering and thus highly efficient multiple scattering above the threshold temperature (yielding a TSFD with efficient overheating protection performance).

However, in order to establish profoundly justified structure-property-relationships between established overheating protection performance of TSFD on the one hand side and polymer-physical properties of TSFD constituents (matrix, additive) and morphology of TSFD on the other hand side as well as with regard to processing related aspects, numerous TSFD had to be formulated and characterised with regard to the desired information. Thus, the so far most comprehensive study on TSFD employing a systematic material formulation strategy (outlined in chapter 2) was designed. It comprised a variety in kind and number of matrix materials (thermoplastic resins,

UV-curable acrylate resins) and thermotropic additives (paraffin waxes, fatty acids and their derivatives, polymers and other substances) investigated, that was never established before. The publications presented hereafter discuss these issues more in detail. Publication 1 deals with the pre-selection and sound-polymer physical characterisation of TSFD constituents, their assessment with regard to suitability for TSFD formulation based primarily on their thermo-refractive properties, the formulation of promising TSFD and their characterisation with regard to overheating protection performance. Subsequently, publication 2 deals with characterisation of the morphology of the formulated TSFD and the establishment of structure-property-relationships between achieved overheating protection performance of TSFD, the polymer-physical properties of TSFD constituents, the morphology of TSFD and processing related aspects. Based on these profound structure-property-relationships, optimisation strategies are derived. Their effectiveness with regard to establishment of a TSFD with efficent overheating protection performance is assessed in this thesis subsequently.

4.1 References

[1] K. Resch and G. M. Wallner, 'Morphology of phase-separated thermotropic layers based on UV cured acrylate resins', *Polymers for Advanced Technologies*, vol. 20, no. 12, pp. 1163–1167, 2009, ISSN: 10427147. DOI: 10.1002/pat.1393.

[2] K. Resch and G. M. Wallner, 'Thermotropic Resin Systems: Relationships Between Formulation Parameters, Material Structure and Optical Properties', in *Proceedings of ISES Solar World Congress 2007*, D. Y. Goswami and Y. Zhao, Eds., Berlin: Springer, 2007, pp. 541–545, ISBN: 978-3-540-75996-6. DOI: 10.1007/978-3-540-75997-3_98.

[3] K. Resch, R. Hausner and G. M. Wallner, 'All Polymeric Flat-Plate Collector — Potential of Thermotropic Layers to Prevent Overheating', in *Proceedings of ISES Solar World Congress 2007*, D. Y. Goswami and Y. Zhao, Eds., Berlin: Springer, 2007, pp. 561–565, ISBN: 978-3-540-75996-6. DOI: 10.1007/978-3-540-75997-3_102.

[4] K. Resch, G. M. Wallner and R. W. Lang, 'Spectroscopic Investigations of Phase-Separated Thermotropic Layers Based on UV Cured Acrylate Resins', *Macromolecular Symposia*, vol. 265, no. 1, pp. 49–60, 2008, ISSN: 10221360. DOI: 10.1002/masy.200850506.

[5] K. Resch, G. M. Wallner and R. Hausner, 'Phase separated thermotropic layers based on UV cured acrylate resins – Effect of material formulation on overheating protection properties and application in a solar collector', *Solar Energy*, vol. 83, no. 9, pp. 1689–1697, 2009, ISSN: 0038092X. DOI: 10.1016/j.solener.2009.06.006.

5 Publication 1

5.1 Bibliographic Information

- Title: Thermotropic Glazings for Overheating Protection I: Material Pre-selection, Formulation and Light-Shielding Efficiency
- Authors:
  - Andreas Weber[1]
  - Katharina Resch[2]
    1. Polymer Competence Center Leoben GmbH, Roseggerstrasse 12, 8700 Leoben, Austria
    2. Department Polymer Engineering and Science, Materials Science and Testing of Polymers, University of Leoben, Otto Glöckel-Strasse 2, 8700 Leoben, Austria
- Periodical: Journal of Applied Polymer Science
- DOI: 10.1002/app.39950

Statement with regard to publication: The manuscript presented here is an adapted accepted manuscript in order to fit the formatting of the thesis and does not necessarily reflect exactly the actually published version.

5.2 Abstract

This paper presents a systematic strategy for formulation and optimisation of thermotropic layers for overheating protection purposes. Specifically, thermotropic systems with fixed domains (TSFD) which consist of a thermotropic additive finely dispersed in a matrix material are considered. Based on systematic material (component) pre-selection regarding thermo-analytical characteristics and refractive indices, numerous thermotropic layers were formulated. TSFD with thermoplastic matrix were produced by compounding and compression moulding. TSFD with resin matrix were produced by UV-curing. The thermotropic layers were analysed as to solar optical properties, threshold temperature, switching process and residual transmittance in the opaque state applying UV/Vis/NIR spectrometry equipped with a heating stage. Best performing materials exhibited solar hemispheric transmittance in the range of 72.2 to 84.5 % and between 59.6 and 83.7 % in the clear and opaque state, respectively. Threshold temperatures between 45 and 75 °C were realised. Refractive index difference between matrix and additive and solar hemispheric transmittance displayed a close correlation. Hence, refractometry was shown to be an appropriate tool for material pre-selection. Furthermore, investigations revealed a close correlation of thermal transitions of thermotropic additives recorded by differential scanning calorimetry (DSC) and threshold temperatures of thermotropic layers formulated therewith. However, thermotropic layers formulated so far have to be optimised with respect to light-shielding performance for efficient overheating protection.

5.3 Introduction

Thermotropic glazings change their light transmittance from transparent to opaque upon reaching a certain threshold temperature reversibly [1], [2]. Their application in passive and active solar energy utilisation allows tailoring solar gains to climatic, user and/or technical demands [3], [4]. Design of façades with thermotropic glazings enhances thermal and visual comfort of building occupants and reduces primary energy consumption for space heating/cooling and artificial daylighting due to solar contributions [3], [5]–[8]. Design of solar thermal collectors with thermotropic glazings limits

collector stagnation temperature to temperatures below 130 °C [4]. Limiting the stagnation temperature of solar thermal flat-plate collectors to values below the long-term service temperature of cost-efficient plastics (approx. 125 °C) allows for utilisation of these polymers as absorber material, thus yielding significant cost-reduction potential [4]. Application of thermotropic glazings in solar thermal collectors at the glazing unit or the absorber requires threshold temperatures of 55 to 60 °C and 75 to 80 °C respectively [4]. To maintain efficient overheating protection for a solar thermal collector, solar hemispheric transmittance has to change from >85 % in the transparent state to <60 % in the opaque state [4]. Such global requirements cannot be derived for window applications due to complex situation of glazing in the architectural context (building usage, lighting requirements, local climate, orientation, structural design, etc.) [1], [7]–[10]. Furthermore, materials shall exhibit a rapid and steep switching process within a small temperature range [4]. Among different thermotropic materials, thermotropic systems with fixed domains (TSFD) exhibit probably the highest potential for these applications [11]. Ease of adjustment of switching threshold, high reversibility, long-term stability and a steep switching process with low hysteresis are significant advantages of TSFD [12]. The key for the superior performance of TSFD is their inherent persistent two-phase material structure: TSFD consist of a thermotropic additive that is finely dispersed in a polymeric matrix material [1], [3]. Below the threshold temperature, the refractive indices of both components are almost equal, resulting in a transparent appearance of the TSFD [1]. With increasing temperature a phase transition (e.g. melting) of the thermotropic additive causes the refractive index difference of matrix and additive to change steeply [1], [3]. Thus incident radiation is multiply scattered at the interfaces of the matrix and the scattering domains formed by thermotropic additive [13]. Consequently, the layer turns opaque.

Nevertheless, TSFD reported in scientific literature so far do not meet the performance requirements described above [3], [4], [14]–[16]. However, the material portfolio investigated so far is limited [12]. Thus, the overall objective of this study is to perform an extensive evaluation of the overheating protection potential of combinations of numerous different matrix materials and thermotropic additives. Therefore, a systematic material formulation strategy is applied. First, a comprehensive polymer-physical characterisation of candidate TSFD components is carried out. Subsequently, various

TSFD are formulated and characterised as to their performance characteristics. Finally, the overheating protection characteristics of the TSFD are related to component properties.

5.4 Systematic Material Formulation Strategy

Refractive index difference of matrix and additive and TSFD morphology are of paramount importance for scattering performance and thus overheating protection performance of TSFD [5]. Hence, for the development of novel TSFD a systematic material formulation strategy – which is depicted in Figure 5.1 – has been established in order to account for these factors. The strategy comprises seven different steps. Steps which are addressed within the present paper are coloured grey. First, a comprehensive literature review concerning material properties is carried out in order to evaluate candidate matrix materials and thermotropic additives: Matrix materials exhibit preferably high transition temperatures (glass transition, melting), high transmittance and a refractive index as low as possible. Thermotropic additives must display a thermal transition – preferably melting – between 30 °C and 105 °C along with a rapid and steep change of refractive index. Subsequently, a comprehensive polymer-physical characterisation of candidate matrix materials and thermotropic additives with regard to thermal, thermo-mechanical and optical properties is carried out. In the second step appropriate combinations of candidate matrix materials and thermotropic additives are identified by assessment of refractive index match/mismatch. Based on this evaluation procedure promising TSFD are formulated and characterised as to light-shielding efficiency, switching characteristics and threshold temperature. Finally, a comprehensive characterisation of morphology (scattering domain size, shape, distribution) is carried out and structure-property-relationships are established. Based on these interrelationships, the optimisation potential of the TSFD is deduced. However, these final steps are addressed in a subsequent publication [17].

Figure 5.1

As the steps outlined above have different requirements with regard to the desired information on polymer-physical characteristics of the materials, it is considered more appropriate to present the experimental details of each step of the systematic

Figure 5.1.: Systematic material formulation strategy.

material formulation strategy in the section where they apply (instead of a cumulative experimental part).

5.4.1 Evaluation and Characterisation of Potential Material Constituents

5.4.1.1 Materials

For matrix materials the material selection focussed on polymers exhibiting the following desired properties. The transition temperature of polymers – glass transition for amorphous polymers and melting for semi-crystalline polymers – was required to be as high as possible but at least as high as 120 °C. Furthermore, high transparency was desirable. The transparency requirement was most likely to be fulfilled by polymers lacking intrinsic scattering domains (i.e. crystallites). Polymers lacking crystallites like amorphous polymers (thermoplastic resins, thermosets) were most promising but also semi-crystalline thermoplastic resins exhibiting crystallites with reduced size and thus less scattering (so called “micro-crystalline” thermoplastic resins) were considered. Besides that, materials not prone or even less than other materials to UV-induced degradation were preferred, including UV-stabilised material grades. That was also important because initially non-polymeric resin matrices had to be UV-curable. Furthermore, a proper match of refractive index of matrices and potential thermotropic additives at room temperature was required. Especially acrylic-esters are recognised to withstand UV-irradiation [18]. Thus, focus was on acrylic polymers, but also UV-stabilized polyamide and polycarbonate were considered.

For the thermotropic additives – as outlined before – a thermal transition in the desired temperature range between 30 and 105 °C accompanied by a steep change

in refractive index of the thermotropic additive was desirable. As outlined before, a proper match of refractive index of matrices and potential thermotropic additives at room temperature was required. As acrylic polymers have refractive indices around 1.5 [19], focus was on potential thermotropic additives having a refractive index around 1.5 at room temperature also.

Table 5.1 A total of seven matrix materials were selected, which are listed in Table 5.1 . The material portfolio comprised three thermoplastics: A poly (methyl methacrylate) (PMMA: Plexiglas FT15, Evonik Röhm GmbH; M1), a semi-crystalline polyamide PA PACM 12 (PA: Trogamid CX9703, Evonik Degussa GmbH; M2) and a polycarbonate (PC: Makrolon ET3127, Bayer Materials Science AG; M3). Four different UV-curable resin systems were employed: A hexa-functional aromatic urethane acrylate (based on oligomer Ebecryl 220; M4), a di-functional aliphatic urethane acrylate (based on oligomer Ebecryl 284; M5), a di-functional epoxy acrylate (based on oligomer Ebecryl 600; M6), and a tetra-functional polyester acrylate (based on oligomer Ebecryl 800; M7). Ebecryl resins were provided by Allnex Belgium SA/NV (former Cytec Surface Specialites Inc.).

Table 5.1.: Candidate matrix materials.

Matrix	Material type
M1	Poly (methyl methacrylate)
M2	Polyamide
M3	Polycarbonate
M4	Aromatic urethane acrylate
M5	Aliphatic urethane acrylate
M6	Epoxy acrylate
M7	Polyester acrylate

Table 5.2 In Table 5.2 the selected thermotropic additives are listed (all materials are technical grades and probably only a small fraction of ingredients is disclosed by suppliers, thus exact chemical structures cannot be presented). The material portfolio comprised a low (A1) and high molecular paraffin wax (A2), which were the most non-polar additives investigated. The latter is a Fischer-Tropsch wax. Furthermore, fatty acids

Table 5.2.: Candidate thermotropic additives.

Additive	Material type
A1	Paraffin, low molecular weight
A2	Paraffin, high molecular weight
A3	Fatty acids (mixture)
A4	Glycerine tristearate
A5	Hydrogenated castor oil [a]
A6	Pentaerythritol tetrastearate
A7	Hydroxystearic acid
A8	Glycerine monostearate
A9	Montan wax
A10	Hydrogenated castor oil [a]
A11	E-co-GMA (8 %)
A12	E-co-MA (24 %)-co-GMA (8 %)
A13	E-co-BA (17 %)-co-MAH (3.1 %)
A14	E-co-MA (16 %)-co-MAH (3.1 %)
A15	E-co-MA (20 %)-co-MAH (0.3 %)
A16	E-co-EA (29 %)-co-MAH (1.3 %)
A17	E-co-VA (28 %)
A18	E-co-VA (33 %)
A19	E-co-MA (30 %)
A20	PS
A21	PETG
A22	Naphthalene
A23	Sodium tetraborate decahydrate
A24	Sodium sulfate decahydrate

[a] different suppliers

and their derivatives were considered: fatty acid mixture (A3), glycerine tristearate (A4), hydrogenated castor oil (A5; main component: glycerine trihydroxystearate), pentaerythritol tetrastearate (A6), hydroxystearic acid (A7), glycerine monostearate (A8), a montan wax (A9) and again a hydrogenated castor oil (A10; main component: glycerine trihydroxystearate). A5 and A10 were provided by different suppliers. In general, fatty acids and fatty acid esters are more polar than paraffin waxes due to their carboxyl-group. However, within the group of fatty acids and derivatives one may discriminate between more and less polar substances: The longer the lipophilic tails of the fatty acids or alcohols are, the less polar the ester will be for example. This applies for instance for montan wax (A8) with esters of montanic acid (a C_{28} carboxylic acid) as an important component. On the contrary, fatty acids or derivatives (including their esters) of fatty acids with shorter lipohilic chains compared to montanic acid or with additional polar groups on these are considered more polar. A proper example would be A7, a C_{16} carboxylic acid chain with a hydroxyl moiety attached to the lipophilic tail. As a rule of a thumb: the longer the alkyl moiety, the less polar a molecule is (and lipophilicity increases).

Furthermore various polymers like a copolymer of ethylene (E) and glycidyl methacrylate (GMA) (Lotader AX8840, Arkema; A11), a terpolymer of E, methyl acrylate (MA) and GMA (Lotader AX8900, Arkema; A12), a terpolymer of E, butyl acrylate (BA) and maleic anhydride (MAH) (Lotader 3410, Arkema; A13), two terpolymers of E, MA and MAH with varying contents of MA and MAH (Lotader 3430, Arkema; A14; Lotader 4503, Arkema; A15), a terpolymer of E, ethyl acrylate (EA) and MAH (Lotader 4700, Arkema; A16), two copolymers of E and vinyl acetate (VA) with lower and higher VA-content (Evatane 28-03, Arkema; A17; Evatane 33-45, Arkema; A18), a copolymer of E and MA (Elvaloy 1330AC, DuPont de Nemours (Deutschland) GmbH; A19), a polystyrene (PS) (Empera 116N, Ineos Nova; A20), a glycol-modified poly (ethylene terephthalate) (PETG) (Eastar 6763, Eastman; A21), naphthalene (A22), sodium tetraborate decahydrate (A23) and sodium sulfate decahydrate (A24) were selected.

5.4.1.2 Experimental

Specimen Preparation For dynamic mechanical analysis (DMA), UV/Vis/NIR measurements and determination of refractive index plate-like specimens were prepared. Thermoplastics were compression moulded to 800 µm thick plates on a press P200PV (Dr. Collin GmbH, Ebersberg, DE). Plates from UV-curable resin systems were prepared by mixing 57 wt% oligomers, 40 wt% reactive diluent trimethylol propane triacrylate (TMPTA) and 3 wt% photoinitiator (blend of benzophenone and 1-hydroxycyclohexyl phenyl ketone). The mixtures were poured in the intervening space between two glass panes, which were sealed around the edge. Layers were cured by UV-radiation (dose: 2.1 J cm^{-2}) from a Light Hammer 6 equipped with a mercury-lamp and a LC6E Benchtop Conveyor (Fusion UV Systems Inc., Gaithersburg, MD, US). Free standing layers with a thickness of 900 µm were obtained after removal of the glass panes.

Differential Scanning Calorimetry (DSC) The thermal transitions of candidate matrix materials and thermotropic additives were determined by differential scanning calorimetry (DSC). Thermograms were recorded in static air on a DSC822^e (Mettler Toledo GmbH, Schwerzenbach, CH). For samples exhibiting a glass transition only, a heating rate of 20 K min^{-1} was used in order get a distinct glass transition signal. A heating rate of 10 K min^{-1} was applied to samples exhibiting melting in order to be able to discriminate between individual transitions more clearly (e.g. between solid phase transition and melting which probably would be displayed as a single peak upon application of higher heating rates). In general, high heating rates are recommended in order to detect effects of small magnitude (like glass transitions) but resolution is decreased compared to lower heating rates [20]. The sample mass was 10 ± 1 mg. Glass transition temperature and melting temperature were evaluated as mid-point temperature and peak temperature, respectively, according to ISO 11357-1 from the second heating run. The data were averaged over two measurements.

Dynamic Mechanical Analysis (DMA) Thermo-mechanical properties of films produced from the different matrix resins M1 to M7 were characterised by dynamic mechanical analysis (DMA) on a DMA/SDTA 861^e (Mettler Toledo GmbH, Schwerzenbach,

CH). Rectangular specimens (17 mm x 4 mm x 0.8–0.9 mm) were cut from plate-like samples with a saw Diadisc 5200 (Mutronic Präzisionsgerätebau GmbH & Co. KG, Rieden am Forggensee, DE). The gauge length was 9 mm. DMA was carried out in tensile mode applying sinusoidal strain amplitude at a frequency of 1 Hz. Strain amplitudes (determined by strain-sweep procedure) and measurement temperature ranges applied for the different material types are summarised in Table 5.3 . Scans were run with a heating rate of 3 K min^{-1}. From DMA, storage modulus (E'), loss modulus (E") and loss factor (tanδ) curves, were generated as a function of specimen temperature. The temperature at the maximum in loss modulus was taken as the glass transition temperature. Thermo-mechanical properties were averaged over two measurements.

Table 5.3

Table 5.3.: Applied strain amplitudes for DMA and measurement temperature range.

Matrix	Strain amplitude [µm]	Start temperature [°C]	End temperature [°C]
M1	5	−50	180
M2	5	−50	200
M3	5	−50	180
M4	4	−80	160
M5	4	−80	160
M6	4	−80	160
M7	5	−80	160

UV/Vis/NIR Spectrometry Solar transmittance, reflectance and absorptance of the matrix materials were determined applying UV/Vis/NIR spectrometry. A double beam UV/Vis/NIR spectrophotometer Lambda 950 (Perkin Elmer Inc., Waltham, MA, US) equipped with an Ulbricht-sphere (diameter 150 mm) was utilised. For the given measurement apparatus the radiation passing through (transmittance) or being reflected (reflectance) from the specimen outside a cone of approximately 5° relative to the incident beam direction was defined as diffuse (scattered) component. Hemi-

spheric and diffuse transmittance and reflectance were recorded at normal incidence in the spectral region from 250 to 2500 nm. The integral solar transmittance and reflectance were determined by weighting the recorded spectral data in steps of 5 nm by the AM1.5 global solar irradiance source function. A single determination was carried out for each material.

Refractometry Refractive indices as a function of temperature of matrix materials and thermotropic additives were determined on an Abbé-type refractometer AR4 (A. Krüss Optronic GmbH, Hamburg, DE) equipped with a water bath Ecoline E306 (Lauda Dr. R. Wobser GmbH & Co. KG, Lauda-Königshofen, DE) to maintain operation temperature. Measurements were conducted in a temperature range between ambient temperature and a maximum of 90 °C. A LED illumination unit with a wavelength of 589 nm was used. The temperature of the prisms was recorded with a two-channel temperature measurement instrument T900 (Dostmann electronic GmbH, Wertheim-Reicholzheim, DE) equipped with a precision K-type thermocouple. Measured prism temperatures were cross-checked by measurement of the refractive index of water as a function of temperature and comparison with tabulated values [21]. The cross-check confirmed the accuracy of temperature values detected by the two-channel instrument. Refractive indices were averaged over three measurements.

5.4.1.3 Results

Table 5.4 summarises melting temperature, glass transition temperature, solar-optical properties at ambient temperature and refractive index at 29 °C of matrix materials investigated. The application temperature limits for amorphous and semi-crystalline thermoplastic materials from a thermo-mechanical point of view are below glass transition and melting temperature, respectively [22]. Thermosets are applicable up to their decomposition temperature [22]. For semi-crystalline material M2 a melting peak at 250 °C was detected. DSC and DMA yielded glass transitions around 125 °C, 130 °C and 148 °C for thermoplastic matrix materials M1, M2 and M3. No decomposition was detected. Whereas glass transition was not observed by DSC for UV-curable resin systems M4 to M7, DMA revealed glass transitions at −6 °C, 24 °C and 17 °C of

Table 5.4

materials M4, M5 and M6, respectively. For material M7 a broad plateau in E”-curve was ascertained. Thus an exact designation of glass transition temperature was not possible for this material. The plateau ranged from −2 to 10 °C. For systems M4 to M7, no decomposition was detected up to the maximum investigation temperatures of 150 and 160 °C in DSC and DMA, respectively.

Matrix materials have to be mechanically stable during operation. Hence, all matrix materials are appropriate for collector application (stagnation temperature of collector approx. 128 °C [4]) according to the criteria mentioned above, except for M1. For window applications all materials are appropriate (this estimation is based on the maximum recorded air-temperature on earth, which is approx. 57 °C [23]).

Refractive indices of matrix materials M1 to M7 varied between 1.502 and 1.587. Solar hemispheric transmittance and reflectance ranged from 83 to 85 % and 7 to 8 %, respectively. Absorptance varied between 7 and 10 %. However, for maintaining high efficiency of a solar thermal flat-plate collector equipped with thermotropic overheating protection glazing, a transmittance of at least 85 % is required in the clear state of the TSFD [4]. Transmittance can be increased by reducing the layer thickness on the one hand side. On the other hand side, reflectance can be minimised (i.e. increase in transmittance) by reducing refractive index of matrix material [24]. However, the latter approach would require the replacement of the matrix material.

Table 5.5

Table 5.5 summarises the transition temperatures, the transition temperature interval and the kind of transition of thermotropic additives. Furthermore, Table 5.5 comprises refractive indices of the thermotropic additives below (at 29 °C) and above the phase transition temperature. Solid phase transitions and subsequent melting upon increasing temperature were detected for additives A1 [25]–[29], A5, A6 [30], A8 [31]–[33] and A10. Melting of two polymorphs with recrystallization between these melting processes were evident for additive A4 [34]–[37]. Additive A7 displayed two melting peaks. The lower temperature peak was attributed to melting of impurities [38]. Solely melting was detected for additives A2 [26], A3, A9 and A11 to A19. DSC thermograms revealed glass transitions for additives A20 and A21.

Although additive A22 exhibited a rather narrow endothermic peak at 85 °C, naphthalene was rejected from further investigations due to high degree of supercooling

(crystallisation at 58 °C). Furthermore, it is suspected to be carcinogenic [39]. For additive A23 an endothermic double peak with maxima at 77 and 99 °C was ascertained in the first heating run. The first maximum correlated with melting of the salt hydrate. The second peak was ascribed to evaporation of water. Due to lack of water and thus lacking formation of salt hydrate, no transition was observed in the second heating run within the investigated temperature range (20 to 130 °C). Most salt hydrates display separation of water and salt during melting yielding irreversible behaviour during a melting/solidification cycle [40], [41]. Additive A24 was used as received. It displayed no thermal transition between −20 and 80 °C, although a melting point of 32 °C is reported [41].

Table 5.4.: Basic characteristics of matrix materials: Melting temperatures detected by DSC (T_m), glass transition temperatures (T_g) detected by DSC and DMA, solar hemispheric transmittance (τ_{nh}), solar hemispheric reflectance (ρ_{nh}), absorbtance (α) and refractive index at 29 °C (n^D_{29}).

Matrix	T_m (DSC) [°C]	T_g (DSC) [°C]	T_g (DMA) [°C]	τ_{nh} [%]	ρ_{nh} [%]	α [%]	n^D_{29} [1]
M1	—	125	122	85	8	7	1.502
M2	250	131	128	83	7	10	1.516
M3	—	147	148	84	8	8	1.587
M4	—	—[a]	−6	84	8	8	1.525
M5	—	—[a]	24	84	8	8	1.512
M6	—	—[a]	17	84	8	8	1.551
M7	—	—[a]	−2 to 10[b]	85	8	7	1.521

[a] not detectable

[b] broad plateau in E”-curve detected

Refractive indices of additives A1 to A21 ranged between 1.482 and 1.586 at 29 °C. Additives A1 to A19 exhibited rather distinct changes ($\geq$0.025) in refractive index when exceeding the transition temperature. For additives A20 and A21 only minor reductions (approx. 0.01) were achieved. The refractive index $n^D_{T>T(transition)}$ of additive A21 was recorded at the maximum operation temperature (90 °C) of the refractometer. Transition temperatures given in Table 5.5 already allow for material classification in

terms of applicability. Hence, thermotropic additives exhibiting distinct or transient phase transitions in the temperature range between 30 and 105 °C are labelled “pass” in Table 5.5. Those displaying no phase transition or irreversible effects are labelled “reject”. Therefore, additives A22 to A24 were excluded from further investigations and are hence not displayed in subsequent tables and figures.

Table 5.5.: Transition temperatures, kind of transition, transition interval of candidate thermotropic additives detected by DSC along with refractive indices below (n^{D}_{29}) and above ($n^{D}_{T>T(transition)}$) the transition temperature and classification of eligibility for TSFD formulation.

Additive	Transition temperature [°C]	Kind of transition	Transition interval ΔT [°C]	n^{D}_{29} [1]	$n^{D}_{T>T(transition)}$ [1]	Classification
A1	35	Solid phase transition	31	1.497	1.435	pass
	55	Melting	22			
A2	86	Melting	37	1.514	1.435	pass
A3	64	Melting	32	1.529	1.434	pass
A4	51	Melting	18	1.495	1.445	pass
	54	Recrystallisation	3			
	61	Melting	9			
A5	59	Solid phase transition	19	1.503	1.462	pass
	80	Solid phase transition	17			
	87	Melting	10			
A6	47	Solid phase transition	–	1.503	1.449	pass
	57	Solid phase transition	27			
	62	Melting	7			

Table 5.5.: continued

Additive	Transition temperature [°C]	Kind of transition	Transition interval ΔT [°C]	n^{D}_{29} [1]	$n^{D}_{T>T(transition)}$ [1]	Classification
A7	55	Melting	23	1.500	1.443	pass
	78	Melting	26			
A8	52	Solid phase transition	30	1.502	1.448	pass
	60	Melting				
A9	81	Melting	53	1.506	1.447	pass
A10	61	Solid phase transition	27	1.502	1.460	pass
	80	Solid phase transition	16			
	86	Melting	9			
A11	106	Melting	>50	1.507	1.478	pass
A12	63	Melting	>50	1.484	1.459	pass
A13	90	Melting	>50	1.493	1.459	pass
A14	87	Melting	>50	1.495	1.460	pass
A15	82	Melting	>50	1.493	1.458	pass
A16	66	Melting	>50	1.485	1.454	pass
A17	77	Melting	>50	1.488	1.458	pass
A18	63	Melting	>50	1.482	1.455	pass

Table 5.5.: continued

Additive	Transition temperature [°C]	Kind of transition	Transition interval ΔT [°C]	n^D_{29} [1]	$n^D_{T>T(transition)}$ [1]	Classification
A19	55 [a]	Melting	>50	1.487	1.460	pass
A20	90	Glass transition	30	1.586	1.574	pass
A21	80	Glass transition	24	1.565	1.551 [b]	pass
A22	85	Melting	12			reject
A23	77	Melting	55			reject
	99	Evaporation				
A24	—	—	No transition detectable			reject
						reject

[a] no distinct maximum detectable

[b] transition not completed at maximum operation temperature of refractometer

5.4.2 Assessment of Refractive Index Match/Mismatch

Figure 5.2, 5.3

In Figures 5.2 and 5.3 the refractive index difference between matrix and additive below (black) and above (grey) the transition temperature of the additive is presented for thermoplastic matrix materials (M1, M2 and M3) and for UV-curable matrix materials (M4, M5, M6 and M7), respectively. For additives exhibiting phase transitions at temperatures equal or higher than the maximum operation temperature of the refractometer (90 °C), refractive index data are presented for 29 °C only in order to avoid misleading interpretation of refractive index difference at temperatures above the transition temperature. For additives A11 to A19, which exhibited a broad transition temperature range ΔT>50 °C (see Table 5.5) with peak temperatures up to 106 °C and additives A20 and A21 with glass transitions close to 90 °C refractive index data were selected as follows: If the vast majority of the transition was already done at the maximum measurement temperature of the refractometer (90 °C), refractive index difference data was included. At 90 °C this was true for all materials except for additives A11 and A20 (see section 5.4.1.3). Thus, their data was excluded at 90 °C.

Refractive index difference between matrix material and thermotropic additive below the phase transition temperature of the additive has to be as low as possible [5]. Thus, if the refractive index difference between matrix and additive was smaller than 0.02 below (29 °C) the phase transition temperature of the thermotropic additive, the material combination was categorised as “appropriate” Combinations of matrix and additive with refractive index difference from 0.02 to lower than 0.03 at 29 °C were categorised as “appropriate with limitation”. Matrix/additive combinations not complying with these criteria were rejected. When exceeding the phase transition temperature, refractive index difference is required to be as high as possible [5]. Thus, combinations displaying a refractive index difference $\geq$0.03 above the phase transition temperature of the additive were considered as “appropriate”, whereas those with a refractive index difference $<$0.03 were considered as “inappropriate” and therefore rejected. As to the nomenclature, a system composed of Matrix M1 and Additive A1 is named M1A1.

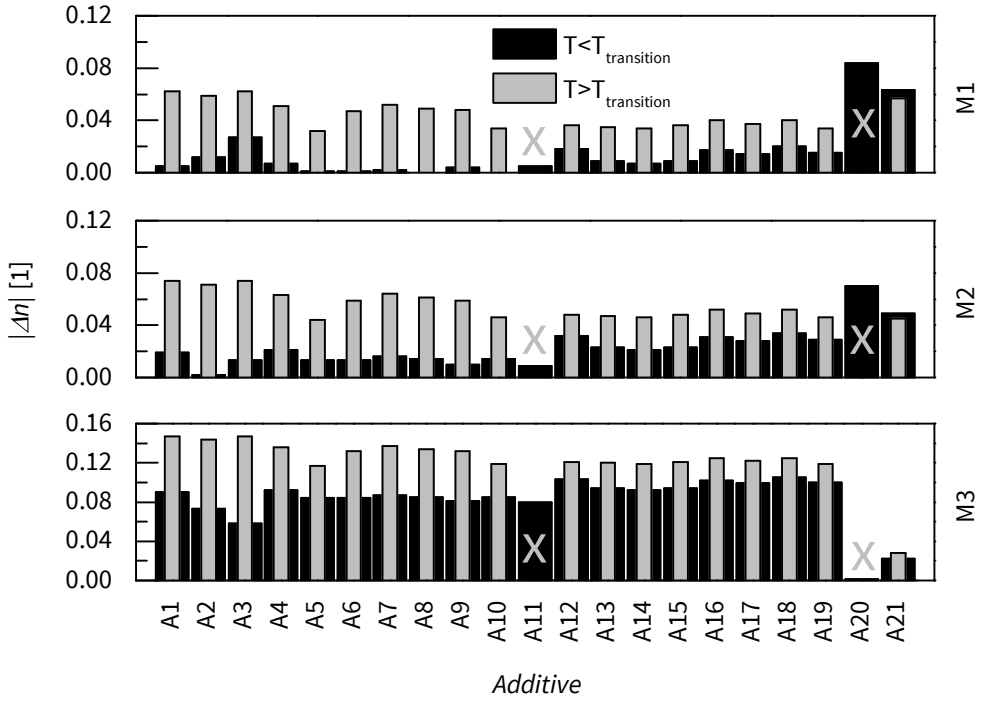

Figure 5.2.: Refractive index difference between matrix and additive below (at 29 °C; black) and above (at $T>T_{transition}$; grey) the transition temperature of the additive for thermoplastic matrix materials M1, M2 and M3. Grey symbol (x) denotes excluded data.

According to these criteria, material combinations M1A1, M1A2, M1A4 to M1A10, M1A12 to M1A17, M1A19, M2A1 to M2A3 and M2A5 to M2A10 were appropriate for formulation. Material combinations M1A11, M2A11 and M3A20 showed refractive index difference <0.02 at 29 °C, which may yield high transmittance at ambient conditions. Thus, regardless of omitted refractive index difference at high temperatures (omission due to technical reasons as pointed out above), these material combinations were considered for formulation. Combinations M1A3, M1A18, M2A4, M2A13 to M2A15, M2A17 and M2A19 were appropriate with limitation for formulation according to the criteria defined above. Material combinations M1A20, M1A21, M2A12, M2A16, M2A18, M2A20, M2A21 and M3A1 to M3A19 were rejected from further investigations due to inappropriate refractive index difference. Combination M3A21 displayed refractive index differences of 0.022 and 0.028 at temperatures below and above the glass

transition, respectively. Nevertheless, this combination was accepted for formulation due to not completed thermal transition of the additive at the maximum operation temperature of the refractometer.

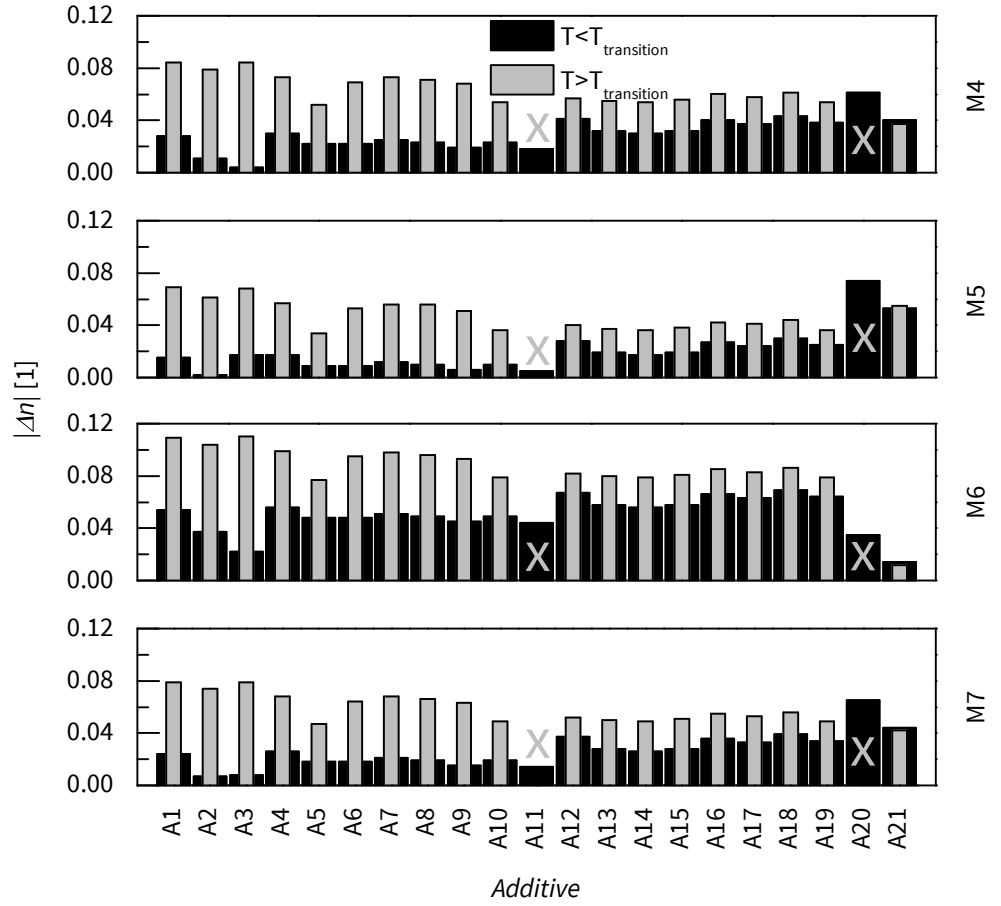

Figure 5.3.: Refractive index difference between matrix and additive below (at 29 °C; black) and above (at $T>T_{transition}$; grey) the transition temperature of the additive for UV-curable matrix materials M4, M5, M6 and M7. Grey symbol (x) denotes excluded data.

Material combinations M4A2, M4A3, M4A9, M5A1 to M5A10, M5A13 to M5A15, M7A2, M7A3, M7A5, M7A6 and M7A8 to M7A10 were appropriate for formulation according to the criteria defined above. Material combinations M4A11, M5A11 and M7A11 exhibited refractive index difference <0.02 at 29 °C, respectively. Low refractive index differences of combinations M4A11, M5A11 and M7A11 were likely to yield high

transmittance at ambient conditions. Thus, regardless of omitted refractive index difference at high temperatures (omission due to technical reasons as pointed out above), these material combinations were considered for formulation. Combinations M4A1, M4A5 to M4A8, M4A10, M5A12, M5A16, M5A17, M5A19, M6A3, M7A1, M7A4, M7A7 and M7A13 to M7A15 were considered appropriate with limitation for formulation. Material combinations M4A4, M4A12 to M4A21, M5A18, M5A20, M5A21, M6A1, M6A2, M6A4 to M6A21, M7A12 and M7A16 to M7A21 were rejected from formulation due to inappropriate refractive index difference.

5.4.3 Formulation of promising Material Combinations

TSFD with thermoplastic matrices were manufactured at APC Advanced Polymer Compounds (Gai, AT) by melt blending on a compounder Coperion ZSK 26 Mcc (Coperion GmbH, Stuttgart, DE). From the compound 800 µm thick plates were obtained by compression moulding on a press P200PV (Dr. Collin GmbH, Ebersberg, DE). Thermotropic layers based on UV-curable resin matrix were prepared by dissolving the thermotropic additive above its transition temperature in the photo-crosslinkable matrix solution, which consisted of 57 wt% oligomers, 40 wt% reactive diluent TMPTA and 3 wt% photoinitiator (blend of benzophenone and 1-hydroxycyclohexyl phenyl ketone). The dissolutions were poured in the intervening space between two glass panes, which were sealed around the edge. Afterwards the samples were stored at ambient temperature for 10 min allowing for precipitation of the additive. Next the mixtures were cured by UV-radiation (dose: 2.1 J cm^{-2}) from a Light Hammer 6 equipped with a mercury-lamp and a LC6E Benchtop Conveyor (Fusion UV Systems Inc., Gaithersburg, MD, US). Free standing layers with a thickness of 900 µm were obtained after removal of the glass panes. TSFD based on UV-curable resin matrix were annealed at the temperature at which mixing of the matrix solution with the corresponding additive was carried out. For both, thermoplastic and resin based TSFD, the theoretical additive concentration was 5 wt%.

Matrix/additive combinations which were chosen for formulation of TSFD are depicted in Table 5.6 . Selection was mainly based on refractive index data discussed above. For combinations of matrix M1 and ethylene co- and terpolymer additives A11 to A19 *Table 5.6*

exhibiting a moderate difference in refractive index above the transition temperature, M1A11 was compounded in order to represent this material class (ethylene co- and terpolymers). M1A11 showed the best refractive index match of the components below the transition temperature. Furthermore, additive A11 was the only ethylene co- or terpolymer that fitted matrix M2 properly with regard to refractive index at low temperatures. Furthermore, combinations M1A1, M1A2, M2A2, M2A3, M2A5, M2A6, M3A20 and M3A21 were compounded. Materials M1A2, M1A11, M2A2, M2A6, M2A11, M3A20 and M3A21 were processable properly. However, compounding of matrix M1 and additive A1 resulted in partial liquid leakage of additive at machine joints due to large differences in melt viscosity of the components. Large differences in viscosity of polymer melt and molten additives led to inaccurate miscibility of matrix M2 and additives A3 and A5 also. TSFD based on UV-curable matrix M4A1 to M4A3, M4A5 to M4A10, M5A1 to M5A10, M6A3 and M7A1 to M7A10 were formulated successfully. Combinations M6A1, M6A2 and M6A10, which were inappropriate for formulation due to high refractive index difference at ambient temperature, were investigated additionally in order to study the effect of refractive index difference on solar optical properties of TSFD. Whereas, mixtures of UV-curable matrix materials and additives A3 to A10 were stable during processing, mixtures of M4, M5, M6 or M7 with additives A1 or A2 exhibited limited miscibility, sometimes resulting in separation of macroscopic additive domains with dimensions in the range of millimetres. For any system with UV-curable resin matrix (M4 to M7), additives A11 to A21 were rejected from formulation due to a lack of processability.

5.4.4 Characterisation of Light-Shielding Performance

5.4.4.1 Experimental

Solar transmittance as a function of temperature, threshold temperature and switching process of TSFD were determined applying UV/Vis/NIR spectrometry. Deviant from the procedure described in section 5.4.1.2, the spectrophotometer was adapted by a heating stage to adjust sample temperature within a range from ambient temperature to maximum 115 °C. Measurements were performed in steps of 5 K for one sample of

Table 5.6.: Actually formulated TSFD.

	M1	M2	M3	M4	M5	M6	M7
A1	+	–	–	+	+	+	+
A2	+	+	–	+	+	+	+
A3	–	+	–	+	+	+	+
A4	–	–	–	–	+	–	+
A5	–	+	–	+	+	–	+
A6	–	+	–	+	+	–	+
A7	–	–	–	+	+	–	+
A8	–	–	–	+	+	–	+
A9	–	–	–	+	+	–	+
A10	–	–	–	+	+	+	+
A11	+	+	–	–	–	–	–
A12	–	–	–	–	–	–	–
A13	–	–	–	–	–	–	–
A14	–	–	–	–	–	–	–
A15	–	–	–	–	–	–	–
A16	–	–	–	–	–	–	–
A17	–	–	–	–	–	–	–
A18	–	–	–	–	–	–	–
A19	–	–	–	–	–	–	–
A20	–	–	+	–	–	–	–
A21	–	–	+	–	–	–	–

\+ materials formulated

– materials *not* formulated

each TSFD. Replicate measurements (samples two and three) were conducted at ambient temperature and at a temperature above the switching threshold of the respective TSFD. Prior to measurement, the samples were allowed to equilibrate for five minutes at the selected temperature. The heating stage was equipped with a control system consisting of a heating stage-internal J-type thermocouple as temperature sensor and the control unit HS-W-35/M (Heinz Stegmeier Heizelemente HS-Heizelemente GmbH, Fridingen, DE). Within the heating stage the sample was positioned in close proximity of the port hole of the Ulbricht-sphere. In situ front- and backside sample surface temperatures as a function of set-point value of the control unit were recorded on a prototype sample with a two-channel temperature measurement instrument T900 (Dostmann electronic GmbH, Wertheim-Reicholzheim, DE) equipped with a precision K-type thermocouple. Sample temperature was assumed as the average of both recorded surface temperatures. Required set-point values to maintain average sample temperatures were calculated from a second order polynomial fit of the temperatures recorded in measurements of the prototype sample. Hemispheric and diffuse solar transmittance were averaged over three measurements. A dependent t-test for paired samples was applied to measured values of solar hemispheric transmittance in order to determine whether transmittance change was significant or not. Equality of mean values of solar hemispheric transmittance below ($\tau_{nh,\,cold}$) and above threshold temperature ($\tau_{nh,\,hot}$) was the null hypothesis (H_0: $\tau_{nh,\,hot} = \tau_{nh,\,cold}$ equal to $\tau_{nh,\,hot} - \tau_{nh,\,cold} = 0$) [42]. H_0 was tested against alternative hypothesis H_A that $\tau_{nh,\,hot} < \tau_{nh,\,cold}$ (equal to $\tau_{nh,\,hot} - \tau_{nh,\,cold} < 0$) or $\tau_{nh,\,hot} > \tau_{nh,\,cold}$ (equal to $\tau_{nh,\,hot} - \tau_{nh,\,cold} > 0$) [42]. H_A were tested one at a time, not at the same time. Thus a one-tailed t-test was applied. Test variable t_d was calculated according to Montgomery [43]. Test scenario 1: Testing H_0 ($\tau_{nh,\,hot} - \tau_{nh,\,cold} = 0$) against H_A ($\tau_{nh,\,hot} - \tau_{nh,\,cold} < 0$) led to rejection of H_0 if $t_d < -t_{1-\alpha;n-1}$. The symbol α denoted the alpha error and n-1 was the degree of freedom (in case of three pairs it was two). Test scenario 2: Testing H_0 ($\tau_{nh,\,hot} - \tau_{nh,\,cold} = 0$) against H_A ($\tau_{nh,\,hot} - \tau_{nh,\,cold} > 0$) led to rejection of H_0 if $t_d > t_{1-\alpha;n-1}$. Transmittance difference was classified according to Kleppmann [44]: H_0 not rejected at $\alpha = 0.05$ meant no significant difference, whereas rejection at $\alpha = 0.05$ meant indifferent increase/decrease. Rejection of H_0 at $\alpha = 0.01$ and 0.001 meant significant and highly significant increase/decrease of solar hemispheric transmittance, respectively.

5.4.4.2 Results

In Table 5.7 the threshold temperature, temperature interval of the major switching process, mean of solar hemispheric and diffuse transmittance below and above the threshold temperature (empirical standard deviation [45] to the right of the mean), and test variable t_d are summarised for TSFD based on thermoplastic matrix. Solar hemispheric transmittance changed from between 36.7 and 80.7 % to values between 53.3 and 83.5 % upon exceeding the threshold temperature. Solar diffuse transmittance ranged from 15.2 to 44.1 % at room temperature. Upon exceeding the threshold temperature it changed to values between 31.4 and 65.9 %. *Table 5.7*

Whereas TSFD M3A21 displayed an indifferent increase in solar hemispheric transmittance, layers M2A2 and M3A20 exhibited an insignificant change in solar hemispheric transmittance. Compared to other layers, the standard deviation of solar hemispheric and diffuse transmittance above the threshold temperature for layer M2A2 was very high (around 13.6 and 12.0 %, respectively). In general, high standard deviation of solar hemispheric transmittance above the threshold temperature is an indication for sample inhomogeneity. At least a significant increase in solar hemispheric transmittance was evident for layers M1A1, M1A2, M1A11 and M2A6. The increase of solar hemispheric transmittance attained for these layers violated predictions from refractive index data. This is attributed to different coefficients of thermal expansion (CTE) of matrix and additive most likely. For example CTE for PMMA and paraffin are in the range of 6–8 $\times$ 10^{-5} K^{-1} and 0.7–1.1 $\times$ 10^{-3} K^{-1}, respectively [46], [47]. Upon cooling during manufacturing, the higher CTE of paraffin leads to more intense contraction of the embedded additive domains compared to surrounding matrix PMMA. Combined with limited adhesion at the interface of matrix and additive, vacuoles are formed. The high refractive index difference between matrix and vacuoles (n=1) yields intense scattering and thus a low solar hemispheric transmittance at room temperature. Upon heating and especially upon melting the additive expands and fills the cavity completely. Thus, the refractive index difference at the scattering interface is reduced, yielding an increase in solar hemispheric transmittance. Detailed investigations concerning layer morphology and to confirm this assumptions are currently under way. On the contrary, a highly significant decrease in solar hemispheric

transmittance from 78.9 to 63.3 % was evident for layer M2A11 upon exceeding the threshold temperature. At temperatures below 75 °C the hemispheric transmittance decreased rather smoothly, whereas between 75 and 100 °C the reduction was steeper. The gradual switching process was in agreement with the broad melting range and the gradual refractive index change of the thermotropic additive A11, detected by DSC and refractometry, respectively. Probably no vacuoles were formed for material combination M2A11. This was likely to be attributed to the epoxy-moiety in additive A11, which is able to form covalent bonds with amide-groups in PA (M2) [48].

Table 5.7.: Threshold temperature T_{th}, major switching interval ΔT_{major}, solar hemispheric and diffuse transmittance below and above the threshold temperature of TSFD based on thermoplastic matrix, and test variable t_d.

TSFD	T_{th} [°C]	ΔT_{major} [°C]	Solar transmittance below threshold temperature [%]				Solar transmittance above threshold temperature [%]				t_d	Remarks [a]
			hemisph.		diffuse		hemisph.		diffuse			
			mean	sdev	mean	sdev	mean	sdev	mean	sdev		
M1A1	45	15	36.7	0.7	36.4	0.6	53.3	1.6	52.0	1.4	26.5	++
M1A2	65	30	37.0	1.4	37.0	1.4	66.1	5.6	65.9	5.1	11.8	+
M1A11	75	20	39.6	2.8	35.4	1.6	64.6	3.2	55.9	1.7	51.5	++
M2A2	70	40	46.2	2.5	44.1	2.6	61.6	13.6	59.7	12.0	2.4	o
M2A6	55	10	59.9	1.3	38.2	0.3	71.8	1.9	44.2	0.2	35.0	++
M2A11	75	25	78.9	0.8	15.2	1.1	63.3	1.2	33.2	2.3	−52.2	−− [b]
M3A20	80	10	80.0	0.9	28.7	3.1	78.0	4.5	37.1	1.9	−0.9	o [c]
M3A21	—	—	80.7	1.1	28.7	4.8	83.5	0.3	31.4	3.5	5.4	+o

[a] Symbols applied: “++” highly significant increase, “+” significant increase, “+o” indifferent increase, “o” insignificant increase/decrease, “–o” indifferent decrease, “–” significant decrease, “––” highly significant decrease

[b] gradual switching process

[c] intermediate reduction

Table 5.8 In Table 5.8 the threshold temperature, temperature interval of the major switching process, mean of solar hemispheric and diffuse transmittance below and above the threshold temperature (empirical standard deviation [45] to the right of the mean) and test variable t_d are summarised for TSFD based on UV-curable resin matrix. Solar hemispheric transmittance changed from between 62.2 and 84.5 % to values between 59.6 and 85.0 % upon exceeding the threshold temperature. Solar diffuse transmittance ranged from 17.5 to 64.8 % at room temperature. Upon exceeding the threshold temperature it changed to values between 28.1 and 81.4 %.

Materials M6A1 and M7A2 exhibited a significant increase of solar hemispheric transmittance above the switching threshold. An indifferent increase was evident for layers M4A1, M5A1 and M5A7. Layers M4A2, M4A6, M5A2, M5A4, M6A2 and M7A1 showed an increase in mean solar hemispheric transmittance upon switching. However, high standard deviation of transmittance change yielded these changes to be insignificant. High standard deviation of transmittance change indicates low sample homogeneity. The increase of solar hemispheric transmittance detected for these layers violated predictions from refractive index data. The observed increase in transmittance instead of the theoretically suggested decrease was attributed to vacuoles (refractive index n=1) which are probably formed at the perimeter of the scattering domains, yielding intense scattering at ambient conditions. Suggested vacuole formation mechanism is slightly different for these systems compared to TSFD based on thermoplastics. During curing procedure components of pre-fabricated mixtures of UV-curable resin and thermotropic additive are exposed to radiation yielding crosslinking reaction in the matrix and heating up of thermotropic mixture due to absorption. Upon cooling, the embedded additive particles contract more intense than the surrounding matrix due to higher CTE of thermotropic additive compared to the matrix material. Combined with limited adhesion at the interface of matrix and additive, vacuoles are formed. The increase of solar hemispheric transmittance upon heating is ascribed to the same mechanisms as already described above. Solar hemispheric transmittance changes between −2.8 and 2.4 % achieved for layers M4A5, M4A7, M4A9, M4A10, M5A5, M5A6, M5A9, M5A10, M7A4, M7A6, M7A7 and M7A10 were insignificant. However, samples of M4A9 showed strongly differing solar hemispheric transmittance at room temperature (sample 1: 82.0 %; sample 2: 80.3 %; sample 3: 61.6 %), whereas

transmittance changed to 75.9 % upon heating. Sample 3 probably contains vacuoles, whereas samples 1 and 2 does not. An indifferent decrease of solar hemispheric transmittance was detected for layers M4A8, M7A5 and M7A9. Solar hemispheric transmittance decrease by −2.3 to −6.9 % was evident for these materials. Solar hemispheric transmittance reduction by −4.7 to −13.5 % was attained for layers M4A3, M5A3, M5A8, M6A3, M6A10, M7A3 and M7A8. The t-test revealed these changes to be at least significant for TSFD M4A3, M5A8, M6A3, M6A10, M7A3 and M7A8. However, transmittance change for layer M5A3 was insignificant. Investigations revealed incoherent switching behaviour of the three samples investigated: The best performing sample, which was one out of three replicates of M5A3, exhibited a change in solar hemispheric transmittance from 84.4 to 52.7 %. However, the switching was partially irreversible.

Table 5.8.: Threshold temperature T_{th}, major switching interval ΔT_{major}, solar hemispheric and diffuse transmittance below and above the threshold temperature of TSFD based on UV-curable resin matrix, and test variable t_d.

TSFD	T_{th} [°C]	ΔT_{major} [°C]	Solar transmittance below threshold temperature [%]				Solar transmittance above threshold temperature [%]				t_d	Remarks [a]
			hemisph.		diffuse		hemisph.		diffuse			
			mean	sdev	mean	sdev	mean	sdev	mean	sdev		
M4A1	30	25	63.5	1.4	56.1	0.4	75.4	6.1	73.7	5.6	3.26	+o
M4A2	70	10	76.6	0.4	26.1	3.1	80.0	3.0	48.6	1.4	2.24	o
M4A3	50	10	79.2	2.5	55.6	6.3	70.9	1.7	61.8	2.9	−11.9	–
M4A5	70	10	80.5	1.1	42.1	2.5	77.7	3.0	73.5	2.1	−1.52	o
M4A6	50	15	71.0	19.3	51.3	3.7	81.3	1.6	78.2	1.0	0.99	o
M4A7	60	10	83.3	1.3	40.7	9.3	85.0	0.2	69.8	4.0	2.19	o
M4A8	50	10	75.9	3.4	51.2	2.8	69.0	5.6	61.5	3.8	−5.36	–o
M4A9	60	15	74.7	11.3	53.2	2.2	75.9	0.8	61.7	4.6	0.21	o
M4A10	70	10	80.4	1.0	42.7	3.3	78.4	3.2	71.5	1.2	−1.21	o
M5A1	45	20	82.2	1.1	52.5	1.0	84.0	1.0	81.4	1.0	6.22	+o
M5A2	55	25	74.7	9.4	43.6	3.3	82.2	1.2	71.5	2.3	1.23	o
M5A3	55	>60	83.1	1.2	41.5	8.2	75.0	19.4	28.1	14.7	−0.68	o [b]
M5A4	50	10	69.4	6.1	53.6	2.2	78.5	0.7	75.9	0.4	2.85	o
M5A5	65	15	81.1	1.0	24.2	5.9	81.9	1.8	67.7	2.8	0.80	o

Table 5.8.: continued

TSFD	T_{th} [°C]	ΔT_{major} [°C]	Solar transmittance below threshold temperature [%]				Solar transmittance above threshold temperature [%]				t_d	Remarks [a]
			hemisph.		diffuse		hemisph.		diffuse			
			mean	sdev	mean	sdev	mean	sdev	mean	sdev		
M5A6	40	25	82.2	1.3	33.1	4.8	82.4	1.0	77.2	1.9	0.12	o
M5A7	60	10	81.1	2.7	39.2	8.8	84.5	0.9	28.3	7.1	3.17	+o
M5A8	50	15	77.9	0.5	37.2	3.9	73.2	0.7	66.5	0.8	−38.8	−−
M5A9	65	10	80.4	1.7	64.8	5.1	78.0	1.0	68.6	3.3	−2.74	o
M5A10	70	10	82.8	0.5	17.5	4.9	82.9	1.2	68.4	2.7	0.20	o
M6A1	45	10	62.2	3.5	54.2	2.7	77.3	1.6	74.6	1.8	8.15	+
M6A2	55	20	69.9	10.2	42.9	11.3	80.4	2.1	72.6	1.5	1.89	o
M6A3	50	10	72.3	4.6	53.5	7.4	59.6	3.7	54.0	2.7	−27.1	−−
M6A10	65	15	72.2	3.3	64.3	2.3	65.3	2.0	64.2	2.0	−8.07	−
M7A1	45	10	69.6	8.3	48.9	7.2	82.9	1.5	79.1	1.9	2.69	o
M7A2	60	15	63.4	3.4	45.0	2.1	81.7	1.2	72.8	0.8	7.06	+
M7A3	50	10	78.8	1.0	51.2	0.9	65.3	2.1	57.3	1.2	−17.5	−
M7A4	50	20	73.1	4.9	50.9	0.7	75.5	0.9	70.6	0.9	0.70	o
M7A5	75	5	81.0	0.6	33.5	6.6	78.7	1.8	74.0	2.8	−3.19	−o
M7A6	45	20	80.3	2.2	49.2	4.3	81.0	0.8	77.2	0.8	0.56	o

Table 5.8.: continued

TSFD	T_{th} [°C]	ΔT_{major} [°C]	Solar transmittance below threshold temperature [%]				Solar transmittance above threshold temperature [%]				t_d	Remarks [a]
			hemisph.		diffuse		hemisph.		diffuse			
			mean	sdev	mean	sdev	mean	sdev	mean	sdev		
M7A7	65	5	84.5	0.6	20.0	8.4	83.7	0.7	51.2	4.4	−2.10	o
M7A8	50	15	76.4	1.1	48.9	3.6	67.2	0.6	61.7	0.5	−12.0	–
M7A9	45	30	80.5	1.8	63.5	1.3	75.2	0.3	70.1	0.8	−6.18	–o
M7A10	60	20	80.6	1.2	34.9	4.0	78.8	2.6	72.9	1.5	−2.09	o

[a] Symbols applied: “++” highly significant increase, “+” significant increase, “+o” indifferent increase, “o” insignificant increase/decrease, “–o” indifferent decrease, “–” significant decrease, “––” highly significant decrease

[b] irreversible degradation

Figure 5.4

In Figure 5.4 the hemispheric transmittance of sample 1 of layer M5A3 is displayed at room temperature (solid line) and at 115 °C (dotted line). A distinct reduction of transmittance over the entire wavelength range between 375 and 2250 nm was observed upon heating. The dashed line represents a spectrum recorded after cooling to ambient temperature and sufficient equilibration time (hemispheric transmittance 64.7 %). The area between the dashed and the dotted line may represent the reversible portion of the process. It may be attributed to solidification of the additive and thus reduction of refractive index difference of matrix and additive. The area between the solid and the dashed line corresponds to an irreversible process. The irreversible portion may be ascribed to formation of crack-like structures inside the sample occurring after exposure to elevated temperatures. These cracks (refractive index n=1) may act as persistent scattering domains, thus yielding a permanent reduction of hemispheric transmittance. Interestingly, the two other samples produced from material M5A3 displayed an increase of hemispheric solar transmittance upon heating. As a consequence standard deviation of hemispheric solar transmittance above the threshold temperature given in Table 5.8 was reasonable high (19.4 %). Nevertheless, hazy areas were also observed for these layers even though in less lateral extension than for sample one. These specimens displayed minor irreversible portion of transmittance change as indicated by hemispheric transmittance of 82.0 or 82.9 % and 78.1 or 76.6 % before and after the heating cycle, respectively.

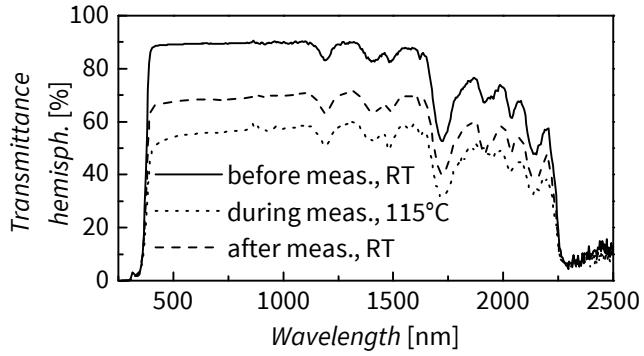

Figure 5.4.: Hemispheric transmittance of sample one of M5A3 before acquisition of solar-optical properties of layers formulated with additive A3 as a function of temperature (solid line), during acquisition (dotted line) and after acquisition (dashed line).

Figure 5.5

Figure 5.5 displays solar hemispheric transmittance of TSFD as a function of the absolute of refractive index difference of matrix and additive below and above the switching threshold. Merely matrix/additive combinations yielding a reduction in hemispheric solar transmittance above the switching threshold are considered. The data scatter reveals a slight trend: The higher the refractive index difference between matrix and additive, the lower the solar hemispheric transmittance. This indicates clearly, that refractometry is an appropriate tool for material pre-selection for formulation of TSFD. Nevertheless, exact prediction of transmittance reduction from refractive index data as a function of temperature of matrix and additive is not possible due to the significant effect of TSFD morphology (scattering domain size and shape) on scattering performance [5], [49], [50].

With regard to refractive index data every formulated TSFD has the potential to display a reduction of solar hemispheric transmittance upon exceeding the threshold temperature in principle. However, morphology of TSFD has a significant effect on switching characteristics of a TSFD also [5], [15], [49], [50]. Thus, observed increase of solar hemispheric transmittance of several TSFD might be ascribed to inappropriate sample morphology (e.g. vacuoles).

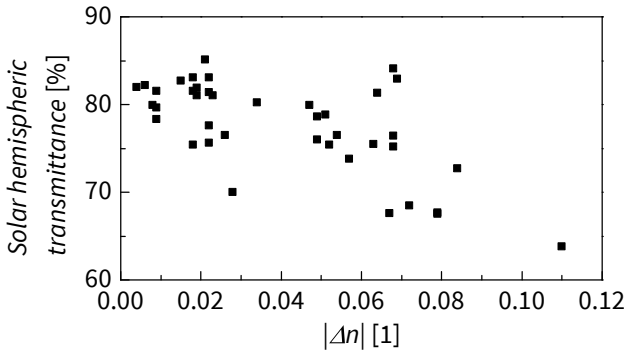

Figure 5.5.: Solar hemispheric transmittance of selected TSFD as a function of the absolute of refractive index difference of matrix and additive.

Detected threshold temperatures ranged from 30 to 75 °C. For several of these materials, switching interval was rather narrow within a frame of 5 to 10 °C. A more transient transition with a broader switching interval between 15 and 30 °C was attained for

TSFD M4A1, M4A6, M4A9, M5A1, M5A2, M5A5, M5A6, M5A8, M6A2, M6A10, M7A2, M7A4, M7A6, M7A8, M7A9 and M7A10. The transition interval of M5A3 was $>60\,^{\circ}C$. In Figure 5.6 the threshold temperatures of TSFD detected by UV/Vis/NIR spectrometry are depicted as a function of transition temperature of the corresponding thermotropic additives detected by DSC. A good correlation is discernible which is in agreement with findings by Resch et al. [15], [51]. Thus, DSC is an appropriate tool for selection of thermotropic additives in order to tune the threshold temperature of TSFD [15], [51]. However, attempts in order to determine the DSC thermograms of formulated TSFD revealed no reasonable results due to the low concentration (5 wt%) of the thermotropic additives and hence low sensibility to thermal transitions of the thermotropic additives.

Figure 5.6

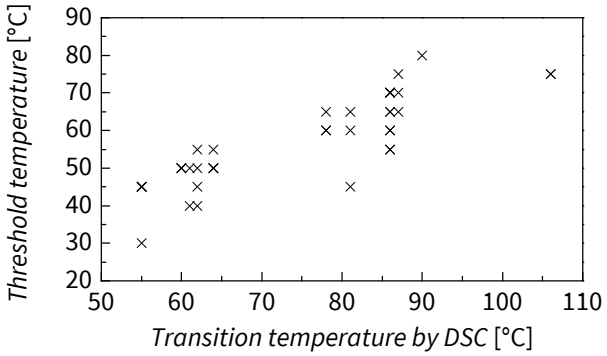

Figure 5.6.: Threshold temperatures of TSFD detected by UV/Vis/NIR spectrometry as a function of transition temperature of corresponding thermotropic additives detected by DSC.

5.5 Conclusions and Outlook

In this paper a systematic material formulation strategy was applied in order to establish a thermotropic systems with fixed domains (TSFD) providing efficient overheating protection. Systematic pre-selection of matrix materials and thermotropic additives was carried out utilising thermo-analytical methods and refractometry. Promising TSFD were formulated based on assessment of refractive index match of matrix and additive. Whereas most TSFD were producible properly, several TSFD based on ther-

moplastics lacked miscibility of matrix and additive due to high viscosity differences. Investigations revealed a good correlation of transition temperature of the thermotropic additives detected by differential scanning calorimetry (DSC) and the threshold temperature of the layers formulated therewith, thus enabling adjustment of switching threshold by selecting adequate thermotropic additives with transition temperature in the desired range (e.g. for window application or solar thermal collectors). A close correlation of refractive index difference and measured solar transmittance was observed, which is in good agreement with theoretical considerations [5]. Thus refractometry is an appropriate tool for pre-selection of candidate combinations of matrix materials and thermotropic additives. A little number of formulated TSFD exhibited no thermo-responsive behaviour. Other materials were showing either an increase or a decrease of hemispheric solar transmittance upon exceeding the switching threshold. In general, the overheating protection potential of the TSFD formulated within this study is limited. Recent studies ascribe the limited overheating protection potential of TSFD to inappropriate size and shape of scattering domains [49], [50]. Thus a related paper [17] will deal with a comprehensive characterisation of morphology with specific focus on scattering domain shape and size. Subsequently, structure-property-relationships will be established and optimisation strategies will be presented.

5.6 Acknowledgements

This research project is funded by the State Government of Styria, Department Zukunftsfonds (Project number 5019). The efforts in determination of solar-optical properties of parts of the formulated TSFD by Alexander KLUTZ (Polymer Competence Center Leoben GmbH, PCCL, Leoben, AT), Astrid RAUSCHENBACH (PCCL) and Andrea SCHMID (Department of Polymer Engineering and Science, University of Leoben, AT) and support concerning UV equipment by Sandra SCHLÖGL (PCCL) and compounding of materials with thermoplastic matrix by Karl SCHNETZINGER (APC Advanced Polymer Compounds, Gai, AT) are gratefully acknowledged. Furthermore, the authors wish to acknowledge the contributions of Arkema GmbH (Düsseldorf, DE), Baerlocher GmbH (Unterschleissheim, DE), Bayer Materials Science AG (Leverkusen, DE), Biesterfeld In-

terowa GmbH & Co. KG (Wien, AT), Brenntag CEE GmbH (Traun, AT), Chemson Polymer Additive AG (Arnoldstein, AT), Allnex Belgium SA/NV (formerly Cytec Surface Specialities Inc.; Drogenbos, BE), DuPont de Nemours (Deutschland) GmbH (Neu-Isenburg, DE), Evonik Degussa GmbH, High Performance Polymers (Marl, DE), Evonik Röhm GmbH (Darmstadt, DE), HDS-Chemie Handelsgesmbh (Wien, AT), Sasol Wax GmbH (Hamburg, DE) and Senoplast Klepsch GmbH (Piesendorf, AT).

5.7 References

[1] P. Nitz and H. Hartwig, 'Solar control with thermotropic layers', *Solar Energy*, vol. 79, no. 6, pp. 573–582, 2005, ISSN: 0038092X. DOI: 10.1016/j.solener.2004.12.009.

[2] A. Seeboth, J. Schneider and A. Patzak, 'Materials for intelligent sun protecting glazing', *Solar Energy Materials and Solar Cells*, vol. 60, no. 3, pp. 263–277, 2000, ISSN: 09270248. DOI: 10.1016/S0927-0248(99)00087-2.

[3] P. Nitz and A. Wagner, 'Schaltbare und regelbare Verglasungen', *BINE Themeninfo*, vol. I/02, no. I/02, pp. 1–12, 2002, ISSN: 1610-8302.

[4] G. M. Wallner, K. Resch and R. Hausner, 'Property and performance requirements for thermotropic layers to prevent overheating in an all polymeric flat-plate collector', *Solar Energy Materials and Solar Cells*, vol. 92, no. 6, pp. 614–620, 2008, ISSN: 09270248. DOI: 10.1016/j.solmat.2007.12.005.

[5] P. Nitz, 'Optical modelling and characterisation of thermotropic systems', Dissertation, Albert-Ludwigs-University, Freiburg i.B., 1999.

[6] T. Inoue, 'Solar shading and daylighting by means of autonomous responsive dimming glass: practical application', *Energy and Buildings*, vol. 35, no. 5, pp. 463–471, 2003, ISSN: 03787788. DOI: 10.1016/S0378-7788(02)00143-3.

[7] J. Yao and N. Zhu, 'Evaluation of indoor thermal environmental, energy and daylighting performance of thermotropic windows', *Building and Environment*, vol. 49, pp. 283–290, 2012, ISSN: 03601323. DOI: 10.1016/j.buildenv.2011.06.004.

[8] H. Hartwig, 'Konzepte für die Integration selbstregelnder, thermotroper Schichten in moderne Gebäudehüllen zur passiven Nutzung der Sonnenenergie', Dissertation, Technische Universität München, München, 2003.

[9] A. Raicu, H. R. Wilson, P. Nitz, W. Platzer, V. Wittwer and E. Jahns, 'Facade systems with variable solar control using thermotropic polymer blends', *Solar Energy*, vol. 72, no. 1, pp. 31–42, 2002, ISSN: 0038092X. DOI: 10.1016/S0038-092X(01)00093-7.

[10] H. Manz and U.-P. Menti, 'Energy performance of glazings in European climates', *Renewable Energy*, vol. 37, no. 1, pp. 226–232, 2012, ISSN: 09601481. DOI: 10.1016/j.renene.2011.06.016. (visited on 08/02/2012).

[11] K. Resch and A. Weber, 'Smart Windows - Smart Collectors: Entwicklung von funktionalen Überhitzungsschutzverglasungen für Gebäudeverglasungen und thermische Solarkollektoren', *Berg- und Hüttenmännische Monatshefte*, vol. 156, no. 11, pp. 429–433, 2011, ISSN: 0005-8912. DOI: 10.1007/s00501-011-0031-2.

[12] K. Resch and G. M. Wallner, 'Thermotropic layers for flat-plate collectors—A review of various concepts for overheating protection with polymeric materials', *Solar Energy Materials and Solar Cells*, vol. 93, no. 1, pp. 119–128, 2009, ISSN: 09270248. DOI: 10.1016/j.solmat.2008.09.004.

[13] P. Nitz, J. Ferber, R. Stangl, H. R. Wilson and V. Wittwer, 'Simulation of multiply scattering media', *Solar Energy Materials and Solar Cells*, vol. 54, no. 1-4, pp. 297–307, 1998, ISSN: 09270248. DOI: 10.1016/S0927-0248(98)00081-6.

[14] O. Muehling, A. Seeboth, T. Haeusler, R. Ruhmann, E. Potechius and R. Vetter, 'Variable solar control using thermotropic core/shell particles', *Solar Energy Materials and Solar Cells*, vol. 93, no. 9, pp. 1510–1517, 2009, ISSN: 09270248. DOI: 10.1016/j.solmat.2009.03.029.

[15] K. Resch, G. M. Wallner and R. Hausner, 'Phase separated thermotropic layers based on UV cured acrylate resins – Effect of material formulation on overheating protection properties and application in a solar collector', *Solar Energy*, vol. 83, no. 9, pp. 1689–1697, 2009, ISSN: 0038092X. DOI: 10.1016/j.solener.2009.06.006.

[16] K. Resch, G. M. Wallner and R. W. Lang, 'Spectroscopic Investigations of Phase-Separated Thermotropic Layers Based on UV Cured Acrylate Resins', *Macromolecular Symposia*, vol. 265, no. 1, pp. 49–60, 2008, ISSN: 10221360. DOI: 10.1002/masy.200850506.

[17] A. Weber, A. Schmid and K. Resch, 'Thermotropic Glazings for Overheating Protection II: Morphology and Structure-Property-Relationships', *Journal of Applied Polymer Science*, ISSN: 0021-8995. DOI: 10.1002/app.39910.

[18] G. W. Ehrenstein and S. Pongratz, *Beständigkeit von Kunststoffen*. München: Hanser, 2007, ISBN: 978-3-446-21851-2.

[19] J. C. Seferis, 'Refractive Indices of Polymers', in *Polymer Handbook*, J. Brandrup, E. H. Immergut and E. A. Grulke, Eds., New York: Wiley, 1999, pp. VI/571–VI/582, ISBN: 0-471-16628-6.

[20] G. W. Ehrenstein, G. Riedel and P. Trawiel, *Praxis der thermischen Analyse von Kunststoffen*, 2nd ed. München: Hanser, 2003, ISBN: 9783446223400.

[21] P. Schiebener, J. Straub, J. M. H. Levelt Sengers and J. S. Gallagher, 'Refractive index of water and steam as function of wavelength, temperature and density', *Journal of Physical and Chemical Reference Data*, vol. 19, no. 3, pp. 677–718, 1990, ISSN: 00472689. DOI: 10.1063/1.555859.

[22] W. Hellerich, G. Harsch and S. Haenle, *Werkstoff-Führer Kunststoffe: Eigenschaften, Prüfungen, Kennwerte*, 9th ed. München: Hanser, 2004, ISBN: 3446225595.

[23] K. I. El Fadli, R. S. Cerveny, C. C. Burt, P. Eden, D. Parker, M. Brunet, T. C. Peterson, G. Mordacchini, V. Pelino, P. Bessemoulin, J. L. Stella, F. Driouech, M. A. Wahab and M. B. Pace, 'World Meteorological Organization Assessment of the Purported World Record 58°C Temperature Extreme at El Azizia, Libya (13 September 1922)', *Bulletin of the American Meteorological Society*, vol. 94, pp. 199–204, 2013, ISSN: 0003-0007. DOI: 10.1175/BAMS-D-12-00093.1.

[24] W. Demtröder, *Experimentalphysik 2: Elektrizität und Optik*, 4th ed. Berlin: Springer, 2006, ISBN: 9783540337942.

[25] A. Hammami and A. K. Mehrotra, 'Thermal behaviour of polymorphic n-alkanes: effect of cooling rate on the major transition temperatures', *Fuel*, vol. 74, no. 1, pp. 96–101, 1995, ISSN: 00162361. DOI: 10.1016/0016-2361(94)P4338-3. [Online]. Available: http://www.sciencedirect.com/science/article/pii/0016236194P43383 (visited on 09/02/2012).

[26] A. Luyt and I. Krupa, 'Thermal behaviour of low and high molecular weight paraffin waxes used for designing phase change materials', *Thermochimica Acta*, vol. 467, no. 1-2, pp. 117–120, 2008, ISSN: 00406031. DOI: 10.1016/j.tca.2007.11.001.

[27] A. Briard, M. Bouroukba, D. Petitjean, N. Hubert, J. Moise and M. Dirand, 'Thermodynamic and structural analyses and mechanisms of the crystallisation of multi-alkane model mixtures similar to petroleum cuts', *Fuel*, vol. 85, no. 5-6, pp. 764–777, 2006, ISSN: 00162361. DOI: 10.1016/j.fuel.2005.07.020. (visited on 09/02/2012).

[28] V. M. Egorov, V. A. Marikhin and L. P. Myasnikova, 'Phase transitions in paraffins, n-alkane alcohols, and α,ω-alkane diols with different chain lengths', *Polymer Science Series A: Polymer Physics*, vol. 49, no. 12, pp. 1366–1376, 2007, ISSN: 0965-545X. DOI: 10.1134/S0965545X07120103. (visited on 09/02/2012).

[29] L. Ventola, M. A. Cuevas-Diarte, T. Calvet, I. Angulo, M. Vivanco, M. Bernar, G. Bernar, M. Melero and D. Mondieig, 'Molecular alloys as phase change materials (MAPCM) for energy storage and thermal protection at temperatures from 70 to 85°C', *Journal of Physics and Chemistry of Solids*, vol. 66, no. 10, pp. 1668–1674, 2005, ISSN: 00223697. DOI: 10.1016/j.jpcs.2005.06.001. (visited on 08/02/2012).

[30] W. Gu, 'Factor analysis of phase transitions and conformational changes in pentaerythritol tetrastearate', *Analytical Chemistry*, vol. 65, no. 6, pp. 827–833, 1993, ISSN: 0003-2700. DOI: 10.1021/ac00054a030.

[31] J. Vereecken, W. Meeussen, I. Foubert, A. Lesaffer, J. Wouters and K. Dewettinck, 'Comparing the crystallization and polymorphic behaviour of saturated and unsaturated monoglycerides', *Food Research International*, vol. 42, no. 10, pp. 1415–1425, 2009, ISSN: 09639969. DOI: 10.1016/j.foodres.2009.07.006.

[32] R. O'Laughlin, C. Sachs, H. Brittain, E. Cohen, P. Timmins and S. Varia, 'Effects of variations in physicochemical properties of glyceryl monostearate on the stability of an oil-in-water cream', *Journal of the Society of Cosmetic Chemists*, vol. 40, no. 4, pp. 215–229, 1989. [Online]. Available: http://www.scopus.com/inward/record.url?eid=2-s2.0-0024821463\&partnerID=40\&md5=600d7f87bb0c63bc13583684c82418a8.

[33] J. Chen, H. Chen, S. Cui, B. Xue, J. Tian, S. Achilefu and Y. Gu, 'Glucosamine derivative modified nanostructured lipid carriers for targeted tumor delivery', *Journal of Materials Chemistry*, vol. 22, no. 12, p. 5770, 2012, ISSN: 0959-9428. DOI: 10.1039/c2jm15830b.

[34] H.-D. Belitz, W. Grosch and P. Schieberle, *Lehrbuch der Lebensmittelchemie*, 6th ed. Berlin: Springer, 2008, ISBN: 978-3-540-73201-3.

[35] R. W. Hartel, *Crystallization in foods*. Gaithersburg: Aspen Publishers, 2001, ISBN: 0834216345.

[36] F. Lavigne, C. Bourgeaux and M. Ollivon, 'Phase transitions of saturated triglycerides', *Journal de Physique IV*, vol. 03, no. C8, pp. 137–140, 1993, ISSN: 1155-4339. DOI: 10.1051/jp4:1993825.

[37] J.-H Oh, A. McCurdy, S. Clark and B. Swanson, 'Characterization and Thermal Stability of Polymorphic Forms of Synthesized Tristearin', *Journal of Food Science*, vol. 67, no. 8, pp. 2911–2917, 2002, ISSN: 0022-1147. DOI: 10.1111/j.1365-2621.2002.tb08837.x.

[38] J. P. Eloundou, E. Girard-Reydet, J.-F. Gérard and J.-P. Pascault, 'Calorimetric and rheological studies of 12-hydroxystearic acid / digycidyl ether of bisphenol A blends', *Polymer Bulletin*, vol. 53, no. 5-6, pp. 367–375, 2005, ISSN: 0170-0839. DOI: 10.1007/s00289-005-0345-x.

[39] IFA, *GESTIS-Stoffdatenbank: Naphthalin*, Institut für Arbeitsschutz der Deutschen Gesetzlichen Unfallversicherung, Ed., 2012. [Online]. Available: http://gestis.itrust.de/nxt/gateway.dll/gestis_de/015510.xml?f=templates\$fn=default.htm\$3.0 (visited on 22/03/2012).

[40] L. Cabeza, A. Castell, C. Barreneche, A. d. Gracia and A. Fernández, 'Materials used as PCM in thermal energy storage in buildings: A review', *Renewable and Sustainable Energy Reviews*, vol. 15, no. 3, pp. 1675–1695, 2011, ISSN: 13640321. DOI: 10.1016/j.rser.2010.11.018.

[41] A. Sharma, V. Tyagi, C. Chen and D. Buddhi, 'Review on thermal energy storage with phase change materials and applications', *Renewable and Sustainable Energy Reviews*, vol. 13, no. 2, pp. 318–345, 2009, ISSN: 13640321. DOI: 10.1016/j.rser.2007.10.005.

[42] L. Sachs, *Angewandte Statistik: Anwendung statistischer Methoden*, 11th ed. Berlin: Springer, 2004, ISBN: 3-540-40555-011.

[43] D. C. Montgomery, *Design and analysis of experiments*, 7th ed. Hoboken: Wiley, 2009, ISBN: 0470128666.

[44] W. Kleppmann, *Taschenbuch Versuchsplanung: Produkte und Prozesse optimieren*, 6th ed. München: Hanser, 2009, ISBN: 3446420339.

[45] H.-J. Bartsch, *Taschenbuch mathematischer Formeln für Ingenieure und Naturwissenschaftler*, 22nd ed. München: Hanser, 2011, ISBN: 978-3-446-42927-7.

[46] E. Baur, S. Brinkmann, T. A. Osswald and E. Schmachtenberg, *Saechtling-Kunststoff-Taschenbuch*, 30. Auflage. München: Hanser, 2007, ISBN: 9783446403529.

[47] M. Schimmelpfennig, K. Weber, F. Kalb, K.-H. Feller, T. Butz and M. Matthäi, 'Volumenausdehnung von Paraffinen aus Steigrohr-Messungen', in *Jahrbuch für den Praktiker 2007*, B. Ziolkowsky, Ed., vol. 50, Augsburg: Verlag für chemische Industrie, 2007, pp. 417–429.

[48] C. Koning, M. Van Duin, C. Pagnoulle and R. Jerome, 'Strategies for compatibilization of polymer blends', *Progress in Polymer Science*, vol. 23, no. 4, pp. 707–757, 1998, ISSN: 00796700. DOI: 10.1016/S0079-6700(97)00054-3. (visited on 08/02/2012).

[49] K. Resch and G. M. Wallner, 'Morphology of phase-separated thermotropic layers based on UV cured acrylate resins', *Polymers for Advanced Technologies*, vol. 20, no. 12, pp. 1163–1167, 2009, ISSN: 10427147. DOI: 10.1002/pat.1393.

[50] A. Weber and K. Resch, 'Effect of Temperature-Cycling on the Morphology of Polymeric Thermotropic Glazings for Overheating Protection Applications', *Journal of Polymer Research*, vol. 19:9888, no. 6, pp. 1–8, 2012, ISSN: 1022-9760. DOI: 10.1007/s10965-012-9888-3.

[51] K. Resch and G. M. Wallner, 'Thermotropic Resin Systems: Relationships Between Formulation Parameters, Material Structure and Optical Properties', in *Proceedings of ISES Solar World Congress 2007*, D. Y. Goswami and Y. Zhao, Eds., Berlin: Springer, 2007, pp. 541–545, ISBN: 978-3-540-75996-6. DOI: 10.1007/978-3-540-75997-3_98.

6 Publication 2

6.1 Bibliographic Information

- Title: Thermotropic Glazings for Overheating Protection II: Morphology and Structure-Property-Relationships
- Authors:
  - Andreas Weber[1]
  - Andrea Schmid[2]
  - Katharina Resch[2]
    1. Polymer Competence Center Leoben GmbH, Roseggerstrasse 12, 8700 Leoben, Austria
    2. Department Polymer Engineering and Science, Materials Science and Testing of Polymers, University of Leoben, Otto Glöckel-Strasse 2, 8700 Leoben, Austria
- Periodical: Journal of Applied Polymer Science
- DOI: 10.1002/app.39910

Statement with regard to publication: The manuscript presented here is an adapted accepted manuscript in order to fit the formatting of the thesis and does not necessarily reflect exactly the actually published version.

6.2 Abstract

This paper completes a systematic strategy for formulation and optimisation of thermotropic systems with fixed domains (TSFD) for overheating protection purposes. Focus was on characterisation of morphology and on revealing optimisation potential. A comprehensive characterisation of scattering domain size and shape was done applying optical microscopy and scanning electron microscopy. In general, scattering domains exhibited inappropriate size and/or shape for optimum overheating protection performance. Moreover, several TSFD displayed defects (vacuoles, voids) resulting from thermo-mechanical or physico-chemical interaction of matrix material and thermotropic additive during manufacturing. Morphological features along with solar optical and thermo-refractive properties allowed for establishment of structure-property-relationships. Light-shielding efficiency of TSFD correlated well with scattering domain size and shape. The majority of TSFD showing defects exhibited an increase of solar hemispheric transmittance upon heating. Several strategies to overcome defect formation and to improve scattering morphology were suggested and proof of concept was shown partially, thus indicating a significant optimisation potential of the established TSFD.

6.3 Introduction

A feasible way to prevent buildings and solar thermal collectors from overheating are thermotropic glazings [1]–[3]. Thermotropic glazings change their light transmittance from highly transmitting to highly reflecting upon reaching a certain threshold temperature reversibly [3]–[5]. Besides other classes of thermotropic glazings, thermotropic systems with fixed domains (TSFD) gained interest in recent research due to their specific advantages like high reversibility, low hysteresis, ease of adjustment of switching threshold, high long-term stability and their steep switching process [6]–[17]. TSFD consist of a thermotropic additive finely dispersed in a matrix material [3], [4]. Refractive index difference of matrix and additive and TSFD morphology are of paramount importance for scattering performance and thus overheating protection performance of TSFD [18]. Refractive indices of matrix and additive are almost equal below the

phase transition temperature (e.g. melting temperature) of the additive yielding transparent appearance of the TSFD [4]. Upon exceeding the switching threshold the refractive index difference between matrix and additive increases steeply resulting in a reduction of solar hemispheric transmittance [4]. Maximum light-shielding efficiency is attained by spherical scattering domains with diameters in the range between 200 and 400 nm [18].

So far with TSFD only moderate overheating protection performance was achieved. Limited light-shielding performance was primarily ascribed to inappropriate scattering domain size and shape [6]–[10], [12], [16]. Thus, Weber and Resch [17] carried out a systematic and comprehensive evaluation of numerous TSFD based on a novel material formulation and characterisation strategy in order to evaluate overheating protection and optimisation potential. Candidate matrix materials and thermotropic additives were characterised comprehensively based on sound polymer-physical principles. Promising material combinations were formulated. On the one hand side, TSFD exhibiting the aspired decrease in solar hemispheric transmittance upon exceeding the threshold temperature were achieved. On the other hand side, TSFD displaying an increase in solar hemispheric transmittance were attained. Hence, the major objective of this paper is to establish relationships between observed switching characteristics and TSFD specific material properties (thermo-refractive properties of matrix and additive, morphology, etc.). For this purpose a comprehensive characterisation of TSFD morphology is carried out. Subsequently, material optimisation approaches are derived in order to improve overheating protection performance.

6.4 Systematic Material Formulation Strategy

Refractive index difference of matrix and additive and TSFD morphology are of paramount importance for scattering performance and thus overheating protection performance of TSFD [18]. Hence, for the development of novel TSFD a systematic material formulation strategy has been established in order to account for these factors. The strategy comprises seven different steps. First a comprehensive literature review concerning material properties is carried out in order to evaluate candidate matrix

materials and thermotropic additives: Matrix materials exhibit preferably high transition temperatures (glass transition, melting), high transmittance and a refractive index as low as possible. Thermotropic additives must display a thermal transition – preferably melting – between 30 °C and 105 °C along with a rapid and steep change of refractive index. Subsequently, a comprehensive polymer-physical characterisation of candidate matrix materials and thermotropic additives with regard to thermal, thermo-mechanical and optical properties is carried out. In the second step appropriate combinations of candidate matrix materials and thermotropic additives are identified by assessment of refractive index match/mismatch. Based on this evaluation procedure promising TSFD are formulated and characterised as to light-shielding efficiency, switching characteristics and threshold temperature. Finally, a comprehensive characterisation of morphology (scattering domain size, shape, distribution) is carried out and structure-property-relationships are established. Based on these interrelationships optimisation potential of TSFD is deduced. These final steps (coloured grey) are addressed within the present paper. The preceding steps are already covered in a previous publication [17].

6.5 Characterisation of Morphology

6.5.1 Experimental

6.5.1.1 Materials and Sample Preparation

Three thermoplastic matrix materials (M1 to M3), four UV-curable resin systems (M4 to M7) and 13 different thermotropic additives (A1 to A11, A20 and A21) were utilised for formulation of TSFD. A detailed description of matrix materials and thermotropic additives is given in the preceding publication [17]. TSFD with thermoplastic matrix were manufactured at APC Advanced Polymer Compounds (Gai, AT) by melt blending on a compounder Coperion ZSK 26 Mcc (Coperion GmbH, Stuttgart, DE). From the compound 800 µm thick plates were obtained by compression moulding on a press P200PV (Dr. Collin GmbH, Ebersberg, DE). Thermotropic layers based on UV-curable resin matrix were prepared by dissolving the thermotropic additive in the

UV-crosslinkable matrix solution, which consisted of 57 wt% oligomers, 40 wt% reactive diluent and 3 wt% photo-initiator [17]. The dissolutions were poured in the intervening space between two glass panes which were sealed around the edge and stored at ambient temperature for 10 min allowing for precipitation of the additive. Afterwards the mixtures were cured by UV-radiation (dose: 2.1 J cm^{-2}) from a Light Hammer 6 equipped with a mercury-lamp and a LC6E Benchtop Conveyor (Fusion UV Systems Inc., Gaithersburg, MD, US). Free standing layers with a thickness of 900 µm were obtained after removal of the glass panes. TSFD based on UV-curable resin matrix were annealed at the mixing temperature of matrix solution and the corresponding additive. For both, thermoplastic and resin based TSFD, the theoretical additive concentration was 5 wt%. As to nomenclature, a system composed of Matrix M1 and Additive A1 is named M1A1 [17].

6.5.1.2 Characterisation Methodology

Morphological characterisation of TSFD was carried out applying optical light microscopy (LiMi) and scanning electron microscopy (SEM). Optical micrographs were obtained with an optical microscope Olympus BX51 (Olympus Austria Ges. m. b. H., Wien, AT) in transmitted light mode from TSFD without further preparation. Samples intended for scanning electron microscopy (SEM) were cut with a knife in order to achieve a fragment of approx. 14 mm $\times$ 5 mm $\times$ 0.9 mm. Fragment was fixed with a Plastic Specimen Support Clip (Buehler, Lake Bluff, IL, US), inserted in a beaker and embedded in a mixture of EpoThin Epoxy Resin and EpoThin Epoxy Hardener (Buehler, Lake Bluff, IL, US). After hardening, specimens were ground successively with different abrasive disks (P 600, P 1200, P 2400, P 4000) applying a force of 15 N under constant water flow in counter-rotating mode (200 rpm) on a grinder/polisher Phoenix Beta (Buehler, Lake Bluff, IL, US). Subsequently specimens were polished with MetaDi Monocrystalline Diamond Suspension on Polishing Cloth and with lubricant MetaDi Fluid, Dialub SW (Buehler, Lake Bluff, IL, US). Specimens were rinsed thoroughly with water between the individual grinding/polishing steps. Prior to imaging with SEM DSM 962 (Carl Zeiss SMT AG, Oberkochen, DE), the specimens were sputtered with gold.

Domain size was evaluated with measurement tools of software analySIS (Soft Imaging System GmbH, Münster, DE). Minimum and maximum of individual scattering domain dimensions were evaluated. Multiple determinations were carried out on a representative specimen for each TSFD. An increased number of specimens (up to three) were investigated for TSFD with inconsistent (i.e. divergence) switching behaviour detected by UV/Vis/NIR spectrophotometry.

6.5.2 Results

Figure 6.1

Figure 6.1 depicts the four prevalent scattering domain types detected for TSFD investigated within this study. SEM images are shown only due inappropriate contrast of optical micrographs for printing. Several TSFD exhibited spherical scattering domains. Additionally, some of these TSFD displayed significant gaps at the circumference (vacuoles) of the spherical scattering domains (Figure 6.1a,b). However, most of these vacuoles appeared rather like a dent in the additive domain than like a shell around the additive particle. Other TSFD showed scattering domains resembling plate-like features (Figure 6.1c,d). Furthermore, scattering domains resembling balls of filaments, thus named filament spheres, with a significant number of voids between the individual filaments were observed (Figure 6.1e,f). Other TSFD displayed structures characterised by individual branches originating from a central node and successive sub-branches, thus named dendrites (Figure 6.1g,h).

Table 6.1, 6.2

Table 6.1 and Table 6.2 summarise morphological features detected by optical light microscopy (LiMi) and SEM of different TSFD. If domains were detectable, their shape and size are stated, otherwise cells are left blank. Cells are partially left blank if one parameter was not detected by LiMi but by SEM or vice versa. Size parameters are divided in two dimensions in order to be able to handle non-spherical domains also. Dimension L_1 represents the major dimension of the scattering domain (e.g. diameter) whereas dimension L_2 is only valid for non-spherical scattering domains representing the minor dimension (e.g. thickness). Detected defects (e.g. vacuoles) are listed in a separate column. Table 6.1 summarises morphological features for TSFD with thermoplastic matrix material. TSFD M1A1, M1A2, M1A11, M2A2, M2A6, M2A11, M3A20 and M3A21 exhibited spherical scattering domains with diameters ranging between

0.31 and 123 µm. Moreover, micrographs revealed existence of vacuoles for layers M1A1, M1A2, M1A11, M2A2 and M2A6. For several TSFD the scattering domain sizes detected by LiMi and SEM differ significantly. On the one hand side, that may be attributed to higher accuracy of measurements in SEM images compared to optical light micrographs due to higher achievable magnification and thus higher resolution. This is especially relevant for small features. On the other hand side, that can be an indication for low uniformity of the layers. Certain regions in a TSFD might exhibit a higher concentration of specifically sized scattering domains than other regions.

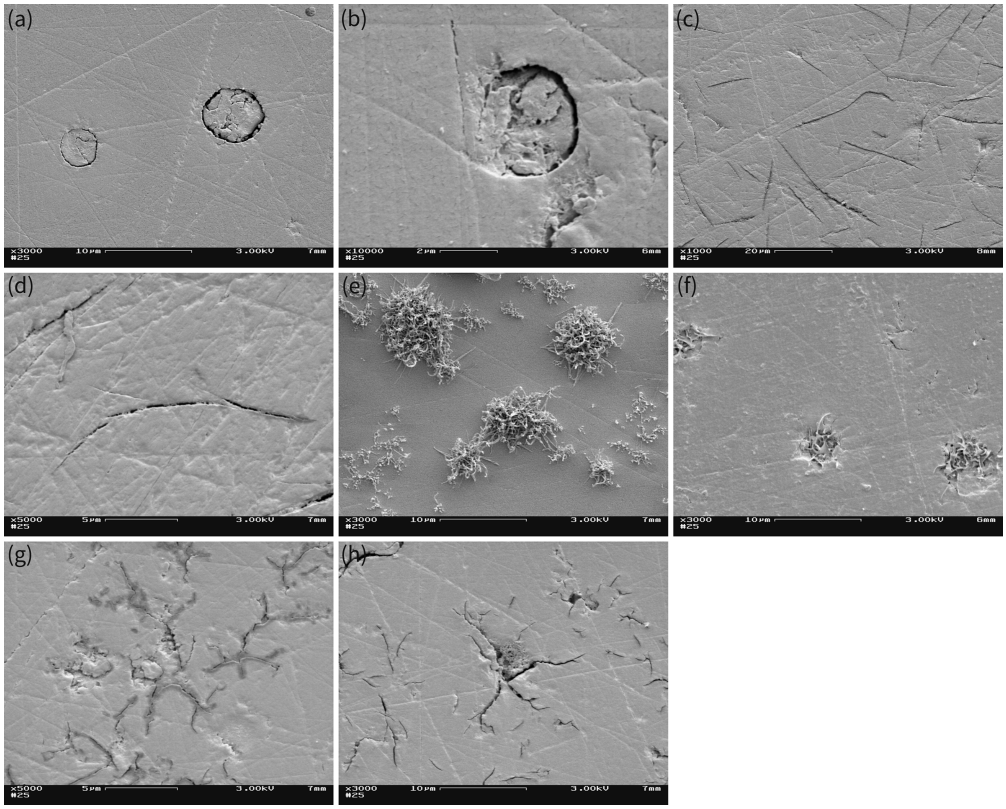

Figure 6.1.: Representative SEM micrographs of scattering domain shapes distinguished within this study: Spherical domains, with vacuoles from TSFD **(a)** M7A1 and **(b)** M5A2; plate-like domains from TSFD **(c)** M6A3 and **(d)** M4A3; filament spheres from TSFD **(e)** M5A7 and **(f)** M7A4; and dendrites from TSFD **(g)** M4A8 and **(h)** M7A8.

Table 6.2 summarises morphological features of TSFD with UV-curable resin matrix. TSFD M4A1, M4A2, M4A6, M4A8, M4A9, M5A1, M5A2, M5A6, M5A9, M6A1, M6A2, M7A1,

M7A2, M7A6 and M7A9 displayed spherical scattering domains with diameters in the range between 0.50 and 235 µm. Micrographs revealed existence of vacuoles for layers M4A1, M4A2, M4A6, M4A9, M5A1, M5A2, M5A6, M6A1, M6A2, M7A1 and M7A2. However, in M4A9 only one out of three samples displayed a significant number of vacuoles. Layers M4A3, M5A3, M6A3 and M7A3 exhibited plate-like scattering domains with diameters and thicknesses ranging from 3.24 to 75.5 µm and from 0.11 to 2.75 µm, respectively. In TSFD M5A3 persistent cracks were formed upon heating. TSFD M5A4, M5A7, M7A4 and M7A7 showed scattering domains resembling filament spheres with diameters between 0.59 and 133 µm and voids between the filaments. Thickness of the single filaments varied between 0.05 and 3.37 µm. Layers M4A5, M4A7, M4A8, M4A10, M5A5, M5A8, M5A10, M6A10, M7A5, M7A8 and M7A10 displayed dendritic scattering domains with diameters and thicknesses of branches varying from 0.5 to 48.9 µm and between 0.08 and 5.74 µm, respectively. Interestingly, for TSFD M4A8 two different scattering domain shapes – spheres and dendrites – were distinguished. None of the TSFD investigated exhibited optimal scattering domain shape and size for efficient overheating protection performance [18]. For several TSFD the scattering domain sizes detected by LiMi and SEM differ significantly. On the one hand side, that may be attributed to higher accuracy of measurements in SEM images compared to optical light micrographs due to higher achievable magnification and thus higher resolution. This is especially relevant for small features. On the other hand side, that can be an indication for low uniformity of the layers. Certain regions in a TSFD might exhibit a higher concentration of specifically sized scattering domains than other regions.

Table 6.1.: Shape of scattering domains, minima and maxima of dimensions L_1 (major dimension) and L_2 (minor dimension, if applicable) and detected defects of TSFD formulated with thermoplastic matrix materials.

Material	Shape of domains	Dim. $L_{1,\,min}$ [µm]		Dim. $L_{1,\,max}$ [µm]		Dim. $L_{2,\,min}$ [µm]		Dim. $L_{2,\,max}$ [µm]		Vacuoles
		LiMi	SEM	LiMi	SEM	LiMi	SEM	LiMi	SEM	
M1A1	Spheres	0.39	1.06	12.1	67.3	na	na	na	na	Vacuoles
M1A2	Spheres	0.41	3.25	13.3	32.3	na	na	na	na	Vacuoles
M1A11	Spheres	0.50	6.62	7.64	123	na	na	na	na	Vacuoles
M2A2	Spheres	0.44	1.90	30.8	13.5	na	na	na	na	Vacuoles
M2A6	Spheres	0.39	—	8.88	—	na	na	na	na	Vacuoles
M2A11	Spheres	0.59	—	5.30	—	na	na	na	na	
M3A20	Spheres	0.50	—	9.97	—	na	na	na	na	
M3A21	Spheres	0.31	—	8.85	—	na	na	na	na	

[na] not applicable

[–] not evaluable/not detectable

Table 6.2.: Shape of scattering domains, minima and maxima of dimensions L_1 (major dimension) and L_2 (minor dimension, if applicable) and detected defects of TSFD formulated with UV-curable resin matrix.

Material	Shape of domains	Dim. $L_{1,\,min}$ [µm]		Dim. $L_{1,\,max}$ [µm]		Dim. $L_{2,\,min}$ [µm]		Dim. $L_{2,\,max}$ [µm]		Vacuoles
		LiMi	SEM	LiMi	SEM	LiMi	SEM	LiMi	SEM	
M4A1	Spheres	0.84	2.55	194	235	na	na	na	na	Vacuoles
M4A2	Spheres	0.78	0.87	67.9	143	na	na	na	na	Vacuoles
M4A3	Plates	6.77	3.24	50.0	54.2	0.20	0.16	1.79	0.57	
M4A5	Dendrites	0.50	4.69	39.3	22.7	0.39	0.81	0.98	4.50	
M4A6	Spheres	0.50	1.04	65.8	32.1	na	na	na	na	Vacuoles
M4A7	Dendrites	13.7	7.38	48.9	23.5	0.44	1.01	1.27	3.92	
M4A8	Dendrites	—	3.47	—	15.2	—	0.08	—	0.35	
	Spheres	—	1.47	—	8.34	na	na	na	na	
M4A9	Spheres	6.47	—	158	—	na	na	na	na	Vacuoles
M4A10	Dendrites	13.3	13.1	28.9	30.7	0.50	1.1	1.79	2.72	
M5A1	Spheres	1.49	1.04	64.6	43.6	na	na	na	na	Vacuoles
M5A2	Spheres	1.71	2.04	55.2	22.3	na	na	na	na	Vacuoles
M5A3	Plates	8.04	7.02	65.3	75.5	0.20	0.25	2.75	1.91	Cracks
M5A4	Filament spheres [a]	4.85	2.93	54.5	56.1	—	0.18	—	0.55	Voids
M5A5	Dendrites	6.62	6.50	22.7	23.4	0.44	0.48	0.84	2.42	

Table 6.2.: continued

Material	Shape of domains	Dim. $L_{1, min}$ [µm]		Dim. $L_{1, max}$ [µm]		Dim. $L_{2, min}$ [µm]		Dim. $L_{2, max}$ [µm]		Vacuoles
		LiMi	SEM	LiMi	SEM	LiMi	SEM	LiMi	SEM	
M5A6	Spheres	0.74	1.40	52.2	31.2	na	na	na	na	Vacuoles
M5A7	Filament spheres [a]	0.59	3.97	17.6	23.9	—	0.07	—	3.37	Voids
M5A8	Dendrites	1.38	3.53	24.1	12.1	—	0.18	—	0.89	
M5A9	Spheres	7.41	12.2	40.5	45.6	na	na	na	na	
M5A10	Dendrites	7.95	5.45	17.0	16.1	0.39	0.71	1.00	1.74	
M6A1	Spheres	0.87	2.49	5.02	139	na	na	na	na	Vacuoles
M6A2	Spheres	2.07	1.88	7.95	3.83	na	na	na	na	Vacuoles
M6A3	Plates	6.47	4.06	52.1	44.0	0.62	0.11	2.23	1.12	
M6A10	Dendrites	9.66	9.52	20.9	25.3	0.59	0.88	1.85	5.74	
M7A1	Spheres	3.87	1.88	60.3	59.6	na	na	na	na	Vacuoles
M7A2	Spheres	0.93	0.93	58.0	2.92	na	na	na	na	Vacuoles
M7A3	Plates	10.8	6.26	69.1	46.0	0.59	0.17	2.48	1.59	
M7A4	Filament spheres [a]	2.07	13.8	133	94.4	—	0.17	—	1.08	Voids
M7A5	Dendrites	13.1	5.7	24.2	23.0	0.93	0.88	2.99	3.75	
M7A6	Spheres	0.59	8.19	42.3	40.3	na	na	na	na	
M7A7	Filament spheres [a]	7.18	1.22	50.5	37.6	0.39	0.05	1.31	0.30	Voids

Table 6.2.: continued

Material	Shape of domains	Dim. $L_{1, min}$ [µm]		Dim. $L_{1, max}$ [µm]		Dim. $L_{2, min}$ [µm]		Dim. $L_{2, max}$ [µm]		Vacuoles
		LiMi	SEM	LiMi	SEM	LiMi	SEM	LiMi	SEM	
M7A8	Dendrites	—	3.49	—	22.5	—	0.16	—	0.70	
M7A9	Spheres	13.3	12.1	45.0	62.2	na	na	na	na	
M7A10	Dendrites	15.2	3.48	28.7	29.6	1.17	0.58	2.34	2.55	

[a] spheres built up from filaments

[na] not applicable

[—] not evaluable/not detectable

6.6 Establishment of Structure-Property-Relationships

Figure 6.2 to 6.6

In Figures 6.2 to 6.6 average solar hemispheric (τ_{nh}; base colour white) and diffuse transmittance (τ_{nd}; base colour grey) investigated within this study are depicted for a temperature below (no pattern) and above (hatching pattern) the threshold temperature, respectively (Figurs 6.2a to 6.6a). Data originates from part I of this publication series [17]. Absolute refractive index difference of matrix material and thermotropic additive below (white column) and above the threshold temperature (hatched column) are also illustrated (Figures 6.2b to 6.6b). Unless otherwise is stated in general, for each of the TSFD discussed herein refractive index data theoretically indicate a reduction of solar hemispheric transmittance above the switching threshold [17]. Furthermore in Figures 6.2 to 6.6 observed domain shape is indicated by symbols ("O" spheres; "/" plates; "θ" filament spheres; "*" dendrites). The dimensions L_1 (diameter: O, /, θ, *; Figurs 6.2c to 6.6c) and L_2 (thickness of plate/filament/dendrite branch: /, θ, *; Figurs 6.2d to 6.6d) of these domains are represented by floating columns. Size ranges of scattering domains detected by optical microscopy (no pattern) and SEM (hatching pattern) are displayed separately. Optimum diameter range of spherical scattering domains is bounded by dashed lines. For clarity reasons, in the following layers displaying the same domain shape are grouped for discussion: Structure-property-relationships of TSFD exhibiting scattering domains with appropriate shape for optimum light-shielding efficiency (spherical) are discussed in the first place for each figure. Subsequently, structure-property-relationships of TSFD displaying scattering domains with inappropriate shape for efficient overheating protection performance (plate-like domains, filament spheres, dendrites) are discussed.

Figure 6.2

Figure 6.2 represents parameters indicated above for TSFD with thermoplastic matrix material. For these TSFD merely spherical scattering domains ("O") were observed. Spherical scattering domains of TSFD M1A1, M1A2, M1A11, M2A2 and M2A6 exhibited diameters hardly in the optimum range between 200 and 400 nm for efficient light-shielding performance and vacuoles at their perimeter (interface matrix/additive). Vacuole formation may be attributed to different coefficient of thermal expansion (CTE) of matrix material and additive. The CTE of PMMA and paraffin for example are in the range of 6–8 $\times$ 10^{-5} K^{-1} and 0.7–1.1 $\times$ 10^{-3} K^{-1}, respectively [19], [20]. The

higher CTE of paraffin forced the embedded additive to contract more intense than the surrounding matrix PMMA upon cooling during manufacturing, thus yielding formation of vacuoles when implying limited adhesion at the interface matrix/additive [17], [21], [22]. All of these layers displayed an increase in solar hemispheric and diffuse transmittance upon heating.

Morphological investigations now confirm assumptions concerning relations between increase in solar hemispheric transmittance and the presence of vacuoles [17]. Dimensions of dent-like vacuoles were theoretically equal (maximum) to or smaller than the size of the cavity provided by the matrix. Accordingly the rest of the cavity was filled with additive. Shell-like vacuoles theoretically had the same diameter as their respective matrix cavities but were larger than the corresponding additive domain inside the cavity. However, thickness of the shell-like vacuoles was low compared to diameter. Thus, a virtual (envisaged) vacuole size distribution probably showed a significantly lower minimum and mean and a slightly higher maximum compared to the additive domain size distribution. Virtually merging these two size distributions in a thought experiment yielded a broad “virtual” size distribution of scattering domains. The high difference in refractive index of matrix material (n approx. 1.5) and vacuole (n=1) along with smaller size of vacuoles compared to additive domains resulted in intense scattering and hence low solar hemispheric transmittance at room temperature [17]. On the contrary, the refractive index difference of matrix and additive below the switching threshold was negligible. Thus, effect of additive domains on forward scattering intensity was low, yielding low solar diffuse transmittance. Upon heating and especially upon melting the additive expanded and filled the cavity completely, yielding a decrease in refractive index difference at the scattering interface. Moreover, the virtual size distribution narrowed upon disappearance of the vacuoles and thus was identical with the actual size distribution of the additive domains. Thus, mean value of scattering domain size was also shifted to higher values. In general, solar hemispheric transmittance gained from a decrease in refractive index difference due to a reduction of overall scattering performance. An isolated increase in scattering domain size increased anisotropy of scattering field yielding reduced back-scattering and increased forward-scattering efficiency. Accordingly, a simultaneous reduction of refractive index difference along with an increase in scattering domain size reduced

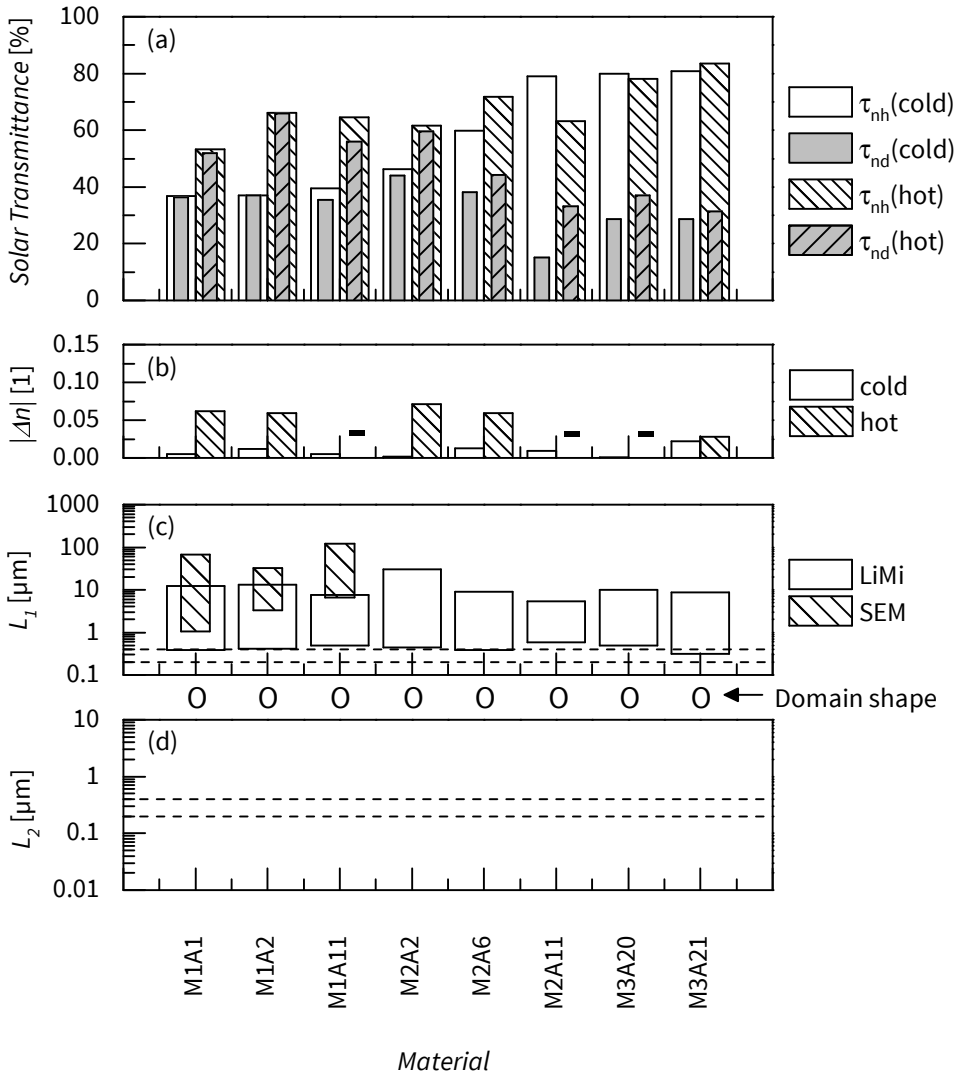

Figure 6.2.: (a) Solar hemispheric (τ_{nh}; base colour white) and solar diffuse transmittance (τ_{nd}; base colour grey) of TSFD formulated with thermoplastic matrix material below (no pattern) and above (hatching pattern) the threshold temperature (data from part I [17]). **(b)** Refractive index difference of matrix and additive below (no pattern) and above (hatching pattern) the threshold temperature. Omitted values are indicated by "—". Observed scattering domain shapes indicated with symbols ("O" spheres) and their respective dimensions **(c)** L_1 (diameter) and **(d)** L_2 (if applicable, thickness of plates/filaments/dendrite branches) detected by optical light microscopy (LiMi; no pattern) and SEM (hatching pattern). Optimum scattering domain size range for spherical scattering domains is bounded by dashed lines.

the overall scattering performance of the TSFD and made the scattering field more anisotropic. Thus solar hemispheric transmittance increased upon heating. An increase in scattering field anisotropy did not necessarily yield an increase in solar diffuse transmittance. Especially for non-spherical scattering domain effects of geometry and potential domain internal boundaries (e.g. voids inside the additive domain) might be rather complex, either yielding an increase or a decrease in solar diffuse transmittance. However, the effect of vacuoles on switching characteristics of TSFD is going to be addressed as "effect of the temporary vacuoles" within this study.

In contrast, for layers displaying spherical scattering domains with inappropriate size for efficient light-shielding performance but lacking vacuoles a rather moderate reduction of solar hemispheric transmittance was expected upon heating. Simultaneously an increase in solar diffuse transmittance was anticipated. Nevertheless, this required a sufficient increase in refractive index difference between matrix and additive to be established upon heating. A prominent example for consistency of these predictions is TSFD M2A11, which showed spherical scattering domains with inappropriate diameter. Thus, the layer exhibited merely a moderate reduction of solar hemispheric transmittance upon exceeding the threshold temperature, along with an increase in solar diffuse transmittance. Although refractive index difference above the threshold temperature (75 °C [17]) is not stated due to experimental reasons (for details refer to WEBER AND RESCH [17]), observed switching characteristics implied an increase of refractive index difference upon switching. The lack of vacuoles within this TSFD may be attributed to the capability of amide-groups of matrix M2 and epoxy-moieties of A11 to form covalent bonds. Spherical scattering domains with inappropriate size for efficient light-shielding performance were detected for layers M3A20 and M3A21. Only minor changes in solar hemispheric transmittance were obtained for these TSFD along with a slight increase in solar diffuse transmittance. Refractive index difference of layer M3A20 is not stated for temperatures above the switching temperature (80 °C [17]) due to experimental reasons [17]. However, negligible reduction of solar hemispheric transmittance implied only minor changes in refractive index difference. Layer M3A21 displayed a smooth change in transmittance rather than distinct switching [17]. This was attributed to insufficient change in refractive index difference.

For layers based on thermoplastic resin matrix, the observation of solely spherical scattering domains for non-polar thermotropic additives like paraffin waxes (A1, A2) on the one hand side as well as for rather polar additives with maleic anhydride moieties (A11) on the other hand side was detected. That leads to the conclusion that establishment of TSFD morphology for these systems was governed by system rheology: In emulsions, spheres or ellipsoids are the prevalent droplet shapes [23].

Figure 6.3 represents parameters indicated above for TSFD with UV-curable matrix material M4. Observed domain shapes were spheres (“O”), plate-like domains (“/”) and dendrites (“*”). Spherical scattering domains with inappropriate diameter for efficient light-shielding performance and with vacuoles at their perimeter (interface matrix/additive) were detected for TSFD M4A1, M4A2 and M4A6. Vacuole formation was ascribed to processing effects [17]: Mixtures of UV-curable resin and thermotropic additive were exposed to UV-radiation yielding crosslinking reaction in the matrix and heating up of the mixture due to absorption [17]. Upon cooling during manufacturing its higher CTE forced the embedded additive to contract more intensively than the surrounding matrix material, thus yielding formation of vacuoles when implying limited adhesion at the interface matrix/additive [17], [21], [22]. Layers M4A1, M4A2 and M4A6 displayed an increase in solar hemispheric and diffuse transmittance upon exceeding the threshold temperature. This was attributed to vacuoles rather than to inappropriate scattering domain size, as already described above. *Figure 6.3*

Spherical scattering domains with inappropriate size for efficient light-shielding performance were detected for TSFD M4A9. Samples one and two of these TSFD displayed a negligible concentration of vacuoles. However, sample three displayed a significant concentration of vacuoles. Samples one, two and three displayed solar hemispheric transmittance of approx. 81 % (one, two) and approx. 62 % (three) at room temperature, respectively, resulting in high standard deviation of mean transmittance [17]. The foremost samples attained a decrease of solar hemispheric transmittance to approx. 76 % upon heating, whereas solar hemispheric transmittance of the latter sample increased to approx. 75 %. Low solar hemispheric transmittance at room temperature and its increase for sample three were attributed to significant concentration of vacuoles. For samples one and two the increase in solar diffuse transmittance upon heating was attributed to inappropriate size of scattering domains. Solar diffuse

transmittance increase in sample three was ascribed to the effect of temporary vacuoles. A specific reason for selective formation of a high number of vacuoles in sample three was not identified, because all layers were produced simultaneously.

Plate-like domains with inappropriate diameter but almost optimum thickness for efficient light-shielding performance were detected for TSFD M4A3, yielding a moderate reduction of solar hemispheric transmittance and an increase in solar diffuse transmittance upon exceeding the threshold temperature. Dendritic scattering domains with inappropriate diameter and thickness of dendrite branches for efficient overheating protection performance were evident for layers M4A5, M4A7 and M4A10. Thus, solar hemispheric transmittance remained almost unchanged (insignificant change [17]) upon heating whereas solar diffuse transmittance increased. TSFD M4A8 displayed scattering domains with spherical and dendritic shape, exhibiting inappropriate diameters for efficient light-shielding. However, thickness of dendrite branches was almost optimum for back-scattering. Hence, a slight reduction of solar hemispheric transmittance was ascertained upon heating along with an increase in solar diffuse transmittance.

Figure 6.4

Figure 6.4 represents parameters indicated above for TSFD with UV-curable matrix material M5. Observed domain shapes were spheres (“O”), plate-like domains (“/”), filament spheres (“θ”) and dendrites (“*”). Spherical scattering domains with inappropriate size for optimum light-shielding and with vacuoles at their perimeter (interface matrix/additive) were detected for TSFD M5A1, M5A2 and M5A6. Layers M5A1 and M5A2 displayed an increase of solar hemispheric and diffuse transmittance upon heating due to effects resulting from vacuoles as already described above (effect of the temporary vacuoles). On the contrary solar hemispheric transmittance of layer M5A6 remained almost unchanged upon heating probably due to concentration effects (lower number of vacuoles yielded a vacuole effect of minor extent). Solar diffuse transmittance of TSFD M5A6 also increased upon heating. This was primarily attributed to inappropriate scattering domain size. TSFD M5A9 displayed spherical scattering domains with inappropriate diameter for efficient light-shielding performance, yielding a minor reduction in solar hemispheric transmittance along with an increase in solar diffuse transmittance upon heating.

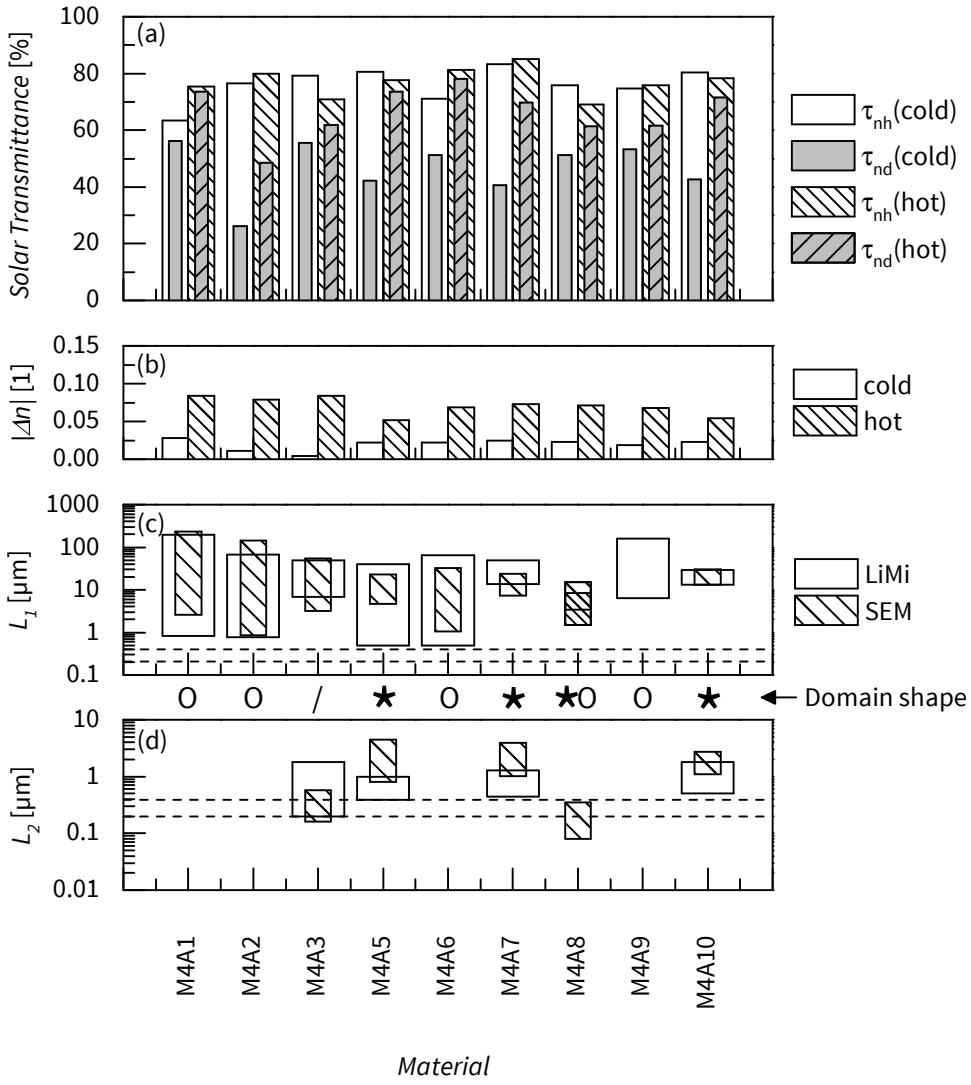

Figure 6.3.: (a) Solar hemispheric (τ_{nh}; base colour white) and solar diffuse transmittance (τ_{nd}; base colour grey) of TSFD with UV-curable matrix material M4 below (no pattern) and above (hatching pattern) the threshold temperature (data from part I [17]). **(b)** Refractive index difference of matrix and additive below (no pattern) and above (hatching pattern) the threshold temperature. Observed scattering domain shapes indicated with symbols ("O" spheres; "/" plates; "*" dendrites) and their respective dimensions **(c)** L_1 (diameter) and **(d)** L_2 (if applicable, thickness of plates/filaments/dendrite branches) detected by optical light microscopy (LiMi; no pattern) and SEM (hatching pattern). Optimum scattering domain size range for spherical scattering domains is bounded by dashed lines.

Plate-like domains with inappropriate diameter but almost optimal thickness for efficient light-shielding performance were evident for TSFD M5A3. However, investigations revealed incoherent switching behaviour of the three samples investigated [17]. One sample displayed a decrease of solar hemispheric transmittance upon heating along with an increase in solar diffuse transmittance. The onset of the observed decrease in solar hemispheric transmittance of sample one at 55 °C corresponds with the melting of the additive [17]. However, after cooling to room temperature, solar hemispheric and diffuse transmittance was lower and higher than in initial state (before heating), respectively. Maybe cracks (vacuum inside, refractive index 1) formed during measurement process acted as additional scattering domains [17], thus increasing scattering volume. As a consequence low solar hemispheric transmittance and high solar diffuse transmittance was attained. In contrast, two other samples of layer M5A3 displayed a moderate increase of solar hemispheric transmittance upon heating along with a distinct reduction of solar diffuse transmittance. However, after cooling to room temperature, solar hemispheric and diffuse transmittance was lower and higher than in initial state (before heating), respectively, which was attributed to cracks as described above.

Regarding the crack formation process, only a hypothesis was established. Upon melting of the thermotropic additive, solar hemispheric transmittance of sample decreased due to melting and probably due to solubilisation of additive molecules in the matrix. Due to concentration gradients of additive molecules, they started to diffuse inside the matrix. These molecules probably filled the free space close to the molecule chains of the matrix, yielding inability of these molecule chains to move unhindered (anti-plasticiser effect). The constraint of molecular movement probably yielded the inability to relax thermally induced stress upon increasing temperature, hence yielding crack formation. This corresponds with the continuous decrease in solar hemispheric transmittance of sample one up to 115 °C (increment 5 °C). In contrast, solar transmittances of samples two and three were detected at room temperature and 115 °C only. Thus, time for migration of molten additive was very short, yielding less progress of crack formation process. This corresponds with the observation of small hazy areas evident in samples two and three, whereas sample one displayed large hazy areas and distinct cracks [17].

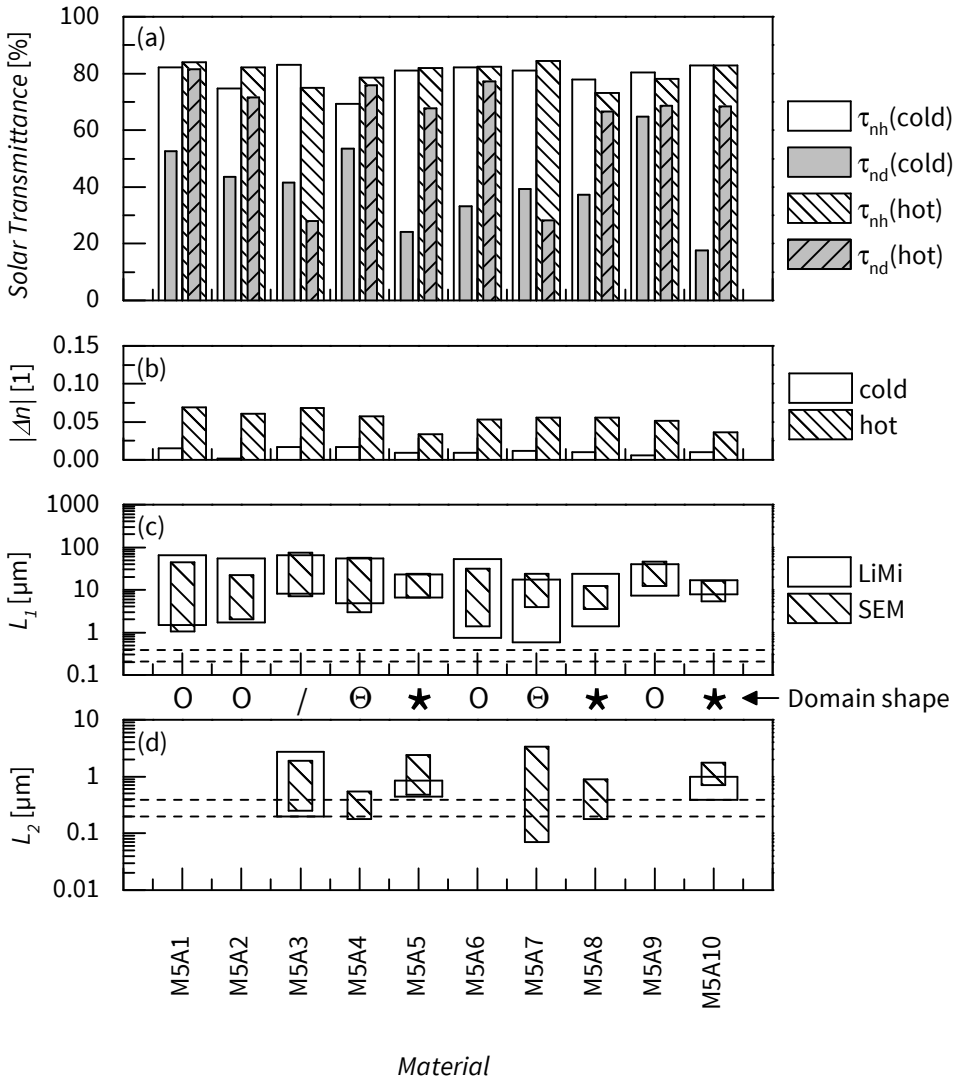

Figure 6.4.: (a) Solar hemispheric (τ_{nh}; base colour white) and solar diffuse transmittance (τ_{nd}; base colour grey) of TSFD with UV-curable matrix material M5 below (no pattern) and above (hatching pattern) the threshold temperature (data from part I [17]). **(b)** Refractive index difference of matrix and additive below (no pattern) and above (hatching pattern) the threshold temperature. Observed scattering domain shapes indicated with symbols (“O” spheres; “/” plates; “θ” filament spheres; “*” dendrites) and their respective dimensions **(c)** L_1 (diameter) and **(d)** L_2 (if applicable, thickness of plates/filaments/dendrite branches) detected by optical light microscopy (LiMi; no pattern) and SEM (hatching pattern). Optimum scattering domain size range for spherical scattering domains is bounded by dashed lines.

Micrographs of TSFD M5A4 and M5A7 revealed spherical scattering domains built from filaments. The diameters of these domains were inappropriate for optimum back-scattering. Thickness of the filaments was detected to be almost optimal for efficient light-shielding. However, between these filaments, voids were observed. Voids were assumed to act in the same manner as vacuoles. Thus, the ascertained increase of solar hemispheric transmittance of layers M5A4 and M5A7 was attributed to voids (effect of the temporary vacuoles/voids). Solar diffuse transmittance of TSFD M5A4 increased upon heating. In contrast, solar diffuse transmittance of M5A7 decreased upon switching. Divergence in change of solar diffuse transmittance of layers M5A4 and M5A7 is most likely due to effects of scattering domain geometry (e.g. slight differences in void concentration or distribution), yielding different scattering performance of the filament spheres. However, formation of voids seemed to be due to physico-chemical interaction (nucleation, surface tension, etc.) of matrix material and thermotropic additive. If it was an additive related effect solely, layer M4A7 would have shown filament spheres also. Layers formulated with UV-curable matrix M4 contracted more upon exposure to UV-radiation compared to layers formulated with matrices M5, M6 and M7. Stronger contraction of the matrix likely introduced higher internal stress in the layer. Hence, high internal stress probably forced the additive to crystallise in filament sphere shape rather than in dendritic shape as in TSFD M5A7 and M7A7.

Dendritic scattering domains with inappropriate diameter for light-shielding purposes were detected for TSFD M5A5, M5A8 and M5A10. Whereas thickness of dendrite branches of layers M5A5 and M5A10 was detected to be inadequate for efficient light scattering it was almost optimal for M5A8. Thus, TSFD M5A8, in contrast to layers M5A5 and M5A10, exhibited a highly significant reduction in solar hemispheric transmittance [17]. Solar diffuse transmittance of layers M5A5, M5A8 and M5A10 increased due to inappropriate diameter of dendrites.

Figure 6.5

Figure 6.5 represents parameters indicated above for TSFD with UV-curable matrix material M6. Observed domain shapes were spheres (“O”), plate-like domains (“/”) and dendrites (“*”). TSFD M6A1 and M6A2 displayed spherical scattering domains with inappropriate size for optimum light-shielding efficiency and with vacuoles at their perimeter (interface matrix/additive). The achieved increase in solar hemispheric

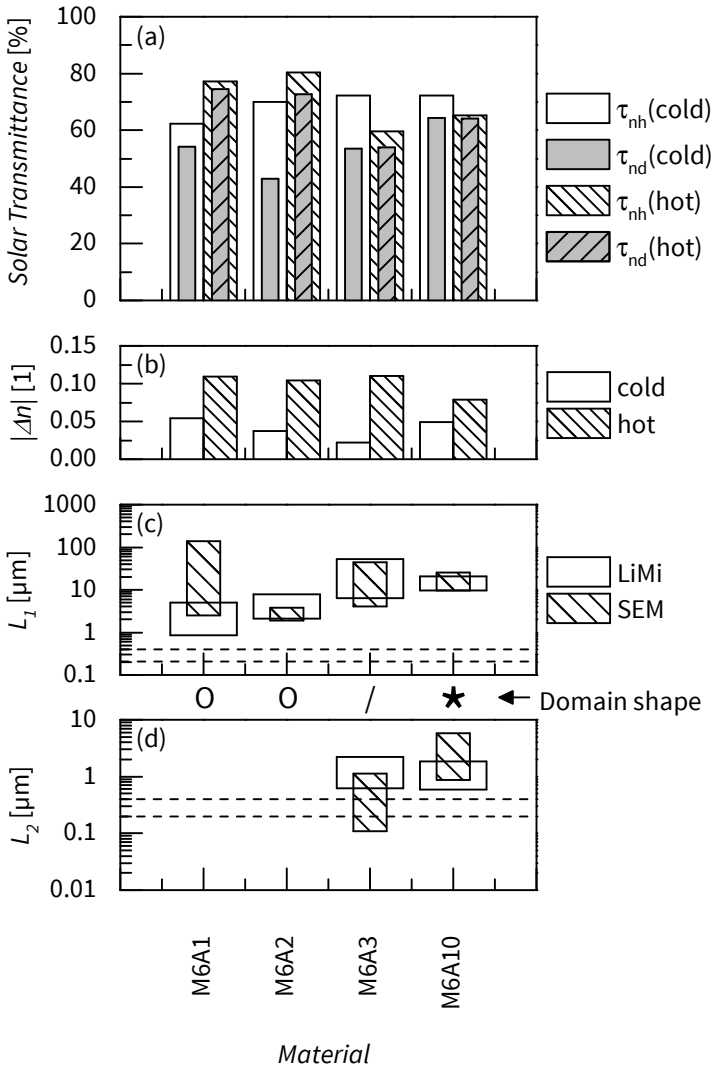

Figure 6.5.: (a) Solar hemispheric (τ_{nh}; base colour white) and solar diffuse transmittance (τ_{nd}; base colour grey) of TSFD with UV-curable matrix material M6 below (no pattern) and above (hatching pattern) the threshold temperature (data from part I [17]). **(b)** Refractive index difference of matrix and additive below (no pattern) and above (hatching pattern) the threshold temperature. Observed scattering domain shapes indicated with symbols ("O" spheres; "/" plates; "*" dendrites) and their respective dimensions **(c)** L_1 (diameter) and **(d)** L_2 (if applicable, thickness of plates/filaments/dendrite branches) detected by optical light microscopy (LiMi; no pattern) and SEM (hatching pattern). Optimum scattering domain size range for spherical scattering domains is bounded by dashed lines.

and diffuse transmittance was ascribed to the effect of the temporary vacuoles. Micrographs of layer M6A3 revealed plate-like domains with inappropriate diameter but almost optimal thickness for efficient back-scattering. Thus a significant reduction of solar hemispheric transmittance was ascertained upon heating. Solar diffuse transmittance of layer M6A3 remained almost constant upon exceeding the threshold temperature. However, the ratio of solar diffuse to solar hemispheric transmittance increased upon switching, which was attributed to the suboptimal scattering domain diameter.

Thickness of branches and diameter of dendrites observed for TSFD M6A10 were detected to be inappropriate for optimal back-scattering. Hence, merely a slight reduction of solar hemispheric transmittance was ascertained. The solar diffuse transmittance of layer M6A10 remained almost unchanged. Due to the increasing ratio of solar diffuse to solar hemispheric transmittance – similar to the observations for layer M6A3 – again an increase in overall scattering efficiency and especially forward scattering was evident. This was attributed to the low thickness of dendrite branches and high diameter of dendrites, respectively.

Figure 6.6

Figure 6.6 represents parameters indicated above for TSFD with UV-curable matrix material M7. Observed domain shapes were spheres (“O”), plate-like domains (“/”), filament spheres (“θ”) and dendrites (“*”). Spherical scattering domains with inappropriate diameter for optimal light-shielding performance were detected for TSFD M7A1 and M7A2. Micrographs revealed vacuoles in these layers. Thus, these layers displayed an increase of solar hemispheric and diffuse transmittance upon heating due to the effect of the temporary vacuoles. Spherical scattering domains with inappropriate diameter were evident for layers M7A6 and M7A9. TSFD M7A6 exhibited no vacuoles. Nevertheless, solar hemispheric transmittance change upon heating was insignificant [17]. According to the inappropriate scattering domain diameter, solar diffuse transmittance increased upon switching. Although scattering domain size was inappropriate for optimum back-scattering in TSFD M7A9, a slight decrease of solar hemispheric transmittance was detected upon heating. Accordingly, solar diffuse transmittance increased significantly.

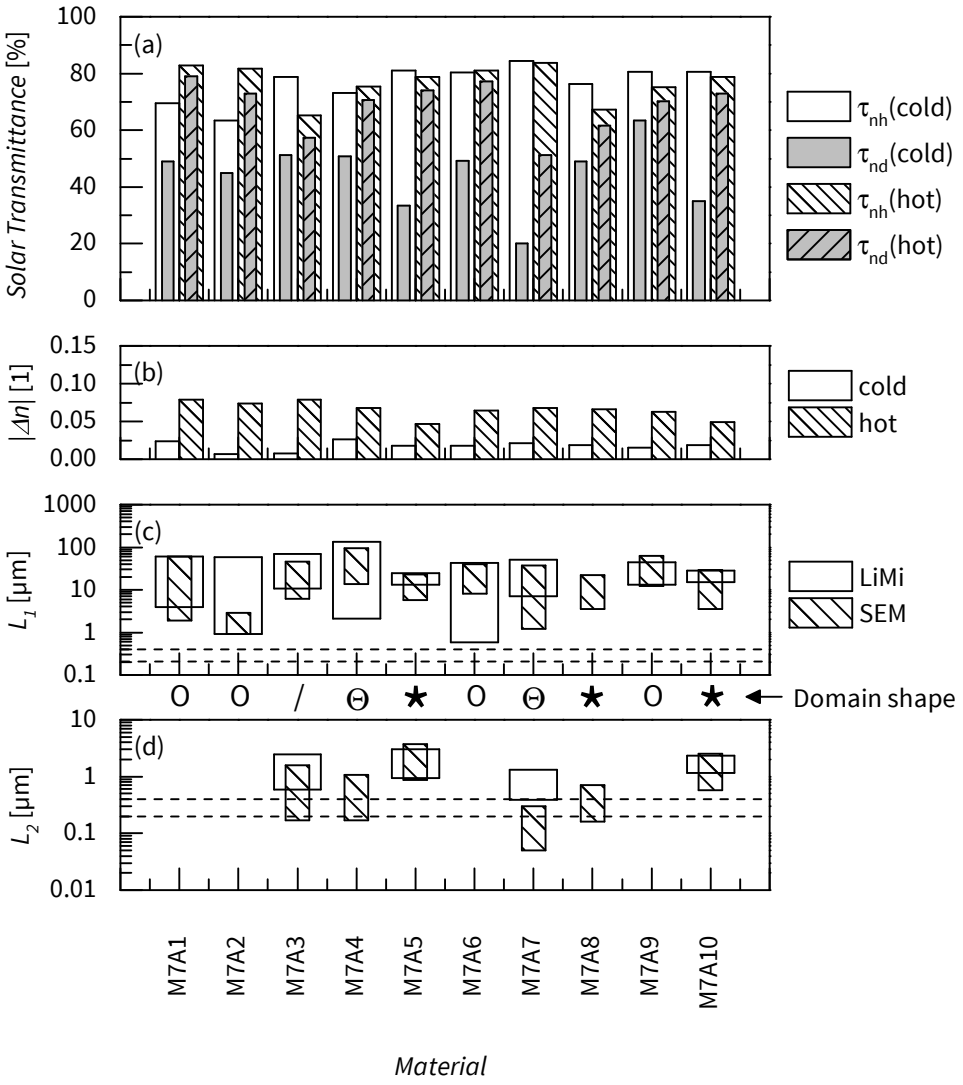

Figure 6.6.: (a) Solar hemispheric (τ_{nh}; base colour white) and solar diffuse transmittance (τ_{nd}; base colour grey) of TSFD with UV-curable matrix material M7 below (no pattern) and above (hatching pattern) the threshold temperature (data from part I [17]). **(b)** Refractive index difference of matrix and additive below (no pattern) and above (hatching pattern) the threshold temperature. Observed scattering domain shapes indicated with symbols ("O" spheres; "/" plates; "θ" filament spheres; "*" dendrites) and their respective dimensions **(c)** L_1 (diameter) and **(d)** L_2 (if applicable, thickness of plates/filaments/dendrite branches) detected by optical light microscopy (LiMi; no pattern) and SEM (hatching pattern). Optimum scattering domain size range for spherical scattering domains is bounded by dashed lines.

Almost optimal thickness of plate-like domains for efficient overheating protection performance provided a reduction of solar hemispheric transmittance for layer M7A3 upon exceeding the threshold temperature. However, diameter of plates was inappropriate for efficient back-scattering. Thus, solar diffuse transmittance increased upon heating. Micrographs of TSFD M7A4 and M7A7 revealed spherical scattering domains built from filaments. The diameters of these domains were inappropriate for optimum light-shielding whereas the thickness of the filaments was almost optimal. However, between these filaments, voids were observed. Voids were assumed to act in the same manner as vacuoles. Thus, the increase of solar hemispheric transmittance of layer M7A4 was attributed to these voids (effect of the temporary vacuoles). Despite existence of voids, layer M7A7 showed a slight reduction in solar hemispheric transmittance. That might be attributed to a lower concentration of voids, thus yielding a mitigated effect on solar hemispheric transmittance. Both layers displayed an increase in solar diffuse transmittance due to the effect of the temporary vacuoles/voids as already described above. Dendritic scattering domains with inappropriate diameter for back-scattering were recorded for layers M7A5, M7A8 and M7A10. Thickness of branches of dendrites was detected to be appropriate for efficient light-shielding in layer M7A8 solely. Thus, out of these three TSFD, layer M7A8 displayed a significant reduction of solar hemispheric transmittance upon heating solely [17]. The increase in solar diffuse transmittance was attributed to the inappropriate scattering domain size.

For TSFD formulated with UV-curable resin matrix, these findings may lead to the conclusion that thermotropic additives exhibiting only little or almost no polar groups like paraffin waxes (A1, A2) or montan wax (A9) were not able to solubilise in the matrix resin upon melting due to the lack of interaction with the matrix (e.g. lack of hydrogen bonding). Consequently, the high interfacial tension established between matrix and additive forced the additive to form spheres in order to reduce overall interfacial forces. On the contrary, for more polar substances like fatty acids and fatty acid esters (with shorter non-polar section compared to e.g. paraffin waxes or montan wax) polar interaction forces were effectual in order to maintain solubilisation of – at least significant fractions of – thermotropic additive upon melting of the additive. Upon cooling of the cast mixture of resin matrix and thermotropic additive prior to curing

process, these thermotropic additives were forced to crystallise. Crystallisation led to separation of additive from the resin matrix yielding two phase morphology. This transition from a solubilised/liquid to a non-solubilised/solid state was effectual to establish non-spherical scattering domains. This was ascribed to the lack of viscous forces governing the additive droplet shape in the liquid state because there were no liquid additive droplets. In general, the spherical shape is usually in favour compared to other particle shapes due to its low surface/volume-ratio reducing interfacial forces compared to non-spherical shape of particles. Instead, crystallisation of rather polar additives and thus domain form was governed by crystallographic alignment (predominant crystal form) of the thermotropic additives rather by viscous forces.

Summarising, inappropriate scattering domain shape and/or size decreased solar hemispheric transmittance reduction upon heating and thus attenuated overheating protection performance of TSFD. This is according to scattering theory [18], [24]. Defects (vacuoles, voids) resulting from processing yielded increasing solar hemispheric transmittance upon exceeding the threshold temperature (effect of temporary vacuoles). This is attributable to intense scattering at the boundary of matrix and scattering domain (matrix/vacuum interface), which is reduced upon melting of the additive.

6.7 Conclusion

Provided that refractive index data are appropriate, structure-property-relationships established in section 6.6 yielded two major requirements for producing thermotropic systems with fixed domains (TSFD) with enhanced overheating protection performance:

- Prevention of defects (vacuoles, voids)
- Optimisation of scattering domain shape and size by maintaining spherical scattering domains with diameters between 200 and 400 nm.

Vacuole formation in TSFD with thermoplastic matrix upon manufacturing was ascribed to different coefficient of thermal expansion (CTE) of matrix and additive combined

with limited adhesion at the matrix/additive interface. Reducing the effect of thermal expansion by lowering processing temperature is not feasible due to processing reasons. Thus, vacuole formation in these TSFD might be prevented merely by adhesion promotion via covalent bonds between reactive moieties of matrix and additive [19], [25]–[28]. TSFD M2A11 of this study is a prominent example for the potential of this approach.

In TSFD formulated with UV-curable resin matrix vacuole formation was ascribed to thermo-mechanical effects of different CTE of matrix and additive due to heat generation upon irradiation, cross-linking reaction and limited adhesion at the interface matrix/additive. In acrylate-based systems covalent bonds between matrix and additive cannot be achieved by introduction of epoxy or maleic-anhydride grafts. Hence, reduction of heat generation seems more feasible. Reduction of heat generation requires lowering absorbed energy by reducing the intensity and dose of UV-radiation. Investigations by RESCH AND CO-WORKERS [9], [11] suggest viability of this approach. TSFD with similar UV-curable resin matrix and paraffin-type additive were produced by curing with low intensity UV-radiation. The samples lacked vacuoles and displayed a reduction of solar hemispheric transmittance upon exceeding the threshold temperature [8], [9], [11], [16].

Strategies for optimising scattering domain size and shape can be deduced from scientific literature in related fields. Smaller scattering domains might result from increasing number of crystallisation nuclei (i.e. addition of nucleating agent) similar to achieved spherulite size reduction in polymers [29], [30]. Heterogeneous nucleation in phase change materials is not only induced by “classical” nucleating agents but also by surfactants [31]–[34]. Surfactants might also change droplet size in emulsions of matrix materials and thermotropic additives during processing [35]. Nucleating agents and surfactants might also influence the shape of the scattering domains by changing matrix/additive interactions.

Another approach to maintain controlled size and shape of scattering domains is encapsulation of additives [36], [37]. Simultaneously vacuole formation may be prevented when incorporating these capsules in a matrix material at temperatures

close to ambient conditions. To the best of our knowledge Muehling et al. [12] were the first to apply this technique for TSFD formulation.

With respect to the optimisation strategies regarding manufacturing process and TSFD formulation already pointed out, the optimisation potential of TSFD formulated so far is considered to be high.

6.8 Acknowledgements

This research project is funded by the State Government of Styria, Department Zukunftsfonds (Project number 5019). The efforts in determination of solar-optical properties of parts of the formulated TSFD by Astrid Rauschenbach (Polymer Competence Center Leoben GmbH, Leoben, AT (PCCL)), valuable input regarding scattering processes and scattering theory by Dieter P. Gruber (PCCL), support concerning UV equipment by Sandra Schlögl (PCCL) and compounding of materials with thermoplastic matrix by Karl Schnetzinger (APC Advanced Polymer Compounds, Gai, AT) are gratefully acknowledged. Furthermore, the authors wish to acknowledge the contributions of Arkema GmbH (Düsseldorf, DE), Baerlocher GmbH (Unterschleissheim, DE), Bayer Materials Science AG (Leverkusen, DE), Biesterfeld Interowa GmbH & Co. KG (Wien, AT), Brenntag CEE GmbH (Traun, AT), Chemson Polymer Additive AG (Arnoldstein, AT), Allnex Belgium SA/NV (formerly Cytec Surface Specialities Inc.; Drogenbos, BE), DuPont de Nemours (Deutschland) GmbH (Neu-Isenburg, DE), Evonik Degussa GmbH, High Performance Polymers (Marl, DE), Evonik Röhm GmbH (Darmstadt, DE), HDS-Chemie HandelsgesmbH (Wien, AT), Sasol Wax GmbH (Hamburg, DE) and Senoplast Klepsch GmbH (Piesendorf, AT).

6.9 References

[1] J. Yao and N. Zhu, 'Evaluation of indoor thermal environmental, energy and daylighting performance of thermotropic windows', *Building and Environment*, vol. 49, pp. 283–290, 2012, ISSN: 03601323. DOI: 10.1016/j.buildenv.2011.06.004.

[2] G. M. Wallner, K. Resch and R. Hausner, 'Property and performance requirements for thermotropic layers to prevent overheating in an all polymeric flat-plate collector', *Solar Energy Materials and Solar Cells*, vol. 92, no. 6, pp. 614–620, 2008, ISSN: 09270248. DOI: 10.1016/j.solmat.2007.12.005.

[3] P. Nitz and A. Wagner, 'Schaltbare und regelbare Verglasungen', *BINE Themeninfo*, vol. I/02, no. I/02, pp. 1–12, 2002, ISSN: 1610-8302.

[4] P. Nitz and H. Hartwig, 'Solar control with thermotropic layers', *Solar Energy*, vol. 79, no. 6, pp. 573–582, 2005, ISSN: 0038092X. DOI: 10.1016/j.solener.2004.12.009.

[5] A. Seeboth, J. Schneider and A. Patzak, 'Materials for intelligent sun protecting glazing', *Solar Energy Materials and Solar Cells*, vol. 60, no. 3, pp. 263–277, 2000, ISSN: 09270248. DOI: 10.1016/S0927-0248(99)00087-2.

[6] K. Resch and G. M. Wallner, 'Thermotropic Resin Systems: Relationships Between Formulation Parameters, Material Structure and Optical Properties', in *Proceedings of ISES Solar World Congress 2007*, D. Y. Goswami and Y. Zhao, Eds., Berlin: Springer, 2007, pp. 541–545, ISBN: 978-3-540-75996-6. DOI: 10.1007/978-3-540-75997-3_98.

[7] K. Resch and G. M. Wallner, 'Thermotropic layers for flat-plate collectors—A review of various concepts for overheating protection with polymeric materials', *Solar Energy Materials and Solar Cells*, vol. 93, no. 1, pp. 119–128, 2009, ISSN: 09270248. DOI: 10.1016/j.solmat.2008.09.004.

[8] K. Resch and G. M. Wallner, 'Morphology of phase-separated thermotropic layers based on UV cured acrylate resins', *Polymers for Advanced Technologies*, vol. 20, no. 12, pp. 1163–1167, 2009, ISSN: 10427147. DOI: 10.1002/pat.1393.

[9] K. Resch, G. M. Wallner and R. Hausner, 'Phase separated thermotropic layers based on UV cured acrylate resins – Effect of material formulation on overheating protection properties and application in a solar collector', *Solar Energy*, vol. 83, no. 9, pp. 1689–1697, 2009, ISSN: 0038092X. DOI: 10.1016/j.solener.2009.06.006.

[10] K. Resch, G. M. Wallner and R. W. Lang, 'Spectroscopic Investigations of Phase-Separated Thermotropic Layers Based on UV Cured Acrylate Resins', *Macromolecular Symposia*, vol. 265, no. 1, pp. 49–60, 2008, ISSN: 10221360. DOI: 10.1002/masy.200850506.

[11] K. Resch and A. Weber, 'Smart Windows - Smart Collectors: Entwicklung von funktionalen Überhitzungsschutzverglasungen für Gebäudeverglasungen und thermische Solarkollektoren', *Berg- und Hüttenmännische Monatshefte*, vol. 156, no. 11, pp. 429–433, 2011, ISSN: 0005-8912. DOI: 10.1007/s00501-011-0031-2.

[12] O. Muehling, A. Seeboth, T. Haeusler, R. Ruhmann, E. Potechius and R. Vetter, 'Variable solar control using thermotropic core/shell particles', *Solar Energy Materials and Solar Cells*, vol. 93, no. 9, pp. 1510–1517, 2009, ISSN: 09270248. DOI: 10.1016/j.solmat.2009.03.029.

[13] F. S. Bühler and M. Hewel, 'Reversibly thermotropic transparent molding material, useful e.g. in glazing or covers for shading and light-heat regulation in houses and cars etc.', pat. DE19841234C1, 1999.

[14] C. DeArmitt and G. E. Mc Kee, 'Moulded article with temperature dependent transparency', pat. EP1985663A1, 2008.

[15] A. Weber and K. Resch, 'Thermotropic glazings for overheating protection applications: Tuning the light-shielding efficiency by systematic material preselection and formulation', in *Solar Building Skins*, Economic Forum, Ed., Munich, 2011, pp. 73–77, ISBN: 978-3-981205343.

[16] A. Weber and K. Resch, 'Effect of Temperature-Cycling on the Morphology of Polymeric Thermotropic Glazings for Overheating Protection Applications', *Journal of Polymer Research*, vol. 19:9888, no. 6, pp. 1–8, 2012, ISSN: 1022-9760. DOI: 10.1007/s10965-012-9888-3.

[17] A. Weber and K. Resch, 'Thermotropic Glazings for Overheating Protection I: Material Pre-selection, Formulation and Light-Shielding Efficiency', *Journal of Applied Polymer Science*, ISSN: 0021-8995. DOI: 10.1002/app.39950.

[18] P. Nitz, 'Optical modelling and characterisation of thermotropic systems', Dissertation, Albert-Ludwigs-University, Freiburg i.B., 1999.

[19] E. Baur, S. Brinkmann, T. A. Osswald and E. Schmachtenberg, *Saechtling-Kunststoff-Taschenbuch*, 30. Auflage. München: Hanser, 2007, ISBN: 9783446403529.

[20] M. Schimmelpfennig, K. Weber, F. Kalb, K.-H. Feller, T. Butz and M. Matthäi, 'Volumenausdehnung von Paraffinen aus Steigrohr-Messungen', in *Jahrbuch für den Praktiker 2007*, B. Ziolkowsky, Ed., vol. 50, Augsburg: Verlag für chemische Industrie, 2007, pp. 417–429.

[21] J.-F. Su, X.-Y. Wang, S.-B. Wang, Y.-H. Zhao, K.-Y. Zhu and X.-Y. Yuan, 'Interface stability behaviors of methanol-melamine-formaldehyde shell microPCMs/epoxy matrix composites', *Polymer Composites*, vol. 32, no. 5, pp. 810–820, 2011, ISSN: 02728397. DOI: 10.1002/pc.21102.

[22] X.-Y. Wang, J.-F. Su, S.-B. Wang and Y.-H. Zhao, 'The effect of interface debonding behaviors on the mechanical properties of microPCMs/epoxy composites', *Polymer Composites*, vol. 32, no. 9, pp. 1439–1450, 2011, ISSN: 02728397. DOI: 10.1002/pc.21174.

[23] S. R. Derkach, 'Rheology of emulsions', *Advances in Colloid and Interface Science*, vol. 151, no. 1-2, pp. 1–23, 2009, ISSN: 00018686. DOI: 10.1016/j.cis.2009.07.001.

[24] P. Nitz, J. Ferber, R. Stangl, H. R. Wilson and V. Wittwer, 'Simulation of multiply scattering media', *Solar Energy Materials and Solar Cells*, vol. 54, no. 1-4, pp. 297–307, 1998, ISSN: 09270248. DOI: 10.1016/S0927-0248(98)00081-6.

[25] C. Koning, M. Van Duin, C. Pagnoulle and R. Jerome, 'Strategies for compatibilization of polymer blends', *Progress in Polymer Science*, vol. 23, no. 4, pp. 707–757, 1998, ISSN: 00796700. DOI: 10.1016/S0079-6700(97)00054-3. (visited on 08/02/2012).

[26] Y. Kayano, H. Keskkula and D. Paul, 'Evaluation of the fracture behaviour of nylon 6/SEBS-g-MA blends', *Polymer*, vol. 38, no. 8, pp. 1885–1902, 1997, ISSN: 00323861. DOI: 10.1016/S0032-3861(96)00703-3. (visited on 08/02/2012).

[27] A. Luyt, I. Krupa, H. Assumption, E. Ahmad and J. Mofokeng, 'Blends of polyamide 12 and maleic anhydride grafted paraffin wax as potential phase change materials', *Polymer Testing*, vol. 29, no. 1, pp. 100–106, 2010, ISSN: 01429418. DOI: 10.1016/j.polymertesting.2009.09.010.

[28] I. Novák, I. Krupa and A. S. Luyt, 'Improvement of the polarity of polyethylene with oxidized Fischer-Tropsch paraffin wax and its influence on the final mechanical properties', *Journal of Applied Polymer Science*, vol. 95, no. 5, pp. 1164–1168, 2005, ISSN: 0021-8995. DOI: 10.1002/app.21283. (visited on 09/02/2012).

[29] G. W. Ehrenstein, G. Riedel and P. Trawiel, *Praxis der thermischen Analyse von Kunststoffen*, 2nd ed. München: Hanser, 2003, ISBN: 9783446223400.

[30] S. Fairgrieve, *Nucleating agents*, ser. Rapra Review Reports. Shawbury: Rapra Technology Ltd., 2006, vol. Vol. 16, No. 7, Report 187.

[31] K. W. Smith, K. Bhaggan, G. Talbot and K. F. v. Malssen, 'Crystallization of Fats: Influence of Minor Components and Additives', *Journal of the American Oil Chemists' Society*, vol. 88, no. 8, pp. 1085–1101, 2011, ISSN: 0003-021X. DOI: 10.1007/s11746-011-1819-7.

[32] X.-x. Zhang, Y.-f. Fan, X.-m. Tao and K.-l. Yick, 'Crystallization and prevention of supercooling of microencapsulated n-alkanes', *Journal of Colloid and Interface Science*, vol. 281, no. 2, pp. 299–306, 2005, ISSN: 00219797. DOI: 10.1016/j.jcis.2004.08.046.

[33] E. Günther, L. Huang, H. Mehling and C. Dötsch, 'Subcooling in PCM emulsions – Part 2: Interpretation in terms of nucleation theory', *Thermochimica Acta*, vol. 522, no. 1-2, pp. 199–204, 2011, ISSN: 00406031. DOI: 10.1016/j.tca.2011.04.027.

[34] K. Chari, B. Antalek, J. Kowalczyk, R. S. Eachus and T. Chen, 'Polymer—Surfactant Interaction and Stability of Amorphous Colloidal Particles', *The Journal of Physical Chemistry B*, vol. 103, no. 45, pp. 9867–9872, 1999, ISSN: 1520-6106. DOI: 10.1021/jp992032i.

[35] T. F. Tadros, 'Emulsion Science and Technology: A General Introduction', in *Emulsion science and technology*, T. F. Tadros, Ed., Weinheim: Wiley-VCH, 2009, pp. 1–56, ISBN: 3527325255.

[36] C. Zhao and G. Zhang, 'Review on microencapsulated phase change materials (MEPCMs): Fabrication, characterization and applications', *Renewable and Sustainable Energy Reviews*, vol. 15, no. 8, pp. 3813–3832, 2011, ISSN: 13640321. DOI: 10.1016/j.rser.2011.07.019.

[37] K. Landfester, 'Miniemulsionspolymerisation und Struktur von Polymer- und Hybridnanopartikeln', *Angewandte Chemie*, vol. 121, no. 25, pp. 4556–4576, 2009, ISSN: 00448249. DOI: 10.1002/ange.200900723. (visited on 09/02/2012).

Part IV.

In-situ Optimisation Strategies

7 Introduction to Publication 3

So far, TSFD exhibiting efficient overheating protection performance were not established upon application of the systematic material formulation strategy outlined in the previous chapters. Nevertheless, experiments revealed valuable structure-property-relationships based on sound polymer-physical characterisation of the formulated TSFD. The achieved limited overheating protection performance was ascribed to inappropriately shaped and/or sized scattering domains primarily. However, the established TSFD faced an additional challenge compared to previous publications [1]–[5]: The formation of defects in numerous TSFD. The defects resulted in an undesirable increase in solar hemispheric transmittance upon exceeding the threshold temperature. The most prominent defect type were vacuoles. Vacuole formation was ascribed to differences in coefficient of thermal expansion (CTE) of matrix and thermotropic additive. Upon cooling down the TSFD to room temperature during manufacturing process, the embedded additive domains contracted more intense than the surrounding matrix yielding vacuole formation at the perimeter of the additive domains. The established temperatures exceeding room temperature – and thus causing defect formation – resulted either from manufacturing requirements (thermoplasts are conventionally processable at temperatures exceeding glass transition (amorphous thermoplastics) or melting temperature (semi-crystalline thermoplastics) only) or from dissipative heating of the matrix due to absorption of radiation (chromophores in UV-curable resin matrix – including the photo-initiator – can undergo a wide variety of photo-physical processes upon irradiation, including energy dissipation to heat).

For TSFD formulated with thermoplastic matrix, adhesion promotion via covalent bonds was considered as a potential remedy in order to prevent defect formation.

Although this approach worked rather well with polymeric adhesion promoters exhibiting functional groups being capable to form covalent bonds with matrix M2, the achieved overheating protection performance was limited and thus results are not published here. Another attempt was to graft thermotropic additive A2 with maleic anhydride (MAH) groups. Although the grafting process was successful [6], mixing the MAH-grafted A2 with matrix M2 (polyamide) did not result in a TSFD with reasonable overheating protection performance. Thus, these results are not presented here.

For TSFD formulated with UV-curable resin matrix, reduction of absorbed energy by reduction of radiation intensity and dose upon curing process was considered as promising defect prevention strategy. Defect formation occured primarily in TSFD formulated with paraffin waxes (A1, A2) as thermotropic additives. Thus, TSFD M7A1 was chosen as prototype system for the subsequent investigations in order to represent TSFD formulated with paraffin waxes and with UV-curable resin matrix. These investigations focussed on an evaluation of the effectiveness strategies to prevent defect formation. The defect prevention strategies evaluated and their underlying considerations and hypotheses are outlined in the subsequent paper in detail.

7.1 References

[1] K. Resch and G. M. Wallner, 'Morphology of phase-separated thermotropic layers based on UV cured acrylate resins', *Polymers for Advanced Technologies*, vol. 20, no. 12, pp. 1163–1167, 2009, ISSN: 10427147. DOI: 10.1002/pat.1393.

[2] K. Resch and G. M. Wallner, 'Thermotropic Resin Systems: Relationships Between Formulation Parameters, Material Structure and Optical Properties', in *Proceedings of ISES Solar World Congress 2007*, D. Y. Goswami and Y. Zhao, Eds., Berlin: Springer, 2007, pp. 541–545, ISBN: 978-3-540-75996-6. DOI: 10.1007/978-3-540-75997-3_98.

[3] K. Resch, R. Hausner and G. M. Wallner, 'All Polymeric Flat-Plate Collector — Potential of Thermotropic Layers to Prevent Overheating', in *Proceedings of ISES Solar World Congress 2007*, D. Y. Goswami and Y. Zhao, Eds., Berlin: Springer, 2007, pp. 561–565, ISBN: 978-3-540-75996-6. DOI: 10.1007/978-3-540-75997-3_102.

[4] K. Resch, G. M. Wallner and R. W. Lang, 'Spectroscopic Investigations of Phase-Separated Thermotropic Layers Based on UV Cured Acrylate Resins', *Macromolecular Symposia*, vol. 265, no. 1, pp. 49–60, 2008, ISSN: 10221360. DOI: 10.1002/masy.200850506.

[5] K. Resch, G. M. Wallner and R. Hausner, 'Phase separated thermotropic layers based on UV cured acrylate resins – Effect of material formulation on overheating protection properties and application in a solar collector', *Solar Energy*, vol. 83, no. 9, pp. 1689–1697, 2009, ISSN: 0038092X. DOI: 10.1016/j.solener.2009.06.006.

[6] K. Resch, A. Weber, D. Gruber, K. Schnetzinger and W. Kern, *Smart Windows - Smart Collectors: Entwicklung, Modellierung und Vermessung von Überhitzungsschutzverglasungen für Fassaden- und Kollektoranwendungen: Zwischenbericht 2: WPR-NKP.09.014-02*, Leoben, 2012.

8 Publication 3

8.1 Bibliographic Information

- Title: Effect of Formulation and Processing Conditions on Light Shielding Efficiency of Thermotropic Systems with Fixed Domains Based on UV Curing Acrylate Resins
- Authors:
  - Andreas Weber[1]
  - Sandra Schlögl[1]
  - Katharina Resch[2]
    1. Polymer Competence Center Leoben GmbH, Roseggerstrasse 12, 8700 Leoben, Austria
    2. Department Polymer Engineering and Science, Materials Science and Testing of Polymers, University of Leoben, Otto Glöckel-Strasse 2, 8700 Leoben, Austria
- Periodical: Journal of Applied Polymer Science 2013, 130(5), 3299–3310
- DOI: 10.1002/app.39571

Statement with regard to publication: The manuscript presented here is an adapted accepted manuscript in order to fit the formatting of the thesis and does not necessarily reflect exactly the actually published version, as the latter one was subject to processing and editing by the typesetter of the journal.

8.2 Abstract

Within this study relationships between material formulation and processing parameters and the morphology (vacuole formation) of thermotropic systems with fixed domains (TSFD) for overheating protection purposes were investigated. Main aim was on improving light shielding efficiency of TSFD based on UV curable acrylate resins by optimisation of selected key parameters including photo-initiator type and content, type of reactive diluent, radiation intensity/dose and thermal treatment of layers during manufacturing. Variations of type of reactive diluent and thermal treatment had a minor effect on overheating protection performance. Utilization of photo-bleaching photo-initiator of acylphospine oxide type instead of a blend of conventional type I (α-hydroxy ketone type) and type II (benzophenone) photo-initiators enabled reduction of radiation dose to achieve properly cured layers. The results revealed that a significant reduction of radiation intensity/dose prevented formation of vacuoles. Consequently light shielding efficiency of TSFD was enhanced significantly. Nevertheless, obtained scattering domain size was inappropriate for optimum light shielding efficiency and requires further optimisation strategies.

8.3 Introduction

Thermotropic glazings providing efficient overheating protection for buildings and solar thermal collectors undergo a transmittance reduction upon exceeding the threshold temperature, reversibly [1]–[5]. Besides other classes of thermo-responsive glazing materials, thermotropic systems with fixed domains (TSFD) gained interest in recent research due to their specific advantages like high reversibility, low hysteresis, ease of adjustment of switching threshold, high long term stability and steep switching process [6]–[19]. TSFD consist of a thermotropic additive finely dispersed in a matrix material [1], [5]. Refractive index difference of matrix and additive and TSFD morphology are of paramount importance for scattering performance and thus overheating protection performance [20]. Refractive indices of matrix and additive are almost equal below the phase transition temperature (e.g. melting temperature) of the additive yielding transparent appearance of the TSFD [1]. Upon exceeding

the switching threshold the refractive index difference between matrix and additive increases steeply resulting in a reduction of solar hemispheric transmittance [1]. Maximum light shielding efficiency is attained by spherical scattering domains with diameters in the range between 200 and 400 nm[20].

The most systematic and extensive study on TSFD so far was performed by Weber and co-workers [17], [18]. In total seven different matrix materials (three thermoplastics, four UV-curable resins systems) and 24 different additives were included. More than 40 material formulations were produced and characterised comprehensively based on sound polymer physical principles. Parameters such as refractive index, light shielding efficiency and morphology were investigated. Fundamental structure-property-relationships were established and material optimisation potential and strategies were revealed. From a theoretical point of view thermo-refractive properties of matrix and additive were sufficient in order to achieve a significant reduction of solar hemispheric transmittance upon exceeding the threshold temperature [17], [21]. However, investigations revealed inappropriate size and/or shape of scattering domains for achieving optimum light shielding efficiency [18]. Accordingly, overheating protection performance of investigated TSFD was limited [17], [18]. Moreover, several TSFD displayed vacuoles at the perimeter of scattering domains, which were adversely affecting overheating protection performance: the vast majority of TSFD exhibiting vacuoles showed an increase in solar hemispheric transmittance upon switching [17], [18]. The high refractive index difference between matrix (n 1.5) and vacuole (n=1) along with small size of vacuoles yielded intense scattering and thus low solar hemispheric transmittance at room temperature. Upon heating and especially upon melting the additive expanded and filled the cavity provided by the matrix material. Thus vacuoles disappeared and a decrease in refractive index difference at the scattering interface (matrix/molten additive) was achieved. Consequently, solar hemispheric transmittance was high above the switching threshold due to lower overall scattering. Details regarding this effect addressed as “effect of the temporary vacuoles” are available from a preceding publication [18].

Thus, the major objective of the present study is to investigate the relationships between material formulation and processing parameters and the morphology (vacuole formation) of TSFD, in order to improve the light shielding efficiency. Effects are

investigated by factorial design. Focus is on TSFD produced from UV curing acrylate systems. TSFD based on thermoplastics are not covered within this study, due to limited feasibility of varying processing conditions [18].

8.4 Vacuole Prevention Strategies

In TSFD with UV-curable resin matrix, vacuole formation is ascribed to thermo-mechanical effects of different coefficients of thermal expansion (CTE) of matrix and additive and limited adhesion at the interface matrix/additive [18], [19]. Reduction of irradiation intensity and dose would possibly prevent radiation induced heating up of matrix material and thus vacuole formation [18]. However, reduction of radiation intensity might decrease the final degree of conversion of the matrix resin and thus may yield partially uncured layers [22].

Hence, more efficient curing would be required. Efficient curing means to decrease radiation dose and yet achieve properly cured layers. A feasible way to increase efficiency of curing process would be the use of photo-bleaching photo-initiator. A photo-bleaching initiator species absorbing at the initiation wavelength is destroyed upon irradiation [23], [24]. Thus incident radiation can successively penetrate deeper into the layer, yielding a steady progress of polymerisation front towards deeper lying sections of the layer [23], [24]. In contrast, according to Lambert-Beer Law, in systems with conventional photo-initiator intensity of radiation at initiation wavelength decreases steadily throughout the layer thickness due to absorption. Hence, more energy is required than for systems formulated with photo-bleaching photo-initiator in order to achieve properly cured layers. Thus, especially for thick layers, photo-bleaching photo-initiators are more efficient (faster and higher conversion) than conventional photo-initiators [23]–[26].

For laminate systems with the UV-curable resin between two glass panes, similar to the curing setup in this and preceding studies [17]–[19], DECKER AND CO-WORKERS [27], [28] demonstrated a significant effect of glass induced filtering (wavelengths below 330 nm extincted) on conversion profiles of a polyurethane acrylate resin depending on the photo-initiator utilized. Due to filtering of incident radiation by the

glass cover, utilization of photo-initiators absorbing above 330 nm is recommended [27], [28]. Compared to a conventional α-hydroxyketone initiator (Irgacure 184) an acylphospine oxide photo-initiator (Lucirin TPO) gives superior curing response in a polyurethane acrylate resin laminated between glass panes due to better absorption characteristic upon exposure to filtered UV-light [27]. Thus, regarding production of TSFD, better absorption characteristics when exposed to filtered UV-light and more effective polymerisation initiation (more photo-initiator decomposition, less dissipative heat generation by initiator fragments) of photo-bleaching photo-initiator would allow for reduction of irradiation intensity and dose as well as for reduction of initiator content. That probably benefits a reduction of radiation induced heating up of the layers upon curing. However, as photo-initiator is only one out of many chromophores within the resin matrix, experiments have to prove the positive effect of reducing photo-initiator content on dissipative heating and thus vacuole formation.

An alternative approach to inhibit vacuole formation might be minimising differences in CTE of matrix and additive. Due to lower CTE of matrix material compared to thermotropic additive (e.g. $6 \times 10^{-5}\ K^{-1}$ to $8 \times 10^{-5}\ K^{-1}$ for PMMA [29] versus $0.7 \times 10^{-3}\ K^{-1}$ to $1.1 \times 10^{-3}\ K^{-1}$ for paraffin [30]), an increase in matrix CTE is desired. An increase in matrix CTE is probably attained by maintaining higher chain mobility. High chain mobility is achieved at temperatures above glass transition temperature and upon lowering crosslinking density [29], [31]. Crosslinking density decreases upon decreasing functionality of reactive diluent [24], [32]. In preceding studies [17]–[19], tri-functional reactive diluent trimethylol propane triacrylate (TMPTA) was utilized for formulation of UV-curable matrix resin. Substitution of TMPTA with either a tri-functional reactive diluent with longer flexible spacers between the individual acrylate moieties than in TMPTA or with a bi-functional reactive diluent (lowering number of reactive sites per reactive diluent molecule) might provide more chain mobility and thus probably affect CTE in the desired way.

Investigations by Resch and co-workers [9], [11] suggest viability of these approaches as a bundle of measures. They manufactured TSFD with UV-curable resin matrix formulated with bi-functional reactive diluent hexanediol diacrylate (HDDA) and paraffin-type additive and cured by low intensity UV-light. The samples lacked vacu-

oles and displayed a reduction of solar hemispheric transmittance upon exceeding the threshold temperature [8], [9], [11], [16].

Another idea to manipulate vacuole formation is to apply different thermal treatment on cast layers during processing. Upon storage of cast mixture at temperatures below room temperature prior to curing, thermotropic additive domains may stay in a less expanded state than at room temperature. However, upon irradiation matrix temperature increases more intense than additive temperature and likely exceeds room temperature. Both temperatures cannot equilibrate on the short time scales of radiation induced polymerisation (below 30 s) due to low thermal conductivity of polymer and additive. Thus, matrix contracts and thermotropic additive expands upon equilibration to room temperature after curing process. Hence, vacuole formation might be prevented by convergent expansion behaviour of matrix cavity and respective additive domain. Moreover, thermal treatment might also affect crystallisation process of thermotropic additive and hence probably scattering domain size. Mikl [33] demonstrated effects of temperature conditions during manufacturing process on the light shielding efficiency of TSFD. Anyway, information on the morphology of these TSFD was not provided.

Summarising, factors probably affecting TSFD morphology and being detailed investigated within this study are:

- Radiation intensity and dose
- Photo-initiator type and content
- Type of reactive diluent
- Thermal treatment during processing

Due to reasons described above (photo-physical processes by chromophores in matrix and photo-initiator, adjusting fit of available radiation and absorption spectrum of photo-initiator) photo-initiator type is assumed to have the most significant effect on morphology of TSFD. Thus the following experimental part of this paper is differentiated by photo-initiator type (conventional photo-initiator and photo-bleaching photo-initiator).

8.5 Experimental

8.5.1 Materials and Sample Preparation

8.5.1.1 Materials

Polyester acrylate oligomer, reactive diluents and conventional photo-initiator were supplied by Cyctec Surface Specialities Inc. (Drogenbos, B). Photo-bleaching photo-initiator was obtained from BASF SE (Ludwigshafen, D). Paraffin was supplied by Sasol Wax GmbH (Hamburg, D) and HDS-Chemie HandelsgesmbH (Wien, A).

8.5.1.2 TSFD formulated with Conventional Photo-Initiator

Figure 8.1 displays the different formulation and processing parameters applied for TSFD formulated with conventional photo-initiator. Factors varied within these investigations were radiation intensity and dose (factor levels: 0.055 and 0.097 W cm^{-2} yielding 1.2 and 2.1 J cm^{-2}) and type of reactive diluent (factor levels: trimethylolpropane triacrylate (TMPTA), propoxylated glycerol esterified with acrylic acid (OTA), hexanediole diacrylate (HDDA)). Photo-initiator content and thermal treatment were not varied. Thus, the test design resembles a 2×3-mixed level full factorial design. TSFD were manufactured as follows:

Figure 8.1

A polyester acrylate oligomer was utilized as the major component of the UV-curable resin matrix. Tri-functional TMPTA, OTA and bi-functional HDDA were chosen as reactive diluents. Conventional photo-initiator was a blend of benzophenone and 1-hydroxy cyclohexyl phenyl ketone. Thermotropic additive was paraffin with its melting point at 55 °C [17]. Thermotropic layers were prepared by dissolving the thermotropic additive in the UV-curable matrix solution consisting of 57 wt% oligomer, 40 wt% reactive diluent and 3 wt% photo-initiator. Dissolutions were poured in the intervening space between two glass panes which were sealed around the edge and stored for 10 min at room temperature prior and post curing (treatment RT). Thermotropic mixtures were cured with varying intensities of irradiation and thus doses, either 0.055 or 0.097 W m^{-2} yielding 1.2 or 2.1 J cm^{-2}, respectively. UV-source

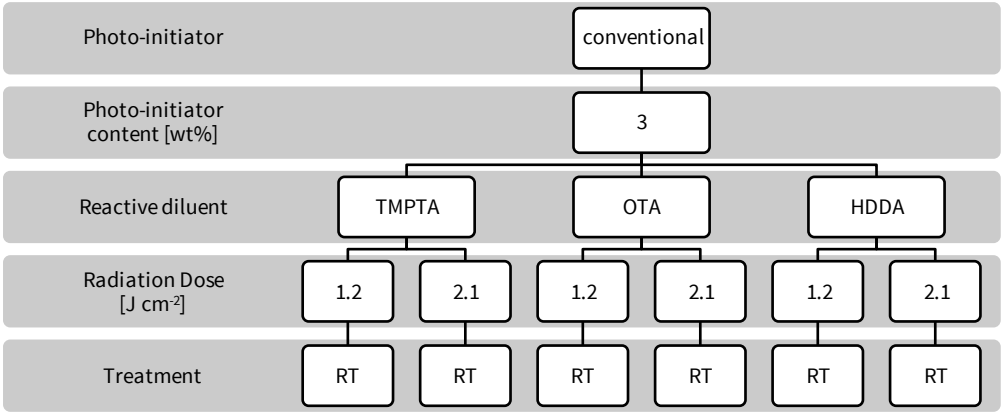

Figure 8.1.: Variations regarding processing conditions and formulation of TSFD (factor levels) formulated with conventional photo-initiator.

was a Light Hammer 6 equipped with a mercury-lamp ("H" bulb) and a LC6E Benchtop Conveyor (Fusion UV Systems Inc., Gaithersburg, MD, USA). Free standing layers with a thickness of 900 µm were obtained after removal of the glass panes. The theoretical additive content was 5 wt%. TSFD were annealed at the mixing temperature of matrix solution and the additive. As to nomenclature, a layer formulated with reactive diluent TMPTA (index "TMPTA"), 3 wt% conventional photo-initiator (index "c3"), applied treatment RT (index "RT") and exposed to a dose of 2.1 J cm^{-2} (index "2.1") is named M7A1-TMPTA-c3-RT-2.1. Because these layers are based on layer M7A1 from preceding publications [17], [18], M7A1 is set as pre-fix. In Table 8.1 the nomenclature of all layers formulated with conventional photo-initiator is presented.

Table 8.1

8.5.1.3 TSFD formulated with Photo-Bleaching Photo-Initiator

Figure 8.2

Figure 8.2 displays the different formulation and processing parameters applied for TSFD formulated with photo-bleaching photo-initiator. Factors varied within the initial investigation were radiation intensity and dose (factor levels: 0.12, 0.39 or 0.57 W cm^{-2} yielding 0.6, 2.1 and 3.1 J cm^{-2}), photo-initiator content (factor levels: 1 and 3 wt%) and thermal treatment (factor levels: DF and RT). Type of reactive diluent was not varied. Thus the initial test design resembled a $3 \times 2 \times 2$-mixed level full

Table 8.1.: Nomenclature of TSFD formulated with conventional photo-initiator

Nomenclature	Reactive diluent	Photo-initiator type	Photo-initiator content [wt%]	Treat-ment	Dose [J cm^{-2}]
M7A1-TMPTA-c3-RT-1.2	TMPTA	conventional	3	RT	1.2
M7A1-TMPTA-c3-RT-2.1[a]	TMPTA	conventional	3	RT	2.1
M7A1-OTA-c3-RT-1.2	OTA	conventional	3	RT	1.2
M7A1-OTA-c3-RT-2.1	OTA	conventional	3	RT	2.1
M7A1-HDDA-c3-RT-1.2	HDDA	conventional	3	RT	1.2
M7A1-HDDA-c3-RT-2.1	HDDA	conventional	3	RT	2.1

[a] Identical with M7A1 from previous publications [17], [18]

factorial design. For in detail investigations, additional factor levels were introduced (see Figure 8.2). TSFD were manufactured as follows:

A polyester acrylate oligomer and tri-functional reactive diluent OTA along with photo-bleaching photo-initiator (ethyl 2,4,6-trimethylbenzoyl phenyl phosphinate) were utilized for formulation of UV-curable resin matrix. Thermotropic additive was paraffin with its melting point at 55 °C [17]. Thermotropic layers were prepared by dissolving the thermotropic additive in the UV-curable matrix solution consisting of 59 or 57 wt% oligomer, 40 wt% reactive diluent and 1 or 3 wt% photo-initiator. Dissolutions were poured in the intervening space between two glass panes which were sealed around the edge and different thermal treatment was applied prior to curing process. Either the layers were stored at −20 °C (treatment DF) or at room temperature (treatment RT) for 10 min prior and post curing. Thermal treatment option HOT (additional factor level not considered initially) was applied for selected systems only as indicated in Figure 8.2. Upon treatment HOT, the dissolution of molten additive and UV-curable resin were immediately cured after casting process and subsequently stored at room temperature for 10 min after curing. Thermotropic mixtures were cured with varying intensities of 0.12, 0.39 or 0.57 W cm^{-2} from a gallium doped lamp (“V” bulb) of Light Hammer 6, yielding doses of 0.6, 2.1 or 3.1 J cm^{-2}. Additionally, evaluation process

required utilization of 366 nm lamp of Universal-UV-Lamp (Camag, Muttenz, CH) as UV-source of very low intensity of 4.6 µW cm^{-2} yielding 8.3 mJ cm^{-2} (additional factor level). Free standing layers with a thickness of 900 µm were obtained after removal of the glass panes. The theoretical additive content was 5 wt%. TSFD were annealed at the mixing temperature of matrix solution and the additive except for samples irradiated with Universal-UV-Lamp. The latter samples not necessarily required tempering due to rather homogeneous appearance. Furthermore, the effect of tempering on overheating protection performance of TSFD irradiated with Universal-UV-Lamp will be addressed in a forthcoming publication. As to nomenclature, a layer formulated with reactive diluent OTA (index "OTA"), 3 wt% photo-bleaching photo-initiator (index "p3"), applied treatment RT (index "RT") and exposed to a dose of 0.6 J cm^{-2} (index "0.6") is named M7A1-OTA-p3-RT-0.6. In Tables 8.2 and 8.3 the nomenclature of all layers formulated with 1 wt% and 3 wt% photo-bleaching photo-initiator is presented, respectively.

Table 8.2, 8.3

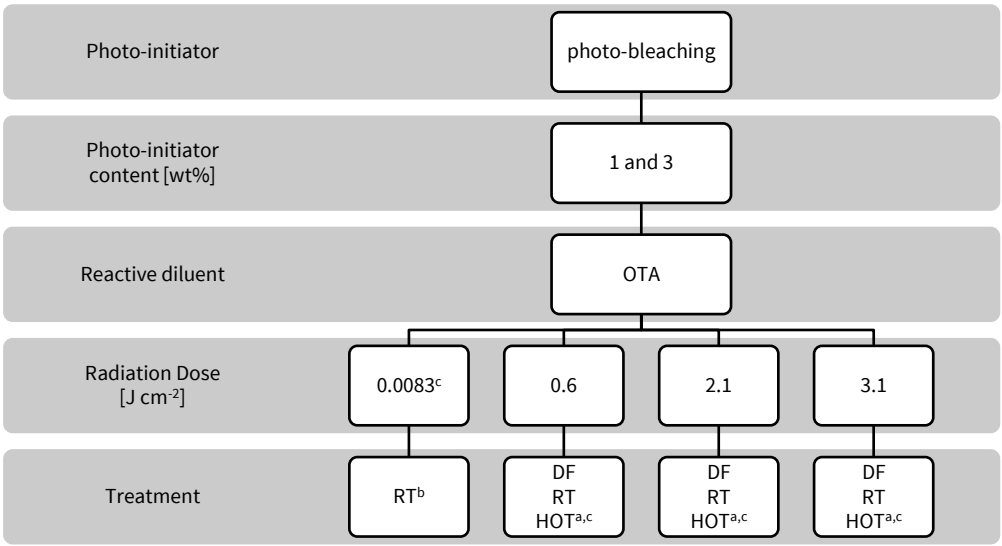

Figure 8.2.: Variations regarding processing conditions and formulation of TSFD (factor levels) formulated with photo-bleaching photo-initiator. ([a] for 1 wt% photo-initiator content only; [b] without tempering after curing; [c] additional factor level)

Table 8.2.: Nomenclature of TSFD formulated with 1 wt% photo-bleaching photo-initiator

Nomenclature	Reactive diluent	Photo-initiator type	Photo-initiator content [wt%]	Treat-ment	Dose [J cm^{-2}]
M7A1-OTA-p1-DF-0.6	OTA	photo-bl.	1	DF	0.6
M7A1-OTA-p1-DF-2.1	OTA	photo-bl.	1	DF	2.1
M7A1-OTA-p1-DF-3.1	OTA	photo-bl.	1	DF	3.1
M7A1-OTA-p1-RT-0.008	OTA	photo-bl.	1	RT	0.0083
M7A1-OTA-p1-RT-0.6	OTA	photo-bl.	1	RT	0.6
M7A1-OTA-p1-RT-2.1	OTA	photo-bl.	1	RT	2.1
M7A1-OTA-p1-RT-3.1	OTA	photo-bl.	1	RT	3.1
M7A1-OTA-p1-HOT-0.6	OTA	photo-bl.	1	HOT	0.6
M7A1-OTA-p1-HOT-2.1	OTA	photo-bl.	1	HOT	2.1
M7A1-OTA-p1-HOT-3.1	OTA	photo-bl.	1	HOT	3.1

Table 8.3.: Nomenclature of TSFD formulated with 3 wt% photo-bleaching photo-initiator

Nomenclature	Reactive diluent	Photo-initiator type	Photo-initiator content [wt%]	Treat-ment	Dose [J cm^{-2}]
M7A1-OTA-p3-DF-0.6	OTA	photo-bl.	3	DF	0.6
M7A1-OTA-p3-DF-2.1	OTA	photo-bl.	3	DF	2.1
M7A1-OTA-p3-DF-3.1	OTA	photo-bl.	3	DF	3.1
M7A1-OTA-p3-RT-0.008	OTA	photo-bl.	3	RT	0.0083
M7A1-OTA-p3-RT-0.6	OTA	photo-bl.	3	RT	0.6
M7A1-OTA-p3-RT-2.1	OTA	photo-bl.	3	RT	2.1
M7A1-OTA-p3-RT-3.1	OTA	photo-bl.	3	RT	3.1

8.5.2 Characterisation Methodology

8.5.2.1 Light Shielding Efficiency

Overheating protection performance of TSFD was determined applying UV/Vis/NIR spectrometry. A double beam UV/Vis/NIR spectrophotometer Lambda 950 (Perkin Elmer Inc., Waltham, MA, USA) equipped with an Ulbricht-sphere (diameter 150 mm) was employed. For the given measurement apparatus the radiation passing through (transmittance) the specimen outside a cone of approximately 5° relative to the incident beam direction was defined as diffuse (scattered) component. Hemispheric and diffuse transmittance was recorded at normal incidence in the spectral region from 250 to 2500 nm. The integral solar transmittance was determined by weighting the recorded spectral data in steps of 5 nm by the AM1.5 global solar irradiance source function. The spectrophotometer was adapted by a heating stage to adjust sample temperature within a range from ambient temperature to maximum 115 °C [17]. Measurements were performed in steps of 5 °C. Prior to measurement the samples were allowed to equilibrate for five minutes at the selected temperature. The heating stage was equipped with a control system consisting of a heating stage-internal J-type thermocouple as temperature sensor and the control unit HS-W-35/M (Heinz Stegmeier Heizelemente HS-Heizelemente GmbH, Fridingen, D). Within the heating stage the sample was positioned in close proximity of the port hole of the Ulbricht-sphere. In situ front- and backside sample surface temperatures as a function of set-point value of the control unit were recorded on a prototype sample with a two-channel temperature measurement instrument T900 (Dostmann electronic GmbH, Wertheim-Reicholzheim, D) equipped with a precision K-type thermocouple. Sample temperature was assumed as the average of both recorded surface temperatures. Required set-point values to maintain average sample temperatures were calculated from a second order polynomial fit of the temperatures recorded in measurements of the prototype sample.

8.5.2.2 Morphology

Morphological characterisation of TSFD was carried out applying an optical microscope Olympus BX51 (Olympus Austria Ges. m. b. H., Wien, A) in transmitted light mode. TSFD were investigated without further preparation. Domain size was evaluated with measurement tools of software analySIS (Soft Imaging System GmbH, Münster, D). Minimum and maximum sizes of scattering domains were evaluated.

8.6 Results and Discussion

8.6.1 TSFD formulated with Conventional Photo-Initiator

Figure 8.3

In Figure 8.3 the optical micrographs of layers M7A1-TMPTA-c3-RT-1.2 (Figure 8.3a), M7A1-OTA-c3-RT-1.2 (Figure 8.3b), M7A1-HDDA-c3-RT-1.2 (Figure 8.3c), M7A1-TMPTA-c3-RT-2.1 (Figure 8.3d), M7A1-OTA-c3-RT-2.1 (Figure 8.3e) and M7A1-HDDA-c3-RT-2.1 (Figure 8.3f) are presented. Layers exhibited spherical scattering domains with diameters ranging from 1.10 to 150 µm (M7A1-TMPTA-c3-RT-1.2, Figure 8.3a), 3.31 to 85.6 µm (M7A1-OTA-c3-RT-1.2, Figure 8.3b), 1.93 to 229 µm (M7A1-HDDA-c3-RT-1.2, Figure 8.3c), 2.48 to 167 µm (M7A1-TMPTA-c3-RT-2.1, Figure 8.3d), 2.48 to 139 µm (M7A1-OTA-c3-RT-2.1, Figure 8.3e) and 3.86 to 242 µm (M7A1-HDDA-c3-RT-2.1, Figure 8.3f). For all these layers domain size is inappropriate for efficient overheating protection. Largest domains were ascertained for layers formulated with HDDA. This may be attributed to lower viscosity of dissolutions formulated with HDDA compared to systems formulated with tri-functional TMPTA or OTA. Low viscosity systems probably yield faster aggregation of additive droplets prior to solidification. Furthermore layers displayed distinct vacuoles at the perimeter of the additive domains (black areas).

A distinct effect of radiation dose and type of reactive diluent on vacuole formation was evident. For layers formulated with HDDA (M7A1-HDDA-c3-RT-1.2 (Figure 8.3c) and M7A1-HDDA-c3-RT-2.1 (Figure 8.3f)), no distinct correlation between irradiation dose and vacuole concentration was ascertainable. Nearly every scattering domain exhibited a vacuole. On the contrary, a significant effect of radiation dose on vacuole

concentration was observed for layers formulated with TMPTA and OTA: lower irradiation dose yielded a reduction of vacuoles (compare: M7A1-TMPTA-c3-RT-1.2 (Figure 8.3a) and M7A1-TMPTA-c3-RT-2.1 (Figure 8.3d); M7A1-OTA-c3-RT-1.2 (Figure 8.3b) and M7A1-OTA-c3-RT-2.1 (Figure 8.3e)). As described above, the reduction of irradiation intensity and dose decreases dissipative heating up of the matrix material and may affect vacuole formation. However, irradiation intensity and dose and hence dissipative heating did not affect concentration of vacuoles in layers formulated with HDDA. Due to its moderate curing response bi-functional reactive diluent HDDA is probably not able to fix established structures fast enough, giving the vacuoles sufficient time to establish, independent on temperature. On the contrary, vacuoles were formed to a minor extent upon reduction of irradiation intensity and dose for layers formulated with tri-functional TMPTA or OTA. Besides decreased dissipative heating also fast curing response of tri-functional reactive diluents, yielding rather fast fixation of established structures and thus limiting vacuole formation, may positively affect layer morphology.

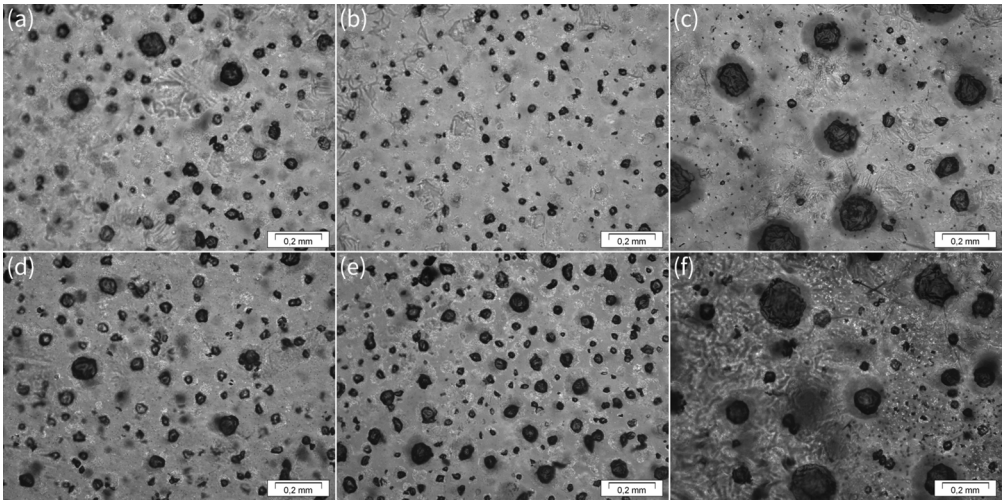

Figure 8.3.: Optical micrographs of TSFD formulated with different reactive diluents and irradiated with different doses from "H" bulb of LightHammer 6 after storage at room temperature (treatment RT) **(a)** M7A1-TMPTA-c3-RT-1.2 **(b)** M7A1-OTA-c3-RT-1.2 **(c)** M7A1-HDDA-c3-RT-1.2 **(d)** M7A1-TMPTA-c3-RT-2.1 **(e)** M7A1-OTA-c3-RT-2.1 **(f)** M7A1-HDDA-c3-RT-2.1

Figure 8.4

Figure 8.4 displays the solar hemispheric (square) and diffuse (triangle) transmittance as a function of temperature of TSFD M7A1-TMPTA-c3-RT-1.2 (Figure 8.4a), M7A1-

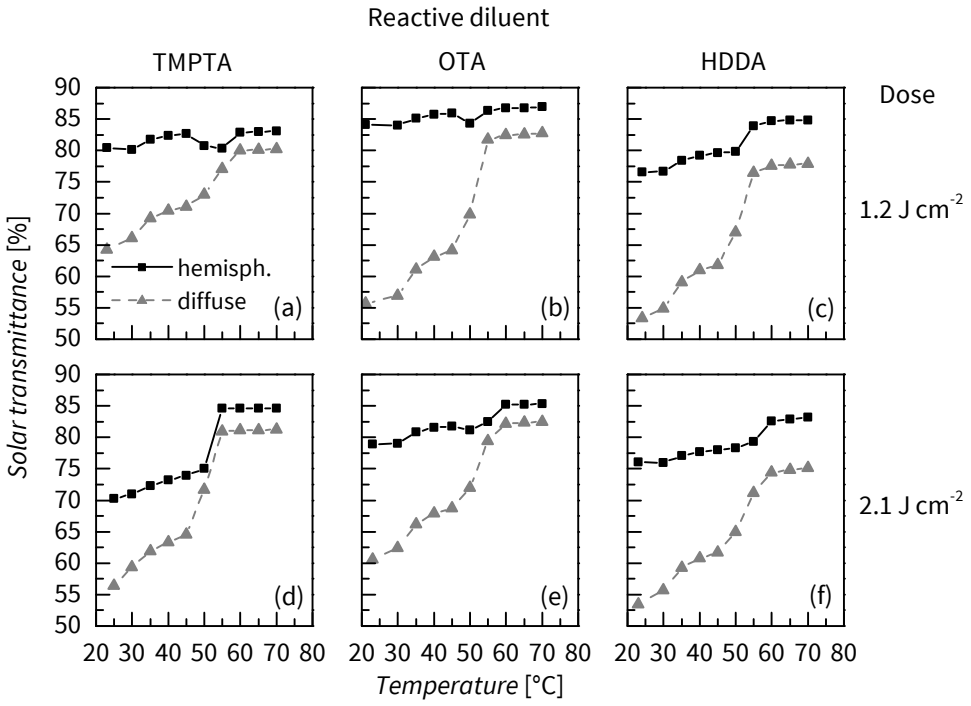

Figure 8.4.: Solar hemispheric and diffuse transmittance as a function of temperature of TSFD formulated with 3 wt% conventional photo-initiator and different reactive diluents, irradiated with different doses from "H" bulb of LightHammer 6 after storage at room temperature (treatment RT) **(a)** M7A1-TMPTA-c3-RT-1.2 **(b)** M7A1-OTA-c3-RT-1.2 **(c)** M7A1-HDDA-c3-RT-1.2 **(d)** M7A1-TMPTA-c3-RT-2.1 **(e)** M7A1-OTA-c3-RT-2.1 **(f)** M7A1-HDDA-c3-RT-2.1

OTA-c3-RT-1.2 (Figure 8.4b), M7A1-HDDA-c3-RT-1.2 (Figure 8.4c), M7A1-TMPTA-c3-RT-2.1 (Figure 8.4d), M7A1-OTA-c3-RT-2.1 (Figure 8.4e) and M7A1-HDDA-c3-RT-2.1 (Figure 8.4f). The solar hemispheric transmittance of layers M7A1-TMPTA-c3-RT-1.2, M7A1-OTA-c3-RT-1.2 and M7A1-HDDA-c3-RT-1.2 increased from 80.4, 84.1 and 76.6 % at ambient conditions to 83.1, 86.9 and 84.8 % at 70 °C, respectively. These layers exhibited an increase in solar diffuse transmittance from between 53.3 and 64.2 % to values ranging from 77.9 to 82.8 % upon heating. The solar hemispheric transmittance of layers M7A1-TMPTA-c3-RT-2.1, M7A1-OTA-c3-RT-2.1 and M7A1-HDDA-c3-RT-2.1 increased from 70.3, 78.9 and 76.1 % at ambient conditions to 84.6, 85.3 and 83.1 % at 70 °C, respectively. These layers exhibited an increase in solar diffuse transmittance from between 53.5 and 60.6 % to values ranging from 75.1 to 82.5 % upon heating. The

observed increase in solar hemispheric transmittance around the switching threshold was ascribed to the effect of temporary vacuoles as already described above. Upon heating also a slight increase in solar hemispheric and diffuse transmittance was detected around 35 °C, which is corresponding to solid phase transition of the thermotropic additive [17]. Probably due to expansion of additive upon solid phase transmittance several vacuoles vanish, yielding lower vacuole concentration and thus lower overall scattering performance. Whereas this effect was rather weak upon further heating for solar hemispheric transmittance, solar diffuse transmittance increased steadily. Upon melting of the additive around 55 °C [17], a more or less distinct increase in both, solar hemispheric and diffuse transmittance occurred. This effect was ascribed to disappearance of vacuoles due to expansion of additive upon melting, thus filling the complete domain cavity provided by the surrounding matrix [18]. Accordingly, the scattering domains with inappropriate diameter for back scattering yielded strong forward scattering.

Differences in switching characteristics of these TSFD were attributed to different layer morphology (vacuoles), and hence correlated with radiation intensity and dose applied and type of reactive diluent used. Layers formulated with bi-functional HDDA displayed rather congruent curves of solar hemispheric and diffuse transmittance as a function of temperature. This was ascribed to the invariance of vacuole concentration upon changes in radiation intensity and dose (Figure 8.3). In contrast, layers formulated with tri-functional TMPTA or OTA displayed a lower solar hemispheric transmittance at room temperature along with a more distinct increase in solar hemispheric transmittance upon switching if irradiated with higher dose. This corresponded well with higher vacuole concentration detected for layers irradiated with 2.1 J cm^{-2} compared to layers irradiated with 1.2 J cm^{-2} (Figure 8.3). Among layers formulated with tri-functional reactive diluents (TMPTA and OTA), higher solar hemispheric transmittance was achieved by layers formulated with OTA, irrespective of applied radiation dose and reference temperature (room temperature or 70 °C). OTA exhibits longer spacers between vinyl-moieties compared to TMPTA, thus yielding higher matrix flexibility due to higher chain mobility.

8.6.2 TSFD formulated with Photo-Bleaching Photo-Initiator

In layers formulated with conventional photo-initiator and with tri-functional reactive diluents TMPTA or OTA a reduction in radiation dose yielded a decrease of vacuole concentration. Hence, the following investigations will also address very low curing intensities. Anyway, as further reduction of radiation dose would yield partially uncured layers, a photo-bleaching photo-initiator will be used. Furthermore subsequent investigations focus on systems formulated with OTA. Layers formulated with OTA exhibited higher solar hemispheric transmittance than layers formulated with TMPTA (see Figure 8.4).

8.6.2.1 Effects of Radiation Dose, thermal Treatment, and Photo-Initiator Content on Light-Shielding Efficiency

For evaluation of the effects of the factors radiation dose, thermal treatment and photo-initiator content on light shielding efficiency of TSFD a test design resembling a mixed level full-factorial design was established. Factor levels were 0.6, 2.1 and 3.1 J cm^{-2} for radiation dose, DF and RT for thermal treatment and 1 and 3 wt% for photo-initiator content, respectively.

Tables 8.4 and 8.5 present diameters of spherical scattering domains for layers irradiated with different doses from "V" bulb of Light Hammer 6 (0.6, 2.1 and 3.1 J cm^{-2}) and different thermal treatment (treatment DF and RT) formulated with 3 and 1 wt% photo-initiator content, respectively. In general no effect of photo-initiator content, radiation dose and thermal treatment on sample morphology was observed (factor levels: DF or RT; 0.6, 2.1 or 3.1 J cm^{-2}). Scattering domain size varied between 1.10 and 258 µm. Furthermore nearly every scattering domain exhibited a vacuole. Anyway, the scattering domain sizes detected for these layers were inappropriate for efficient overheating protection. *Table 8.4, 8.5*

Figure 8.5 presents the mean plots regarding the factors radiation dose applied from "V" bulb of Light Hammer 6 (0.6, 2.1 and 3.1 J cm^{-2}), photo-initiator content (1 and 3 wt%) and thermal treatment (treatment DF or RT) on solar hemispheric (square symbols) and diffuse transmittance (triangle symbols) of TSFD formulated with reactive *Figure 8.5*

diluent OTA. Data were recorded at room temperature RT (solid symbols) and 70 °C (open symbols). Mean and standard deviation of solar hemispheric and diffuse transmittance of layers regarding applied radiation dose were calculated by merging data of TSFD M7A1-OTA-p1-DF-0.6, M7A1-OTA-p1-RT-0.6, M7A1-OTA-p3-DF-0.6 and M7A1-OTA-p3-RT-0.6 for a dose of 0.6 J cm^{-2} for example. The mean and standard deviation of solar transmittances regarding other factor levels were calculated accordingly.

Table 8.4.: Scattering domain size in TSFD formulated with 40 wt% OTA and 3 wt% photo-bleaching photo-initiator for different thermal treatment prior to UV-exposure ("V" bulb) of the layers

	Radiation dose					
	0.6 J cm^{-2}		2.1 J cm^{-2}		3.1 J cm^{-2}	
Treatment	d_{min} [µm]	d_{max} [µm]	d_{min} [µm]	d_{max} [µm]	d_{min} [µm]	d_{max} [µm]
DF	2.48	126	1.38	113	1.66	189
RT	1.10	85.6	3.04	224	2.21	144

Table 8.5.: Scattering domain size in TSFD formulated with 40 wt% OTA and 1 wt% photo-bleaching photo-initiator for different thermal treatment prior to UV-exposure ("V" bulb) of the layers

	Radiation dose					
	0.6 J cm^{-2}		2.1 J cm^{-2}		3.1 J cm^{-2}	
Treatment	d_{min} [µm]	d_{max} [µm]	d_{min} [µm]	d_{max} [µm]	d_{min} [µm]	d_{max} [µm]
DF	1.24	113	1.52	74.5	1.10	142
RT	3.17	95.2	2.07	171	4.42	258
HOT	2.48	86.9	2.76	112	2.62	126

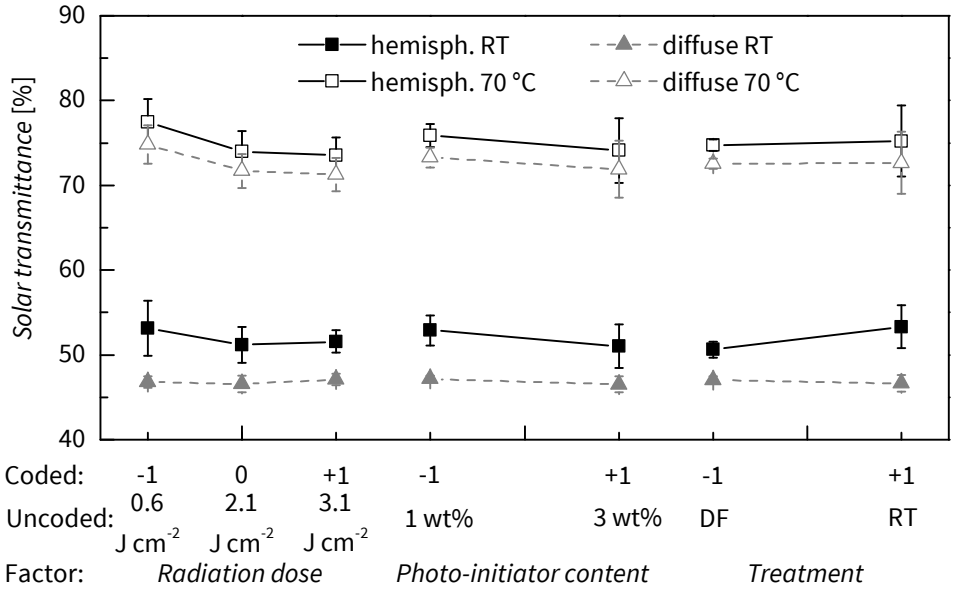

Figure 8.5.: Mean plot regarding effects of factors radiation dose applied from "V" bulb of LightHammer 6 (factor levels: 0.6, 2.1, and 3.1 Jcm^{-2}), photo-initiator content (factor levels: 1 and 3 wt%) and thermal treatment (factor levels: DF: –20 °C/10 min prior and post curing; RT: room temperature/10 min prior and post curing) on solar hemispheric and diffuse transmittance of TSFD formulated with reactive diluent OTA and photo-bleaching photo-initiator. Data were recorded at room temperature RT and 70 °C, respectively.

As to solar transmittance, three general trends were evident: (1) Solar hemispheric transmittance increased from between 49.4 and 56.0 % at ambient temperature to values between 70.3 and 80.8 % upon exceeding the threshold temperature. The increase is attributable to the effect of temporary vacuoles. (2) Detected diameters of scattering domains yielded intense forward scattering thus resulting in rather high solar diffuse transmittance of around 47 and 73 % at room temperature and 70 °C, respectively. (3) Applied radiation dose, thermal treatment and photo-initiator content do not affect the level of solar transmittance significantly. The invariance against the two factors radiation dose and photo-initiator content was ascribed to the high curing efficiency of the photo-bleaching photo-initiator, yielding fast curing response also upon low intensities and low photo-initiator content. However, invariance against these two parameters also indicated that dissipation of irradiated energy was too high in order to mitigate vacuole formation and thus to achieve a reduction of solar hemi-

spheric transmittance upon heating. The invariance of solar transmittance against photo-initiator content revealed an insignificant contribution of photo-initiator content to overall radiation dissipation. The effect of other chromophores inside the matrix resin is higher.

Upon variation of thermal treatment slight changes in solar transmittances were achieved. Solar hemispheric transmittance at room temperature was slightly higher for treatment RT (53.3 ± 2.5 %) than for treatment DF (50.60 ± 0.92 %). However, initial considerations anticipated a higher solar hemispheric transmittance at room temperature for layers exposed to treatment DF than for those exposed to treatment RT. Thus, additional investigations regarding this effect are carried out in the subsequent section. Nevertheless, solar diffuse transmittance at room temperature did not vary upon change in thermal treatment (DF: 47.00 ± 0.47 %; RT: 46.70 ± 0.97 %). This was ascribed to similar scattering domain sizes detected for the respective layers (see Tables 8.4, 8.5).

At 70 °C high solar hemispheric transmittance of 75.0 ± 2.9 % was achieved. This was attributed to the absence of vacuoles at this temperature. Solar diffuse transmittance was 72.6 ± 2.5 %. The high diffuse fraction of the solar hemispheric transmittance was attributed to inappropriate scattering domain size for efficient back-scattering.

8.6.2.2 Effect of higher Temperature of thermal Treatment on Light-Shielding Efficiency

The variation of thermal treatment revealed a slight effect on solar hemispheric transmittance (see above). Thus in the following an additional factor level is evaluated for this factor. Due to invariance of solar hemispheric transmittance upon changes in photo-initiator content, layers formulated with 1 wt% photo-bleaching photo-initiator were chosen as model system (see Figure 8.2). Hence, this test design resembles a 3x3 full factorial design.

Table 8.5 Table 8.5 presents diameters of spherical scattering domains detected for layers irradiated with different doses from "V" bulb of Light Hammer 6 (0.6, 2.1 and 3.1 J cm^{-2}) and different thermal treatment (treatment DF, RT and HOT) formulated with 1 wt%

photo-initiator. In general no effect of radiation dose and thermal treatment on sample morphology was observed (factor levels: DF, RT or HOT; 0.6, 2.1 or 3.1 J cm^{-2}). Scattering domain size varied between 1.10 and 258 µm. Furthermore nearly every scattering domain exhibited a vacuole. Anyway, the scattering domain sizes detected for these layers were inappropriate for efficient overheating protection.

Figure 8.6 presents the mean plots regarding the factors radiation dose applied from "V" bulb of Light Hammer 6 (0.6, 2.1 and 3.1 J cm^{-2}) and thermal treatment (treatment DF, RT and HOT) on solar hemispheric (square symbols) and diffuse transmittance (triangle symbols) of TSFD formulated with reactive diluent OTA and 1 wt% photo-bleaching photo-initiator. Data were recorded at room temperature RT (solid symbols) and 70 °C (open symbols). *Figure 8.6*

Solar transmittances did not vary upon changes in radiation dose (Figure 8.6). Solar hemispheric transmittance was around 57 and 78 % at room temperature and 70 °C, respectively. Solar diffuse transmittance was around 45 and 72 % at room temperature and 70 °C, respectively. The observed increase in solar hemispheric and diffuse transmittance upon heating was attributed to the effect of temporary vacuoles. The high diffuse fraction of solar hemispheric transmittance was ascribed to inappropriate scattering domain size for efficient back-scattering.

In contrast, thermal treatment applied during manufacturing affected solar hemispheric transmittance significantly. With increasing treatment temperature (order DF<RT<HOT) solar hemispheric transmittance increased. At room temperature solar hemispheric transmittance of 51.4, 54.3 and 65.2 % were detected for factor levels DF, RT and HOT, respectively. At the same time a solar diffuse transmittance of 42.2 % at room temperature was evident for treatment HOT. Treatments DF and RT yielded a solar diffuse transmittance of 47.4 and 46.9 % at room temperature, respectively.

Deviant from what was expected (see section 8.4), the actually detected level of solar hemispheric transmittance at room temperature was in the order DF<RT<HOT. Observed order indicates that layers exposed to treatment HOT probably exhibited a bigger average size of vacuoles yielding less efficient back-scattering. That might be due to a more left-tailed size distribution of scattering domains for layers exposed to treatment HOT, yielding a more left tailed size distribution of vacuoles compared to

layers exposed to treatment DF or RT. Hence, the actually detected order was likely due to lower back-scattering efficiency of bigger vacuoles.

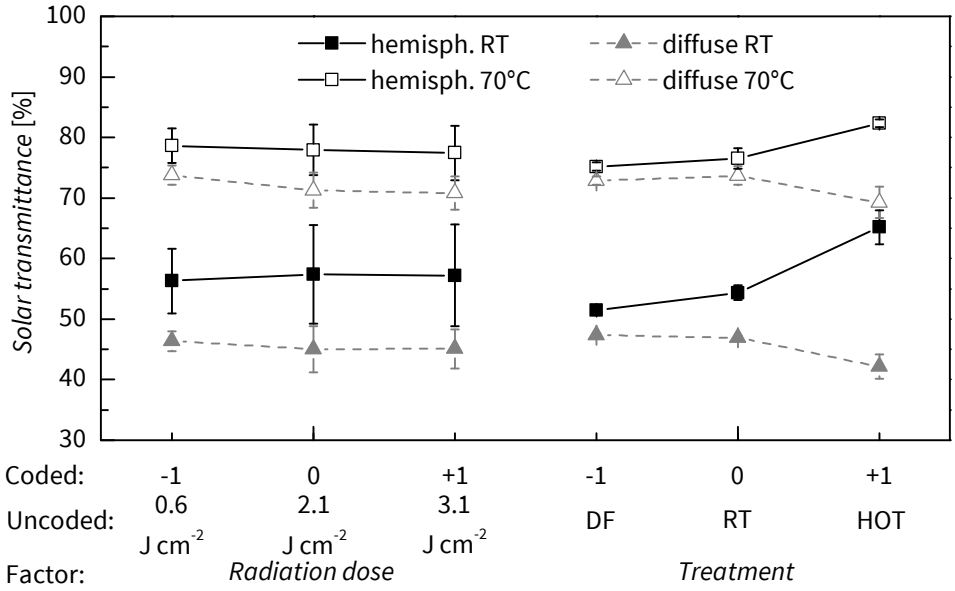

Figure 8.6.: Mean plot regarding effects of factors radiation dose applied from "V" bulb of LightHammer 6 (factor levels: 0.6, 2.1, and 3.1 Jcm^{-2}) and thermal treatment (factor levels: DF: –20 °C/10 min prior and post curing; RT: room temperature/10 min prior and post curing; HOT: immediately cured in the hot state after casting, storage at room temperature/10 min post curing) on solar hemispheric and diffuse transmittance of TSFD formulated with reactive diluent OTA and 1 wt% photo-bleaching photo-initiator. Data were recorded at room temperature RT and 70 °C, respectively.

These trends were also observed for solar transmittances recorded at 70 °C. Solar hemispheric transmittance was 75.2, 76.5 and 82.3 % for treatments DF, RT and HOT, respectively. The enhanced solar hemispheric transmittance at 70 °C for treatment HOT compared to treatments DF and RT was probably a side effect of the vacuole size distribution issue. Maybe not all vacuoles disappeared upon exceeding the threshold temperature for treatments DF and RT, thus yielding residual back scattering. At the same time solar diffuse transmittance was 72.9, 73.7 and 69.3 % for treatments DF, RT and HOT, respectively. This was probably due to a reduced concentration of larger scattering domains in layers exposed to treatment HOT compared to layer exposed to treatments DF or RT.

8.6.2.3 Effect of reduced Irradiation Intensity on Light-Shielding Efficiency

The results achieved so far indicate that temperature difference between matrix and additive is probably the most crucial parameter affecting light-shielding performance. However, further increasing treatment temperature is not feasible due to deterioration and evaporation of TSFD constituents. Thus, preventing dissipative heating up of the matrix might be more beneficial. Hence, for the following discussion layers formulated with either 1 or 3 wt% photo-bleaching photo-initiator were exposed to radiation of low intensity (4.6 µW cm^{-2} yielding 8.3 mJ cm^{-2}) of 366 nm lamp of Universal-UV-Lamp. With respect to a potential practical application in future, thermal treatment RT was applied solely (see Figure 8.2).

Figure 8.7 displays optical micrographs of the layers M7A1-OTA-p1-RT-0.008 (Figure 8.7a) and M7A1-OTA-p3-RT-0.008 (Figure 8.7b). The layers displayed spherical scattering domains with diameters ranging from 3.31 to 84.2 µm and from 2.76 to 116 µm for layers formulated with 1 and 3 wt% photo-initiator, respectively. For both layers only few vacuoles were evident at the perimeter of the scattering domains. The vacuole concentration was significantly lower for these TSFD compared to the layers discussed above (e.g. Figure 8.3). This was ascribed to the very low irradiation intensity preventing excessive dissipative heating up of the matrix material. *Figure 8.7*

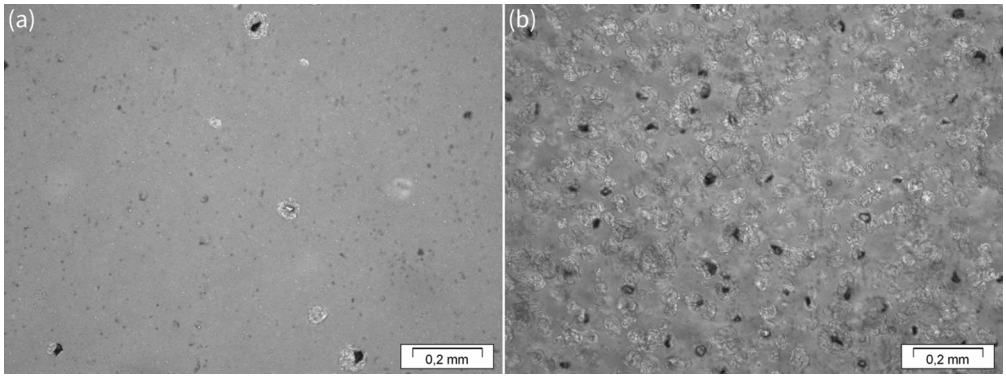

Figure 8.7.: Optical micrographs of TSFD formulated with reactive diluent OTA and either **(a)** 1 wt% or **(b)** 3 wt% photo-bleaching photo-initiator and irradiated with Universal-UV-lamp after storage at room temperature (treatment RT)

Figure 8.8

In Figure 8.8 the solar hemispheric (square) and diffuse (triangle) transmittance of TSFD M7A1-OTA-p1-RT-0.008 (Figure 8.8a) and M7A1-OTA-p3-RT-0.008 (Figure 8.8b) is depicted as a function of temperature. For layer M7A1-OTA-p1-RT-0.008 solar hemispheric transmittance of 81.9 and 80.8 % were evident at ambient conditions and 70 °C, respectively. Diffuse transmittance increased from 37.7 to 75.5 %. Layer M7A1-OTA-p3-RT-0.008 exhibited a solar hemispheric transmittance of 81.2 and 78.5 % at ambient conditions and 70 °C, respectively. Diffuse transmittance increased from 56.2 to 75.2 %. Thus, by lowering irradiation intensity and dose a significant improvement of light shielding efficiency was achieved. This is correlating well with layer morphology. Nevertheless, for optimum overheating protection performance solar hemispheric transmittances of $>$85 % and $<$60 % are required in the transparent and opaque state, respectively [4]. Inappropriate light-shielding efficiency achieved for layers M7A1-OTA-p1-RT-0.008 and M7A1-OTA-p3-RT-0.008 within the present study is attributable to inappropriate scattering domain size. Hence, future work should focus on optimising scattering domain size. As already pointed out in a preceding study [18], adjustment of scattering domain size might be achieved by manipulation of surface energy of the additive by surface active substances, chemical modification of the additive or covalent bonding for example.

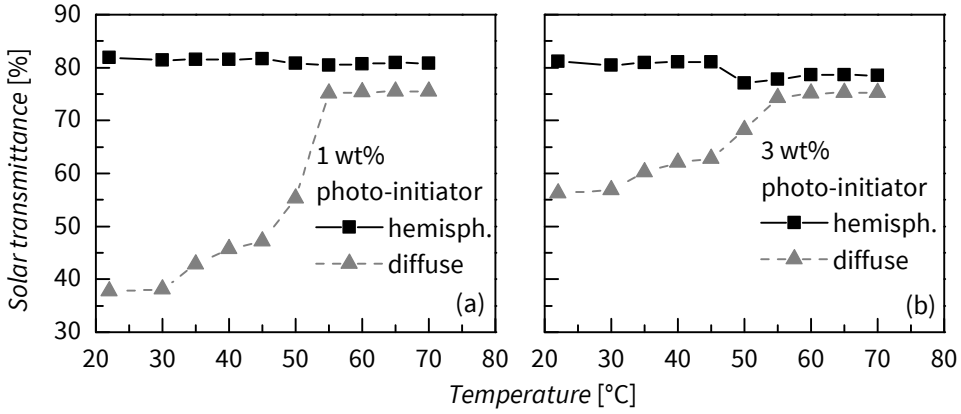

Figure 8.8.: Solar hemispheric (square) and diffuse (triangle) transmittance of TSFD formulated with reactive diluent OTA and either **(a)** 1 wt% or **(b)** 3 wt% photo-bleaching photo-initiator and irradiated with Universal-UV-lamp after storage at room temperature (treatment RT)

8.7 Summary and Conclusion

In this paper the effect of formulation and processing conditions on the light-shielding properties of TSFD formulated with paraffin type additive were investigated applying UV/Vis/NIR-spectrometry and microscopy. Type of reactive diluent and applied radiation dose and intensity were found to have significant effects on light shielding characteristics of TSFD formulated with conventional photo-initiator. Highest transmittance values at room temperature were obtained by utilizing reactive diluent OTA and by lowering applied irradiation dose/intensity. Nevertheless, these layers displayed an increase in solar hemispheric transmittance upon exceeding the threshold temperature, due to vacuoles formed at the perimeter of the spherical scattering domains during manufacturing.

However, further reduction of irradiation dose/intensity required application of a photo-bleaching photo-initiator in order to achieve properly cured TSFD. TSFD formulated with photo-bleaching photo-initiator displayed an increase of solar hemispheric transmittance upon heating due to vacuoles at the perimeter of the scattering domains also. Nevertheless, upon significant reduction of irradiation dose/intensity, TSFD exhibiting a transmittance reduction upon exceeding the threshold temperature were ascertained. The improvement of light-shielding efficiency was ascribed to a reduction of vacuole concentration. The reduction in vacuole concentration was attributed to a reduction of dissipative heating of matrix material and thus to a low temperature difference between matrix and additive during processing. Anyway, size of scattering domains persisted inappropriate for efficient overheating protection. Thus, future work has to focus on improvement of scattering domain size. As pointed out previously [18], surfactants and nucleating agents might have positive effects on scattering domain size by introducing additional crystallisation loci for the thermotropic additive and by probably maintaining smaller additive droplets in matrix/additive dispersions during manufacturing process.

8.8 Acknowledgement

This research project is funded by the State Government of Styria, Department Zukunftsfonds (Project number 5019). The efforts in determination of solar-optical properties of parts of the formulated TSFD by Astrid Rauschenbach (PCCL) and Alexander Klutz (Department Polymer Engineering and Science, University of Leoben) are gratefully acknowledged. Furthermore the authors want to acknowledge the contributions of Cytec Surface Specialities Inc. (Drogenbos, B), Sasol Wax GmbH (Hamburg, D), HDS-Chemie HandelsgesmbH (Wien, A) and BASF SE (Ludwigshafen, D).

8.9 References

[1] P. Nitz and H. Hartwig, 'Solar control with thermotropic layers', *Solar Energy*, vol. 79, no. 6, pp. 573–582, 2005, ISSN: 0038092X. DOI: 10.1016/j.solener.2004.12.009.

[2] A. Seeboth, J. Schneider and A. Patzak, 'Materials for intelligent sun protecting glazing', *Solar Energy Materials and Solar Cells*, vol. 60, no. 3, pp. 263–277, 2000, ISSN: 09270248. DOI: 10.1016/S0927-0248(99)00087-2.

[3] J. Yao and N. Zhu, 'Evaluation of indoor thermal environmental, energy and daylighting performance of thermotropic windows', *Building and Environment*, vol. 49, pp. 283–290, 2012, ISSN: 03601323. DOI: 10.1016/j.buildenv.2011.06.004.

[4] G. M. Wallner, K. Resch and R. Hausner, 'Property and performance requirements for thermotropic layers to prevent overheating in an all polymeric flat-plate collector', *Solar Energy Materials and Solar Cells*, vol. 92, no. 6, pp. 614–620, 2008, ISSN: 09270248. DOI: 10.1016/j.solmat.2007.12.005.

[5] P. Nitz and A. Wagner, 'Schaltbare und regelbare Verglasungen', *BINE Themeninfo*, vol. I/02, no. I/02, pp. 1–12, 2002, ISSN: 1610-8302.

[6] K. Resch and G. M. Wallner, 'Thermotropic Resin Systems: Relationships Between Formulation Parameters, Material Structure and Optical Properties', in *Proceedings of ISES Solar World Congress 2007*, D. Y. Goswami and Y. Zhao, Eds., Berlin: Springer, 2007, pp. 541–545, ISBN: 978-3-540-75996-6. DOI: 10.1007/978-3-540-75997-3_98.

[7] K. Resch and G. M. Wallner, 'Thermotropic layers for flat-plate collectors—A review of various concepts for overheating protection with polymeric materials', *Solar Energy Materials and Solar Cells*, vol. 93, no. 1, pp. 119–128, 2009, ISSN: 09270248. DOI: 10.1016/j.solmat.2008.09.004.

[8] K. Resch and G. M. Wallner, 'Morphology of phase-separated thermotropic layers based on UV cured acrylate resins', *Polymers for Advanced Technologies*, vol. 20, no. 12, pp. 1163–1167, 2009, ISSN: 10427147. DOI: 10.1002/pat.1393.

[9] K. Resch, G. M. Wallner and R. Hausner, 'Phase separated thermotropic layers based on UV cured acrylate resins – Effect of material formulation on overheating protection properties and application in a solar collector', *Solar Energy*, vol. 83, no. 9, pp. 1689–1697, 2009, ISSN: 0038092X. DOI: 10.1016/j.solener.2009.06.006.

[10] K. Resch, G. M. Wallner and R. W. Lang, 'Spectroscopic Investigations of Phase-Separated Thermotropic Layers Based on UV Cured Acrylate Resins', *Macromolecular Symposia*, vol. 265, no. 1, pp. 49–60, 2008, ISSN: 10221360. DOI: 10.1002/masy.200850506.

[11] K. Resch and A. Weber, 'Smart Windows - Smart Collectors: Entwicklung von funktionalen Überhitzungsschutzverglasungen für Gebäudeverglasungen und thermische Solarkollektoren', *Berg- und Hüttenmännische Monatshefte*, vol. 156, no. 11, pp. 429–433, 2011, ISSN: 0005-8912. DOI: 10.1007/s00501-011-0031-2.

[12] O. Muehling, A. Seeboth, T. Haeusler, R. Ruhmann, E. Potechius and R. Vetter, 'Variable solar control using thermotropic core/shell particles', *Solar Energy Materials and Solar Cells*, vol. 93, no. 9, pp. 1510–1517, 2009, ISSN: 09270248. DOI: 10.1016/j.solmat.2009.03.029.

[13] F. S. Bühler and M. Hewel, 'Reversibly thermotropic transparent molding material, useful e.g. in glazing or covers for shading and light-heat regulation in houses and cars etc.', pat. DE19841234C1, 1999.

[14] C. DeArmitt and G. E. Mc Kee, 'Moulded article with temperature dependent transparency', pat. EP1985663A1, 2008.

[15] A. Weber and K. Resch, 'Thermotropic glazings for overheating protection applications: Tuning the light-shielding efficiency by systematic material preselection and formulation', in *Solar Building Skins*, Economic Forum, Ed., Munich, 2011, pp. 73–77, ISBN: 978-3-981205343.

[16] A. Weber and K. Resch, 'Effect of Temperature-Cycling on the Morphology of Polymeric Thermotropic Glazings for Overheating Protection Applications', *Journal of Polymer Research*, vol. 19:9888, no. 6, pp. 1–8, 2012, ISSN: 1022-9760. DOI: 10.1007/s10965-012-9888-3.

[17] A. Weber and K. Resch, 'Thermotropic Glazings for Overheating Protection I: Material Pre-selection, Formulation and Light-Shielding Efficiency', *Journal of Applied Polymer Science*, ISSN: 0021-8995. DOI: 10.1002/app.39950.

[18] A. Weber, A. Schmid and K. Resch, 'Thermotropic Glazings for Overheating Protection II: Morphology and Structure-Property-Relationships', *Journal of Applied Polymer Science*, ISSN: 0021-8995. DOI: 10.1002/app.39910.

[19] A. Weber and K. Resch, 'Thermotropic glazings for overheating protection', *Energy Procedia*, vol. 30, pp. 471–477, 2012, ISSN: 18766102. DOI: 10.1016/j.egypro.2012.11.056.

[20] P. Nitz, 'Optical modelling and characterisation of thermotropic systems', Dissertation, Albert-Ludwigs-University, Freiburg i.B., 1999.

[21] D. P. Gruber, G. Winkler, A. Weber and K. Resch, 'Novel approach to the solution of the scattering problem in a thermotropic medium', vol. unpublished manuscript, 2013.

[22] C. Decker, 'The use of UV irradiation in polymerization', *Polymer International*, vol. 45, no. 2, pp. 133–141, 1998, ISSN: 0959-8103. DOI: 10.1002/(SICI)1097-0126(199802)45:2<133::AID-PI969>3.0.CO;2-F.

[23] V. V. Ivanov and C. Decker, 'Kinetic study of photoinitiated frontal polymerization', *Polymer International*, vol. 50, no. 1, pp. 113–118, 2001, ISSN: 0959-8103. DOI: 10.1002/1097-0126(200101)50:1<113::AID-PI594>3.0.CO;2-X.

[24] C. Decker, 'Photoinitiated crosslinking polymerisation', *Progress in Polymer Science*, vol. 21, no. 4, pp. 593–650, 1996, ISSN: 00796700. DOI: 10.1016/0079-6700(95)00027-5.

[25] G. A. Miller, L. Gou, V. Narayanan and A. B. Scranton, 'Modeling of photobleaching for the photoinitiation of thick polymerization systems', *Journal of Polymer Science Part A: Polymer Chemistry*, vol. 40, no. 6, pp. 793–808, 2002, ISSN: 0887-624X. DOI: 10.1002/pola.10162.

[26] C. Decker, K. Zahouily, D. Decker, T. Nguyen and T. Viet, 'Performance analysis of acylphosphine oxides in photoinitiated polymerization', *Polymer*, vol. 42, no. 18, pp. 7551–7560, 2001, ISSN: 00323861. DOI: 10.1016/S0032-3861(01)00221-X.

[27] C. Decker, 'Kinetic Study and New Applications of UV Radiation Curing', *Macromolecular Rapid Communications*, vol. 23, no. 18, pp. 1067–1093, 2002, ISSN: 10221336. DOI: 10.1002/marc.200290014. (visited on 09/02/2012).

[28] C. Decker and K. Moussa, 'UV-curable acrylic resins for production of glass laminates', *Journal of Applied Polymer Science*, vol. 55, no. 2, pp. 359–369, 1995, ISSN: 0021-8995. DOI: 10.1002/app.1995.070550218.

[29] E. Baur, S. Brinkmann, T. A. Osswald and E. Schmachtenberg, *Saechtling-Kunststoff-Taschenbuch*, 30th ed. München: Hanser, 2007, ISBN: 978-3-446-41437-2.

[30] M. Schimmelpfennig, K. Weber, F. Kalb, K.-H. Feller, T. Butz and M. Matthäi, 'Volumenausdehnung von Paraffinen aus Steigrohr-Messungen', in *Jahrbuch für den Praktiker 2007*, B. Ziolkowsky, Ed., vol. 50, Augsburg: Verlag für chemische Industrie, 2007, pp. 417–429.

[31] G. W. Ehrenstein, *Polymer-Werkstoffe: Struktur - Eigenschaften - Anwendung*, 3rd ed. München: Hanser, 2011, ISBN: 978-3-446-42283-4.

[32] J. A. Arceneaux and K. Willard, *UV&EB Chemistry and Technology*, 2013. [Online]. Available: http://72.52.184.8/~radtecho/pdfs/PrinterGuideChemistry.pdf (visited on 10/01/2013).

[33] M. J. Mikl, ‘Herstellung und Charakterisierung von thermotropen Systemen mit fixierten Domänen’, Diplomarbeit, University of Leoben, Leoben, 2010.

9 Introduction to Publication 4

The challenge of preventing vacuole formation in TSFD formulated with paraffin wax as thermotropic additive and UV-curable resin matrix was successfully accomplished in chapter 8. Nevertheless, a major challenge remained unsolved so far: Diameters of scattering domains formed by paraffin wax are still inappropriate for efficient overheating protection. Earlier publications [1]–[3] highlighted this issue as hampering the establishment of TSFD with efficient overheating protection performance. However, they were not able to solve this problem. Furthermore, as outlined earlier, several TSFD formulated with more polar thermotropic additives faced an additional challenge: Not only the scattering domain dimensions were inappropriate for overheating protection. Indeed, the observed scattering domain shapes were inappropriate as well. The formation of inappropriate scattering domain shapes was ascribed to a rather complex effect: Upon manufacturing of the TSFD, temperatures exceeding the melting temperatures of the thermotropic additives were maintained. Due to matrix/additive interactions the additives were solubilised in the resin matrix and a one-phase mixture was formed. Upon cooling, a two-phase system was established by precipitation of the thermotropic additive. The precipitation was induced by additive crystallisation and thus the energetically most favourable shape of the additive domains was established. Obviously, in several cases this was a non-spherical shape. Attempts to establish spherical instead of non-spherical scattering domains in these TSFD by addition of additives – like potential nucleation agents – failed and thus are only presented in the respective project report [4].

In view of these results, it was considered to be more promising to tune the scattering domain size in TSFD that already exhibit spherical scattering domains (e.g. like TSFD formulated with paraffin wax as thermotropic additive and UV-curable resin matrix).

Thus, mixtures of matrix and thermotropic additive that were showing insignificant solubilisation of the additive in the matrix were considered to be relevant. Such kind of mixtures form a persistent liquid/liquid two-phase mixture during manufacturing and thus form predominantly spherical or ellipsoidal additive droplets, similar as in conventional emulsions [5]. Upon crystallisation of the additive, the droplet shape may persist and thus spherical or ellipsoidal additive domains are formed. Hence, only the size of the droplets has to be adjusted in order to be appropriate for efficient back-scattering. Subsequently, considerations with regard to size adjustment of the droplets are discussed more in detail.

In two-phase mixtures, the established size of the minor phase is dependent on a wide variety of factors including rheological aspects (shear flow, elongational flow, viscosity ratio of the phases, etc.) and interaction of major and minor phase for example [5]–[8]. In conventional O/W-emulsions for example, the interactions of major and minor phase can obviously be tuned by addition of surfactants yielding a change in interfacial tension between major and minor phase and thus a potenial reduction in droplet size of the minor phase. From similarity considerations (prior to curing, a mixture of UV-curable resin matrix and thermotropic additive form a liquid/liquid two-phase system) manipulation of interaction of both phases of TSFD were considered to be a promising approach in order to reduce diameter of established scattering domains.

Another promising approach was to enhance the number of additive domains and thus to form smaller droplets due to mass conservation. With regard to these considerations, the introduction of additional crystallisation nuclei by changing processing temperature (affecting homogeneous nucleation of additive crystallisation) and/or addition of potential nucleation agent (heterogeneous nucleation) were considered to be reasonable. In the subsequent manuscript the outlined hypotheses are exploited more in detail and the viability of the suggested measures in order to enhance the overheating protection performance of TSFD is evaluated.

9.1 References

[1] K. Resch and G. M. Wallner, 'Morphology of phase-separated thermotropic layers based on UV cured acrylate resins', *Polymers for Advanced Technologies*, vol. 20, no. 12, pp. 1163–1167, 2009, ISSN: 10427147. DOI: 10.1002/pat.1393.

[2] K. Resch, G. M. Wallner and R. W. Lang, 'Spectroscopic Investigations of Phase-Separated Thermotropic Layers Based on UV Cured Acrylate Resins', *Macromolecular Symposia*, vol. 265, no. 1, pp. 49–60, 2008, ISSN: 10221360. DOI: 10.1002/masy.200850506.

[3] A. Weber and K. Resch, 'Effect of Temperature-Cycling on the Morphology of Polymeric Thermotropic Glazings for Overheating Protection Applications', *Journal of Polymer Research*, vol. 19:9888, no. 6, pp. 1–8, 2012, ISSN: 1022-9760. DOI: 10.1007/s10965-012-9888-3.

[4] K. Resch, A. Weber, D. Gruber, K. Schnetzinger and W. Kern, *Smart Windows - Smart Collectors: Entwicklung, Modellierung und Vermessung von Überhitzungsschutzverglasungen für Fassaden- und Kollektoranwendungen: Endbericht WPR-NKP.09.014-01: Projekt NKP.09.014*, Leoben, 2013.

[5] S. R. Derkach, 'Rheology of emulsions', *Advances in Colloid and Interface Science*, vol. 151, no. 1-2, pp. 1–23, 2009, ISSN: 00018686. DOI: 10.1016/j.cis.2009.07.001.

[6] P. Walstra, 'Principles of emulsion formation', *Chemical Engineering Science*, vol. 48, no. 2, pp. 333–349, 1993, ISSN: 00092509. DOI: 10.1016/0009-2509(93)80021-H.

[7] C. Dalmazzone, 'Génération mécanique des émulsions: Mechanical Formation of Emulsions', *Oil & Gas Science and Technology*, vol. 55, no. 3, pp. 281–305, 2000, ISSN: 1294-4475. DOI: 10.2516/ogst:2000020.

[8] H. P. Grace, 'Dispersion phenomena in high viscosity immisible fluid systems and application of static mixers as dispersion devices in such systems', *Chemical Engineering Communications*, vol. 14, no. 3-6, pp. 225–277, 1982, ISSN: 0098-6445. DOI: 10.1080/00986448208911047.

10 Publication 4

10.1 Bibliographic Information

- Title: Thermotropic Overheating Protection Glazings: Effect of Functional Additives and Processing Conditions on Light-Shielding Efficiency
- Authors:
  - Andreas Weber[1]
  - Katharina Resch[2]
    1. Polymer Competence Center Leoben GmbH, Roseggerstrasse 12, 8700 Leoben, Austria
    2. Department Polymer Engineering and Science, Materials Science and Testing of Polymers, University of Leoben, Otto Glöckel-Strasse 2, 8700 Leoben, Austria
- Periodical: Journal of Polymer Engineering
- Status: submitted

Statement with regard to publication: The manuscript presented here is an adapted manuscript in order to fit the formatting of the thesis and does not necessarily reflect exactly the actually published version.

10.2 Abstract

Within this study the effect of functional additives and processing conditions on the light-shielding efficiency of thermotropic systems with fixed domains (TSFD) for overheating protection purposes was evaluated. Focus was on improving overheating protection performance of a prototype TSFD based on UV curable acrylate resin by optimisation of material constitution (addition of functional additives like surfactants and nucleating agents) and processing conditions (temperature conditions during manufacturing, annealing). For the evaluated system an effect of nucleating agent on the light-shielding efficiency was ascertained. Furthermore, omission of an annealing step improved light-shielding efficiency slightly.

10.3 Introduction

Thermotropic glazings change optical appearance from transparent to opaque upon exceeding a certain threshold temperature reversibly [1], [2]. Their utilisation in the façade of a building can maintain a reduction in energy consumption for heating, cooling and artificial day-lighting (smart window) [3]–[5]. Thus, a reduction in overall energy demand of a building is achievable [3]–[5]. Furthermore, thermotropic glazings can provide efficient overheating protection for solar thermal collectors and thus can limit stagnation temperatures to less than 130 °C (smart collector) [6]. Hence, stagnation control by thermotropic glazings can alleviate thermal load on solar thermal systems (especially collectors) and heat carrier fluid and thus prevent those from deterioration, ageing and failure [7]. Especially for polymeric solar thermal systems stagnation control is a prerequisite in order not to exceed the long-term service temperatures of utilised – preferably cost-efficient – polymeric materials [6]–[9].

Besides other classes of thermotropic glazing materials, thermotropic systems with fixed domains (TSFD) gained interest in recent research due to their specific advantages like ease of adjustment of switching threshold, high long-term stability, low hysteresis, high reversibility and steep switching process [9]–[30]. TSFD consist of a

thermotropic additive which is finely dispersed in a matrix material [1], [3]. Below the threshold temperature refractive indices of matrix and additive are almost equal yielding transparent appearance of the TSFD [1]. Upon exceeding the threshold temperature (i.e. the melting temperature of the additive) a steep increase in refractive index difference between matrix and additive is imparted with the onset of intense light-scattering and thus a transmittance reduction [1]. Besides refractive index difference, TSFD morphology is of paramount importance for overheating protection performance [31], [32]. Maximum light-shielding efficiency is attained by spherical scattering domains with diameter in the range between 200 and 400 nm [31].

Recent studies regarding TSFD revealed limited overheating protection performance of the layers due to inappropriate scattering domain size and/or shape for optimum light-shielding efficiency [17], [19], [26], [28], [30]. In a preceding study, potential remedies in order to adjust scattering domain shape and size were outlined [30]. During manufacturing, uncured matrix material (i.e. a mixture of an oligomer, reactive diluent and photo-initiator) and thermotropic additive form a kind of emulsion. In conventional emulsions the addition of surfactants yields a reduction in droplet size by changing interfacial energy between continuous and disperse phase [33]–[36]. In analogy, the addition of surfactants to mixtures of matrix material and additive might also reduce scattering domain size. However, surfactants may also induce heterogeneous nucleation in additive domains. This was observed in emulsions of phase change materials for example [37]. Usually, heterogeneous nucleation is induced by intentional addition of nucleating agents to a crystallisable substance [38]–[42]. Addition to mixtures of matrix material and additive may probably yield a reduction in size of scattering domains by increasing number of crystallisation loci and by affecting free energy for crystallisation. Furthermore, temperature conditions during manufacturing process may affect the overheating protection performance of TSFD significantly [14], [29], due to temperature-affected variations in nucleation of crystallisation which probably induce changes in scattering domain size distribution. Furthermore, an annealing step employed after curing probably enhances homogeneity of TSFD.

Thus, the major objective of the present study is to investigate the effect of surfactants and nucleating agents on scattering domain parameters and hence the light-shielding

efficiency of TSFD produced from UV-curable resin. As the light-shielding properties of TSFD are directly related to the TSFD morphology, determining the solar optical properties of TSFD is an appropriate index in order to quantify the effect of the employed measures on TSFD morphology. Furthermore, the effect of processing conditions (thermal treatment, annealing) on the overheating protection performance of TSFD is studied. Effects are investigated by employing tools of factorial design.

10.4 Experimental

10.4.1 Materials and Formulation

To address the aspects discussed above TSFD M7A1-OTA-p3-RT-0.008 – which was already developed in a preceding publication [29] – was selected as prototype system. That specific layer was selected because it exhibited appropriate scattering domain shape (spherical) but inappropriate scattering domain diameter for efficient overheating protection. A reduction in scattering domain diameter is likely to enhance the light-shielding efficiency significantly.

The layers formulated within this study were thus derivatives of TSFD M7A1-OTA-p3-RT-0.008. UV-curable resin matrix consisted of 57 wt% polyester acrylate oligomer Ebecryl 800 (Allnex Belgium SA/NV, former Cytec Surface Specialities, Drogenbos, BE), 40 wt% reactive diluent OTA-480 (abbr. OTA) – a propoxylated glycerol esterified with acrylic acid (Allnex) – and 3 wt% photo-bleaching photo-initiator Lucirin TPO-L (BASF SE, Ludwigshafen, DE). Thermotropic additive was paraffin wax Sasolwax 5005 (additive A1; Sasol Wax GmbH, Hamburg, DE) with melting point at 55 °C [28]. The nomenclature of the thermotropic additive is consistent with previous publications [28]–[30]. Functional additives were non-ionic surfactant Lutensol AT11 (BTC Europe GmbH, Köln, DE) and the potential nucleating agent synthetic Indigo (Sigma-Aldrich Handels GmbH, Wien, AT). Initially, Indigo was chosen as potential nucleation agent from analogy considerations: Paraffin waxes and polyolefins have similar structure. In polypropylene (a polyolefin) Indigo was recognised as efficient nucleating agent [43], [44]. Thus Indigo is supposed to act as a nucleating agent in paraffin waxes also. Table 10.1 shows the factors and factor levels employed upon TSFD formulation.

Table 10.1

Whereas the factor levels employed for the factor AT11 concentration were either 0.01 or 0.02 mol kg^{-1}, the factor levels maintained for the factor Indigo concentration were either 0 or 0.001 mol kg^{-1}. Thermotropic layers were prepared by dissolving the thermotropic additive and functional additives in the UV-curable matrix solution. Dissolutions were poured in the intervening space between two glass panes which were sealed around the edge and stored at either −20 °C (factor level "DF") or room temperature (factor level "RT") for 10 min prior and post curing. Thermotropic mixtures were cured with an intensity of 4.6 µW cm^{-2} yielding a dose of 8.3 mJ cm^{-2} from 366 nm lamp of Universal-UV-Lamp (Camag, Muttenz, CH). Free standing layers with a thickness of 900 µm were obtained after removal of the glass panes. Theoretical additive concentration was 5 wt%. TSFD were either annealed at the mixing temperature (100 °C) of resin matrix and the thermotropic additive (factor level 1) or not annealed (factor level −1). Accordingly, the parental layer M7A1-OTA-p3-RT-0.008 represents the factor combination AT11: 0 mol kg^{-1}; Indigo: 0 mol kg^{-1}; Treatment: RT; Annealing: no).

Table 10.1.: Factors and factor levels employed for formulation of TSFD.

Factors and Levels	c(AT11) [mol kg^{-1}][a]		c(Indigo) [mol kg^{-1}][a]		Treatment[b] [—]		Annealing[c] [—]	
Coded	−1	+1	−1	+1	−1	+1	−1	+1
Uncoded	0.01	0.02	0	0.001	RT	DF	no	yes

[a] mol functional additive related to kilograms of thermotropic mixture (matrix + thermotropic additive)

[b] RT: storage at room temperature for 10 min prior and post curing; DF: storage at −20 °C for 10 min prior and post curing

[c] at the mixing temperature of resin matrix and thermotropic additive

10.4.2 Characterisation Methodology

10.4.2.1 Light-Shielding Efficiency

Overheating protection performance of TSFD was determined applying UV/Vis/NIR spectrometry. A double beam UV/Vis/NIR spectrophotometer Lambda 950 (Perkin

Elmer Inc., Waltham, MA, US) equipped with an Ulbricht-sphere (diameter 150 mm) was employed. For the given measurement apparatus the radiation passing through (transmittance) the specimen outside a cone of approximately 5° relative to the incident beam direction was defined as diffuse (scattered) component. Hemispheric and diffuse transmittance was recorded at normal incidence in the spectral region from 250 to 2500 nm. The integral solar transmittance was determined by weighting the recorded spectral data in steps of 5 nm by the AM1.5 global solar irradiance source function. The spectrophotometer was adapted by a heating stage to adjust sample temperature within a range from ambient temperature to maximum 115 °C [28]. Measurements were performed at room temperature and 70 °C. Prior to measurement, the samples were allowed to equilibrate for five minutes at the selected temperature. The heating stage was equipped with a control system consisting of a heating stage-internal J-type thermocouple as temperature sensor and the control unit HS-W-35/M (Heinz Stegmeier Heizelemente HS-Heizelemente GmbH, Fridingen, DE). Within the heating stage the sample was positioned in close proximity of the port hole of the Ulbricht-sphere. In situ front- and backside sample surface temperatures as a function of set-point value of the control unit were recorded on a prototype sample with a two-channel temperature measurement instrument T900 (Dostmann electronic GmbH, Wertheim-Reicholzheim, DE) equipped with a precision K-type thermocouple. Sample temperature was assumed as the average of both recorded surface temperatures. Required set-point values to maintain average sample temperatures were calculated from a second order polynomial fit of the temperatures recorded in measurements of the prototype sample. A double determination was carried out.

10.4.2.2 Morphology

Morphological characterisation of TSFD was carried out applying an optical microscope Olympus BX51 (Olympus Austria Ges. m. b. H., Wien, AT) in transmitted light mode. TSFD were investigated without further preparation. Domain size was evaluated with measurement tools of software analySIS (Soft Imaging System GmbH, Münster, DE). Minimum and maximum sizes of scattering domains were evaluated.

10.5 Results and Discussion

Table 10.2 presents the response – solar hemispheric transmittance detected either at room temperature ($\tau_{nh}{}^{RT}$) or at 70 °C ($\tau_{nh}{}^{70}$) – of the investigated TSFD upon application of different factor combinations during manufacturing process. Factors varied were concentration of functional additives AT11 and Indigo as well as thermal treatment and annealing (see Table 10.1). Solar hemispheric transmittance varied between 67.3 and 82.3 % at room temperature on the one hand side and between 66.1 and 82.3 % at 70 °C on the other hand side. The layers formulated with Indigo displayed the lowest solar hemispheric transmittance: Their transmittance varied between 67.3 and 76.0 % (layers without Indigo 78.8–82.3 %) at room temperature and between 66.1 and 76.3 % (layers without Indigo 79.6–82.3 %) at 70 °C. That was attributed to the colouration of TSFD induced by Indigo. In Figure 10.1 hemispheric transmittance spectra at room temperature of layers formulated without (solid line; factor combination AT11: 0.01 mol kg^{-1}; Indigo: 0 mol kg^{-1}; Treatment: RT; Annealing: no) or with (dash-dotted line; factor combination AT11: 0.01 mol kg^{-1}; Indigo: 0.001 mol kg^{-1}; Treatment: RT; Annealing: no) Indigo are presented. Around 600 nm, the layer formulated with Indigo displayed a lower transmittance compared to the layer formulated without Indigo. That was ascribed to absorption characteristics of Indigo. Furthermore, Indigo introduced inhomogeneities to the TSFD: In optical micrographs, individual pigment particles of Indigo were discernible. Figure 10.2 shows an optical micrograph of a layer formulated without Indigo (Figure 10.2a) along with the optical micrograph of a layer formulated with Indigo (Figure 10.2b). Both layers exhibited spherical scattering domains (bright spots) with similar size. Apart from the scattering domains, the layer formulated with Indigo showed plate-like structures (black arrows are pointing on several ones) additionally. These structures were Indigo (pigment) particles. These particles are distributed in the matrix and are not nucleating an additive domain. Thus, Indigo seems to be not as effective in nucleating the thermotropic additive A1 as desired. Furthermore, the layers formulated with Indigo exhibited agglomerates of Indigo, yielding heterogeneous colouration.

Table 10.2

Figure 10.1

Figure 10.2

Table 10.2.: Response of formulated TSFD regarding solar hemispheric transmittance at room temperature ($\tau_{nh}{}^{RT}$) and 70 °C ($\tau_{nh}{}^{70}$).

c(AT11) [mol kg^{-1}]	c(Indigo) [mol kg^{-1}]	Treatment [—]	Annealing [—]	$\tau_{nh,1}{}^{RT}$ [%]	$\tau_{nh,2}{}^{RT}$ [%]	$\tau_{nh,1}{}^{70}$ [%]	$\tau_{nh,2}{}^{70}$ [%]
0.01	0	RT	no	81.4	82.3	80.6	81.5
0.02	0	RT	no	81.5	81.7	81.7	81.9
0.01	0.001	RT	no	75.8	74.7	75.7	74.1
0.02	0.001	RT	no	73.4	73.8	72.4	72.8
0.01	0	DF	no	80.5	81.5	79.8	80.0
0.02	0	DF	no	81.0	82.1	81.1	81.6
0.01	0.001	DF	no	74.4	74.2	73.4	72.3
0.02	0.001	DF	no	68.1	72.6	66.1	69.8
0.01	0	RT	yes	80.4	78.8	81.2	81.2
0.02	0	RT	yes	80.7	80.2	82.3	81.0
0.01	0.001	RT	yes	73.7	73.3	73.0	71.3
0.02	0.001	RT	yes	75.7	75.3	76.3	75.5
0.01	0	DF	yes	79.4	80.6	79.6	80.3
0.02	0	DF	yes	80.7	80.5	80.4	80.0
0.01	0.001	DF	yes	67.7	67.3	70.1	69.4
0.02	0.001	DF	yes	76.0	73.3	75.8	74.6

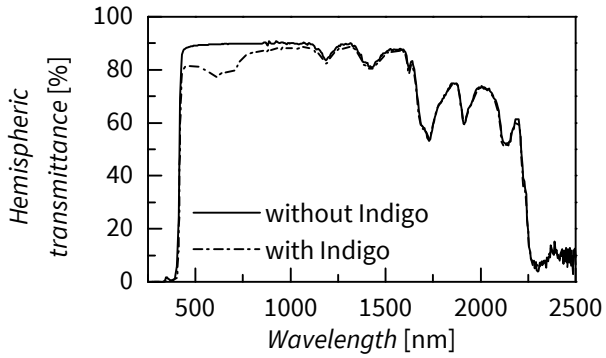

Figure 10.1.: Hemispheric transmittance of TSFD formulated without (solid line; treatment combination AT11: 0.01 mol kg^{-1}; Indigo: 0 mol kg^{-1}; Treatment: RT; Annealing: no) and with (dash-dotted line; treatment combination AT11: 0.01 mol kg^{-1}; Indigo: 0.001 mol kg^{-1}; Treatment: RT; Annealing: no) Indigo.

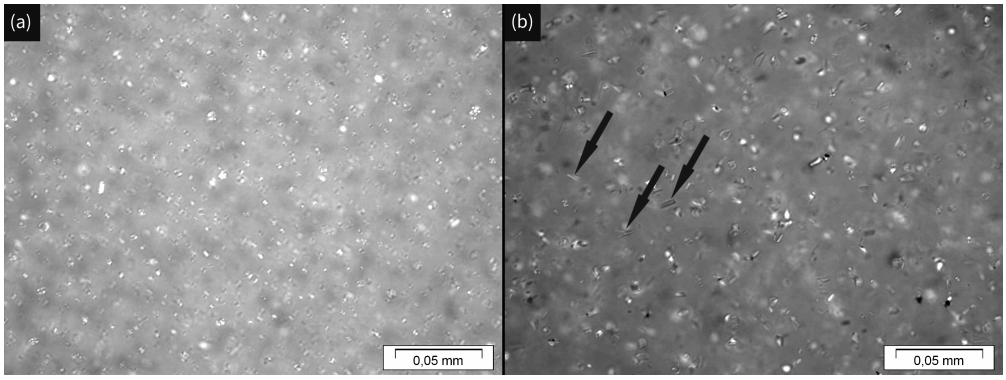

Figure 10.2.: Optical micrographs of layers formulated **(a)** without (treatment combination: AT11: 0.01 mol kg^{-1}; Indigo: 0 mol kg^{-1}; Treatment: RT; Annealing: no) and **(b)** with (treatment combination: AT11: 0.01 mol kg^{-1}; Indigo: 0.001 mol kg^{-1}; Treatment: RT; Annealing: no) Indigo. Black arrows are pointing on several Indigo particles. Contrast of the image was enhanced by image processing software.

Summarizing, the addition of Indigo yielded a transmittance reduction of the prototype TSFD which was ascribed to the predominating effect of absorption of incident radiation. Moreover, the desired nucleating agent-induced reduction in scattering domain-size by addition of Indigo as potential nucleating agent for the thermotropic additive was not achieved. This may be ascribed to a lack of nucleating potential of Indigo for the utilised paraffin wax. Anyway, due to the observed inhomogeneities –

caused by Indigo agglomerates – which yielded a potential bias for statistical analysis, subsequent discussion is going to omit TSFD formulated with Indigo.

Analysis of variance (ANOVA; coded factor levels according to Table 10.1 were employed upon calculation of the factor effects) of the data presented in Table 10.2 revealed the most important factors with regard to solar hemispheric transmittance. For solar hemispheric transmittance at room temperature, the effect of the factor Annealing was significant only (see Table 10.3). The other factors displayed insignificant effects. On the contrary, for solar hemispheric transmittance at 70 °C the effect of factor Treatment was significant only (see Table 10.4). Except for the factor AT11 concentration – its effect was indifferent – all other factors exhibited insignificant effects.

Table 10.3

Table 10.4

Table 10.3.: Results of the Analysis of Variance of the quasi-2^3 full factorial design regarding solar hemispheric transmittance of formulated TSFD at room temperature ($\tau_{nh}{}^{RT}$). Layers formulated with Indigo were omitted.

Factors	Effect	P-Value [a] for test regarding factor effect on $\tau_{nh}{}^{RT}$	Effect significance assessment [b]
c(AT11)	0.445	0.237	–
Treatment	−0.061	0.865	–
Annealing	−1.327	0.005	+
c(AT11)×Treatment	0.137	0.704	–
c(AT11)×Annealing	0.275	0.453	–
Treatment×Annealing	0.348	0.347	–
c(AT11)×Treatment×Annealing	−0.264	0.470	–

[a] Test statistics according to Montgomery [45]

[b] according to Kleppmann [46]. Applied symbols: "–" insignificant, "o" indifferent, "+" significant, "++" highly significant

Table 10.4.: Results of the Analysis of Variance of the quasi-2^3 full factorial design regarding solar hemispheric transmittance of formulated TSFD at 70 °C (τ_{nh}^{70}). Layers formulated with Indigo were omitted.

Factors	Effect	P-Value [a] for test regarding factor effect on τ_{nh}^{RT}	Effect significance assessment [b]
c(AT11)	0.727	0.014	o
Treatment	−1.104	>0.001	+
Annealing	−0.299	0.234	-
c(AT11)×Treatment	0.117	0.629	-
c(AT11)×Annealing	−0.362	0.158	-
Treatment×Annealing	−0.303	0.227	-
c(AT11)×Treatment×Annealing	−0.225	0.362	-

[a] Test statistics according to Montgomery [45]

[b] according to Kleppmann [46]. Applied symbols: "–" insignificant, "o" indifferent, "+" significant, "++" highly significant

Figure 10.3

Figure 10.3 displays a plot regarding the factor effects of the factors concentration of functional additive AT11, thermal treatment and annealing on solar hemispheric transmittance at room temperature (RT) and at 70 °C of layers formulated without Indigo. Individual data points are presented for room temperature (squares) and for 70 °C (circles). Furthermore, the change in mean value of solar hemispheric transmittance upon changing a factor level is presented either with a solid line (for RT) or a dashed line (for 70 °C). Results were derived from data presented in Table 10.2. The mean solar hemispheric transmittances at room temperature and 70 °C were both lower for factor level 0.01 mol kg^{-1} than for factor level 0.02 mol kg^{-1} of factor AT11 concentration. The parallel slope of the mean plots indicated that the factor AT11 concentration did not interact with the measurement temperature. Furthermore, for both factor levels of the factor AT11 concentration the mean solar hemispheric transmittance did only change to a minor extent when exceeding the switching threshold. Probably, an increase in AT11 concentration improved the overall transmittance of

the TSFD by affecting the scattering domain size distribution. Imagine two scattering domain size distributions: Whereas one size distribution displays scattering domains with sizes close to the optimum, another size distribution displays bigger domains. Assuming a slight difference in refractive indices of matrix and additive already existing at room temperature, a TSFD exhibiting the latter scattering domain size distribution will show pronounced forward-scattering and reduced back-scattering compared to a TSFD exhibiting optimally sized scattering domains. Thus also solar hemispheric transmittance will be higher. However, the factor effects of the factor AT11 concentration with regard to solar hemispheric transmittance at room temperature and at 70 °C were rather small. Actually, the factor effects were insignificant and indifferent with regard to solar hemispheric transmittance detected at room temperature and 70 °C, respectively (see Tables 10.3, 10.4). The rather small factor effect of the factor AT11 concentration was also related to the calculated insignificance of any factor with regard to the scattering domain diameter minima and maxima (see Table 10.5; diameters varied between 1.4 and 1568 µm). Thus, variation in AT11 concentration did not affect the scattering domain size in the desired way. Furthermore, the additive AT11 seems to be inappropriate to reduce the scattering domain size and thus to yield a significant improvement in light-shielding efficiency because the addition of AT11 was not effectual in order to enhance the difference between solar hemispheric transmittance at room temperature and at 70 °C: For a layer lacking any AT11 (specifically that was layer M7A1-OTA-p3-RT-0.008 [29], which represents a treatment combination of AT11: 0 mol kg^{-1}; Indigo: 0 mol kg^{-1}; Treatment: RT; Annealing: no), a solar hemispheric transmittance of 81.2 and 78.5 % was achieved below and above the threshold temperature, respectively. Upon application of an AT11 concentration of 0.01 mol kg^{-1} solar hemispheric transmittance was recorded to be 81.9 and 81.1 % below and above the threshold temperature, respectively. For an AT11 concentration of 0.02 mol kg^{-1} solar hemispheric transmittance was 81.6 and 81.8 % below and above the threshold temperature, respectively. These mean values were calculated from respective data presented in Table 10.2 – row 1 and 2. Thus, AT11 did not act in the supposed manner (like a surfactant in an emulsion) in the investigated resin systems. However, the two other factors Treatment and Annealing showed more distinct effects, as already demonstrated by ANOVA.

Table 10.5

For both factor levels of the factor Treatment, the mean solar hemispheric transmittances at room temperature were almost the same. For factor level RT, mean solar hemispheric transmittance was higher at 70 °C than at room temperature. On the contrary, for factor level DF the mean solar hemispheric transmittance was lower at 70 °C than at room temperature.

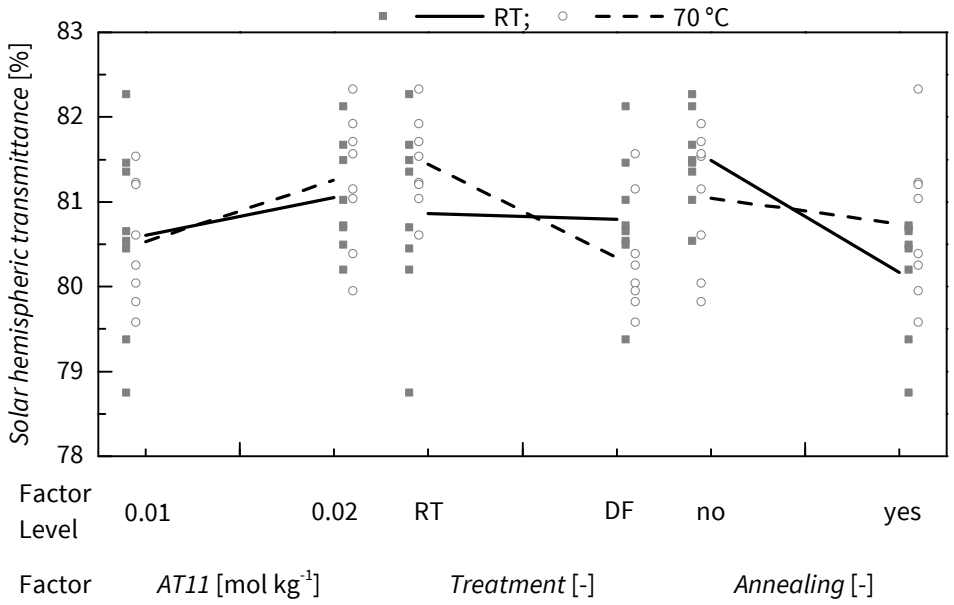

Figure 10.3.: Plot regarding effects of factors concentration of functional additive AT11, thermal treatment (Treatment) applied during manufacturing and Annealing on solar hemispheric transmittance of TSFD at room temperature (RT; single data points represented by squares; change of mean value illustrated by solid line) and at 70 °C (single data points represented by circles; change of mean value illustrated by dashed line) for layers formulated without Indigo.

For factor Annealing, the findings were quite similar. Layers lacking annealing displayed a higher mean solar hemispheric transmittance at room temperature than the annealed layers. For layers lacking annealing, the solar hemispheric transmittance was lower at 70 °C than at room temperature. For the annealed layers, the temperature-dependent behaviour was inverted. Such kind of behaviour was observed already in earlier studies [28]–[30]: TSFD without defects (like vacuoles or voids) showed a decrease in solar hemispheric transmittance upon exceeding the threshold temperature. This behaviour is consistent with the observed increase in refractive index difference between matrix and thermotropic additive upon exceed-

ing the threshold temperature [28], [30]. On the contrary, TSFD displaying defects (especially vacuoles) exhibited an increase in solar hemispheric transmittance upon exceeding the threshold temperature [28]–[30]. The low solar hemispheric transmittance at room temperature was attributed to the high refractive index difference established between matrix/additive (n approx. 1.5) and vacuoles (n = 1). Upon melting of the additive, the vacuoles disappeared and the subsequent reduction in refractive index difference at the scattering interfaces yielded a higher solar hemispheric transmittance than at room temperature. Taking these previous findings into account, the annealed layers were suspected to exhibit defects.

Table 10.5.: Minimum and maximum of scattering domain diameter detected for spherical domains in formulated TSFD.

c(AT11) [mol kg^{-1}]	c(Indigo) [mol kg^{-1}]	Treatment [—]	Annealing [—]	Diam., min. [µm]	Diam., max. [µm]
0.01	0	RT	no	1.4	1568
0.02	0	RT	no	3.2	907
0.01	0.001	RT	no	1.8	170
0.02	0.001	RT	no	3.0	537
0.01	0	DF	no	1.9	949
0.02	0	DF	no	1.9	1198
0.01	0.001	DF	no	1.9	983
0.02	0.001	DF	no	2.1	802
0.01	0	RT	yes	1.9	244
0.02	0	RT	yes	2.5	607
0.01	0.001	RT	yes	2.5	486
0.02	0.001	RT	yes	1.9	410
0.01	0	DF	yes	1.8	374
0.02	0	DF	yes	3.0	657
0.01	0.001	DF	yes	2.4	276
0.02	0.001	DF	yes	1.4	353

The findings for the factors Treatment and Annealing were an indication for possible changes in the internal material structure upon changing factor levels. Thus, in

Figure 10.4 light micrographs of layers formulated upon application of different factor combinations are displayed. Focus is on the different factor levels of the factors Treatment and Annealing. Whereas the layers lacking annealing displayed almost no vacuoles inside the spherical scattering domains (Figures 10.4a,c), the annealed layers exhibited a higher number of vacuoles (dark areas) inside the scattering domains (Figures 10.4b,d). Nevertheless, the vacuole concentration was rather low compared to layers which were not optimised with regard to curing procedure [29]. It can be concluded that in spite of enhancing the homogeneity of TSFD – which was initially supposed – annealing introduced additional vacuoles to the TSFD.

Figure 10.4

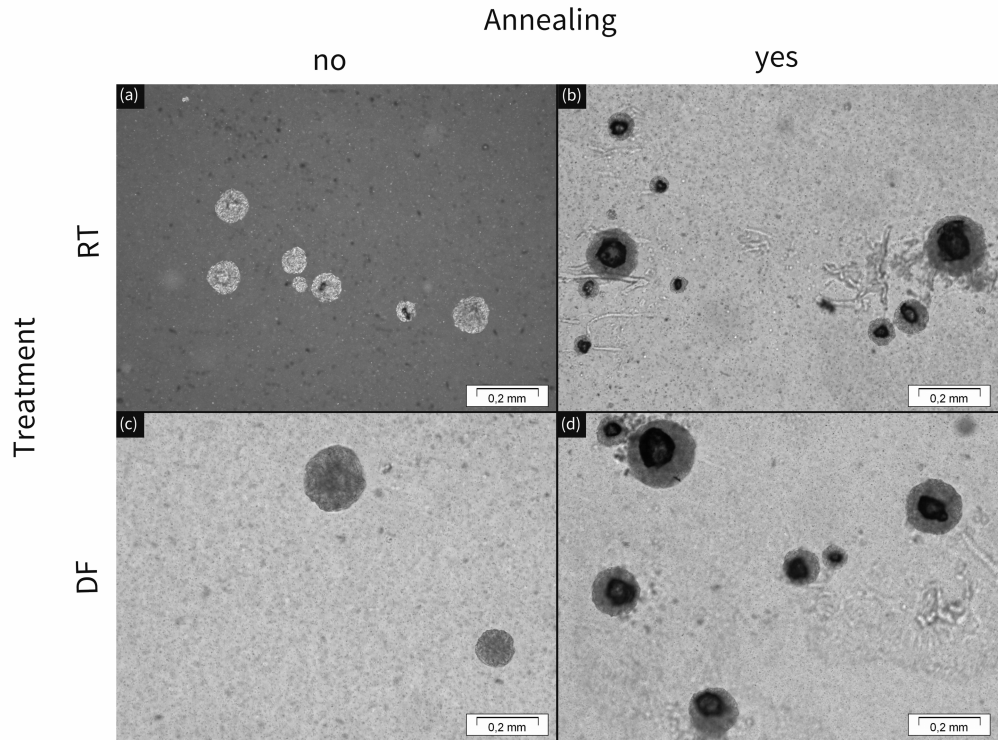

Figure 10.4.: Light micrographs of TSFD obtained upon application of different factor combinations **(a)** AT11: 0.01 mol kg^{-1}; Indigo: 0 mol kg^{-1}; Treatment: RT; Annealing: no **(b)** AT11: 0.01 mol kg^{-1}; Indigo: 0 mol kg^{-1}; Treatment: RT; Annealing: yes **(c)** AT11: 0.01 mol kg^{-1}; Indigo: 0 mol kg^{-1}; Treatment: DF; Annealing: no **(d)** AT11: 0.01 mol kg^{-1}; Indigo: 0 mol kg^{-1}; Treatment: DF; Annealing: yes.

These observations led to the conclusion, that the significant effect of Annealing on the solar hemispheric transmittance at room temperature is associated with these

vacuoles. The vacuoles were probably formed during the annealing process. This was ascribed to a thermally-driven diffusion process of molten additive, leaving less thermotropic additive within the cavity provided by the matrix material after the annealing process. This hypothesis is supported by the observation of thermally induced diffusion processes of thermotropic additive in a preceding study [26], yielding a loss of thermotropic additive inside matrix cavities. Vacuoles have a refractive index equal to unity, yielding a rather high refractive index (RI) difference at the scattering interfaces (boundaries to matrix or additive, which both have a RI around 1.5 at room temperature). Consequently, high scattering efficiency is achieved, yielding a low solar hemispheric transmittance at room temperature. Upon exceeding the threshold temperature, the remaining additive fills the cavity completely due to its higher coefficient of thermal expansion compared to the matrix (e.g. $6 \times 10^{-5}\,K^{-1}$ to $8 \times 10^{-5}\,K^{-1}$ for PMMA [47] versus $0.7 \times 10^{-3}\,K^{-1}$ to $1.1 \times 10^{-3}\,K^{-1}$ for paraffin [48]) and vacuoles vanish. Thus, a lower refractive index difference is established at the scattering interface matrix/additive (RI around 1.5 versus 1.44 for matrix and additive, respectively). Consequently, the achieved lower scattering efficiency yields a higher solar hemispheric transmittance at 70 °C than at room temperature. For layers lacking vacuoles – like those not exposed to the annealing process – an increase in refractive index difference between matrix and scattering domain is achieved upon exceeding the threshold temperature. Consequently, an increase in scattering efficiency and hence a reduction in solar hemispheric transmittance upon exceeding the threshold temperature was achieved for these layers.

The considerations made before indicated that vacuoles are supposed to be absent at 70 °C. This hypothesis is supported by the assignment of an insignificant effect to the factor Annealing with regard to solar hemispheric transmittance at 70 °C. If vacuoles would have been present at 70 °C, the established high refractive index difference at the scattering interfaces would have yielded high scattering efficiency and thus a lower solar hemispheric transmittance compared to layers without vacuoles. The absence of vacuoles is hence also the reason why the layers formulated upon application of the different factor levels of factor Annealing displayed rather similar mean solar hemispheric transmittance at 70 °C.

However, these micrographs do not give a guiding line for the reason why the factor Treatment is the only significant with regard to solar hemispheric transmittance at 70 °C. From the data presented above, it is evident that layers exposed to Treatment factor level DF showed a lower solar hemispheric transmittance at 70 °C compared to layers which were subject to Treatment RT. Upon recognition of the postulated absence of vacuoles at 70 °C, only one reasonable conclusion can be drawn: The lower solar hemispheric transmittance at 70 °C for layers which were subject to Treatment DF compared to layers exposed to Treatment RT can only be due to differences in scattering domain size. This is because the absence of vacuoles implies that refractive index difference at the scattering interface for both factor levels are the same. Lower storage temperature (factor level DF) prior to UV-exposure probably yields faster nucleation and reduced mobility of additive droplets in the matrix due to higher viscosity. Thus, coalescence of additive droplets prior to solidification is probably reduced. Consequently, achievement of more and smaller scattering domains is likely. Provided that refractive index difference between matrix and additive is low, layers with smaller scattering domain diameter and layers with bigger scattering domains are likely to exhibit similar solar hemispheric transmittance at room temperature. However, upon melting of the additive, the smaller scattering domains would yield more efficient back-scattering and thus lower solar hemispheric transmittance of the corresponding layer. Hence, the factor Treatment would have nearly no effect on solar hemispheric transmittance at room temperature but a significant effect on solar hemispheric transmittance change when exceeding the threshold temperature. This hypothesis would fit best to the observed response to variations in factor Treatment. However, morphological analysis did not reveal differences in scattering domain size between layers produced under conditions of factor levels RT and DF: As already pointed out before, no significant differences in scattering domain diameter (neither with regard to minimum nor to maximum) were evident for the different factor combinations. This was ascribed to the small effects of the different applied factors, probably yielding only small changes in scattering domain size, which were not resolvable with light microscopy applied within this study.

Anyway, a key result of this study is that the employed factor combinations did not improve the scattering domain size of the TSFD and hence did not improve the light-

shielding efficiency of the TSFD reasonably. However, the experiments have also shown that light-shielding efficiency of TSFD is very sensible to vacuoles. Vacuole formation has to be avoided under any circumstances. A preceding study [29] pointed out that vacuole formation can be prevented by careful adjustment (i.e. reduction) of radiation intensity and dose employed upon curing of the TSFD. Now evidence is proven that selection of disadvantageous processing conditions others than radiation intensity and dose can also yield undesirable vacuole formation and thus reduction of light-shielding efficiency of the TSFD investigated.

10.6 Summary and Conclusion

For the investigated TSFD system, the addition of Indigo as potential nucleating agent reduced solar hemispheric transmittance at room temperature significantly due to colouration. Indigo also introduced undesirable inhomogeneities into TSFD due to its insolubility and indispersibility in the resin matrix. Furthermore, it was not able to nucleate the thermotropic additive in the desired way and thus to reduce the scattering domain size. This was ascribed to the lacking nucleation potential of Indigo with regard to the employed thermotropic additive. Altogether, the addition of Indigo was not beneficial with regard to TSFD performance. Thus, statistical data analysis was conducted for the layers formulated without Indigo. For these layers the application of an annealing step yielded a lower solar hemispheric transmittance at room temperature than for layers lacking annealing. Furthermore the annealed layers showed an increase in solar hemispheric transmittance upon exceeding the threshold temperature. The observed behaviour of the annealed layers was ascribed to vacuoles which were formed upon annealing. The vacuole formation was attributed to thermally-induced diffusion of the molten additive, yielding an additive loss inside the cavities provided by the surrounding matrix material. The vacuoles introduced a high refractive index difference at the scattering interfaces at room temperature, yielding intense scattering. Upon melting of the thermotropic additive the vacuoles disappeared and the refractive index difference at the scattering interfaces was reduced along with a reduction in scattering efficiency. In contrast, layers lacking annealing displayed no vacuoles. Thus, an increase in refractive index difference at the scattering interfaces

(i.e. matrix/thermotropic additive interfaces) was maintained. Consequently, a high solar hemispheric transmittance at room temperature and a transmittance reduction upon exceeding the threshold temperature was ascertained due to increasing scattering efficiency. Nevertheless, due to absence of vacuoles, morphology of layers annealed and not annealed was likely to be similar above the switching threshold of the TSFD. Consequently, the factor Annealing had no significant effect on solar hemispheric transmittance at 70 °C. On the contrary, the variation of the thermal treatment of the TSFD prior and post curing process (storage at −20 °C for 10 min prior and post curing instead of storage at room temperature) had a significant effect on the solar hemispheric transmittance at 70 °C (but not on transmittance at room temperature). The solar hemispheric transmittance at 70 °C was lower when the TSFD was stored at −20 °C than at room temperature. The lower storage temperature was suspected to enhance (homogeneous) nucleation of additive droplets and their solidification on the one hand side. On the other hand side, a storage temperature reduction increased the matrix viscosity and thus was likely to obstruct additive droplet mobility and coalescence. Hence, formation of a higher number of scattering domains – increasing scattering probability –, which are also smaller (improving scattering efficiency) due to mass conservation, was likely. However, morphological analysis by optical light microscopy revealed no differences with regard to scattering domain size of layers stored at −20 °C or room temperature. Anyway, the employed measures revealed no break-through in attempting a significant improvement of the overheating protection performance of TSFD: Although several of the applied measures slightly improved overheating protection performance of the investigated TSFD, attained light-shielding efficiency was not appropriate in order to maintain efficient overheating protection for a solar thermal collector. This was primarily attributed to inappropriate scattering domain size. Hence, other factors than the investigated might have a more important effect on the scattering domain diameter and thus the light-shielding efficiency. Some of these factors might be the deformation employed upon mixing, interfacial tension matrix/additive, viscosity ratio of the molten additive and the matrix resin, or type of flow field (laminar or turbulent), which seem to play a more important role than initially expected [34], [49]. Thus, future work has to focus on investigating other factors or entirely different approaches in order to improve scattering domain size.

Notwithstanding, formation of vacuoles via thermally induced diffusion of molten thermotropic additive yielding a deterioration of the light-shielding efficiency of TSFD might have severe implications with regard to application of a TSFD as overheating protection glazing. In order to preserve long-term overheating protection performance of TSFD, such diffusion has to be suppressed, probably by encapsulation of the thermotropic additive with a barrier layer. Otherwise, the efficiency of a solar thermal collector equipped with a TSFD exhibiting thermally induced additive diffusion as overheating protection glazing will suffer significantly from the reduced solar hemispheric transmittance of the TSFD. Accordingly, investigations dealing with adjustment of scattering domain size on the one hand side and encapsulation of the additive in order to prevent additive diffusion on the other hand side and subsequent assessment of long-term stability of the obtained TSFD are currently under way.

10.7 Acknowledgements

This research project is funded by the State Government of Styria, Department Zukunftsfonds (Project number 5019). The efforts in determination of solar-optical properties of parts of the formulated TSFD by Alexander KLUTZ (Department Polymer Engineering and Science, University of Leoben, Leoben, AT) are gratefully acknowledged. Furthermore the authors want to acknowledge the contributions of Allnex Belgium SA/NV (former Cytec Surface Specialities Inc., Drogenbos, BE), Sasol Wax GmbH (Hamburg, DE) and HDS-Chemie HandelsgesmbH (Wien, AT), BASF SE (Ludwigshafen, DE) and BTC Europe GmbH (Köln, DE).

10.8 References

[1] P. Nitz and H. Hartwig, 'Solar control with thermotropic layers', *Solar Energy*, vol. 79, no. 6, pp. 573–582, 2005, ISSN: 0038092X. DOI: 10.1016/j.solener.2004.12.009.

[2] A. Seeboth, J. Schneider and A. Patzak, 'Materials for intelligent sun protecting glazing', *Solar Energy Materials and Solar Cells*, vol. 60, no. 3, pp. 263–277, 2000, ISSN: 09270248. DOI: 10.1016/S0927-0248(99)00087-2.

[3] P. Nitz and A. Wagner, 'Schaltbare und regelbare Verglasungen', *BINE Themeninfo*, vol. I/02, no. I/02, pp. 1–12, 2002, ISSN: 1610-8302.

[4] T. Inoue, 'Solar shading and daylighting by means of autonomous responsive dimming glass: practical application', *Energy and Buildings*, vol. 35, no. 5, pp. 463–471, 2003, ISSN: 03787788. DOI: 10.1016/S0378-7788(02)00143-3.

[5] J. Yao and N. Zhu, 'Evaluation of indoor thermal environmental, energy and daylighting performance of thermotropic windows', *Building and Environment*, vol. 49, pp. 283–290, 2012, ISSN: 03601323. DOI: 10.1016/j.buildenv.2011.06.004.

[6] G. M. Wallner, K. Resch and R. Hausner, 'Property and performance requirements for thermotropic layers to prevent overheating in an all polymeric flat-plate collector', *Solar Energy Materials and Solar Cells*, vol. 92, no. 6, pp. 614–620, 2008, ISSN: 09270248. DOI: 10.1016/j.solmat.2007.12.005.

[7] S. Harrison and C. A. Cruickshank, 'A review of strategies for the control of high temperature stagnation in solar collectors and systems', *Energy Procedia*, vol. 30, pp. 793–804, 2012, ISSN: 18766102. DOI: 10.1016/j.egypro.2012.11.090.

[8] K. Resch, R. Hausner, G. M. Wallner and R. W. Lang, 'Thermotropic Layers for Overheating Protection of all-Polymeric Flat Plate Solar Collectors', in *Polymeric materials for solar thermal applications*, M. Köhl, M. G. Meir, P. Papillon, G. M. Wallner and S. Saile, Eds., Weinheim: Wiley-VCH, 2012, pp. 255–266, ISBN: 978-3-527-33246-5.

[9] K. Resch and A. Weber, 'Smart Windows - Smart Collectors: Entwicklung von funktionalen Überhitzungsschutzverglasungen für Gebäudeverglasungen und thermische Solarkollektoren', *Berg- und Hüttenmännische Monatshefte*, vol. 156, no. 11, pp. 429–433, 2011, ISSN: 0005-8912. DOI: 10.1007/s00501-011-0031-2.

[10] F. S. Bühler and M. Hewel, 'Reversibly thermotropic transparent molding material, useful e.g. in glazing or covers for shading and light-heat regulation in houses and cars etc.', pat. DE19841234C1, 1999.

[11] C. DeArmitt and G. E. Mc Kee, 'Moulded article with temperature dependent transparency', pat. EP1985663A1, 2008.

[12] A. Gladen, J. H. Davidson, S. C. Mantell, J. Zhang and Y. Xu, 'A Model of the Optical Properties of a Non-absorbing Media with Application to Thermotropic Materials for Overheat Protection', *Energy Procedia*, vol. 30, pp. 116–124, 2012, ISSN: 18766102. DOI: 10.1016/j.egypro.2012.11.015.

[13] M. Knausz, 'Untersuchung des Schaltverhaltens von thermotropen Gießharzen', Bachelorarbeit, University of Leoben, Leoben, 2009.

[14] M. J. Mikl, 'Herstellung und Charakterisierung von thermotropen Systemen mit fixierten Domänen', Diplomarbeit, University of Leoben, Leoben, 2010.

[15] O. Muehling, A. Seeboth, T. Haeusler, R. Ruhmann, E. Potechius and R. Vetter, 'Variable solar control using thermotropic core/shell particles', *Solar Energy Materials and Solar Cells*, vol. 93, no. 9, pp. 1510–1517, 2009, ISSN: 09270248. DOI: 10.1016/j.solmat.2009.03.029.

[16] K. Resch and G. M. Wallner, 'Thermotropic Resin Systems: Relationships Between Formulation Parameters, Material Structure and Optical Properties', in *Proceedings of ISES Solar World Congress 2007*, D. Y. Goswami and Y. Zhao, Eds., Berlin: Springer, 2007, pp. 541–545, ISBN: 978-3-540-75996-6. DOI: 10.1007/978-3-540-75997-3_98.

[17] K. Resch and G. M. Wallner, 'Morphology of phase-separated thermotropic layers based on UV cured acrylate resins', *Polymers for Advanced Technologies*, vol. 20, no. 12, pp. 1163–1167, 2009, ISSN: 10427147. DOI: 10.1002/pat.1393.

[18] K. Resch and G. M. Wallner, 'Thermotropic layers for flat-plate collectors—A review of various concepts for overheating protection with polymeric materials', *Solar Energy Materials and Solar Cells*, vol. 93, no. 1, pp. 119–128, 2009, ISSN: 09270248. DOI: 10.1016/j.solmat.2008.09.004.

[19] K. Resch, G. M. Wallner and R. Hausner, 'Phase separated thermotropic layers based on UV cured acrylate resins – Effect of material formulation on overheating protection properties and application in a solar collector', *Solar Energy*, vol. 83, no. 9, pp. 1689–1697, 2009, ISSN: 0038092X. DOI: 10.1016/j.solener.2009.06.006.

[20] K. Resch, G. M. Wallner and R. W. Lang, 'Spectroscopic Investigations of Phase-Separated Thermotropic Layers Based on UV Cured Acrylate Resins', *Macromolecular Symposia*, vol. 265, no. 1, pp. 49–60, 2008, ISSN: 10221360. DOI: 10.1002/masy.200850506.

[21] R. Ruhmann, A. Seeboth, O. Muehling and D. Loetzsch, 'Thermotropic Materials for Adaptive Solar Control', *Advances in Science and Technology*, vol. 77, pp. 124–131, 2012, ISSN: 1662-0356. DOI: 10.4028/www.scientific.net/AST.77.124.

[22] A. Schmid, 'Untersuchung der Zusammenhänge zwischen Morphologie und den Überhitzungsschutzeigenschaften von thermotropen Systemen mit fixierten Domänen', Bachelorarbeit, Montanuniversität Leoben, Leoben, 2012. (visited on 14/03/2012).

[23] M. Seemann, 'Charakterisierung des Lichtstreuverhaltens und der Morphologie von thermotropen Verglasungen auf Thermoplastbasis', Masterarbeit, University of Leoben, Leoben, 2010.

[24] A. Weber, 'Analyse der Morphologie und des Schaltvorganges von thermotropen Polymeren mittels Rasterkraftmikroskopie', Master Thesis, University of Leoben, Leoben, 2010.

[25] A. Weber and K. Resch, 'Thermotropic glazings for overheating protection applications: Tuning the light-shielding efficiency by systematic material preselection and formulation', in *Solar Building Skins*, Economic Forum, Ed., Munich, 2011, pp. 73–77, ISBN: 978-3-981205343.

[26] A. Weber and K. Resch, 'Effect of Temperature-Cycling on the Morphology of Polymeric Thermotropic Glazings for Overheating Protection Applications', *Journal of Polymer Research*, vol. 19:9888, no. 6, pp. 1–8, 2012, ISSN: 1022-9760. DOI: 10.1007/s10965-012-9888-3.

[27] A. Weber and K. Resch, 'Thermotropic glazings for overheating protection', *Energy Procedia*, vol. 30, pp. 471–477, 2012, ISSN: 18766102. DOI: 10.1016/j.egypro.2012.11.056.

[28] A. Weber and K. Resch, 'Thermotropic Glazings for Overheating Protection I: Material Pre-selection, Formulation and Light-Shielding Efficiency', *Journal of Applied Polymer Science*, ISSN: 0021-8995. DOI: 10.1002/app.39950.

[29] A. Weber, S. Schlögl and K. Resch, 'Effect of Formulation and Processing Conditions on Light Shielding Efficiency of Thermotropic Systems with Fixed Domains Based on UV Curing Acrylate Resins', *Journal of Applied Polymer Science*, vol. 130, no. 5, pp. 3299–3310, 2013, ISSN: 0021-8995. DOI: 10.1002/app.39571.

[30] A. Weber, A. Schmid and K. Resch, 'Thermotropic Glazings for Overheating Protection II: Morphology and Structure-Property-Relationships', *Journal of Applied Polymer Science*, ISSN: 0021-8995. DOI: 10.1002/app.39910.

[31] P. Nitz, 'Optical modelling and characterisation of thermotropic systems', Dissertation, Albert-Ludwigs-University, Freiburg i.B., 1999.

[32] D. P. Gruber, G. Winkler, A. Weber and K. Resch, 'Novel approach to the solution of the scattering problem in a thermotropic medium', vol. unpublished manuscript, 2013.

[33] T. F. Tadros, 'Emulsion Science and Technology: A General Introduction', in *Emulsion science and technology*, T. F. Tadros, Ed., Weinheim: Wiley-VCH, 2009, pp. 1–56, ISBN: 3527325255.

[34] P. Walstra, 'Principles of emulsion formation', *Chemical Engineering Science*, vol. 48, no. 2, pp. 333–349, 1993, ISSN: 00092509. DOI: 10.1016/0009-2509(93)80021-H.

[35] T. Tadros, P. Izquierdo, J. Esquena and C. Solans, 'Formation and stability of nano-emulsions', *Advances in Colloid and Interface Science*, vol. 108-109, pp. 303–318, 2004, ISSN: 00018686. DOI: 10.1016/j.cis.2003.10.023.

[36] C. Dalmazzone, 'Génération mécanique des émulsions: Mechanical Formation of Emulsions', *Oil & Gas Science and Technology*, vol. 55, no. 3, pp. 281–305, 2000, ISSN: 1294-4475. DOI: 10.2516/ogst:2000020.

[37] E. Günther, L. Huang, H. Mehling and C. Dötsch, 'Subcooling in PCM emulsions – Part 2: Interpretation in terms of nucleation theory', *Thermochimica Acta*, vol. 522, no. 1-2, pp. 199–204, 2011, ISSN: 00406031. DOI: 10.1016/j.tca.2011.04.027.

[38] J. Kurja and N. A. Mehl, 'Nucleating Agents for Semi-crystalline Polymers', in *Plastics Additives Handbook*, H. Zweifel, Ed., München: Hanser, 2001, pp. 949–972, ISBN: 1-56990-295-X.

[39] D. Horn and J. Rieger, 'Organic Nanoparticles in the Aqueous Phase—Theory, Experiment, and Use', *Angewandte Chemie International Edition*, vol. 40, no. 23, p. 4330, 2001, ISSN: 14337851. DOI: 10.1002/1521-3773(20011203)40:23<4330::AID-ANIE4330>3.0.CO;2-W. (visited on 10/02/2012).

[40] G. W. Ehrenstein, G. Riedel and P. Trawiel, *Praxis der thermischen Analyse von Kunststoffen*, 2nd ed. München: Hanser, 2003, ISBN: 9783446223400.

[41] S. Fairgrieve, *Nucleating agents*, ser. Rapra Review Reports. Shawbury: Rapra Technology Ltd., 2006, vol. Vol. 16, No. 7, Report 187.

[42] J. Rieger, 'Polymer Crystallization Viewed in the General Context of Particle Fomration and Crystallization', in *Polymer crystallization*, G. Reiter and J.-U. Sommer, Eds., Berlin: Springer, 2003, pp. 7–16, ISBN: 3-540-44342-8.

[43] J. Karger-Kocsis, *Polypropylene: Structure, blends and composites: 1. Structure and Morphology*. London: Chapman & Hall, 1995, vol. 1, ISBN: 978-0-412-58430-5.

[44] G. Di Marco and M. Pieruccini, 'Lamellar Growth in Melt-Crystallizing Polymers: Some Effect Related to a Nucleating Agent', in *Polymer crystallization*, G. Reiter and J.-U. Sommer, Eds., Berlin: Springer, 2003, pp. 366–377, ISBN: 3-540-44342-8.

[45] D. C. Montgomery, *Design and analysis of experiments*, 7th ed. Hoboken: Wiley, 2009, ISBN: 0470128666.

[46] W. Kleppmann, *Taschenbuch Versuchsplanung: Produkte und Prozesse optimieren*, 6th ed. München: Hanser, 2009, ISBN: 3446420339.

[47] E. Baur, S. Brinkmann, T. A. Osswald and E. Schmachtenberg, *Saechtling-Kunststoff-Taschenbuch*, 30th ed. München: Hanser, 2007, ISBN: 978-3-446-41437-2.

[48] M. Schimmelpfennig, K. Weber, F. Kalb, K.-H. Feller, T. Butz and M. Matthäi, 'Volumenausdehnung von Paraffinen aus Steigrohr-Messungen', in *Jahrbuch für den Praktiker 2007*, B. Ziolkowsky, Ed., vol. 50, Augsburg: Verlag für chemische Industrie, 2007, pp. 417–429.

[49] H. P. Grace, 'Dispersion phenomena in high viscosity immisible fluid systems and application of static mixers as dispersion devices in such systems', *Chemical Engineering Communications*, vol. 14, no. 3-6, pp. 225–277, 1982, ISSN: 0098-6445. DOI: 10.1080/00986448208911047.

Part V.

Ex-situ Optimisation Strategy

11 Introduction to Publication 5

An important lesson learned from previous publication (see chapter 10) was that thermally-induced diffusion of the thermotropic additive in its molten state had deleterious effects on the overheating protection performance of TSFD due to vacuole formation. With regard to practical application of TSFD as an overheating protection glazing in a solar thermal collector, this issue poses a severe challenge because the deterioration of the overheating protection performance of the TSFD which is associated with the thermally-induced additive diffusion will indeed reduce the solar thermal collector efficiency and thus its yield in an undesirable extent during operation. To encapsulate the thermotropic additive with a barrier layer was considered to be a promising approach to suppress thermally-driven diffusion of molten additive.

Notwithstanding, the applied measures in order to adjust the scattering domain size of thermotropic additive paraffin wax – which was the initial motivation to conduct the study outlined in chapter 10 – failed. For example the addition of a surfactant was not effectual in order to affect the interactions of matrix and thermotropic additive and thus to reduce the scattering domain size similar as a surfactant would do in a conventional emulsion. Furthermore, suggested heterogeneous nucleation of thermotropic additive in order to increase the number of crystallisation loci and thus to reduce the scattering domain size did not work. This was attributed to the lack of nucleating potential of the employed nucleating agent with regard to the thermotropic additive utilised. Furthermore, an approach to affect homogeneous nucleation of thermotropic additive was also established by variation of the temperature conditions during TSFD formulation in order to tune the number of crystallisation loci. However, that approach did not work either. Changing the temperature conditions during TSFD formulation do also affect the system rheology by increasing for

instance the resin matrix viscosity. Hence, it was concluded that effects of system rheology of TSFD during formulation on the scattering domain size were probably underestimated. For instance, articles on disperson phenomena (in immiscible fluid systems and emulsions) point out the significant importance of the viscosity ratio of the components of a liquid disperse system with regard to the achievable droplet size of the minor phase [1], [2]: Droplet break-up is easier for liquid/liquid systems with a viscosity ratio close to unity and therefore smaller droplets are achievable. Probably different viscosities of matrix resin and liquid paraffin wax forced the formation of inappropriately sized scattering domains upon TSFD formulation. In order to eliminate these effects in a liquid/liquid mixture, establishment of a liquid resin matrix/solid thermotropic additive mixture upon TSFD formulation was promising. Anyway, that required the adjustment of the scattering domain size towards the optimum and their solidification prior to TSFD formulation and to keep these domains solid during TSFD formulation.

From literature it was recognised that numerous encapsulation processes were capable to form a solid protective shell around a core material [3], [4]. From the numerous encapsulation processes described in the literature, miniemulsion polymerisation was considered to be most promising technique due to the possibility to obtain capsules with diameters below 1 µm [3]–[18]. So far, only Muehling et al. [16] applied miniemulsion polymerisation in order encapsulate a thermotropic additive prior to TSFD formulation. Nevertheless, Muehling et al. [16] employed thermally initiated miniemulsion polymerisation. When striving for encapsulation of thermotropic additives with a low melting point – like Muehling et al. [16] actually did – thermal initiation is considered to be rather unproblematic. However, when striving for the encapsulation of thermotropic additives with a higher melting point, higher temperatures have to be maintained during establishment of the reactants and subsequent emulsification. If these temperatures exceed the decomposition temperature of a utilised thermal initiator, one may lose spatial and temporal control of the start of the polymerisation reaction. Furthermore, at higher temperatures the reaction will likely be faster due to enhanced decomposition frequency of thermal initiators. Thus, decoupling the initiation trigger from the process temperature was considered to be desirable. In this context, photo-initiation was considered to be an elegant way to

trigger the initiation of the polymerisation reaction. Hence, the manuscript presented hereafter describes the development of a photo-initiated miniemulsion process for encapsulation of thermotropic additive (adjustment of scattering domain size) and subsequent TSFD formulation with the reaction product. Consequently, such a process will provide more flexibility with regard to encapsulation of a wide variety of thermotropic additives (exhibiting different melting temperatures). Furthermore, such a process will be reasonably fast.

11.1 References

[1] P. Walstra, 'Principles of emulsion formation', *Chemical Engineering Science*, vol. 48, no. 2, pp. 333–349, 1993, ISSN: 00092509. DOI: 10.1016/0009-2509(93)80021-H.

[2] H. P. Grace, 'Dispersion phenomena in high viscosity immisible fluid systems and application of static mixers as dispersion devices in such systems', *Chemical Engineering Communications*, vol. 14, no. 3-6, pp. 225–277, 1982, ISSN: 0098-6445. DOI: 10.1080/00986448208911047.

[3] C. Zhao and G. Zhang, 'Review on microencapsulated phase change materials (MEPCMs): Fabrication, characterization and applications', *Renewable and Sustainable Energy Reviews*, vol. 15, no. 8, pp. 3813–3832, 2011, ISSN: 13640321. DOI: 10.1016/j.rser.2011.07.019.

[4] O. Seok Kwon, J. Jang and J. Bae, 'A Review of Fabrication Methods and Applications of Novel Tailored Microcapsules', *Current Organic Chemistry*, vol. 17, no. 1, pp. 3–13, 2013, ISSN: 13852728. DOI: 10.2174/13852721380528919 6.

[5] S. Alay, C. Alkan and F. Göde, 'Synthesis and characterization of poly(methyl methacrylate)/n-hexadecane microcapsules using different cross-linkers and their application to some fabrics', *Thermochimica Acta*, vol. 518, no. 1-2, pp. 1–8, 2011, ISSN: 00406031. DOI: 10.1016/j.tca.2011.01.014. (visited on 09/02/2012).

[6] C. Alkan, A. Sarı and A. Karaipekli, 'Preparation, thermal properties and thermal reliability of microencapsulated n-eicosane as novel phase change material for thermal energy storage', *Energy Conversion and Management*, vol. 52, no. 1, pp. 687–692, 2011, ISSN: 01968904. DOI: 10.1016/j.enconman.2010.07.047. (visited on 09/02/2012).

[7] C. Alkan, A. Sarı, A. Karaipekli and O. Uzun, 'Preparation, characterization, and thermal properties of microencapsulated phase change material for thermal energy storage', *Solar Energy Materials and Solar Cells*, vol. 93, no. 1, pp. 143–147, 2009, ISSN: 09270248. DOI: 10.1016/j.solmat.2008.09.009. (visited on 09/02/2012).

[8] Z. Cao and U. Ziener, 'A Versatile Technique to Fabricate Capsules: Miniemulsion', *Current Organic Chemistry*, vol. 17, no. 1, pp. 30–38, 2013, ISSN: 13852728. DOI: 10.2174/138527213805289169.

[9] C. Chen, Z. Chen, X. Zeng, X. Fang and Z. Zhang, 'Fabrication and characterization of nanocapsules containing n-dodecanol by miniemulsion polymerization using interfacial redox initiation', *Colloid and Polymer Science*, vol. 290, no. 4, pp. 307–314, 2012, ISSN: 0303-402X. DOI: 10.1007/s00396-011-2545-2.

[10] Z.-H. Chen, F. Yu, X.-R. Zeng and Z.-G. Zhang, 'Preparation, characterization and thermal properties of nanocapsules containing phase change material n-dodecanol by miniemulsion polymerization with polymerizable emulsifier', *Applied Energy*, vol. 91, no. 1, pp. 7–12, 2012, ISSN: 03062619. DOI: 10.1016/j.apenergy.2011.08.041.

[11] M. G. d. Cortazar and R. Rodríguez, 'Thermal storage nanocapsules by miniemulsion polymerization', *Journal of Applied Polymer Science*, vol. 127, no. 6, pp. 5059–5064, 2013, ISSN: 0021-8995. DOI: 10.1002/app.38124.

[12] M. Fuensanta, U. Paiphansiri, M. D. Romero-Sánchez, C. Guillem, Á. M. López-Buendía and K. Landfester, 'Thermal properties of a novel nanoencapsulated phase change material for thermal energy storage', *Thermochimica Acta*, vol. 565, pp. 95–101, 2013, ISSN: 00406031. DOI: 10.1016/j.tca.2013.04.028.

[13] K. Landfester, 'Miniemulsionspolymerisation und Struktur von Polymer- und Hybridnanopartikeln', *Angewandte Chemie*, vol. 121, no. 25, pp. 4556–4576, 2009, ISSN: 00448249. DOI: 10.1002/ange.200900723. (visited on 09/02/2012).

[14] Y. Luo and X. Zhou, 'Nanoencapsulation of a hydrophobic compound by a miniemulsion polymerization process', *Journal of Polymer Science Part A: Polymer Chemistry*, vol. 42, no. 9, pp. 2145–2154, 2004, ISSN: 0887-624X. DOI: 10.1002/pola.20065.

[15] S. Ma, G. Song, W. Li, P. Fan and G. Tang, 'UV irradiation-initiated MMA polymerization to prepare microcapsules containing phase change paraffin', *Solar Energy Materials and Solar Cells*, vol. 94, no. 10, pp. 1643–1647, 2010, ISSN: 09270248. DOI: 10.1016/j.solmat.2010.05.021.

[16] O. Muehling, A. Seeboth, T. Haeusler, R. Ruhmann, E. Potechius and R. Vetter, 'Variable solar control using thermotropic core/shell particles', *Solar Energy Materials and Solar Cells*, vol. 93, no. 9, pp. 1510–1517, 2009, ISSN: 09270248. DOI: 10.1016/j.solmat.2009.03.029.

[17] A. Sarı, C. Alkan and A. Karaipekli, 'Preparation, characterization and thermal properties of PMMA/n-heptadecane microcapsules as novel solid–liquid microPCM for thermal energy storage', *Applied Energy*, vol. 87, no. 5, pp. 1529–1534, 2010, ISSN: 03062619. DOI: 10.1016/j.apenergy.2009.10.011.

[18] F. Tiarks, K. Landfester and M. Antonietti, 'Preparation of Polymeric Nanocapsules by Miniemulsion Polymerization', *Langmuir*, vol. 17, no. 3, pp. 908–918, 2001, ISSN: 0743-7463. DOI: 10.1021/la001276n.

12 Publication 5

12.1 Bibliographic Information

- Title: Thermotropic Systems with Fixed Domains exhibiting Enhanced Overheating Protection Performance
- Authors:
  - Andreas Weber[1]
  - Katharina Resch[2]
    1. Polymer Competence Center Leoben GmbH, Roseggerstrasse 12, 8700 Leoben, Austria
    2. Department Polymer Engineering and Science, Materials Science and Testing of Polymers, University of Leoben, Otto Glöckel-Strasse 2, 8700 Leoben, Austria
- Periodical: Journal of Applied Polymer Science
- Status: submitted

Statement with regard to publication: The manuscript presented here is an adapted manuscript in order to fit the formatting of the thesis and does not necessarily reflect exactly the actually published version.

12.2 Abstract

Within this study, a time saving photo-initiated miniemulsion polymerisation process (duration of polymerisation was 15 min) was established in order to encapsulate a paraffin wax with an acrylate polymer shell. The obtained freeze-dried latex was an off-white powder exhibiting spherical particles with mean diameters around 400 nm and a concentration of paraffin wax around 56 %. Mixing the reaction product with a UV-curable resin matrix resulted in thermotropic overheating protection glazings with high light-shielding efficiency.

12.3 Introduction

Thermotropic glazings change their optical properties from transparent to opaque upon exceeding a predefined threshold temperature, reversibly [1], [2]. Thus, they can provide efficient overheating protection for buildings as well as for solar thermal collectors [1], [3]–[9]. Upon utilisation in a building's façade, a reduction in primary energy demand is achievable by reduction of energy consumption for heating, cooling and artificial daylighting [3], [4]. In solar thermal collectors, they can limit stagnation temperatures to values below 130 °C which otherwise would exceed 180 °C and thus prevent deterioration, ageing and potential failure of heat carrier fluid and other collector components [9]–[11]. Especially for polymeric solar thermal systems stagnation control is a prerequisite in order not to exceed the long-term service temperatures of utilised – preferably cost-efficient – polymeric materials [9], [10], [12], [13].

Besides other thermotropic glazing systems, thermotropic systems with fixed domains (TSFD) are promising due to specific advantages like ease of adjustment of switching threshold, high long-term stability, low hysteresis, high reversibility and steep switching process [8]. The TSFD itselves consist of a thermotropic additive finely dispersed in a matrix material [1], [6]. Below the threshold temperature, the refractive indices of both components are almost equal, enabling the incident radiation to pass the layer almost un-scattered [1]. Upon exceeding the threshold temperature (i.e. melting of the additive), the refractive index of the thermotropic additive exhibits a

steep change [1]. Thus a significant refractive index difference between matrix and additive is obtained, finally resulting in intense scattering of incident radiation [1]. Besides refractive index difference, layer morphology governs overheating protection of TSFD to a high extent [14], [15]. Most efficient light-shielding is achieved for spherical scattering domains with diameters between 200 and 400 nm [14]. Notwithstanding, the achieved light-shielding efficiency of TSFD established so far is limited, and especially inappropriate for efficient overheating protection of an all-polymeric flat plate collector [8], [9], [13], [16]–[24]. Primarily, this was attributed to inappropriate scattering domain shape and/or size [13], [17], [19]–[23], [25], [26]: Scattering domains were either spherical or non-spherical but too big in general anyway. In 2008, Resch [27] suggested adjustment of scattering domain shape and size prior to TSFD formulation in order to enhance overheating protection performance of TSFD. To the best of our knowledge, Muehling et al. [24] were the first and only ones so far conducting a study devoted to the establishment of properly sized scattering domains for TSFD formulation. However, the established threshold temperature (25 °C [24]) is rather low and thus not appropriate for overheating protection of a solar thermal collector. Overheating protection of a solar thermal collector either requires threshold temperatures in the range between 55 and 60 °C or 75 and 80 °C, respectively [9]. Thus, an objective of this study was to establish a novel process for adjustment of scattering domain size of thermotropic additive with rather high melting point (i.e. 55 °C). Furthermore, formulation of TSFD with these optimally sized scattering domains was an issue.

12.4 Encapsulation of Thermotropic Additive

12.4.1 Background

As suggested earlier [21], [24], encapsulation of thermotropic additive was considered to be a promising approach for adjustment of scattering domain size in order to formulate TSFD with efficient overheating protection performance. Therefore, the considerations which led to the actual setup of the subsequently employed encapsulations process are outlined in the following paragraphs.

For encapsulation of phase change materials in general and alkanes and paraffin waxes – which may also serve as thermotropic additives – more specifically, polymerisation processes employing vinyl monomers are addressed rather frequently in literature [28]–[50]. However, besides other techniques, the most versatile process to establish encapsulated thermotropic additive with controlled size is probably miniemulsion polymerisation [36], [51]–[64]. In miniemulsion polymerisation the polyreactions take place in some kind of "nanoreactors" formed by the disperse phase which are separated from each other by the continuous phase [55], [57], [65]. Extensive reviews on the details of miniemulsion polymerisation – also for encapsulation purposes – are presented elsewhere [55], [57], [58], [61], [65], [66]. One noteworthy aspect of miniemulsion polymerisation is that the "nanoreactor"-droplets have to be stabilised against growth due to Ostwald-ripening by addition of an ultrahydrophobe [55], [57], [65]. For example, the alkane hexadecane was recognised as a very efficient ultrahydrophobe [55], [65]. This is very interesting because with regard to adjustment of the switching threshold of a TSFD, alkanes and paraffin waxes are probably the most versatile thermotropic additives due to rather easy availability of materials displaying a melting transition in the desired temperature ranges (either 55–60 °C or 75–80 °C [9]). Hence, upon miniemulsion polymerisation mediated encapsulation of an alkane or a paraffin wax these substances act as an ultrahydrophobe simultaneously.

However, encapsulation of paraffin waxes exhibiting melting in the previously specified temperature ranges might encounter challenges that are related to standard thermal initiation of miniemulsion polymerisation: To form an emulsion, usually the water- and the oil-phase are assembled separately prior to emulsification [35], [36], [63]. Thereby, the oil-phase contains the monomers (e.g. acrylates) and the paraffin wax (simultaneously acting as ultrahydrophobe in miniemulsion polymerisation). Both phases have to be heated above the melting temperature of the paraffin wax in order to subsequently establish an oil-in-water (O/W) emulsion. High energy emulsification techniques (e.g. ultrasound) are required in order to establish a miniemulsion with narrow size distribution and small mean diameter [24], [57], [65], [67]–[69]. However, the high temperatures employed prior, during and after emulsification and heat dissipation due to emulsification might be a challenge for thermal initiators, especially for oil-soluble ones. Oil-soluble initiators have to be mixed with the oil-phase

prior to emulsification [36]. This may cause uncontrollable polymerisation start due to decomposition of the thermal initiator when exposed to high temperatures during establishment of the miniemulsion. Utilisation of water soluble initiators, which can be added after emulsification and which thus may overcome the previously mentioned shortcomings of oil soluble initiators, is not an option when utilising rather water soluble monomers like methyl methacrylate (MMA). Otherwise nucleation in the aquatic phase and subsequent growth of pure polymer particles (e.g. PMMA) might occur [63], which is undesirable when performing an encapsulation process.

Thus, decoupling the polymerisation initiation from the reactants' temperatures was considered to be an imperative in order to facilitate utilisation of oil soluble initiator while maintaining spatial and temporal control of initiation reaction. That may be achieved via photo-initiation of the polymerisation process [54], [70]. Furthermore, photo-initiation might provide additional advantages compared to thermal initiation, like high reaction rates and feasibility of photo-initiated processes for continuous reactors [70]. Thus, the miniemulsion polymerisation process for encapsulation is considered to be significantly accelerated by substitution of thermal initiation (for example reactions last around 3 h in reference [24]) by photo-initiation. However, photo-initiation for starting polymerisation within an encapsulation process of phase change materials was rarely addressed in the past [37], [46].

Anyway, not virtually any monomer is suitable for encapsulation of paraffin wax intended for use as scattering domain in a TSFD. A proper match of refractive indices (n) of the core and the polymeric shell is required for this purpose. For paraffin waxes (n approx. 1.5), polymers with a proper match of refractive index are derived from acrylate monomers, e.g. Poly (methyl methacrylate) (PMMA; n=1.49) or Poly (isobornyl methacrylate) (PiBoMA; n=1.50) [20], [71]–[73]. Furthermore, polymers based on acrylate esters are recognised rather stable upon exposition to UV-light [74].

12.4.2 Experimental

12.4.2.1 Materials

Monomers methyl methacrylate (MMA; 99 %), ethylene glycol dimethacrylate (EGDMA; 98 %), isobornyl methacrylate (iBoMA; technical grade) and surfactant sodium lauryl sulphate (SDS; $\geq$98.5 %) were purchased from Sigma Aldrich Handels GmbH (Wien, AT). Thermotropic additive paraffin wax (Sasolwax 5005) and photo-initiator (Lucirin TPO-L) were supplied by Sasol Wax GmbH (Hamburg, DE) and BASF SE (Ludwigshafen, DE), respectively. All materials were used as received.

12.4.2.2 Miniemulsion Polymerisation

Monomer mixture either consisted of 4.5 g MMA and 0.5 g EGDMA or 2.5 g MMA, 2.0 g iBoMA and 0.5 g EGDMA. The oil phase was assembled by mixing and stirring the monomer mixture (5 g), paraffin wax (5 g) and photo-initiator Lucirin TPO-L (0.15 g) in a beaker immersed in an oil bath (temperature: 70 °C) until it was clear. The water phase was established by mixing SDS with 50 g deionized water in a beaker also immersed in the oil bath. The required amount of SDS was evaluated in preliminary tests. A concept estimating the area a single surfactant molecule is stabilizing in an emulsion (A_{surf}; see references [52], [53], [60], [75], [76]) was adopted in order to estimate a reasonable starting concentration of surfactant for these tests. Preliminary tests revealed an amount of 8.3 mg SDS to be effectual. To form the emulsion, the oil phase was transferred to the beaker (made from clear Schott DURAN glass) with the water phase and subsequently emulsified by ultrasound from a Sonopuls HD 3200 equipped with a booster horn SH 213 G and a sonotrode KE76 (Bandelin electronic GmbH & Co. KG, Berlin, DE), maintaining an amplitude set-point of 70 % for 5 min. Subsequently, the established emulsion was irradiated through the beaker wall for 900 s at 100 % intensity with radiation from a light-guide attached to OmniCure S 1000 (Lumen Dynamics Group Inc., Mississauga, ON, CA). During irradiation vigorous stirring with a magnetic stirrer bar and continuous nitrogen flow was maintained. The obtained dispersion was freeze-dried.

12.4.2.3 Freeze-Drying

Proof of concept for freeze-drying was established via a laboratory apparatus consisting of a vacuum pump P8Z (Ilmvac GmbH, Illmenau, DE) equipped with a vacuum control unit, a cooling trap cooled with liquid nitrogen and a salt/water/ice-bath for immersion of the round-bottomed flask with the frozen latex. Larger amount of dried latex was obtained by utilising a commercial freeze-dryer Alpha 2-4 (Martin Christ Gefriertrocknungsanlagen GmbH, Osterode am Harz, DE) equipped with a rotary vane pump RV 5 (Edwards Ltd., Crawley, West Sussex, GB).

12.4.2.4 Capsule Characterisation

In order to prove evidence for successfully conducted polymerisation reaction, infrared (IR) spectra of freeze-dried latex were recorded in mode of attenuated total reflection (ATR) employing a Spectrum GX FTIR spectrometer (Perkin Elmer Inc., Waltham, MA, US) equipped with an ATR device GladiATR Vision (PIKE Technologies, Madison, WI, US).

Thermal transitions and melting enthalpies of pristine paraffin wax and of encapsulated wax were determined by differential scanning calorimetry (DSC). Thermograms were recorded under nitrogen flow (40 mL min^{-1}) on a DSC 4000 (Perkin Elmer Inc., Waltham, MA, US) applying a heating/cooling rate of 10 K min^{-1} in the range between −20 and 100 °C. Sample mass was 10±1 mg. Threefold determination was carried out for each sample. Melting temperature (peak temperature) and enthalpy of melting transition were evaluated from the second heating run. Mass content of paraffin wax (w_{Core}) in the capsules was calculated by building the ratio of the specific melting enthalpy of the capsules ($h_{Capsules}$ in J g^{-1}) and the specific melting enthalpy of the pristine paraffin wax (h_{Core} material in J g^{-1}) (see eq. 12.1). *Equation 12.1*

After transferring the particles to a sample mount and subsequent sputtering with gold, capsule morphology was characterised employing scanning electron microscope (SEM) DSM 962 (Carl Zeiss SMT AG, Oberkochen, DE). Capsule size was evaluated with measurement tools of software analySIS (Soft Imaging System GmbH, Münster, DE). From the capsule diameters ($d_{Capsule}$), the core diameters (d_{Core}) were calculated

Equation 12.2

according to eq. 12.2. Density of the core material paraffin wax (ρ_{Core}) and the polymeric shell (ρ_{Shell}) were assumed to be 0.91 (value for a paraffin with melting point around 55 °C [77]) and 1.19 g cm^{-3} (value for PMMA) [78]–[80], respectively.

The core diameter was calculated because it was of major interest with regard to the light-shielding efficiency of TSFD formulated with the obtained capsules. In contrast, the outer diameter of the protective shell of the additive core was of minor interest. Size distribution histograms were established with graphical statistics tool of software Origin 9.0 (OriginLab Corporation, Northampton, MA, US).

$$w_{Core} = \frac{h_{Capsules}}{h_{Core\ material}} \tag{12.1}$$

$$d_{Core} = d_{Capsules} \times \left(1 + \frac{\rho_{Core}}{\rho_{Core}} \times \frac{1 - w_{Core}}{w_{Core}}\right)^{-\frac{1}{3}} \tag{12.2}$$

12.4.3 Results

Figure 12.1

In Figure 12.1 the ATR spectra of pristine paraffin wax (Fig. 12.1a), and of encapsulated paraffin wax with a polymeric shell obtained from either, MMA and EGDMA (Fig. 12.1b), or MMA, iBoMA and EGDMA (Fig. 12.1c) are displayed. Band assignment is based on information provided by literature [81]–[84]. The bands identified for pristine wax were: IR (ATR): ν = 2957 (m, $\nu_{as}(CH_3)$), 2917 (vs, $\nu_{as}(CH_2)$), 2874 (w, $\nu_s(CH_3)$), 2849 (vs, $\nu_s(CH_2)$), 1473 (m, $\delta_s(CH_2)$), 1463 (s, $\delta_s(CH_2)$, $\delta_{as}(CH_3)$), 1378 (w, $\delta_s(CH_3)$), 730 (m, $\rho(CH_2)$), 719 cm^{-1} (s, $\rho(CH_2)$). These bands were also identified for the paraffin wax encapsulated with a shell of either MMA and EGDMA or MMA, iBoMA and EGDMA. Further bands identified for both encapsulated products were: IR (ATR): ν = 1728 (s, ν(C=O)), 1240 (m, ν(C(=O)O)), 1147 (s, ρ'(CH_3)), 988 (w, ν(O-C)), 750 cm^{-1} (w, δ(C=O)). Especially the bands ascribed to the carbonyl-moieties (e.g. at 1240 cm^{-1}) gave evidence for successfully conducted polymerisation. For the product encapsulated with MMA, iBoMA and EGDMA two more bands were evident, which were not detectable or at least much weaker for the product encapsulated with MMA and EGDMA: IR(ATR): ν = 1327 (w, probably a C-H deformation vibration of a ternary C-H group), 1052 cm^{-1} (probably a C-C skeletal vibration of >C(CH_3)$_2$), both indications for the isobornyl-group being present.

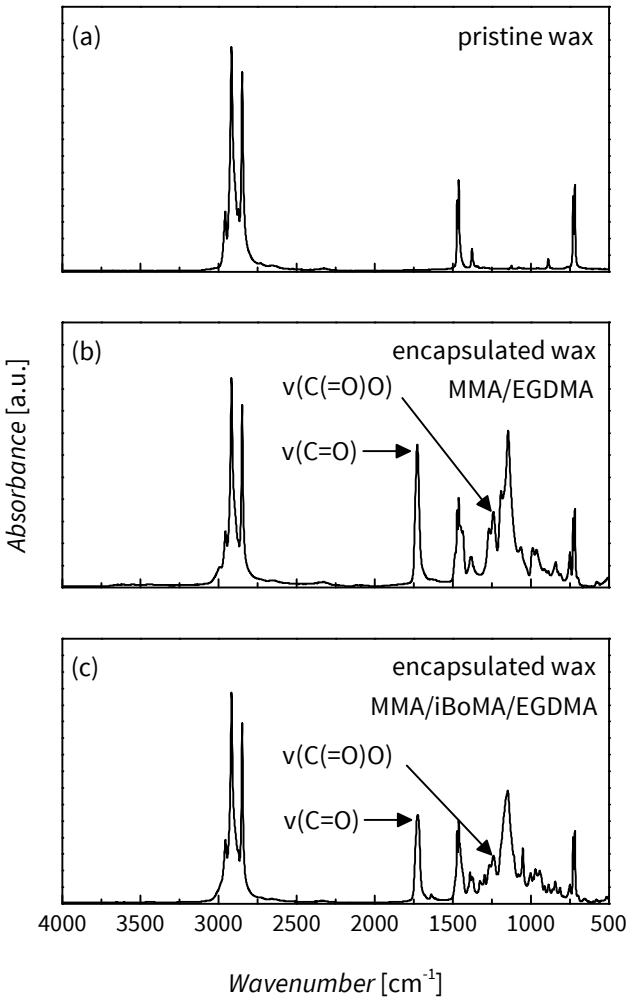

Figure 12.1.: ATR-spectra of **(a)** pristine wax, encapsulated wax with a polymeric shell obtained from **(b)** MMA and EGDMA, or **(c)** MMA, iBoMA and EGDMA.

Figure 12.2

In Figure 12.2 the second DSC heating runs recorded for pristine paraffin wax (Fig. 12.2a), and encapsulated paraffin wax with a polymeric shell obtained from either, MMA and EGDMA (Fig. 12.2b), or MMA, iBoMA and EGDMA (Fig. 12.2c) are depicted. Melting peak temperatures of paraffin wax were 56 °C for the pristine wax (Fig. 12.2a), 55 °C for the wax encapsulated with a polymeric shell resulting from MMA and EGDMA (Fig. 12.2b) and 53 °C for the wax encapsulated with a polymeric shell resulting from MMA, iBoMA

and EGDMA (Fig. 12.2c), respectively. The specific melting enthalpies obtained from
Table 12.1 these thermograms are listed in Table 12.1. Whereas the pristine paraffin wax had a specific melting enthalpy of 204 J g^{-1} ($h_{Core\ Material}$), the wax encapsulated with a shell of MMA and EGDMA displayed a specific melting enthalpy of 112 J g^{-1}. Thus, according to eq. 12.1, the related freeze dried product contained 55 % paraffin wax. For the paraffin wax encapsulated with a shell of MMA, iBoMA and EGDMA the specific melting enthalpy was 117 J g^{-1}, yielding a wax content of 57 %.

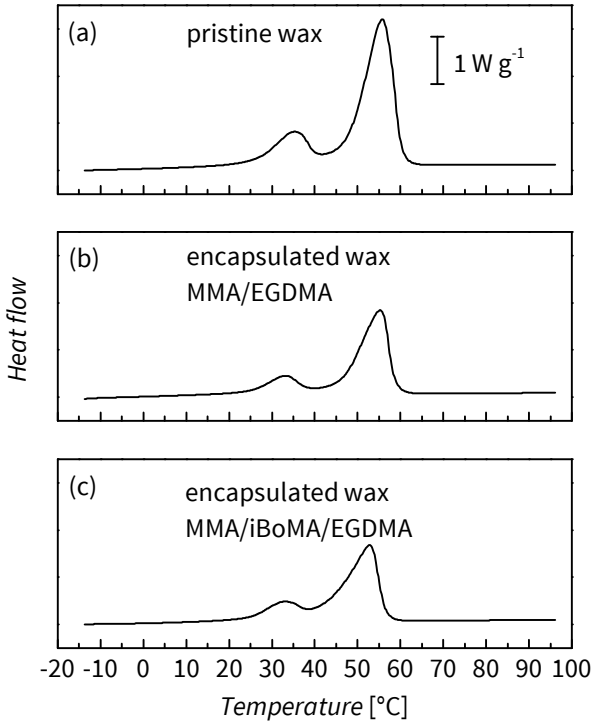

Figure 12.2.: DSC-thermograms (second heating run) of **(a)** pristine wax, encapsulated wax with a polymeric shell obtained from **(b)** MMA and EGDMA, or **(c)** MMA, iBoMA and EGDMA.

Figures 12.3,12.4 Figures 12.3 and 12.4 displays SEM micrographs of the paraffin wax encapsulated with a polymeric shell obtained from either MMA and EGDMA (Fig. 12.3) or MMA, iBoMA and EGDMA (Fig. 12.4) in magnifications of 10000 (Fig. 12.3,12.4a) and 30000 (Fig. 12.3,12.4b). Micrographs display aggregated spherical particles. A survey of individual particles from numerous micrographs enabled establishment of particle size distributions. Furthermore, for each individual particle the calculation of a hypo-

thetical core diameter (according to eq. 12.2; assumption: uniform wax content for all particles) was carried out. The resulting size distribution histograms are depicted in Figures 12.5 and 12.6. For illustration purposes, a logarithmic normal-distribution curve was overlaid on the histograms. The mean and median of the actually detected particle diameters for the wax encapsulated with a shell resulting from MMA and EGDMA were 354 and 280 nm, respectively (histogram see Fig. 12.5a). The size distribution of the core diameters exhibited mean and median of 301 and 238 nm, respectively (histogram see Fig. 12.5b). The vast majority of the particle cores had diameters between 50 and 1000 nm. The mean and median of the actually detected particle diameters for wax encapsulated with a shell resulting from MMA, iBoMA and EGDMA were 487 and 439 nm, respectively (histogram see Fig. 12.6a). The size distribution of the core diameters exhibited mean and median of 419 and 377 nm, respectively (histogram see Fig. 12.6b). The vast majority of these particle cores had diameters between 100 and 1000 nm. Table 12.2 summarises the key findings of the particle characterisation.

Figures 12.5,12.6

Table 12.2

Table 12.1.: Specific melting enthalpies for paraffin wax encapsulated with a polymeric shell obtained from MMA and EGDMA or from MMA, iBoMA and EGDMA and resultant paraffin wax content of the capsules (w_{Core}) calculated based on the specific melting enthalpy of the pristine wax $h_{Core\ Material}$ = 204 J g^{-1}.

Monomer mixture	$h_{Capsules}$[J g^{-1}]	w_{Core} [%]
MMA/EGDMA	112	55
MMA/iBoMA/EGDMA	117	57

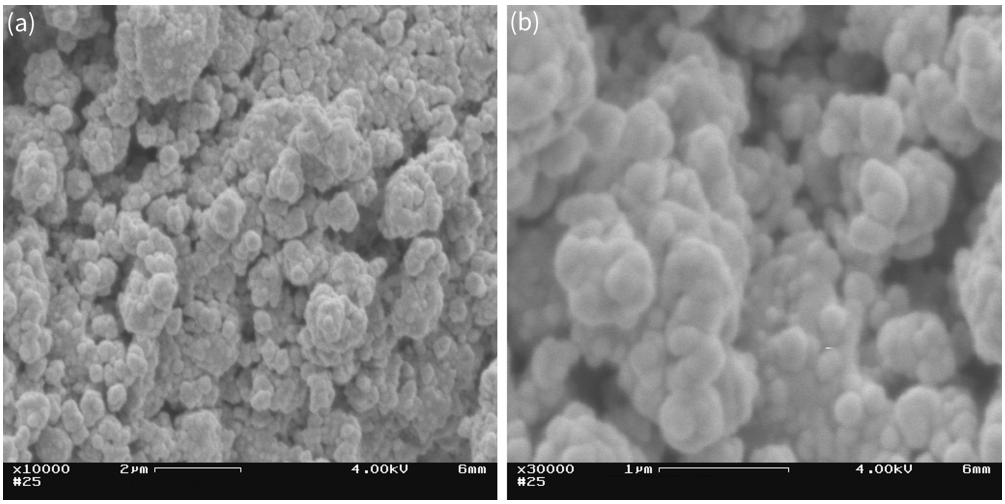

Figure 12.3.: SEM micrographs of paraffin wax encapsulated with a polymeric shell obtained from MMA and EGDMA. Magnifications displayed are **(a)** 10000× and **(b)** 30000×.

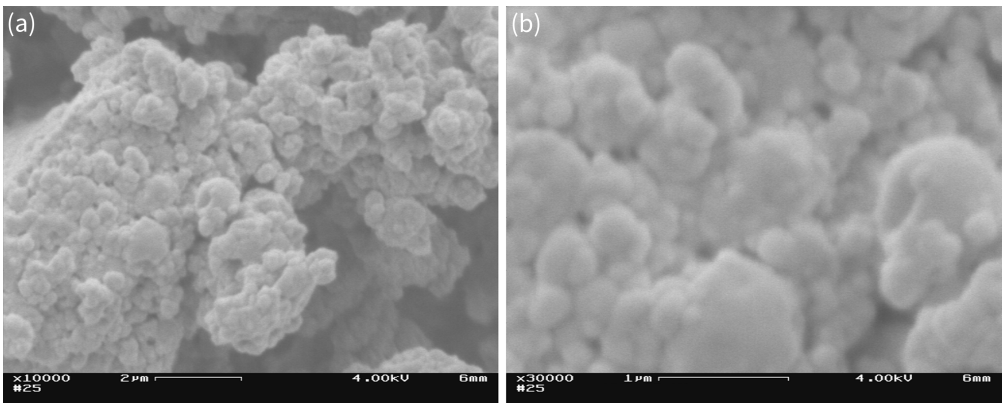

Figure 12.4.: SEM micrographs of paraffin wax encapsulated with a polymeric shell obtained from MMA, iBoMA and EGDMA. Magnifications displayed are **(a)** 10000× and **(b)** 30000×.

In TSFD scattering domains with diameters between 200 and 400 nm are most efficient [14]. However, studies showed that domains with diameters up to 1000 nm are highly efficient in terms of back-scattering [14]. From this point of view the particles produced within this study are rather promising for application in TSFD. Furthermore the established encapsulation process is promising for larger-scale applications with regard to its reasonably low time demand.

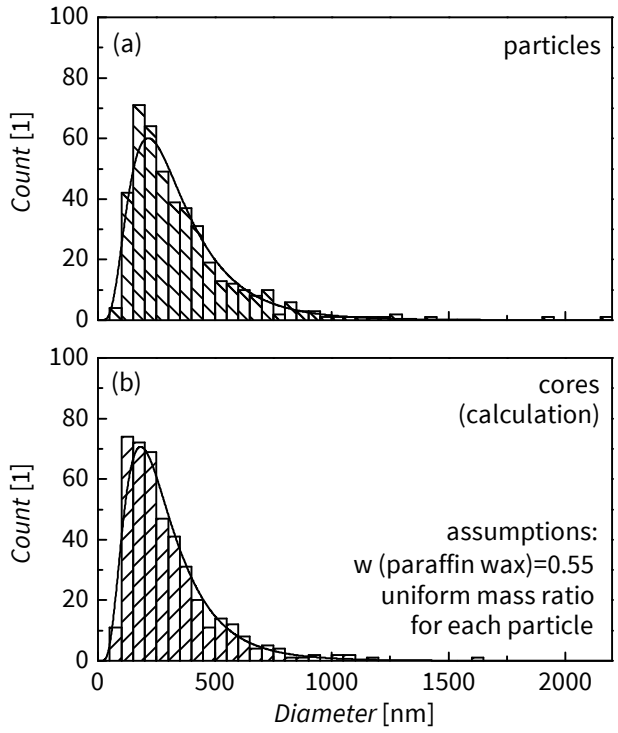

Figure 12.5.: Histograms and overlaid logarithmic normal-distribution of **(a)** diameters of particles with a wax core and a shell made of MMA and EGDMA and **(b)** core diameters calculated from particle diameters (assumption $w_{Core} = 0.55$ be uniform for all particles). Total count of particles: 434.

Table 12.2.: Paraffin wax content (w_{Core}) along with the mean and median of the actually detected capsule diameters ($d_{Capsule}$) and the calculated core diameters (d_{Core}) of capsules with polymeric shell obtained from different monomer mixtures.

Monomer mixture	w_{Core} [%]	$d_{Capsule}$ [nm]		d_{Core} [nm]	
		mean	median	mean	median
MMA/EGDMA	55	354	280	301	238
MMA/iBoMA/EGDMA	57	487	439	419	377

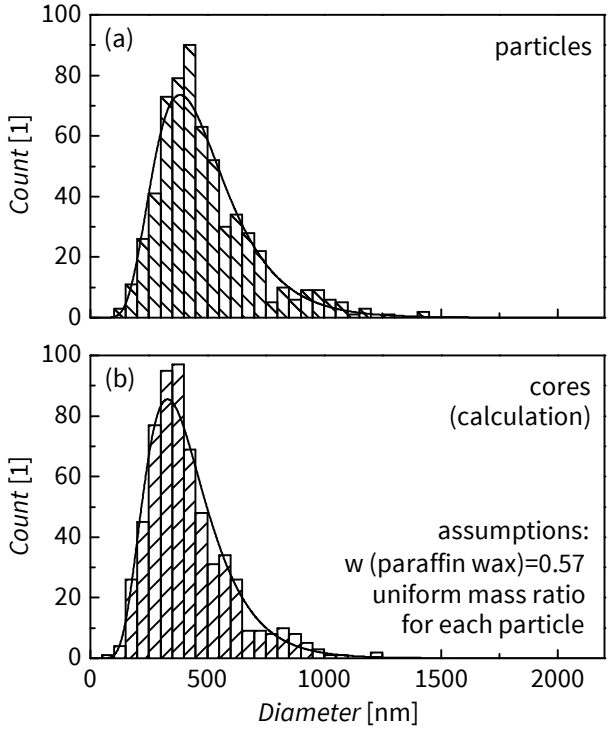

Figure 12.6.: Histograms and overlaid logarithmic normal-distribution of **(a)** diameters of particles with a wax core and a shell made of MMA, iBoMA and EGDMA and **(b)** core diameters calculated from particle diameters (assumption w_{Core} = 0.57 be uniform for all particles). Total count of particles: 609.

12.5 TSFD formulated with Encapsulated Paraffin Wax

12.5.1 Experimental

12.5.1.1 TSFD Formulation

Resin matrix was prepared by mixing 57 wt% oligomer (Ebecryl 800), 40 wt% reactive diluent (OTA-480) and 3 wt% photo-initiator (Lucirin TPO-L). Employed oligomer and reactive diluent were supplied by Allnex Belgium SA/NV (formerly Cytec Surface Specialities Inc.; Drobenbos, BE). Photo-Initiator was provided by BASF. The amount of capsules ($m_{Capsules}$) required to maintain a thermotropic additive content ($w_{Additive}$)

of 5 wt% in a TSFD formulated with a specific amount of resin matrix was calculated according to eq. 12.3. This amount of capsules was added to the resin matrix and dispersed subsequently. The resulting mixtures were poured in the intervening space between two glass panes, which were sealed around the edge. Subsequently the layers were cured by UV-radiation (dose: 8.3 mJ cm^{-2}) from 366 nm bulb of Universal-UV-Lamp (Camag, Muttenz, CH). Removal of the glass panes resulted in approx. 900 µm thick free-standing layers.

Equation 12.3

$$m_{Capsules} = m_{Matrix} \times \left(\frac{w_{Core}}{w_{Additive}} - 1 \right)^{-1} \tag{12.3}$$

12.5.1.2 Determination of Light-Shielding Efficiency

Overheating protection performance of TSFD was determined applying UV/Vis/NIR spectrometry. A double beam UV/Vis/NIR spectrophotometer Lambda 950 (Perkin Elmer Inc., Waltham, MA, US) equipped with an Ulbricht-sphere (diameter 150 mm) was employed. For the given measurement apparatus the radiation passing through (transmittance) the specimen outside a cone of approximately 5° relative to the incident beam direction was defined as diffuse (scattered) component. Hemispheric and diffuse transmittance was recorded at normal incidence in the spectral region from 250 to 2500 nm. The integral solar transmittance was determined by weighting the recorded spectral data in steps of 5 nm by the AM1.5 global solar irradiance source function. The spectrophotometer was adapted by a heating stage to adjust sample temperature within a range from ambient temperature to maximum 115 °C. Measurements were performed in steps of 5 °C. Prior to measurement, the samples were allowed to equilibrate for 5 min at the selected temperature. The heating stage was equipped with a control system consisting of a heating stage-internal J-type thermocouple as temperature sensor and the control unit HS-W-35/M (Heinz Stegmeier Heizelemente HS-Heizelemente GmbH, Fridingen, DE). Within the heating stage the sample was positioned in close proximity of the port hole of the Ulbricht-sphere. In situ front- and backside sample surface temperatures as a function of set-point value of the control unit were recorded on a prototype sample with a two-channel temperature measurement instrument T900 (Dostmann electronic GmbH, Wertheim-

Reicholzheim, DE) equipped with a precision K-type thermocouple. Sample temperature was assumed as the average of both recorded surface temperatures. Required set-point values to maintain average sample temperatures were calculated from a second order polynomial fit of the temperatures recorded in measurements of the prototype sample.

12.5.2 Results and Discussion

Figure 12.7

In Figure 12.7 the solar hemispheric (square symbol) and solar diffuse (triangle symbol) transmittance of TSFD formulated with encapsulated paraffin wax with a polymeric shell obtained from either MMA and EGDMA (Fig. 12.7a) or MMA, iBoMA and EGDMA (Fig. 12.7b) is displayed. Both layers exhibited a distinct reduction in solar hemispheric transmittance upon exceeding the switching threshold (45 °C). The layer formulated with encapsulated paraffin wax with a polymeric shell obtained from MMA and EGDMA showed a reduction in solar hemispheric transmittance from 73.1 (room temperature) to 49.2 % (70 °C). At the same time, the solar diffuse transmittance increased from 40.7 (room temperature) to 47.8 °C (70 °C). The layer formulated with encapsulated paraffin wax with a polymeric shell obtained from MMA, iBoMA and EGDMA showed a reduction in solar hemispheric transmittance from 70.1 (room temperature) to 49.0 °C (70 °C). At the same time, the solar diffuse transmittance increased from 34.6 (room temperature) to 46.8 % (70 °C). In order to validate these results, two additional replicates of each individual TSFD were characterised with regard to their overheating protection performance. The replicate measurements were conducted at room temperature and 70 °C only. Mean and standard deviation of solar hemispheric and diffuse transmittance were calculated for room temperature and 70 °C. The results are presented in Table 12.3. The TSFD formulated with the additive capsules with a polymeric shell obtained from MMA and EGDMA displayed higher solar hemispheric transmittance at room temperature (72.6 %) than the TSFD formulated with the additive capsules with a polymeric shell obtained from MMA, iBoMA and EGDMA (68.6 %). However, the achieved solar hemispheric transmittance at 70 °C was rather similar for both layers (48.9 vs. 48.7 %). The solar diffuse trans-

Table 12.3

mittance of both layers increased slightly upon exceeding the threshold temperature (from 38.8 to 47.4 % and from 35.3 to 46.6 %, respectively).

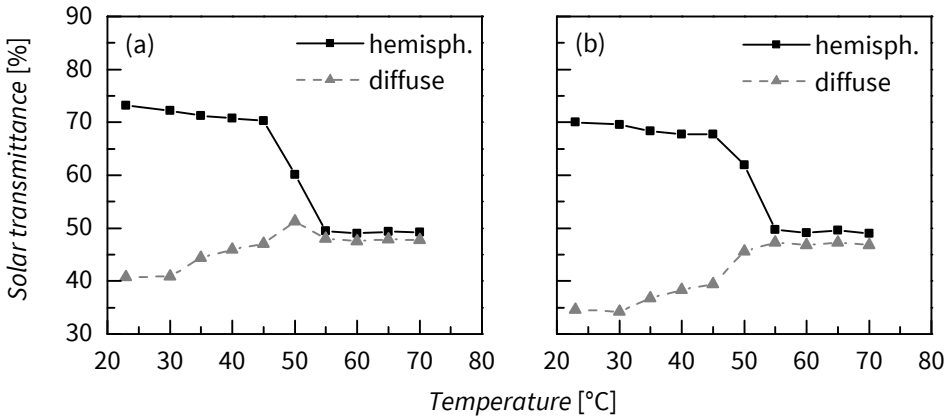

Figure 12.7.: Solar hemispheric (square symbol) and solar diffuse (triangle symbol) transmittance as a function of temperature of TSFD formulated with 5 wt% thermotropic additive content. Thermotropic additive was incorporated in encapsulated form with a polymeric shell obtained from different monomer mixtures, either **(a)** MMA and EGDMA or **(b)** MMA, iBoMA and EGDMA.

The difference in solar hemispheric transmittance at room temperature detected for these two TSFD may be ascribed to a multitude of factors like slight differences in shell-material content, refractive index differences between matrix/shell/additive or slight differences in size distribution.

Anyway, compared to earlier results, a remarkable improvement in overheating protection performance of TSFD was obtained. A TSFD produced from the same matrix and additive type, but additive not being encapsulated (referred to as M7A1-OTA-p3-RT-0.008 [22]) exhibited a reduction in solar hemispheric transmittance from 81.2 (room temperature) to 78.5 % (70 °C). That was ascribed to the inappropriate diameters of spherical scattering domains formed by the additive, ranging from 2.76 to 116 µm.

Thus, the better light-shielding efficiency of the TSFD formulated with encapsulated additive was ascribed to the rather optimal diameter of the scattering domains. However, the detected solar hemispheric transmittance at room temperature of around

70 % is significantly lower compared to the result of 81.2 % detected for the TSFD formulated with the additive not being encapsulated [22]. This may be ascribed to the differences in scattering domain size: For scattering domains that are too big for optimal back-scattering, a low potential refractive index difference between matrix and additive probably yields no distinct effect on solar hemispheric transmittance at room temperature due to low back-scattering efficiency. However, for layers formulated with optimally sized scattering domains, even a small refractive index difference between matrix and additive may yield a significant effect on solar hemispheric transmittance (i.e. a lower transmittance) at room temperature due to high back-scattering efficiency. Thus, future work also has to address the optimisation of the matrix/additive combination more in detail.

Table 12.3.: Mean and standard deviation of solar hemispheric and diffuse transmittance detected at room temperature and 70 °C of TSFD formulated with encapsulated paraffin wax with polymeric shell obtained from different monomer mixtures (results from threefold determination).

Monomer mixture	Solar hemispheric transmittance at room temperature				Solar hemispheric transmittance at 70 °C			
	hemispheric [%]		diffuse [%]		hemispheric [%]		diffuse [%]	
	mean	sdev	mean	sdev	mean	sdev	mean	sdev
MMA/EGDMA	72.6	0.5	38.8	1.7	48.9	0.2	47.4	0.3
MMA/iBoMA/EGDMA	68.6	1.3	35.3	0.8	48.7	0.3	46.6	0.2

12.6 Conclusion and Outlook

Within this study, a photo-initiated miniemulsion polymerisation technique was established in order to encapsulate a thermotropic additive with a polymeric acrylate shell and thereby obtain optimally sized scattering domains for formulation of thermotropic systems with fixed domains (TSFD). The light-shielding efficiency of the TSFD formulated with these capsules was significantly improved compared to layers lacking scattering domains with adjusted size. The improvements in light-shielding efficiency of TSFD were rather remarkable. The obtained solar hemispheric transmittances were around 73 and 49 % at temperatures below and above the switching threshold, respectively. However, efficient overheating protection of an all polymeric flat plate collector requires solar hemispheric transmittances of $>$85 and $<$60 % at temperatures below and above the switching threshold, respectively [9]. An improvement in light-shielding efficiency of the layers is probably achievable upon optimisation of matrix/additive combination. The lower the refractive index difference at room temperature is, the higher the corresponding solar hemispheric transmittance will be. Thus, future work has to focus on an optimisation of material composition of matrix and polymeric shell in order to match the refractive index of thermotropic additive at room temperature as good as possible.

Anyway, the established miniemulsion polymerisation routine would also allow for encapsulation of thermotropic additives with different melting points rather easily and thus easy adjustment of switching threshold of TSFD formulated with these capsules. With regard to encapsulation of thermotropic additives with higher melting temperature, monomer evaporation is an issue, thus carrying out the reaction in pressurised atmosphere (oxygen-free) would be beneficial in order to mitigate monomer losses. Anyway, a major advantage of the photo-initiated process is the process acceleration. The duration of the established photo-initiated polymerisation was 15 min.

Notwithstanding, the way the miniemulsion polymerisation process was carried out has some drawbacks: In photo-initiated polymerisation processes, thickness of the irradiated layer is always an issue. In a reaction vessel the layer thickness – which actually is the diameter of the beaker in this study – is rather high. This is

especially relevant for scale-up of the polymerisation process. In a big stirred tank the miniemulsion with its polymerisable fraction is probably not irradiated properly due to absorption (Lambert-Beer-law) or requires reasonably high residence times in order to get irradiated properly. Thus, a reduction in layer thickness would enhance photo-polymerisation process. Furthermore, for larger scale application a continuous process is desirable.

A promising reactor concept that can probably cope with all these aspects is the spinning disc reactor [85]. With this reactor type, one can control the reaction medium temperature rather easily and maintain a reasonably thin reactant layer [85]. Furthermore, it has proven applicability for UV initiated photo-polymerisation processes [85].

Thus, a potential continuous process for manufacturing of encapsulated thermotropic additive might look like: (1) Establishment of oil and water phase, (2) mixing the phases and subsequent establishment of miniemulsion via ultrasound emulsification in a continuous-flow cell, (3) UV-irradiation under nitrogen atmosphere in a spinning disc reactor equipped with a UV-radiation source and subsequent (4) spray-drying of the obtained latex.

12.7 Acknowledgements

The research work of this paper was performed at the Polymer Competence Center Leoben GmbH (PCCL, Austria) within the framework of the COMET-program of the Federal Ministry for Transport, Innovation and Technology and Federal Ministry for Econoomy, Family and Youth with contributions by University of Leoben (Department Polymer Engineering and Science, Leoben AT). The PCCL is funded by the Austrian Government and the State Governments of Styria and Upper Austria. Parts of this research project were funded by the State Government of Styria, Department Zukunftsfonds (project number 5019).

The authors want to express their gratitude to Sandra Schlögel and Jakob Manhart (PCCL) for their help upon setting up laboratory equipment, to Thomas Griesser and Mathias Edler (Christian Doppler Laboratory for Functional and Polymer Based

Inkjet Inks at University of Leoben, Department Polymer Engineering and Science, Chemistry of Polymeric Materials, Leoben, AT) for providing the ultrasound device and to Carina Tauterer (University of Leoben, Department of Environmental and Energy Process Engineering, Institute of Waste Treatment Technologies and Landfilling) for providing the freeze drying apparatus.

Furthermore the contribution of materials by Allnex Belgium SA/NV (formerly Cytec Surface Specialities Inc.; Drogenbos, BE), BASF SE (Ludwigshafen, DE) and Sasolwax GmbH (Hamburg, DE) are gratefully acknowledged.

12.8 References

[1] P. Nitz and H. Hartwig, 'Solar control with thermotropic layers', *Solar Energy*, vol. 79, no. 6, pp. 573–582, 2005, ISSN: 0038092X. DOI: 10.1016/j.solener.2004.12.009.

[2] A. Seeboth, J. Schneider and A. Patzak, 'Materials for intelligent sun protecting glazing', *Solar Energy Materials and Solar Cells*, vol. 60, no. 3, pp. 263–277, 2000, ISSN: 09270248. DOI: 10.1016/S0927-0248(99)00087-2.

[3] J. Yao and N. Zhu, 'Evaluation of indoor thermal environmental, energy and daylighting performance of thermotropic windows', *Building and Environment*, vol. 49, pp. 283–290, 2012, ISSN: 03601323. DOI: 10.1016/j.buildenv.2011.06.004.

[4] T. Inoue, 'Solar shading and daylighting by means of autonomous responsive dimming glass: practical application', *Energy and Buildings*, vol. 35, no. 5, pp. 463–471, 2003, ISSN: 03787788. DOI: 10.1016/S0378-7788(02)00143-3.

[5] H. Hartwig, 'Konzepte für die Integration selbstregelnder, thermotroper Schichten in moderne Gebäudehüllen zur passiven Nutzung der Sonnenenergie', Dissertation, Technische Universität München, München, 2003.

[6] P. Nitz and A. Wagner, 'Schaltbare und regelbare Verglasungen', *BINE Themeninfo*, vol. I/02, no. I/02, pp. 1–12, 2002, ISSN: 1610-8302.

[7] K. Resch, R. Hausner and G. M. Wallner, 'All Polymeric Flat-Plate Collector — Potential of Thermotropic Layers to Prevent Overheating', in *Proceedings of ISES Solar World Congress 2007*, D. Y. Goswami and Y. Zhao, Eds., Berlin: Springer, 2007, pp. 561–565, ISBN: 978-3-540-75996-6. DOI: 10.1007/978-3-540-75997-3_102.

[8] K. Resch and G. M. Wallner, 'Thermotropic layers for flat-plate collectors—A review of various concepts for overheating protection with polymeric materials', *Solar Energy Materials and Solar Cells*, vol. 93, no. 1, pp. 119–128, 2009, ISSN: 09270248. DOI: 10.1016/j.solmat.2008.09.004.

[9] G. M. Wallner, K. Resch and R. Hausner, 'Property and performance requirements for thermotropic layers to prevent overheating in an all polymeric flat-plate collector', *Solar Energy Materials and Solar Cells*, vol. 92, no. 6, pp. 614–620, 2008, ISSN: 09270248. DOI: 10.1016/j.solmat.2007.12.005.

[10] S. Harrison and C. A. Cruickshank, 'A review of strategies for the control of high temperature stagnation in solar collectors and systems', *Energy Procedia*, vol. 30, pp. 793–804, 2012, ISSN: 18766102. DOI: 10.1016/j.egypro.2012.11.090.

[11] S. A. Kalogirou, 'Solar thermal collectors and applications', *Progress in Energy and Combustion Science*, vol. 30, no. 3, pp. 231–295, 2004, ISSN: 03601285. DOI: 10.1016/j.pecs.2004.02.001.

[12] K. Resch, R. Hausner, G. M. Wallner and R. W. Lang, 'Thermotropic Layers for Overheating Protection of all-Polymeric Flat Plate Solar Collectors', in *Polymeric materials for solar thermal applications*, M. Köhl, M. G. Meir, P. Papillon, G. M. Wallner and S. Saile, Eds., Weinheim: Wiley-VCH, 2012, pp. 255–266, ISBN: 978-3-527-33246-5.

[13] K. Resch and A. Weber, 'Smart Windows - Smart Collectors: Entwicklung von funktionalen Überhitzungsschutzverglasungen für Gebäudeverglasungen und thermische Solarkollektoren', *Berg- und Hüttenmännische Monatshefte*, vol. 156, no. 11, pp. 429–433, 2011, ISSN: 0005-8912. DOI: 10.1007/s00501-011-0031-2.

[14] P. Nitz, 'Optical modelling and characterisation of thermotropic systems', Dissertation, Albert-Ludwigs-University, Freiburg i.B., 1999.

[15] D. P. Gruber, G. Winkler, A. Weber and K. Resch, 'Novel approach to the solution of the scattering problem in a thermotropic medium', vol. unpublished manuscript, 2013.

[16] K. Resch, G. M. Wallner and R. Hausner, 'Phase separated thermotropic layers based on UV cured acrylate resins – Effect of material formulation on overheating protection properties and application in a solar collector', *Solar Energy*, vol. 83, no. 9, pp. 1689–1697, 2009, ISSN: 0038092X. DOI: 10.1016/j.solener.2009.06.006.

[17] K. Resch, G. M. Wallner and R. W. Lang, 'Spectroscopic Investigations of Phase-Separated Thermotropic Layers Based on UV Cured Acrylate Resins', *Macromolecular Symposia*, vol. 265, no. 1, pp. 49–60, 2008, ISSN: 10221360. DOI: 10.1002/masy.200850506.

[18] R. Ruhmann, A. Seeboth, O. Muehling and D. Loetzsch, 'Thermotropic Materials for Adaptive Solar Control', *Advances in Science and Technology*, vol. 77, pp. 124–131, 2012, ISSN: 1662-0356. DOI: 10.4028/www.scientific.net/AST.77.124.

[19] A. Weber and K. Resch, 'Thermotropic glazings for overheating protection', *Energy Procedia*, vol. 30, pp. 471–477, 2012, ISSN: 18766102. DOI: 10.1016/j.egypro.2012.11.056.

[20] A. Weber and K. Resch, 'Thermotropic Glazings for Overheating Protection I: Material Pre-selection, Formulation and Light-Shielding Efficiency', *Journal of Applied Polymer Science*, ISSN: 0021-8995. DOI: 10.1002/app.39950.

[21] A. Weber, A. Schmid and K. Resch, 'Thermotropic Glazings for Overheating Protection II: Morphology and Structure-Property-Relationships', *Journal of Applied Polymer Science*, ISSN: 0021-8995. DOI: 10.1002/app.39910.

[22] A. Weber, S. Schlögl and K. Resch, 'Effect of Formulation and Processing Conditions on Light Shielding Efficiency of Thermotropic Systems with Fixed Domains Based on UV Curing Acrylate Resins', *Journal of Applied Polymer Science*, vol. 130, no. 5, pp. 3299–3310, 2013, ISSN: 0021-8995. DOI: 10.1002/app.39571.

[23] A. Weber and K. Resch, 'Thermotropic Overheating Protection Glazings: Effect of Functional Additives and Processing Conditions on Light-Shielding Efficiency', *Journal of Polymer Engineering*, vol. submitted,

[24] O. Muehling, A. Seeboth, T. Haeusler, R. Ruhmann, E. Potechius and R. Vetter, 'Variable solar control using thermotropic core/shell particles', *Solar Energy Materials and Solar Cells*, vol. 93, no. 9, pp. 1510–1517, 2009, ISSN: 09270248. DOI: 10.1016/j.solmat.2009.03.029.

[25] K. Resch and G. M. Wallner, 'Morphology of phase-separated thermotropic layers based on UV cured acrylate resins', *Polymers for Advanced Technologies*, vol. 20, no. 12, pp. 1163–1167, 2009, ISSN: 10427147. DOI: 10.1002/pat.1393.

[26] A. Weber and K. Resch, 'Effect of Temperature-Cycling on the Morphology of Polymeric Thermotropic Glazings for Overheating Protection Applications', *Journal of Polymer Research*, vol. 19:9888, no. 6, pp. 1–8, 2012, ISSN: 1022-9760. DOI: 10.1007/s10965-012-9888-3.

[27] K. Resch, 'Polymeric Thermotropic Materials for Overheating Protection of Solar Collectors', Dissertation, University of Leoben, Leoben, 2008.

[28] S. Alay, C. Alkan and F. Göde, 'Synthesis and characterization of poly(methyl methacrylate)/n-hexadecane microcapsules using different cross-linkers and their application to some fabrics', *Thermochimica Acta*, vol. 518, no. 1-2, pp. 1–8, 2011, ISSN: 00406031. DOI: 10.1016/j.tca.2011.01.014. (visited on 09/02/2012).

[29] C. Alkan, A. Sarı and A. Karaipekli, 'Preparation, thermal properties and thermal reliability of microencapsulated n-eicosane as novel phase change material for thermal energy storage', *Energy Conversion and Management*, vol. 52, no. 1, pp. 687–692, 2011, ISSN: 01968904. DOI: 10.1016/j.enconman.2010.07.047. (visited on 09/02/2012).

[30] C. Alkan, A. Sarı, A. Karaipekli and O. Uzun, 'Preparation, characterization, and thermal properties of microencapsulated phase change material for thermal energy storage', *Solar Energy Materials and Solar Cells*, vol. 93, no. 1, pp. 143–147, 2009, ISSN: 09270248. DOI: 10.1016/j.solmat.2008.09.009. (visited on 09/02/2012).

[31] C. Chen, Z. Chen, X. Zeng, X. Fang and Z. Zhang, 'Fabrication and characterization of nanocapsules containing n-dodecanol by miniemulsion polymerization using interfacial redox initiation', *Colloid and Polymer Science*, vol. 290, no. 4, pp. 307–314, 2012, ISSN: 0303-402X. DOI: 10.1007/s00396-011-2545-2.

[32] Z.-H. Chen, F. Yu, X.-R. Zeng and Z.-G. Zhang, 'Preparation, characterization and thermal properties of nanocapsules containing phase change material n-dodecanol by miniemulsion polymerization with polymerizable emulsifier', *Applied Energy*, vol. 91, no. 1, pp. 7–12, 2012, ISSN: 03062619. DOI: 10.1016/j.apenergy.2011.08.041.

[33] M. G. d. Cortazar and R. Rodríguez, 'Thermal storage nanocapsules by miniemulsion polymerization', *Journal of Applied Polymer Science*, vol. 127, no. 6, pp. 5059–5064, 2013, ISSN: 0021-8995. DOI: 10.1002/app.38124.

[34] M. Delgado, A. Lázaro, J. Mazo and B. Zalba, 'Review on phase change material emulsions and microencapsulated phase change material slurries: Materials, heat transfer studies and applications', *Renewable and Sustainable Energy Reviews*, vol. 16, no. 1, pp. 253–273, 2012, ISSN: 13640321. DOI: 10.1016/j.rser.2011.07.152.

[35] Y. Fang, S. Kuang, X. Gao and Z. Zhang, 'Preparation and characterization of novel nanoencapsulated phase change materials', *Energy Conversion and Management*, vol. 49, no. 12, pp. 3704–3707, 2008, ISSN: 01968904. DOI: 10.1016/j.enconman.2008.06.027. (visited on 09/02/2012).

[36] Y. Luo and X. Zhou, 'Nanoencapsulation of a hydrophobic compound by a miniemulsion polymerization process', *Journal of Polymer Science Part A: Polymer Chemistry*, vol. 42, no. 9, pp. 2145–2154, 2004, ISSN: 0887-624X. DOI: 10.1002/pola.20065.

[37] S. Ma, G. Song, W. Li, P. Fan and G. Tang, 'UV irradiation-initiated MMA polymerization to prepare microcapsules containing phase change paraffin', *Solar Energy Materials and Solar Cells*, vol. 94, no. 10, pp. 1643–1647, 2010, ISSN: 09270248. DOI: 10.1016/j.solmat.2010.05.021.

[38] Y. Ma, X. Chu, W. Li and G. Tang, 'Preparation and characterization of poly(methyl methacrylate-co-divinylbenzene) microcapsules containing phase change temperature adjustable binary core materials', *Solar Energy*, vol. 86, no. 7, pp. 2056–2066, 2012, ISSN: 0038092X. DOI: 10.1016/j.solener.2012.04.008.

[39] X. Qiu, W. Li, G. Song, X. Chu and G. Tang, 'Fabrication and characterization of microencapsulated n-octadecane with different crosslinked methylmethacrylate-based polymer shells', *Solar Energy Materials and Solar Cells*, vol. 98, pp. 283–293, 2012, ISSN: 09270248. DOI: 10.1016/j.solmat.2011.11.018.

[40] X. Qiu, W. Li, G. Song, X. Chu and G. Tang, 'Microencapsulated n-octadecane with different methylmethacrylate-based copolymer shells as phase change materials for thermal energy storage', *Energy*, vol. 46, no. 1, pp. 188–199, 2012, ISSN: 03605442. DOI: 10.1016/j.energy.2012.08.037.

[41] X. Qiu, G. Song, X. Chu, X. Li and G. Tang, 'Microencapsulated n-alkane with p(n-butyl methacrylate-co-methacrylic acid) shell as phase change materials for thermal energy storage', *Solar Energy*, vol. 91, pp. 212–220, 2013, ISSN: 0038092X. DOI: 10.1016/j.solener.2013.01.022.

[42] X. Qiu, G. Song, X. Chu, X. Li and G. Tang, 'Preparation, thermal properties and thermal reliabilities of microencapsulated n-octadecane with acrylic-based polymer shells for thermal energy storage', *Thermochimica Acta*, vol. 551, pp. 136–144, 2013, ISSN: 00406031. DOI: 10.1016/j.tca.2012.10.027.

[43] A. Sarı, C. Alkan and A. Karaipekli, 'Preparation, characterization and thermal properties of PMMA/n-heptadecane microcapsules as novel solid–liquid microPCM for thermal energy storage', *Applied Energy*, vol. 87, no. 5, pp. 1529–1534, 2010, ISSN: 03062619. DOI: 10.1016/j.apenergy.2009.10.011.

[44] N. Sarier and E. Onder, 'Organic phase change materials and their textile applications: An overview', *Thermochimica Acta*, vol. 540, pp. 7–60, 2012, ISSN: 00406031. DOI: 10.1016/j.tca.2012.04.013.

[45] A. R. Shirin-Abadi, A. R. Mahdavian and S. Khoee, 'New Approach for the Elucidation of PCM Nanocapsules through Miniemulsion Polymerization with an Acrylic Shell', *Macromolecules*, vol. 44, no. 18, pp. 7405–7414, 2011, ISSN: 0024-9297. DOI: 10.1021/ma201509d.

[46] Y. Wang, H. Shi, T. D. Xia, T. Zhang and H. X. Feng, 'Fabrication and performances of microencapsulated paraffin composites with polymethylmethacrylate shell based on ultraviolet irradiation-initiated', *Materials Chemistry and Physics*, vol. 135, no. 1, pp. 181–187, 2012, ISSN: 02540584. DOI: 10.1016/j.matchemphys.2012.04.050.

[47] C. Zhao and G. Zhang, 'Review on microencapsulated phase change materials (MEPCMs): Fabrication, characterization and applications', *Renewable and Sustainable Energy Reviews*, vol. 15, no. 8, pp. 3813–3832, 2011, ISSN: 13640321. DOI: 10.1016/j.rser.2011.07.019.

[48] P. Amrhein, A. Spannagel, H. Ascherl and G. Lang-Wittkowski, 'Microcapsule powder', pat. WO 2006092439A1, 2006.

[49] J. F. Rodriguez Romero, M. L. Sanchez Silva, P. Sanchez Parades, A. De Lucas Martinez and M. L. Torres Barreto, 'Process for microencapsulation of phase change materials, microcapsules obtained and uses thereof', pat. WO 2007107171A1, 2007.

[50] T. Schröder-Grimonpont, H. Willax, B. Katz, J. Brust, S. Altmann and M. Schmidt, 'Microcapsules having a paraffin composition as a capsule core', pat. WO 2012 110443A1, 2012.

[51] Z. Cao and U. Ziener, 'A Versatile Technique to Fabricate Capsules: Miniemulsion', *Current Organic Chemistry*, vol. 17, no. 1, pp. 30–38, 2013, ISSN: 13852728. DOI: 10.2174/138527213805289169.

[52] L. L. Hecht, C. Wagner, K. Landfester and H. P. Schuchmann, 'Surfactant Concentration Regime in Miniemulsion Polymerization for the Formation of MMA Nanodroplets by High-Pressure Homogenization', *Langmuir*, vol. 27, no. 6, pp. 2279–2285, 2011, ISSN: 0743-7463. DOI: 10.1021/la104480s.

[53] L. L. Hecht, C. Wagner, Ö. Özcan, F. Eisenbart, K. Köhler, K. Landfester and H. P. Schuchmann, 'Influence of the Surfactant Concentration on Miniemulsion Polymerization for the Preparation of Hybrid Nanoparticles', *Macromolecular Chemistry and Physics*, vol. 213, no. 20, pp. 2165–2173, 2012, ISSN: 1022-1352. DOI: 10.1002/macp.201200219.

[54] M. Y. Koroleva and E. V. Yurtov, 'Nanoemulsions: the properties, methods of preparation and promising applications', *Russian Chemical Reviews*, vol. 81, no. 1, pp. 21–43, 2012, ISSN: 0036-021X. DOI: 10.1070/RC2012v081n01ABEH004219.

[55] K. Landfester, 'Polyreactions in Miniemulsions', *Macromolecular Rapid Communications*, vol. 22, no. 12, pp. 896–936, 2001, ISSN: 10221336.

[56] K. Landfester, F. Schork and V. A. Kusuma, 'Particle size distribution in miniemulsion polymerization', *Comptes Rendus Chimie*, vol. 6, no. 11-12, pp. 1337–1342, 2003, ISSN: 16310748. DOI: 10.1016/j.crci.2003.07.019. (visited on 09/02/2012).

[57] K. Landfester, 'Miniemulsionspolymerisation und Struktur von Polymer- und Hybridnanopartikeln', *Angewandte Chemie*, vol. 121, no. 25, pp. 4556–4576, 2009, ISSN: 00448249. DOI: 10.1002/ange.200900723. (visited on 09/02/2012).

[58] K. Landfester and C. K. Weiss, 'Encapsulation by Miniemulsion Polymerization', in *Advances in Polymer Science*, F. Caruso, Ed., vol. 229, Berlin: Springer, 2010, pp. 1–49, ISBN: 978-3-642-12873-8. DOI: 10.1007/12_2009_43.

[59] J. P. Rao and K. E. Geckeler, 'Polymer nanoparticles: Preparation techniques and size-control parameters', *Progress in Polymer Science*, vol. 36, no. 7, pp. 887–913, 2011, ISSN: 00796700. DOI: 10.1016/j.progpolymsci.2011.01.001.

[60] A. J. van Zyl, D. d. Wet-Roos, R. D. Sanderson and B. Klumperman, 'The role of surfactant in controlling particle size and stability in the miniemulsion polymerization of polymeric nanocapsules', *European Polymer Journal*, vol. 40, no. 12, pp. 2717–2725, 2004, ISSN: 00143057. DOI: 10.1016/j.eurpolymj.2004.07.021.

[61] F. J. Schork, Y. Luo, W. Smulders, J. P. Russum, A. Butté and K. Fontenot, 'Miniemulsion Polymerization', in *Advances in Polymer Science*, ser. Advances in Polymer Science, M. Okubo, Ed., vol. 175, Berlin: Springer, 2005, pp. 129–255, ISBN: 978-3-540-31565-0. DOI: 10.1007/b100115.

[62] O. Seok Kwon, J. Jang and J. Bae, 'A Review of Fabrication Methods and Applications of Novel Tailored Microcapsules', *Current Organic Chemistry*, vol. 17, no. 1, pp. 3–13, 2013, ISSN: 13852728. DOI: 10.2174/138527213805289196.

[63] F. Tiarks, K. Landfester and M. Antonietti, 'Preparation of Polymeric Nanocapsules by Miniemulsion Polymerization', *Langmuir*, vol. 17, no. 3, pp. 908–918, 2001, ISSN: 0743-7463. DOI: 10.1021/la001276n.

[64] K. Landfester, N. Bechthold, S. Förster and M. Antonietti, 'Evidence for the preservation of the particle identity in miniemulsion polymerization', *Macromolecular Rapid Communications*, vol. 20, no. 2, pp. 81–84, 1999, ISSN: 10221336. DOI: 10.1002/(SICI)1521-3927(19990201)20:2<81::AID-MARC81>3.0.CO;2-G.

[65] M. Antonietti and K. Landfester, 'Polyreactions in miniemulsions', *Progress in Polymer Science*, vol. 27, no. 4, pp. 689–757, 2002, ISSN: 00796700. DOI: 10.1016/S0079-6700(01)00051-X.

[66] J. M. Asua, 'Miniemulsion polymerization', *Progress in Polymer Science*, vol. 27, no. 7, pp. 1283–1346, 2002, ISSN: 00796700. DOI: 10.1016/S0079-6700(02)00010-2. (visited on 09/02/2012).

[67] B. Abismaı¨l, J. Canselier, A. Wilhelm, H. Delmas and C. Gourdon, 'Emulsification by ultrasound: drop size distribution and stability', *Ultrasonics Sonochemistry*, vol. 6, no. 1-2, pp. 75–83, 1999, ISSN: 13504177. DOI: 10.1016/S1350-4177(98)00027-3. (visited on 09/02/2012).

[68] J. P. Canselier, H. Delmas, A. M. Wilhelm and B. Abismaïl, 'Ultrasound Emulsification—An Overview', *Journal of Dispersion Science and Technology*, vol. 23, no. 1-3, pp. 333–349, 2002, ISSN: 0193-2691. DOI: 10.1080/01932690208984209.

[69] P. Walstra, 'Principles of emulsion formation', *Chemical Engineering Science*, vol. 48, no. 2, pp. 333–349, 1993, ISSN: 00092509. DOI: 10.1016/0009-2509(93)80021-H.

[70] A. Chemtob, B. Kunstler, C. Croutxé-Barghorn and S. Fouchard, 'Photoinduced miniemulsion polymerization', *Colloid and Polymer Science*, vol. 288, no. 5, pp. 579–587, 2010, ISSN: 0303-402X. DOI: 10.1007/s00396-010-2190-1. (visited on 09/02/2012).

[71] J. C. Seferis, 'Refractive Indices of Polymers', in *Polymer Handbook*, J. Brandrup, E. H. Immergut and E. A. Grulke, Eds., New York: Wiley, 1999, pp. VI/571–VI/582, ISBN: 0-471-16628-6.

[72] W.-C. Chen and C.-C. Chang, 'Synthesis and characterization of large diameter acrylic polymer light conduits', *Journal of Materials Chemistry*, vol. 9, no. 10, pp. 2307–2312, 1999, ISSN: 0959-9428. DOI: 10.1039/A902742D.

[73] R. V. Slone, 'Methacrylic Ester Polymers', *Encyclopedia of Polymer Science and Technology*, pp. 1–29, 2010. DOI: 10.1002/0471440264.pst196.pub2.

[74] G. W. Ehrenstein and S. Pongratz, *Beständigkeit von Kunststoffen*. München: Hanser, 2007, ISBN: 978-3-446-21851-2.

[75] K. Landfester, N. Bechthold, F. Tiarks and M. Antonietti, 'Formulation and Stability Mechanisms of Polymerizable Miniemulsions', *Macromolecules*, vol. 32, no. 16, pp. 5222–5228, 1999, ISSN: 0024-9297. DOI: 10.1021/ma990299+.

[76] K. Landfester, N. Bechthold, F. Tiarks and M. Antonietti, 'Miniemulsion Polymerization with Cationic and Nonionic Surfactants: A Very Efficient Use of Surfactants for Heterophase Polymerization', *Macromolecules*, vol. 32, no. 8, pp. 2679–2683, 1999, ISSN: 0024-9297. DOI: 10.1021/ma9819438.

[77] M. Freund, R. Csikós, S. Keszthelyi and G. Mózes, 'Paraffin products: Properties, technologies, applications', in *Developments in Petroleum Science*, ser. Developments in Petroleum Science, G. Mózes, Ed., vol. 14, Budapest: Akadémiai Kiadó, 1982, pp. 1–336.

[78] G. W. Ehrenstein, *Polymer-Werkstoffe: Struktur - Eigenschaften - Anwendung*, 3rd ed. München: Hanser, 2011, ISBN: 978-3-446-42283-4.

[79] E. Baur, S. Brinkmann, T. A. Osswald and E. Schmachtenberg, *Saechtling-Kunststoff-Taschenbuch*, 30th ed. München: Hanser, 2007, ISBN: 978-3-446-41437-2.

[80] W. Hellerich, G. Harsch and S. Haenle, *Werkstoff-Führer Kunststoffe: Eigenschaften, Prüfungen, Kennwerte*, 10th ed. München: Hanser, 2010, ISBN: 978-3-446-42572-9.

[81] D. O. Hummel, *Atlas of plastics additives: Analysis by spectrometric methods ; with 62 tables*. Berlin: Springer, 2002, ISBN: 3540424148.

[82] H. Günzler and H. M. Heise, *IR-Spektroskopie: Eine Einführung*, 3rd ed. Weinheim: VCH, 1996, ISBN: 3-527-28759-0.

[83] G. A. L. Verleye, N. P. G. Roeges and M. O. De Moor, *Easy identification of plastics and rubbers*. Shrewsbury: Rapra Technology, 2001, ISBN: 1859572685.

[84] G. Socrates, *Infrared and Raman characteristic group frequencies*, 3rd ed. Chichester: J. Wiley & sons, 2001, ISBN: 9780470093078.

[85] S. D. Pask, O. Nuyken and Z. Cai, 'The spinning disk reactor: an example of a process intensification technology for polymers and particles', *Polymer Chemistry*, vol. 3, no. 10, pp. 2698–2707, 2012, ISSN: 1759-9954. DOI: 10.1039/C2PY20237A.

Part VI.

Summary, Conclusion and Outlook

Summary

Within this thesis, a systematic material formulation stategy was established in order to formulate thermotropic systems with fixed domains (TSFD) with efficient overheating protection performance. Accoring to the strategy, TSFD constituents were characterised prior to TSFD formulation employing sound polymer-physical characterisation methods. TSFD constituents employed were matrix (thermoplastic resins and UV-curable acrylate resins) and thermotropic additives (paraffin waxes, fatty acids and derivatives, polymers, etc.). After assessment of potential TSFD constituents with regard to suitability for TSFD formulation – primarily based on refractive index data of matrix and additive –, layers were formulated either by compounding and compression moulding (TSFD with thermoplastic resin matrix) or mixing of matrix and additive and subsequent curing by UV-radiation (TSFD with UV-curable resin matrix). The established layers were characterised with regard to overheating protection performance and morphology, allowing establishment of structure-property-relationships: In general, scattering domain shape and/or size of these layers were inappropriate for efficient overheating protection. The actually obtained shape of scattering domains was ascribed to effects of rheological issues and/or aspects of matrix/additive interaction (solubility, etc.). The additives beeing likely to show almost no solubility (e.g. paraffin waxes) in the employed matrix materials formed spherical domains. This was ascribed to rheology governing the scattering domain formation process. On the contrary, additives likely exhibiting reasonable solubility (and actually solubilised in the UV-curable resin matrix prior to curing) in the matrix formed non-spherical additive domains because the additive crystals were established in their energetically most favourable shape (and formation was not affected by rheology).

Furthermore, defects evident in several layers had detrimental effects on overheating protection performance. That means an increase in solar hemispheric transmittance was observed upon exceeding the threshold temperature instead of the desired transmittance reduction. The most layers with defects exhibited vacuoles at the perimeter of the scattering domains. Formation of vacoules was ascribed to limited adhesion at the interface of matrix and additive on the one hand side and differences in coefficient of thermal expansion (CTE) of matrix and additive on the other hand side. Based on these findings, optimisation strategies were established in order to (1) prevent defect formation and (2) adjust scattering domain size in order to achieve efficient overheating protection performance (Note: The efforts in order to adjust the scattering domain shape in TSFD is not addressed within this thesis but elsewhere as already pointed out in chapter 9).

The defect prevention focussed on preventing the formation of vacuoles at the perimeter of scattering domains. These investigations were carried out on a prototype system with UV-curable resin matrix and paraffin wax as the thermotropic additive. Experiments revealed the radiation intensity and dose applied upon curing of the layers to be the most important factors governing the defect formation process. A significant reduction in radiation intensity and dose prevented vacuole formation successfully. Thus, the optimised TSFD was further employed as prototype TSFD in subsequent investigations. However, the reduction in intensity and dose required replacement of non-photo-bleaching photo-initiator with a photo-bleaching photo-initiator in order to achieve properly cured layers.

The adjustment of the scattering domain size was a bit more complicated. In a first approach, the effects of adding surfactants and nucleating agents on the one hand side and changes in processing conditions (especially temperatures applied during manufacturing process) on the overheating protection performance of TSFD was investigated. However, these approaches did not improve the overheating protection performance of the investigated prototype TSFD. Notwithstanding, the outcomes of these experiments further improved the established structure-property-relationships. Employing an annealing step after manufacturing the TSFD introduced vacuoles at the perimeter of the scattering domains and thus reduced the achieved solar hemispheric

transmittance below the threshold temperature significantly. This was ascribed to temperature-induced diffusion of the thermotropic additive in the molten state.

Thus, in order to adjust scattering domain size on the one hand side and to suppress a potential temperature-induced additive migration on the other hand side, another strategy for adjustment of the scattering domain size was established. A photo-initiated miniemulsion polymerisation process was developed in order to encapsulate thermotropic additive paraffin wax with an acrylate polymer protective shell and thus adjust the size of the encapsulated thermotropic additive prior to TSFD formulation. The TSFD formulated with the encapsulated thermotropic additive exhibited significantly improved overheating protection performance: Upon exceeding the threshold temperature, a reduction in solar hemispheric transmittance by 24 % from 73 to 49 % was achieved. Just for comparison, a nearly identical layer that was formulated with the thermotropic additive not being encapsulated showed a reduction in solar hemispheric transmittance by 2 % from 81 to 79 % upon exceeding the threshold temperature.

Conclusion and Outlook

One of the major conclusions of this thesis is that prevention of defect formation upon TSFD formulation is a prerequisite in order to achieve TSFD with efficient overheating protection. Defect formation in TSFD had several reasons:

1. poor adhesion between matrix and additive at their interfaces
2. thermally driven effects
    a) different coefficient of thermal expansion (CTE) of matrix and additive
    b) thermally induced diffusion of thermotropic additive in the molten state following an additive concentration gradient

Each measure that triggered these mechanisms led to defect formation in TSFD. On the contrary, if covalent bonds between matrix and additive maintained proper adhesion at their interface, thermally driven mechanisms were *not* able to introduce defects. For example a specific thermotropic additive – a copolymer of ethylene and glycidyl methacrylate (E-co-GMA) – was capable to form covalent bonds with the matrix material polyamide (PA) but not with poly (methyl methacrylate) (PMMA). Thus, TSFD consisting of PA and E-co-GMA did not exhibit vacuoles whereas the layer consisting of PMMA and E-co-GMA did. Consequently, for defect prevention (i.e. prevention of vacuole formation) proper adhesion between matrix material and thermotropic additive is desirable.

For layers with poor adhesion between matrix and additive, mitigation of the effect of different coefficients of thermal expansion (CTE) of matrix and additive upon TSFD manufacturing is desirable in order to suppress defect formation. For these kind of systems apparently no reasonable solution was found when they were formulated

with thermoplastic resin matrix. However, for TSFD exhibiting poor matrix/additive adhesion and being formulated with UV-curable resin matrix, the establishment of low intensity and dose (of the radiation that initiates the polymerisation) upon curing is sufficient in order to prevent vacuole formation. But also these precautions are probably antagonised when thermally induced diffusion of thermotropic additive in the molten state is not suppressed.

One further conclusion was that the establishment of appropriately shaped and sized scattering domain size is an indispensable requirement for maintaining TSFD with efficient overheating protection performance. The encapsulation of the thermotropic additive with a protective polymer shell prior to TSFD formulation was successfully applied in order to adjust scattering domain shape and size on the one hand side and to simultaneously prevent thermally induced additive diffusion on the other hand side. Indeed, upon application of encapsulated thermotropic additive which was appropriately sized, a significant improvement in overheating protection performance of TSFD was achieved.

The promising results of this work with regard to adjustment of the scattering domain shape and size and the significantly enhanced overheating protection performance of TSFD formulated with these domains are an excellent starting point for future investigations. However, several open questions are remaining. First, although adjustment of appropriately shaped and sized scattering domains was achieved, it is not profoundly justified if encapsulation of the thermotropic additive is able to suppress thermally induced diffusion of thermotropic additive in the molten state and thus to overcome defect formation. Although first investigations were rather promising with regard to prevention of thermally induced diffusion of thermotropic additive by the polymeric shell, long-term investigations – which are currently under way – have to confirm the actual effectiveness of the encapsulation in order to prevent the thermotropic additive in the molten state from diffusion. These long-term investigations are also important with regard to the utilisation of TSFD in an architectural context or in solar thermal systems. These goods with rather long life-times require a reasonable long-term stability of TSFD, ideally exceeding the planned life-time of such appliances or other economically relevant times spans (for example depending on regulations for depreciation). Furthermore, TSFD performance has to be evaluated under real-life

conditions in facades and solar thermal collectors. These long-term investigations are also important with regard to the second open question, if encapsulation is able to overcome defect formation by poor adhesion (either between matrix and polymeric shell or polymeric shell and thermotropic additive) and effect of different CTE of polymers (matrix, polymeric shell) and thermotropic additive. Otherwise long-term thermal cycling would probably yield defect formation in TSFD during operation. Consequently, a reduction in solar hemispheric transmittance below the threshold temperature would significantly reduce the solar gains available in buildings or the efficiency of solar thermal collectors equipped with such kind of layers.

Furthermore, future investigations have to focus on the optimisation of the refractive index match between matrix, polymer shell and thermotropic additive: At room temperature, a refractive index difference between these three materials equal to zero is desired. At temperatures exceeding the threshold temperature, the matrix material and the polymeric shell preferably have the same refractive index. On the contrary, the refractive index difference between matrix/polymer shell and thermotropic additive has to be as high as possible.

These remaining challenges have to be carefully addressed (e.g. long-term stability). Nevertheless, based on the established structure-property-relationships and with profound polymer physical knowledge one may derive promising strategies to cope with the remaining issues outlined. For example, thermally induced diffusion of the thermotropic additive in the molten state might be suppressed by employing matrix materials with reasonably low polymer chain mobility (i.e. polymers with a high glass transition temperature) which may hinder additive migration. Taking all these considerations and achievements into account, one might come to the conclusion that the results obtained so far are promising and shall encourage further research in the field of TSFD.